Engineering Sustainable Composites for Lightweight Automotive Applications: Experimental and Theoretical Insights on Hybrid Fibre-reinforced Polymers

by

Shaghayegh Armioun

A thesis submitted in conformity with the requirements

for the degree of PhD

Centre for Biocomposites and Biomaterials Processing (CBBP), Graduate Department of Forestry, John H. Daniels Faculty of Architecture, Landscape, and Design

University of Toronto

Abstract

This study investigates the enhancement of mechanical properties in cellulose microfibre/carbon fibre hybrid composites on PA11-based matrices, aiming to achieve lightweight and sustainable applications in the automotive sector. The use of a PA11-PP blend matrix led to composites with improved thermo-mechanical performance, elevated heat deflection temperatures, and reduced densities, key attributes for semi-structural automotive components where both weight reduction and mechanical reliability are critical.

To support and interpret the experimental findings, a progressive modelling strategy was employed, combining semi-empirical and analytical methods. Classical models such as HROM, Halpin–Tsai, and shear-lag theory were adapted and mathematically refined to predict the tensile modulus of the composites. Using the effective matrix approach, the modified Halpin–Tsai model accurately captured the behaviour of randomly oriented fibres, with best-fit orientation factors (λ_L = 0.481, λ_T = 0.736) aligning closely with theoretical values (0.375 and 0.625), confirming its applicability for reinforcement efficiency in hybrid composites.

To obtain further insight into stress transfer mechanisms and fibre-length-dependent behaviour, particularly relevant in short-fibre composites, the study advanced toward the shear-lag model. Unlike the Halpin-Tsai formulation, which is primarily geometry-based, the shear-lag approach provides a mechanistic description of load transfer between fibres and matrix. The classical shear-lag model was refined through the introduction of a stress transfer efficiency factor (α), defined as a non-linear function of the ratio of fibre length to

its critical length. This analytically modified formulation enabled more realistic and accurate predictions of the tensile modulus in composites reinforced with microfibrillated cellulose and short carbon fibres.

The combined use of semi-empirical and analytically modified models, supported by an effective matrix approach, enabled a deeper understanding of the reinforcing mechanisms in hybrid fibre systems. This framework validates experimental observations and offers a versatile design tool for optimizing the performance of bio-based hybrid composites across a wide range of applications.

Acknowledgment

At the commencement of this PhD journey, which was both exhilarating and challenging, I was surrounded by an extraordinary circle of support and inspiration. It is with profound gratitude that I acknowledge those who have played pivotal roles in making this endeavour possible and a memorable chapter of my life.

First and foremost, my most profound appreciation goes to my supervisor, Professor Mohini Sain. His unwavering support, invaluable guidance, and insightful feedback have been the cornerstone of my research. He has been more than a mentor; he has been a beacon of knowledge and a constant source of motivation. His patience and expertise have shaped this work and my scholarly growth.

I extend my heartfelt thanks to the NSERC Automotive Partnership Canada (APC) program and the in-kind support from the industrial partners, FORD Motor Company of Canada, for their generous funding and support of my project. Their commitment to advancing research and development has provided the financial backbone for this work, enriching my research experience with invaluable industry insights and opportunities. I would like to show my sincerest appreciation to Dr Jimmy Tjong for his constructive feedback.

I extend my sincere appreciation to the Ontario Graduate Scholarship (OGS) and the Queen Elizabeth II Graduate Scholarship in Science and Technology (QEII-GSST) for their generous financial support. The scholarships provided by these prestigious programs have been instrumental in facilitating my research and academic endeavours, allowing me to fully immerse myself in my studies without financial burden.

I would like to thank Professor Ning Yan and Dr. Birat K.C. for their valuable feedback and insightful suggestions, which have contributed meaningfully to the development of this thesis.

Special thanks to Suhara Panthapulakkal for being a great friend, teacher, and co-worker. My work would not have been accomplished without her help and support. My sincere

appreciation also goes to Dr. Omar Faruk for his guidance and support in completing this thesis.

I owe a great deal of gratitude to our lab assistants (Shiang Law and Christian Belachew), whose technical help and collaboration have made the countless hours of research not only productive but also enjoyable. Your shared passion for discovery and innovation has made our lab a nurturing ground for ideas and personal growth.

A special word of thanks to my husband, Navid, whose love, patience, and encouragement have been my stronghold. Your unwavering belief in me has been a source of strength and motivation, making every challenge surmountable. To my son, Edwin, who has been the greatest gift and joined our family while I was accomplishing this study, you bring endless joy and laughter into my life, reminding me of the beautiful balance between work and family.

I am eternally grateful to my parents, whose sacrifices, support, and love laid the foundation for who I am today. Your examples of hard work, perseverance, and kindness have been my guiding stars. Furthermore, to my sister, Arghavan, for being my confidant and cheerleader; thank you for your endless support and for always believing in me.

This thesis stands as a testament to the collective support, guidance, and love of all the individuals mentioned above. I am immensely grateful for every word of encouragement, every piece of advice, and every moment you have invested in me. Thank you for being part of this journey.

Table of Contents

List of Tabl

List of Figures

Nomenclature

3-DEP – Three-dimensional engineered pre-forming
ABS – Acrylonitrile butadiene styrene
ANN – Artificial neural network
ASR – Automobile shredder residue
B4C – Boron carbide
BB – Dimension stone waste or basalt-based (context-specific)
BMCs – Bulk moulding compounds
CF – Carbon fibre
CFRP – Carbon fibre reinforced polymer
CGFR – Continuous glass fibre reinforced
CGFR-PP – Continuous glass fibre reinforced polypropylene
CNN – Convolutional neural network
CTMP – Chemi-thermo mechanical pulp
CZM – Cohesive zone model
DAPA – Dimer fatty acid-based polyamides
DCB – Double cantilever beam
DFA – Desirability function analysis
DMDA – Decamethylenediamine
DMA – Dynamic mechanical analysis
ELV – End-of-life vehicle
EVP – Elasto-viscoplastic
FEA – Finite element analysis
F/BFRP – Flax/basalt fibre reinforced polymer
FFRP – Flax fibre reinforced polymer
GFRP – Glass fibre reinforced polymer
GNP – Graphene nanoplatelet
GSF – Generalized stiffness formulation
HDT – Heat deflection temperature
HFRP – Hybrid fibre reinforced polymer
HMDA – Hexamethylenediamine
HTT-CF – High-heat-treatment carbon fibres
HYP – High yield pulp
IHT-CF – Intermediate-heat-treatment carbon fibres
LCA– Life Cycle Assessment
LCF – Lignin–cellulose fibre
L/D ratio – Length-to-diameter ratio
LHT-CF – Low-heat-treatment carbon fibres
MAPP – Maleic anhydride grafted polypropylene
MFI – Melt flow index
MT – Mori–Tanaka
NFRP – Natural fibre reinforced polymer

OEM – Original equipment manufacturer
PA – Polyamide
PA6 – Polyamide 6
PA11 – Polyamide 11
PAN – Polyacrylonitrile
PCD – Polycrystalline diamond
PEEK – Polyether ether ketone
PEI – Polyetherimide
PEKK – Polyether ketone ketone
PINN – Physics-informed neural network
PMDA – Pentamethylenediamine
PMMA – Polymethyl methacrylate
PP – Polypropylene
PPS – Polyphenylene sulphide
PVDF – Polyvinylidene fluoride
ROM – Rule of mixtures
RSM – Response surface methodology
RTM – Resin transfer moulding
SEM – Scanning electron microscopy
SFRT – Single fibre reinforced thermoplastic
SGFR-PP – Short glass fibre reinforced polypropylene
SMCs – Sheet moulding compounds
TMDA – Tetramethylenediamine
UD – Unidirectional
VARTM – Vacuum-assisted resin transfer moulding
Vf – Fibre volume fraction
Vm – Matrix volume fraction
WF – Wood fibre (cellulose microfibre)
Wt% – Weight percentage

Chapter 1 Introduction: Overview of Research

1.1 Background

Hybrid composites, engineered materials that incorporate two or more distinct constituents, have emerged as a compelling solution for advanced structural applications due to their ability to exhibit synergistic properties that are unattainable by individual components alone (Chagas et al., 2022; Kumar, 2020; Mahmud et al., 2023). The growing interest in sustainable materials has driven research into hybrid composites that integrate synthetic and natural fibres (Shoja et al., 2021; Zolkin et al., 2021). Hybrid composites that combine synthetic and natural fibres offer potential benefits such as improved performance, reduced environmental impact, and cost efficiency (Huang et al., 2023). The careful selection of components and their interactions is essential for realizing the full potential of these hybrid systems. This process yields optimized structural designs that meet both performance requirements and environmental considerations (Kumar, 2020).

Hybridization of composites is crucial for enhancing their mechanical, tribological, or thermal properties while reducing costs (Gaurav et al., 2020; Shoja et al., 2021). Accurate and robust predictive models are necessary to fully capture the complex mechanical behaviour of hybrid composites, resulting from the interaction of synthetic and natural fibres within a shared matrix (Zhang et al., 2021). The interface between natural and synthetic fibres presents a complex challenge in hybrid composites. While natural fibres offer advantages such as lightweighting, biodegradability, and low cost (Martinelli et al., 2023; Simamora et al., 2023), integrating them introduces complexities due to their variability and hydrophilic nature, which affect the composite's mechanical properties and long-term durability (Kurowiak et al., 2023; Seculi et al., 2023).

Understanding the complex behaviour of these materials necessitates advanced modelling techniques that consider variables such as fibre length and orientation, interfacial adhesion, and the varying mechanical properties of the constituent materials (Müzel et al., 2020; Wang et al., 2024; Hage, 2024). The lack of comprehensive and validated models capable of accurately predicting the behaviour of hybrid composites with synthetic and natural fibres poses a significant barrier to the widespread adoption of these materials in demanding engineering applications (Swolfs et al., 2019; Mahmud et al., 2023; Gao et al., 2025). To address this gap, it is necessary to

adopt a comprehensive approach that takes into account the specific properties of synthetic and natural fibres, their interactions within composite materials, and the effects of manufacturing processes on the final product.

1.2 Theoretical Frameworks and Limitations

Current predictive frameworks for fibre-reinforced composites predominantly rely on micromechanical models such as the rule of mixtures, Mori–Tanaka scheme, and Halpin–Tsai equations, along with computational methods including finite element analysis (FEA), cohesive zone models, and phase-field methods (Hu et al., 2021; Seculi et al., 2023; Slamani & Châtelain, 2023). While these classical micromechanical models provide proper estimations of effective composite properties based on constituent properties and volume fractions, they inherently rely on idealized assumptions such as perfect interfacial bonding, homogenous fibre distribution, and isotropic matrix behaviour (Swolfs et al., 2019; Seculi et al., 2023; Przybyszewski et al., 2024). These assumptions are particularly limiting when applied to hybrid composites composed of dissimilar fibre systems, such as natural and synthetic fibres, which inherently exhibit multi-scale variability, interfacial heterogeneity, and thermomechanical anisotropy. As a result, traditional models often fail to capture the complex load transfer mechanisms and nonlinear synergies that emerge from the interaction of reinforcement systems with vastly different stiffness, surface chemistry, and morphological characteristics (Wang et al., 2024; Hage et al., 2024).

To address these limitations, advanced numerical methods, such as cohesive zone models and phase-field methods, have been increasingly employed to simulate progressive damage, interfacial debonding, and microcrack evolution in concrete composite materials (Hu et al., 2021; Li et al., 2020). These techniques provide a more detailed description of failure mechanisms and offer higher predictive fidelity for durability and damage tolerance assessments. Similarly, FEA enables the simulation of stress distributions and failure modes in geometrically complex structures but depends heavily on high-fidelity input data, including experimentally validated material models and interfacial parameters that are often difficult to characterize, especially for bio-based and hybrid systems (Slamani & Châtelain, 2023; Przybyszewski et al., 2024). Despite these advancements, existing models still fail to provide generalizable, practically applicable tools for

predicting the performance of hybrid composites across varying processing conditions, fibre morphologies, and reinforcement architectures.

One of the critical gaps in the literature is the lack of physically meaningful yet computationally efficient models that bridge the gap between empirical observations and theoretical predictions for hybrid systems. Specifically, the interaction between natural and synthetic fibres, including variable dispersion states, orientation distributions, and interfacial stress transfer phenomena, remains poorly characterized in most existing models. This gap is further complicated by the lack of standardized experimental protocols and the inherent variability of natural fibres, which make the calibration and validation of advanced numerical models both resource-intensive and application-specific (Fantuzzi et al., 2020). Moreover, although fully numerical methods such as FEA and phase-field modelling can offer detailed insights, they are not easily generalizable and lack a closed-form relationship that can be practically used for material selection, design optimization, or preliminary performance screening in industrial contexts.

Recognizing these limitations, recent efforts have emphasized the need for semi-empirical and analytically modified models that retain physical interpretability while incorporating correction factors or boundary condition refinements based on experimental observations. Such models aim to strike a balance between accuracy and usability, particularly for hybrid systems where the assumptions of perfect bonding, uniform stress development, or homogeneous dispersion are unrealistic (El-baky et al., 2020). The shear-lag theory, despite its simplicity and widespread adoption, traditionally suffers from these oversimplifications. However, by introducing semi-empirical correction factors along with the effective matrix concepts, grounded in both theoretical analysis and experimental validation, there exists the potential to significantly improve the predictive reliability of shear-lag-based models for hybrid fibre composites. This direction addresses the identified limitations in current modelling approaches. It offers a practical pathway to enhance material design, selection, and optimization for advanced hybrid systems that combine natural and synthetic reinforcements.

The integration of carbon fibre and cellulose microfibre within a thermoplastic matrix has garnered considerable attention (Gaurav et al., 2020). This combination aims to leverage the high strength and stiffness of carbon fibre, combined with the renewability and biodegradability of cellulose,

while the thermoplastic matrix provides processability and recyclability (Arbelaiz et al., 2020). Carbon fibre-reinforced thermoplastic polymers present advantages such as recyclability, ease of processability, flexibility, and shorter production time compared to thermosetting and elastomer polymers, leading to their increased use in hybrid composites (Alshammari et al., 2021). However, the hybridization of these materials is not without its challenges, as achieving optimal dispersion, interfacial adhesion, and compatibility between the dissimilar components is critical to realizing the full potential of the composite (Kumar, 2020). The interface strength between the reinforcement and the matrix is crucial and significantly affects both the physical and mechanical properties of the composites (Aliotta et al., 2020).

Polyamides (PAs) are one of the most widely used engineering polymers in the automotive industry, mainly due to their desirable properties, i.e., excellent thermal stability, high chemical resistance, low flammability, and favourable mechanical performances (Botelho et al., 2003; Nie & Li, 2010; Grozdanov & Bogoeva-Gaceva, 2010; Kuciel et al., 2012; Feldmann & Bledzki, 2014). Characterized mainly through crystalline structure, polyamides are long-chain polymers containing multiple amide groups (–CO–NH–), and their grades are defined by available carbon atoms between the amide bonds (Shen et al., 2010; Kuciel et al., 2012; Brehmer, 2014; Raushan et al., 2024). Polyamides can be entirely or partially derived from renewable resources (Shen et al., 2010; Kuciel et al., 2012; Brehmer, 2014). Bio-sourcing distinguishes between products from petroleum or renewable sources and is limited to available functional groups associated with biomaterials (Brehmer, 2014). Although most organic polymers contain varying proportions of H, C, and O, polyamides and biopolyamides are essentially composed of nitrogen functional groups in the form of their amine bonds (Brehmer, 2014; Gigante et al., 2024).

Due to longer-chain polymers, bio-based polyamides (PA610, PA1010, PA1012, and PA11) perform better in terms of moisture and chemical resistance than conventional shorter-chain polyamides, PA6 and PA66. On the other hand, compared to longer-chain PA12, bio-sourced polyamides exhibit superior thermal resistance and strength properties. Essentially, positioned between short- and long-chain polyamides, bio-based polyamides can exhibit either greater or lower performance, depending on the preferred application, compared to their petroleum-based counterparts (Brehmer, 2014). Polyamide 11 (PA11) has the added advantage of high mechanical and thermal properties along with good processability (Kohan et al., 2007; Shen et al., 2010;

Endres & Siebert-Raths, 2011; Kuciel et al., 2012; Brehmer, 2014; Gigante et al., 2024). In addition, the functional end-groups and amide linkages in the polyamide structure enable hydrogen bonding, thereby facilitating good interfacial bonding with natural fibres (Kuciel et al., 2012; Feldmann & Bledzki, 2014). Having a relatively low amide to methylene ratio (1:10), PA11 performance is quite similar to polyethylene thermoplastic, having outstanding dimensional stability, great impact strength, energy absorption at low temperatures, and good resistance to stress and crack (Kohan et al., 2003; Shen et al., 2010; Gigante et al., 2024).

Polyamide composites reinforced by inorganic filler or fibre are widely used for structural parts in the automotive industry, as these composites have superior mechanical strength and stiffness properties as well as high thermal stability (Holbery & Houston, 2006; Oksman & Sain, 2008; Vaidya, 2011; Faruk et al., 2012; Faruk et al., 2014; Mundhe & Kandasubramanian, 2024; Gigante et al., 2024).

Wood pulp or cellulose microfibres typically exist as fibre bundles, which undergo defibrillation during the compounding process. This results in microfibrils that either remain on the fibre surface or disperse within the polymer matrix (Sain et al., 2015). The formation of microfibrils significantly increases the surface area available for interaction with the matrix, enhancing the mechanical bonding. However, incorporating cellulosic microfibres into certain polymer matrices poses challenges, as the processing temperatures of some polymers can exceed the thermal degradation limits of the cellulosic fibres, leading to the potential loss of fibre integrity and performance during fabrication (Feldmann & Bledzki, 2014; Semba et al., 2014; Corrêa et al., 2014; Kiziltas et al., 2014; Feldmann et al., 2015; Liu et al., 2015; Peng et al., 2015; Aydemir et al., 2015; Chagas et al., 2022; Falkenreck, et al., 2025).

Biopolyamides have relatively lower melting temperatures compared to and are another suitable alternative to develop cellulosic fibre-reinforced composites with superior mechanical characteristics (Botelho et al., 2003; Kuciel et al., 2012; Feldmann & Bledzki, 2014; Thakur et al., 2014; Bahrami et al., 2024; Gigante et al., 2024). Polymer blending is a common approach for improving the performance and properties of polymers used in various applications. It provides flexibility in combining two or more distinct individual polymers to create admixtures with varying properties. In general, blends of polyamides with polyolefins can potentially deliver a wide range

of desirable characteristics, including proper chemical resistance, low water absorption, and reduced cost. Consequently, it is well-suited for an extensive range of industrial applications.

Carbon fibre is often selected as reinforcement for polymer matrices in structurally demanding applications due to its low weight and excellent mechanical properties (Donnet, 1998; Botelho et al., 2003; Morgan, 2005; Nie & Li, 2010; Karsli & Aytac, 2013; El-baky et al., 2020; Raushan et al., 2024). The properties of carbon fibre, including high stiffness, excellent tensile strength, good chemical resistance, high-temperature tolerance, and low thermal expansion, make it suitable for the aerospace and automotive industries (Nie & Li, 2010; Makwana & Shaikh, 2020; Sugimoto et al., 2020). Carbon fibre has the most weight reduction potential among its counterparts.

Carbon fibre-reinforced polyamides are indisputably promising composite materials that have the potential to revolutionize various industries due to their unique properties and lightweight design options (Raushan et al., 2024). The versatility of carbon fibre-reinforced polymers extends to a wide range of applications in various industries. Specifically, these composites can produce mechanically robust structural components in the automotive sector, contributing to weight reduction and enhanced fuel efficiency (Makwana & Shaikh, 2020). While carbon fibre-reinforced polyamides offer numerous advantages in terms of mechanical properties, thermal stability, and weight reduction, several challenges are still associated with their manufacturing (Raushan et al., 2024). One major challenge is the cost of production. Carbon fibre-reinforced polyamides can be more expensive to manufacture than other materials due to the high cost of carbon fibres and the complexity of the manufacturing process.

Hybridizing carbon fibre with cellulose microfibre could be a cost-effective alternative for developing lightweight structural biocomposites. The behaviour of hybrid composites is a balance of the advantages and disadvantages of each component, in which the advantages of one type of fibre could compensate for the lack of the other. However, some challenges need to be addressed:

- The high moisture sensitivity of natural fibres and PA11 presents substantial challenges during composite fabrication, as moisture uptake can deteriorate mechanical performance, induce dimensional instability, and compromise the thermal and rheological properties during processing. Controlling moisture absorption is, therefore, critical for maintaining the integrity and consistency of the final composite material.

- The anisotropic characteristics of fibres in a hybrid system, where fibres with varying structural and mechanical properties are utilized, introduce significant complexities in achieving homogeneous stress distribution. Furthermore, ensuring efficient interfacial bonding between the two fibres (each with distinct surface chemistries and different compatibility with the polymer matrix) presents an additional challenge. Optimizing fibre-matrix and fibre-fibre interactions is crucial to improving load transfer efficiency and enhancing the overall mechanical performance of the composite, particularly in structurally demanding applications.

Efforts to overcome these challenges include enhancing interfacial adhesion by applying maleic anhydride grafted polypropylene (MAPP) and blending the biopolyamide with other polymers, such as polypropylene, to reduce moisture absorption.

1.3 Hypothesis and Objectives

The hypothesis of this study is that the hybridization of carbon fibre with cellulose microfibrils in a PA11 matrix leads to the formation of a pseudo-unified system, as opposed to established two-phase hybrid composites. In this pseudo-unified system, the flexible cellulose microfibrils become interwoven and entangled with the rigid carbon fibres, forming a unified network that exhibits synergistic mechanical behaviour.

It is proposed that the entanglement of the two phases within the polymer matrix could significantly enhance load transfer and energy dissipation, particularly under conditions of mechanical failure. In this system, the cellulose microfibrils initially absorb the applied stress due to their flexibility and act as the primary load-bearing component. Once the microfibrils reach their load-bearing threshold, the residual stress is transferred to the more rigid carbon fibres, distributing the mechanical load throughout the composite. This stress transfer mechanism enables the system to function as a cohesive unit, where the entire structure is anchored to short carbon fibres, creating a robust and interconnected network. The combined action of the flexible microfibrils and stiff carbon fibres is expected to significantly improve the elastic modulus and tensile strength of the composite. Additionally, the mechanical synergy between these two constituents is anticipated to enhance the composite's toughness and failure tolerance, offering superior post-failure

performance compared to other dual-phase composites where the phases remain separate and lack the integrative interaction observed in the proposed system.

The primary objective of this study was to obtain a deeper understanding of the stress-related failure mechanism and its correlation to fibre characteristics in bio-based hybrid fibre-reinforced composites engineered for applications requiring enhanced thermo-mechanical functionalities.

The specific objectives are as follows:

1. To examine the effect of dual fibres' structural anisotropy and chemical compositions on the stress transfer mechanisms within hybrid composites of cellulose microfibres and carbon fibre-reinforced PA11
2. To study the heterogeneity and thermodynamic compatibility of carbon fibres and cellulose microfibrils as a dual-fibre system embedded within the PA11/ PA11-PP matrix
3. To develop mathematically correlated and analytically derived equations to closely predict thermomechanical behaviours of hybrid composites as a function of dual-fibre system and matrix properties.

1.4 Thesis Outline

This thesis presents a comprehensive investigation into the development, characterization, and modelling of bio-based hybrid composites composed of PA11 reinforced with cellulose microfibres and carbon fibres. The primary goal is to optimize the mechanical performance of sustainable composite materials for automotive applications, using both experimental and theoretical approaches.

Part I – Experimental Analysis of Hybrid Composite Systems

The experimental phase was conducted in three key stages, each contributing to a deeper understanding of the effects of fibre selection, processing parameters, and matrix design:

- ***Stage 1: Single-Fibre Reinforcement (Cellulose Microfibre in PA11)***

In this initial stage, PA11 was reinforced only with cellulose microfibre with different compositions (WF10, WF20, and WF30) to establish a baseline for mechanical performance. Tensile, flexural, and impact tests demonstrated the sustainable reinforcement potential of cellulose microfibre-reinforced PA11, while also highlighting limitations in strength and stiffness that demand further enhancements.

- ***Stage 2: Hybrid Reinforcement with Carbon Fibre Addition***

A hybrid approach was employed by incorporating cellulose microfibre and short carbon fibres with different compositions (WF10CF20 and WF20CF10). Consequently, an alternative processing method was introduced by relocating the carbon fibre feeding point from the feeding hopper to the degassing zone of the extruder with different compositions (WF10CF2, WF10CF5, and WF10CF10). The alternative method resulted in preserving carbon fibre lengths during processing and improved dispersion. This method resulted in longer post-process carbon fibre, and consequently, enhanced the mechanical performance of the hybrid composites.

- ***Stage 3: Matrix Modification through PA11–PP Blending***

To further enhance ductility and toughness, PA11 was blended with polypropylene (PP). The hybrid fibre system was then embedded within this modified matrix. Comparative mechanical analysis revealed that PA11/PP matrices exhibited superior impact resistance and processing flexibility compared to PA11-only matrices, making them more suitable for high-stress automotive environments.

Part II – Theoretical and Empirical Analysis of Predictive Modelling

This section examines the empirical evaluation of both classical and modified theoretical models for predicting the mechanical behaviour of the developed hybrid composites. The aim is to determine the accuracy of these models in representing experimental results, identify their limitations, and develop improved formulations tailored for hybrid systems.

- ***Baseline Theoretical Frameworks***

Classical micromechanical models, including the Rule of Mixtures, Halpin-Tsai equations, and the classical shear lag model, were initially employed to predict tensile modulus and strength of the composites. While these models provided a general understanding of reinforcement trends, significant deviations from experimental data highlighted their limitations in capturing the complex interactions in short-fibre hybrid systems.

- ***Empirical Analysis and Model Comparison***

  The study undertook a detailed empirical analysis, comparing model predictions to experimentally measured mechanical properties for various composite configurations. These comparisons revealed that the classical models often underestimated or overestimated mechanical responses, especially in the presence of dual-fibre reinforcements with differing geometries, moduli, and interfacial behaviours.

- ***Effective Matrix Approach and Semi-empirical Analysis***

  To address these discrepancies, a semi-empirical model was introduced using the effective matrix concept, in which PA11 reinforced with 10 wt% cellulose microfibre (WF10) was treated as a homogenized matrix phase. Carbon fibre was then added as the secondary reinforcement to form hybrid systems (WF10CF2, WF10CF5, WF10CF10). This model demonstrated improved alignment with experimental results, particularly in modulus prediction, although it still exhibited notable limitations under certain conditions.

Part III – Development of an Analytically Modified Shear Lag Model

Recognizing the limitations of classical shear lag theory in modelling short-fibre hybrid systems, a new analytical framework was developed:

- ***Boundary Condition Reformation and Hybrid-Specific Factors***

  This modified shear lag model incorporates revised boundary conditions that reflect interfacial interactions and non-uniform stress transfer between the fibre and matrix. The hybrid nature of the reinforcement was also accounted for by considering differences in modulus, volume fractions, and interaction zones between cellulose and carbon fibres.

- ***Critical Fibre Length and Load Transfer Efficiency***

The study also investigated the role of fibre length in stress transfer by comparing the actual fibre lengths to the theoretical critical fibre length (~700 μm for carbon fibres). Since the carbon fibres used in the hybrid composites were shorter than this threshold, the load transfer was less efficient, which influenced both the experimental outcomes and the accuracy of model predictions. This aspect further validated the need for model modifications to account for partial load transfer and fibre inefficiency.

- ***Model Validation and Applicability***

  Comparisons between the modified model, classical models, and experimental data demonstrated that the revised shear lag model significantly improved predictive accuracy, particularly for hybrid systems with short carbon fibres and a cellulose microfibrillated effective matrix.

This study provides a validated experimental-theoretical framework for bio-based hybrid composites, demonstrating their mechanical competence, environmental resilience, and processing feasibility. The analytical refinement of the shear-lag model further contributes to the theoretical understanding of hybrid composites, enabling more accurate design and optimization for structural applications in the automotive sector. The integration of sustainable materials and advanced modelling techniques positions this work as a step toward greener, structurally demanding engineering solutions.

1.4 References

Aliotta, L., & Lazzeri, A. (2020). A proposal to modify the Kelly–Tyson equation to calculate the interfacial shear strength (IFSS) of composites with low aspect ratio fibres. *Composites Science and Technology, 186*, 107920. https://doi.org/10.1016/j.compscitech.2019.107920

Arbelaiz, A., Txueka, U., Mezo, I., & Orue, A. (2020). Biocomposites based on poly(lactic acid) matrix and reinforced with lignocellulosic fibres: The effect of fibre type and matrix modification. *Journal of Natural Fibres, 19*(1), 1–15. https://doi.org/10.1080/15440478.2019.1615499

Aydemir, D., Kiziltas, A., Kiziltas, E. E., Gardner, D. J., & Gunduz, G. (2015). Heat treated wood–nylon 6 composites. *Composites Part B: Engineering, 68*, 414–423. https://doi.org/10.1016/j.compositesb.2014.09.045

Bahrami, M., Butenegro, J. A., Mehdikhani, M., Swolfs, Y., Abenojar, J., & Martinez, M. A. (2024). Tensile, impact, and the damping performance of woven flax-carbon hybrid polyamide biocomposites. *Polymer Composites, 45*(5), 3901–3917. https://doi.org/10.1002/pc.27810

Battegazzore, D., Salvetti, O., Frache, A., Peduto, N., De Sio, A., & Marino, F. (2016). Thermo-mechanical properties enhancement of bio-polyamides (PA10.10 and PA6.10) by using rice husk ash and nanoclay. *Composites Part A: Applied Science and Manufacturing, 81*, 193–201. https://doi.org/10.1016/j.compositesa.2015.11.009

Bernstein, R., Derzon, D. K., & Gillen, K. T. (2005). Nylon 6.6 accelerated aging studies: Thermal-oxidative degradation and its interaction with hydrolysis. *Polymer Degradation and Stability, 88*, 480–488. https://doi.org/10.1016/j.polymdegradstab.2004.11.007

Bledzki, A. K., Faruk, O., & Sperber, V. E. (2006). Cars from bio-fibres. *Macromolecular Materials and Engineering, 291*(5), 449–457. https://doi.org/10.1002/mame.200500378

Botelho, E. C., Figiel, Ł., Rezende, M. C., & Lauke, B. (2003). Mechanical behaviour of carbon fibre reinforced polyamide composites. *Composites Science and Technology, 63*(13), 1843–1855. https://doi.org/10.1016/S0266-3538(03)00186-1

Brehmer, B. (2014). Polyamides from biomass derived monomers. In S. Kabasci (Ed.), *Bio-based plastics: Materials and applications* (pp. 275–293). John Wiley & Sons Ltd.

Chagas, G. N., Barros, M. M., Leão, A. G. d., Tapanes, N. d. L. C. O., Ribeiro, R. C. d. C., & Bastos, D. C. (2022). A hybrid green composite for automotive industry. *Polímeros: Ciência e Tecnologia, 32*(2), e2022013. https://doi.org/10.1590/0104-1428.20220004

Corrêa, A. C., Teixeira, E. M., Carmona, V. B., Teodoro, K. B. R., Ribeiro, C. A., Mattoso, L. H. C., & Marconcini, J. M. (2014). Obtaining nanocomposites of polyamide 6 and cellulose whiskers via extrusion and injection moulding. *Cellulose, 21*(1), 311–322. https://doi.org/10.1007/s10570-013-0124-5

De Almeida, S. F. M., & Neto, Z. d. S. N. (1994). Effect of void content on the strength of composite laminates. *Composite Structures, 28*, 139–145. https://doi.org/10.1016/0263-8223(94)90048-5

De Arcaya, P. A., Retegi, A., Arbelaiz, A., Kenny, J. M., & Mondragon, I. (2009). Mechanical properties of natural fibres/polyamides composites. *Polymer Composites, 30*(3), 257–264. https://doi.org/10.1002/pc.20612

Dhakal, H. N., Zhang, Z. Y., & Richardson, M. O. W. (2007). Effect of water absorption on the mechanical properties of hemp fibre reinforced unsaturated polyester composites. *Composites Science and Technology, 67*(7–8), 1674–1683. https://doi.org/10.1016/j.compscitech.2006.06.019

Du, Y., Yan, N., & Kortschot, M. T. (2012). Investigation of unsaturated polyester composites reinforced by aspen high-yield pulp fibres. *Polymer Composites, 33*(2), 169–177. https://doi.org/10.1002/pc.22134

Du, Y., Wu, T., Yan, N., Kortschot, M. T., & Farnood, R. (2013). Pulp fibre-reinforced thermoset polymer composites: Effects of the pulp fibres and polymer. *Composites Part B: Engineering, 48*, 10–17. https://doi.org/10.1016/j.compositesb.2012.12.011

Du, Y., Yan, N., & Kortschot, M. T. (2014). The use of ramie fibres as reinforcements in composites. In A. K. Mohanty, M. Misra, & L. T. Drzal (Eds.), *Biofibre reinforcements in composite materials* (pp. 104–137). Woodhead Publishing.

El-baky, M. A., Attia, M., Abdelhaleem, M., & Hassan, M. (2020). Mechanical characterization of hybrid composites based on flax, basalt and glass fibres. *Journal of Composite Materials, 54*(27), 4185–4198. https://doi.org/10.1177/0021998319901250

Endres, H. J., & Siebert-Raths, A. (2011). *Engineering biopolymers: Markets, manufacturing, properties and applications* (pp. 95–98). Carl Hanser Verlag.

Fantuzzi, N., Bacciocchi, M., Benedetti, D., & Agnelli, J. (2020). The use of sustainable composites for the manufacturing of electric cars. *Composites Part C: Open Access, 4*, 100096. https://doi.org/10.1016/j.jcomc.2020.100096

Faruk, O., Bledzki, A. K., Fink, H. P., & Sain, M. (2012). Biocomposites reinforced with natural fibres: 2000–2010. *Progress in Polymer Science, 37*(11), 1552–1596. https://doi.org/10.1016/j.progpolymsci.2012.04.003

Faruk, O., Bledzki, A. K., Fink, H. P., & Sain, M. (2014). Progress report on natural fibre reinforced composites. *Macromolecular Materials and Engineering, 299*(1), 9–26. https://doi.org/10.1002/mame.201300008

Feldmann, M., & Bledzki, A. K. (2014). Bio-based polyamides reinforced with cellulosic fibres – Processing and properties. *Composites Science and Technology, 100*, 113–120. https://doi.org/10.1016/j.compscitech.2014.06.021

Feldmann, M., Heim, H., & Zarges, J. (2015). Influence of the process parameters on the mechanical properties of engineering biocomposites using a twin-screw extruder. *Composites Part A: Applied Science and Manufacturing, 76*, 27–36. https://doi.org/10.1016/j.compositesa.2015.05.001

Gao, P., Xie, W., Ling, Y., Xu, H., & Xi, X. (2025). Optimal fibre mix and prediction model for compressive strength of hybrid fibre reinforced concrete. *PLOS ONE, 20*(2), e0318713. https://doi.org/10.1371/journal.pone.0318713

Gaurav, G., Gohal, H., Kumar, V. M., & Jena, H. (2020). Study of natural fibre composite material and its hybridization techniques. *Materials Today: Proceedings, 26*, 1368–1372. https://doi.org/10.1016/j.matpr.2020.02.286

Gigante, V., Cartoni, F., Dal Pont, B., & Aliotta, L. (2024). Extrusion parameters optimization and mechanical properties of bio-polyamide 11-based biocomposites reinforced with short basalt fibres. *Polymers, 16*(21), 3092. https://doi.org/10.3390/polym16213092

Gonçalves, E. S., Poulsen, L., & Ogilby, P. R. (2007). Mechanism of the temperature-dependent degradation of polyamide 66 films exposed to water. *Polymer Degradation and Stability, 92*(10), 1977–1985. https://doi.org/10.1016/j.polymdegradstab.2007.08.003

Grozdanov, A., & Bogoeva-Gaceva, G. (2010). Carbon fibres/polyamide 6 composites based on hybrid yarns. *Journal of Thermoplastic Composite Materials, 23*(1), 99–110. https://doi.org/10.1177/0892705709335877

Hablot, E., Matadi, R., Ahzi, S., & Avérous, L. (2010). Renewable biocomposites of dimer fatty acid-based polyamides with cellulose fibres: Thermal, physical and mechanical properties. *Composites Science and Technology, 70*(3), 504–509. https://doi.org/10.1016/j.compscitech.2009.11.006

Hage, I. S. (2024). A hybrid model for accurate prediction of composite longitudinal elastic modulus. *Computers & Mathematics with Applications, 174*, 287–297. https://doi.org/10.1016/j.camwa.2023.11.030

Hajiha, H., & Sain, M. (2015). High toughness hybrid biocomposite process optimization. *Composites Science and Technology, 111*, 44–49. https://doi.org/10.1016/j.compscitech.2015.03.004

Holbery, J., & Houston, D. (2006). Natural-fibre-reinforced polymer composites in automotive applications. *JOM, 58*(11), 80–86. https://doi.org/10.1007/s11837-006-0234-2

Hu, Z., Suo, X., Jiang, F., & Shen, Y. (2021). A minimalistic approach to simulate multiple failure mechanisms of metal matrix fibre-reinforced composites by the phase field and cohesive zone models. *arXiv*. https://doi.org/10.48550/arXiv.2107.14509

Huang, X., Su, S., Xu, Z., Miao, Q., Li, W., & Wang, L. (2023). Advanced composite materials for structure strengthening and resilience improvement. *Buildings, 13*(10), 2406. https://doi.org/10.3390/buildings13102406

KC, B., Panthapulakkal, S., Kronka, A., Agnelli, J. A. M., Tjong, J., & Sain, M. (2015). Biorenewable composites from cellulose fibres and polyamide. *Journal of Applied Polymer Science, 132*(48). https://doi.org/10.1002/app.42896

Khanna, Y. P., Reimschuessel, A. C., Banerjie, A., & Altman, C. (1988). Memory effects in polymers. II. Processing history vs. crystallization rate of nylon 6—Observation of phenomenon and product behaviour. *Polymer Engineering & Science, 28*(24), 1600–1606. https://doi.org/10.1002/pen.760282407

Khanna, Y. P., Han, P. K., & Day, E. D. (1996). Memory effects in polymers. II. Processing history vs. crystallization rate of nylon 6—Observation of phenomenon and product behaviour. *Polymer Engineering & Science, 36*(14), 1745–1751. https://doi.org/10.1002/pen.10653

Kiziltas, A., Nazari, B., Gardner, D. J., & Bousfield, D. W. (2014). Polyamide 6–cellulose composites: Effect of cellulose composition on melt rheology and crystallization behaviour. *Polymer Engineering & Science, 54*(4), 739–746. https://doi.org/10.1002/pen.23650

Kohan, M. I., Mestemacher, S. A., Pagilagan, R. U., & Redmond, K. (2003). Polyamides. In *Ullmann's Encyclopedia of Industrial Chemistry* (7th ed.). Wiley-VCH. https://doi.org/10.1002/14356007.a21_717

Kuciel, S., Kuzniar, P., & Liber-Knec, A. (2012). Polyamides from renewable sources as matrices of short fibre reinforced biocomposites [Poliamidy ze źródeł odnawialnych jako osnowy biokompozytów wzmacnianych krótkimi włóknami]. *Polimery, 57*(9), 627–634.

Kumar, K. V., Moshi, A. A. M., & Rajadurai, J. S. (2020). Mechanical property analysis on bamboo-glass fibre reinforced hybrid composite structures under different lamina orders. *Materials Today: Proceedings, 45*, 1620–1624. https://doi.org/10.1016/j.matpr.2020.11.091

Kurowiak, J., Klekiel, T., & Będziński, R. (2023). Biodegradable polymers in biomedical applications: A review—Developments, perspectives and future challenges. *International Journal of Molecular Sciences, 24*(23), 16952. https://doi.org/10.3390/ijms242316952

Liu, K., Madbouly, S. A., Schrader, J. A., Kessler, M. R., Grewell, D., & Graves, W. R. (2015). Biorenewable polymer composites from tall oil-based polyamide and lignin-cellulose fibre. *Journal of Applied Polymer Science, 132*(48). https://doi.org/10.1002/app.42883

Magniez, K., Iftikhar, R., & Fox, B. L. (2015). Properties of bio-based polymer nylon 11 reinforced with short carbon fibre composites. *Polymer Composites, 36*(4), 668–674. https://doi.org/10.1002/pc.23042

Mahmud, M. A., Abir, N., Anannya, F. R., Khan, A. N., Rahman, A. N. M. M., & Jamine, N. (2023). Coir fibre as thermal insulator and its performance as reinforcing material in biocomposite production. *Heliyon, 9*(5), e16140. https://doi.org/10.1016/j.heliyon.2023.e16140

Makwana, A. H., & Shaikh, A. A. (2020). Performance assessment and optimization of hybrid composite patch repair of aircraft structure. *Multidiscipline Modelling in Materials and Structures, 16*(5), 887–913. https://doi.org/10.1108/MMMS-01-2020-0011

Martinelli, F. R. B., Ribeiro, F. R. C., Marvila, M. T., Monteiro, S. N., Filho, F. C. G., & Azevedo, A. R. G. (2023). A review of the use of coconut fibre in cement composites. *Polymers, 15*(5), 1309. https://doi.org/10.3390/polym15051309

Mohanty, A. K., Misra, M., & Drzal, L. T. (2002). Sustainable bio-composites from renewable resources: Opportunities and challenges in the green materials world. *Journal of Polymers and the Environment, 10*(1–2), 19–26. https://doi.org/10.1023/A:1021013921916

Müzel, S. D., Bonhin, E. P., Guimarães, N. M., & Guidi, E. S. (2020). Application of the finite element method in the analysis of composite materials: A review. *Polymers, 12*(4), 818. https://doi.org/10.3390/polym12040818

Mundhe, A., & Kandasubramanian, B. (2024). Advancements in natural fibre composites: Innovative chemical surface treatments, characterization techniques, environmental sustainability, and wide-ranging applications. *Hybrid Advances, 7*, 100282. https://doi.org/10.1016/j.hyadv.2024.100282

Mutlu, H., & Meier, M. A. R. (2010). Castor oil as a renewable resource for the chemical industry. *European Journal of Lipid Science and Technology, 112*(1), 10–30. https://doi.org/10.1002/ejlt.200900095

Nie, W. Z., & Li, J. (2010). Effect of carbon fibre content on friction and wear properties of carbon fibre reinforced PA6 composites. *Plastics, Rubber and Composites, 39*(1), 10–15. https://doi.org/10.1179/174328910X12603660527011

Saheb, D. N., & Jog, J. P. (1999). Natural fibre polymer composites: A review. *Advances in Polymer Technology, 18*(4), 351–363. https://doi.org/10.1002/(SICI)1098-2329(199924)18:4<351::AID-ADV6>3.0.CO;2-W

Sugimoto, Y., Shimamoto, D., Imai, Y., & Hotta, Y. (2020). Simultaneous evaluation of tensile strength and interfacial shear strength of short length carbon fibres using fragmentation test. *Carbon, 161*, 83–91. https://doi.org/10.1016/j.carbon.2020.01.041

Ogunniyi, D. S. (2006). Castor oil: A vital industrial raw material. *Bioresource Technology, 97*(9), 1086–1091. https://doi.org/10.1016/j.biortech.2005.03.028

Oksman Niska, K., & Sain, M. (Eds.). (2008). *Wood-polymer composites*. Woodhead Publishing.

Ota, W. N., Amico, S. C., & Satyanarayana, K. G. (2005). Studies on the combined effect of injection temperature and fibre content on the properties of polypropylene-glass fibre composites. *Composites Science and Technology, 65*(5), 873–881. https://doi.org/10.1016/j.compscitech.2004.10.002

Ozen, E., Kiziltas, A., Kiziltas, E. E., & Gardner, D. J. (2013). Natural fibre blend–nylon 6 composites. *Polymer Composites, 34*(4), 544–553. https://doi.org/10.1002/pc.22480

Panthapulakkal, S., Law, S., & Sain, M. (2005). Injection molded natural fibre hybrid composites for automobile applications – Mechanical properties and flammability. *International SAMPE Technical Conference, 37*, 2207–2216.

Panthapulakkal, S., & Sain, M. (2006). Injection molded wheat straw and corn stem filled polypropylene composites. *Journal of Polymers and the Environment, 14*(3), 265–272. https://doi.org/10.1007/s10924-006-0013-4

Panthapulakkal, S., & Sain, M. (2007a). Injection-molded short hemp fibre/glass fibre-reinforced polypropylene hybrid composites – Mechanical, water absorption and thermal properties. *Journal of Applied Polymer Science, 103*(4), 2432–2441. https://doi.org/10.1002/app.25484

Panthapulakkal, S., & Sain, M. (2007b). Studies on the water absorption properties of short hemp-glass fibre hybrid polypropylene composites. *Journal of Composite Materials, 41*(15), 1871–1883. https://doi.org/10.1177/0021998306069880

Peng, Y., Gardner, D. J., & Han, Y. (2015). Characterization of mechanical and morphological properties of cellulose reinforced polyamide 6 composites. *Cellulose, 22*(5), 3199–3215. https://doi.org/10.1007/s10570-015-0715-2

Przybyszewski, B., Kozera, R., Ziętkowska, K., Łabęda, A., Karl, C. W., Pilz, M., & Boczkowska, A. (2024). Effect of UV laser texturization on hydrophobic and anti-icing properties of waterborne polyurethane nanocomposite coatings. *Composites Theory and Practice, 24*(4), 213–220.

Rajput, L., & Jana, P. (2025). Coupled nano-interfacial and agglomeration effects on elastic behaviour of hybrid composites using multi-scale modelling. *International Journal of Mechanical Sciences, 296*, 110273. https://doi.org/10.1016/j.ijmecsci.2023.110273

Raushan, R., Dhande, K. K., & Jamadar, N. I. (2024). Modal analysis of carbon fibre reinforced polyamide66 drive shaft using analytical and finite element approach. *International Journal on Interactive Design and Manufacturing, 19*(4), 2801–2816. https://doi.org/10.1007/s12008-023-01446-9

Rosenau, B. (2007). Polyamides (PA). *Kunststoffe International, 10*, 48–51.

Sain, M., Panthapulakkal, S., & Law, S. (2015). *Natural fibre composite reinforced polymer and method of manufacture*. U.S. Patent No. 8,940,132. https://patents.google.com/patent/US8940132B2/en

Sathish, T., Boobalan, V., Giri, J., Hourani, A. O., Santhosh, A. J., & Nasri, F. (2025). Optimization and enhancement of tensile strength and elongation at failure in basalt/glass fibre polymer composites with MWCNTs + SiO_2 hybrid nanofillers using response surface methodology. *Engineering Reports, 7*(2), e12852. https://doi.org/10.1002/eng2.12852

Scott, E., Peter, F., & Sanders, J. (2007). Biomass in the manufacture of industrial products—the use of proteins and amino acids. *Applied Microbiology and Biotechnology, 75*(4), 751–762. https://doi.org/10.1007/s00253-007-0946-2

Seculi, F., Espinach, F. X., Julián, F., Delgado-Aguilar, M., Mutjé, P., & Tarrés, Q. (2023a). Comparative evaluation of the stiffness of abaca-fibre-reinforced bio-polyethylene and high-density polyethylene composites. *Polymers, 15*(5), 1096. https://doi.org/10.3390/polym15051096

Seculi, F., Espinach, F. X., Julián, F., Delgado-Aguilar, M., Mutjé, P., & Tarrés, Q. (2023b). Evaluation of the interface strength in the abaca-fibre-reinforced bio-polyethylene composites. *Polymers, 15*(12), 2686. https://doi.org/10.3390/polym15122686

Seculi, F., Julián, F., Llorens, J., Espinach, F. X., Mutjé, P., & Tarrés, Q. (2023). Methodologies to evaluate the micromechanics flexural strength properties of natural-fibre-reinforced composites: The case of abaca-fibre-reinforced bio polyethylene composites. *Polymers, 15*(14), 3137. https://doi.org/10.3390/polym15143137

Semba, T., Ito, A., Kitagawa, K., Nakatani, T., Yano, H., & Sato, A. (2014). Thermoplastic composites of polyamide-12 reinforced by cellulose nanofibres with cationic surface modification. *Journal of Applied Polymer Science, 131*(20). https://doi.org/10.1002/app.40744

Shen, L., Worrell, E., & Patel, M. (2010). Present and future development in plastics from biomass. *Biofuels, Bioproducts and Biorefining, 4*(1), 25–40. https://doi.org/10.1002/bbb.189

Shoja, M., Kazemi, R., Mohammadi-Roshandeh, J., Farizeh, T., Shadman, A., & Hemmati, F. (2021). Hybrid mathematical modelling and multi-objective optimization of mechanical properties of green composites based on starch and modified rice straw fillers. *Journal of Applied Polymer Science, 138*(36), e50915. https://doi.org/10.1002/app.50915

Simamora, P., Simanjuntak, J. H. H., Sinulingga, K., & Laksono, A. D. (2023). Mechanical properties of polypropylene composites with different reinforced natural fibres – A comparative study. *Journal of Ecological Engineering, 24*(7), 311–318. https://doi.org/10.12911/22998993/161071

Singha, A. S., Sharma, A., & Thakur, V. K. (2008). Pressure-induced graft co-polymerization of acrylonitrile onto *Saccharum cilliare* fibre and evaluation of some properties of grafted fibres. *Bulletin of Materials Science, 31*(1), 7–13. https://doi.org/10.1007/s12034-008-0002-1

Singha, A. S., & Thakur, V. K. (2008). Fabrication and study of lignocellulosic *Hibiscus sabdariffa* fibre reinforced polymer composites. *BioResources, 3*(4), 1173–1186.

Singha, A. S., Sharma, A., & Thakur, V. K. (2009). Graft copolymerization of acrylonitrile onto *Saccharum cilliare* fibre. *e-Polymers, 9*(1), 1–12. https://doi.org/10.1515/epoly.2009.9.1.1

Singha, A. S., & Thakur, V. K. (2009a). Fabrication and characterization of *Saccharum cilliare* fibre reinforced polymer composites. *Bulletin of Materials Science, 32*(1), 49–58. https://doi.org/10.1007/s12034-009-0008-2

Singha, A. S., & Thakur, V. K. (2009b). Fabrication and characterization of *Hibiscus sabdariffa* fibre reinforced polymer composites. *Polymer-Plastics Technology and Engineering, 48*(4), 482–487. https://doi.org/10.1080/03602550802688897

Singha, A. S., & Thakur, V. K. (2010). Mechanical, morphological, and thermal characterization of compression-molded polymer biocomposites. *International Journal of Polymer Analysis and Characterization, 15*(2), 87–97. https://doi.org/10.1080/10236660903480644

Slamani, M., & Chatelain, J. F. (2023). A review on the machining of polymer composites reinforced with carbon (CFRP), glass (GFRP), and natural fibres (NFRP). *Discover Mechanical Engineering, 2*(4), 1–42. https://doi.org/10.1007/s44217-023-00034-y

Swolfs, Y., Gorbatikh, L., & Verpoest, I. (2019). Recent advances in fibre hybrid composites: Materials selection, design, and performance. *Composites Part B: Engineering, 183*, 107749. https://doi.org/10.1016/j.compositesb.2019.107749

Thakur, V. K., & Singha, A. S. (2010). Evaluation of *Grewia optiva* fibres as reinforcement in polymer biocomposites. *Polymer-Plastics Technology and Engineering, 49*(11), 1101–1107. https://doi.org/10.1080/03602550903361291

Thakur, V. K., Thakur, M. K., & Gupta, R. K. (2014a). Review: Raw natural fibre-based polymer composites. *International Journal of Polymer Analysis and Characterization, 19*(3), 256–271. https://doi.org/10.1080/1023666X.2014.880016

Thakur, V. K., Thakur, M. K., Raghavan, P., & Kessler, M. R. (2014b). Progress in green polymer composites from lignin for multifunctional applications: A review. *ACS Sustainable Chemistry & Engineering, 2*(5), 1072–1092. https://doi.org/10.1021/sc500087x

Vaidya, U. (2011). *Composites for automotive, truck and mass transit: Materials, design, manufacturing*. DEStech Publications.

Wang, M. S., & Huang, J. C. (1994). Nylon 1010 properties and applications. *Journal of Polymer Engineering, 13*(2), 155–174. https://doi.org/10.1515/polyeng.1994.13.2.155

Wang, X., Yang, T., Maeder, M., & Marburg, S. (2024). A novel fractional calculus modelling and physics-informed machine learning study on dynamic performance of hybrid flax/basalt fibre-reinforced composite. *Nonlinear Dynamics, 112*(22), 19917–19937. https://doi.org/10.1007/s11071-023-08820-7

Zhang, H., Zhang, L., Liu, Z., Qi, S., Zhu, Y., & Zhu, P. (2021). Numerical analysis of hybrid (bonded/bolted) FRP composite joints: A review. *Composite Structures, 262*, 113606. https://doi.org/10.1016/j.compstruct.2021.113606

Chapter 2 Literature Review

2.1 Global Automotive Industry Recycling Statistics

The automotive and transportation industries have long been major contributors to global waste generation and resource consumption. As such, there has been an increasing pressure to adopt sustainable practices and reduce environmental impact. The automotive industry is primarily challenged by the exponential increase in petroleum consumption, depletion of fuel resources, rising fuel prices, and increased CO_2 emissions. These concerns necessitate immediate changes in automotive design and manufacturing for a sustainable future (Oksman & Sain, 2008; Faruk et al., 2012; Faruk et al., 2014; Thakur et al., 2014a; Chagas et al., 2022).

The global annual production of automobiles and commercial vehicles is approximately 85-95 million units. The average car weighs around 1.2 tons, producing 102.5 million tons of refined raw material. The structure's composition includes the following components: scrap iron, plastics, tires, non-ferrous metals, glass, foam, vehicle batteries, electrical waste, textiles, and insulation materials (Novotný et al., 2020).

There is a growing trend in the automotive industry to replace metal components with plastic ones. Employing this substitution, vehicle weight is decreased, consequently resulting in reduced fuel consumption. Substituting metals with plastics and composites has been acknowledged as reducing the average vehicle weight by 200 kg. About 75% of a vehicle's fuel consumption is directly correlated to its body weight, and a 10% reduction in vehicle weight can save approximately 6-8% of fuel consumption (Vaidya, 2011; Faruk et al., 2014). The primary objective of the automotive industry is to reduce the weight and cost of vehicles while enhancing their safety and recyclability after use (Bledzki et al., 2006; Vaidya, 2011; Faruk et al., 2014).

The recovery of plastics offers considerable benefits owing to the extensive variety of accessible plastic materials. The vehicles contain a significant amount of polymer, particularly polyolefins (polypropylene (PP) and polyethylene (PE)), which exhibit properties influenced by their molecular weight and degree of crystallinity (Krilek et al., 2020). Waste plastics consisting of polyolefins are fully reclaimed in economically advanced countries. The previously mentioned polymers are used in the manufacturing of foils, board materials, electrical device coverings, injection-moulded parts, irrigation pipes, various crates, and other applications (Zhang & Chen,

2014). Polyvinyl chloride (PVC) and polyurethane (PU) are widely manufactured synthetic polymers with extensive applications in the automotive sector. The qualities of the materials depend on both their manufacturing and the processing technique. PVC waste is used to manufacture sewer pipes, extruded profiles, and boards. Mixed waste, consisting of PVC and polyolefin, is used in the production of pallets and industrial floor components. Additionally, PU waste is used as an additive in mixtures of thermoplastic polyurethanes to enhance dimensional stability and abrasion resistance (Zhang & Chen, 2014; Krilek et al., 2020; Ravina et al., 2023).

To address all previously discussed criteria, the industry has adopted recycling and reusing materials as critical strategies. In the United States, approximately 95% of end-of-life vehicles enter the recycling stream, resulting in the reclamation of around 12 million tons of steel and 800,000 tons of nonferrous metals annually (Fukumori K. et al., 2003). In Europe, the automotive sector accounts for the third-largest share of plastics demand, supplying approximately 9% of the market. In 2018, around 80% of the recycled plastic produced in Europe was reintegrated into the European economy through the manufacturing of new products. A proportion of 3% of this total amount was designated for the automotive industry (Ravina et al., 2023).

On a global scale, regulations have been implemented to reduce the amount of waste generated by vehicles. These regulations emphasized the use of recyclable components, discouraged the introduction of hazardous substances, enabled disassembly-friendly designs, and promoted reusability and recycling. After evaluating the potential for reuse, components must be assessed for energy recovery, followed by recycling (which entails extracting materials from the waste stream for use as basic materials in the production of new products) (Anthony et al., 2017; Ravina et al., 2023). Directive 2018/849 modified European Directive 2000/53/EC, known as the End-of-Life Vehicle (ELV) Directive, established a minimum threshold of 95% of the vehicle weight for the reuse and recovery of ELVs beginning in 2015. Achieving a minimum of 85% reuse and recycling of the vehicle's total weight was imperative within the designated timeframe (Anthony et al., 2017; Ravina et al., 2023). In 2018, the reuse and recycling of ELVs in the European Union progressed to 87.3%. Nonetheless, eleven EU Member States, whose reuse and recycling rates total 90.0%, have contributed to the achievement of this result. Conversely, many European nations still need to fulfill the stipulations delineated in the previously mentioned directive (Adelodun, 2021; Ravina et al., 2023).

At the end of their lifespan, automobiles can be recycled by typical mechanical recycling methods, with metals, tires, and glass comprising around 80-90% of the recyclable materials. The remaining 10-20%, known as automobile shredder residue (ASR), contains a combination of plastic and other non-recyclable elements (Lee et al., 2001; Ruffino et al., 2021; Ravina et al., 2023). These materials are currently disposed of in landfills or recovered using waste-to-energy technology (Ruffino et al., 2021). Typically, ELVs are subjected to the following three phases of processing: decontamination, disassembly, and shredding (which includes material sifting and crushing). Plastic materials may be extracted from ASRs after the comminution procedure or via pre-dismantling separation (Ruffino et al., 2021; Ravina et al., 2023).

Following the recovery of primary materials, the procedure for reusing and recycling materials can be made more streamlined and effective by separating the materials prior to the demolition operation. The recycling of plastics during ELV treatment is a complex procedure, and the existing techniques employed lack sufficient selectivity, resulting in substantial amounts of waste (Kongar & Gupta, 2006; Turner et al., 2015; Gu et al., 2017). The recycling process is hindered by many economic and technical barriers, which collectively contribute to its inefficiency (Vogt et al., 2021; Ravina et al., 2023).

Currently, only the most massive and easily detachable components are recovered. However, many of the remaining plastic components in the vehicle are difficult to detach due to their small size. An additional fundamental aspect to contemplate is the intricacy of every individual component. An increased number of subcomponents increases the probability of encountering a heterogeneous material, which consequently hinders the recycling procedure (Turner et al., 2015; Ravina et al., 2023). According to the 2018 European Automobile Manufacturers Association (ACEA) and European Association of Automotive Suppliers (CLEPA), recycled materials are only suitable for use if they retain the same qualities as the initial virgin material (Go et al., 2011; Vanderreydt et al., 2021; Ravina et al., 2023).

The production, utilization, and disposal of plastic automotive components have detrimental impacts on the environment and the economy. Specific repercussions, such as waste disposal, result in immediate financial expenses, whereas others incur indirect costs associated with environmental deterioration and human health. In the absence of their inclusion in the price of new plastic, these elements are generally considered externalities (European Environment Agency

(EEA), 2021; Afrinaldi & Mat Saman, 2008; Dalberg Advisors, 2021; Vanderreydt et al., 2021; Ravina et al., 2023).

2.2 Transition to Renewable Plastics

Green initiatives are currently a prevalent market trend in the automotive industry. These have inspired the automotive industry to replace petroleum-based materials with bio-based and renewable alternatives. The shift towards bio-based plastics presents an opportunity for the automotive industry to reduce its dependence on petroleum-based plastics, contributing to environmental sustainability. Bio-based plastics are gaining attention as a promising alternative due to their renewable feedstocks and potential for composting or recycling (Vaidya, 2011; Faruk et al., 2014). Utilizing renewable biomass as raw materials can help minimize price fluctuations caused by the finite supply of fossil oil in the short and medium term.

The most significant criteria for selecting bioplastics over petroleum-based plastics are their renewability and biodegradability. Biodegradability refers to a product's ability to break down completely, both chemically and biologically. The biodegradability of bioplastics plays a crucial role in minimizing the environmental effects of plastic products and advancing the overall sustainability of the plastic industry. Bioplastics are presently confined to interior trims and non-structural components in automotive applications. However, ongoing research is being conducted to enhance the properties of bioplastic materials to achieve universal application. The existing production infrastructure for petroleum-based plastics poses challenges for the widespread adoption of bioplastics as a commodity plastic.

While it is essential to consider the adverse impacts of bio-based plastics throughout their lifecycle, this shift can be a step towards reducing environmental and health impacts associated with conventional plastics. Nevertheless, there has been a lack of rapid advancement in alternative materials due to the automotive industry's excessive safety and performance requirements, which significantly limit the range of available materials (Spreafico, 2021). Limitations in materials' properties, including mechanical properties, thermal stability, flammability, and the effect of weathering and humidity, need to be addressed to make these composites suitable for structurally demanding applications (Holbery & Houston, 2006; Bledzki et al., 2006; Vaidya, 2011; Faruk et al., 2014).

2.3 Polyamides in Composites

There are three major types of polymers: thermoplastics, thermosets, and elastomers. Thermoplastics quickly soften when exposed to heat and solidify upon cooling. On the contrary, thermosets undergo a crosslinking reaction by applying heat above a specific temperature, resulting in a 3D network of polymer molecules through the formation of crosslinking bonds. This makes thermosets quite challenging to recycle, as the crosslinked 3D network does not alter with temperature changes, rendering the material irreversible. Some examples of thermoplastics include nylons, polycarbonates, polypropylenes, and polyethylenes, among others. Examples of thermosets include epoxies, phenolics, polyesters, bismaleimides, cyanate esters, and polyimides, among others. Elastomers or rubbers typically exhibit the capability to undergo significant deformations without altering their primary structure and can behave elastically under severe deformations; in this case, the material can recover almost entirely after the removal of the deformation forces (Rauwendaal, 2014; Faruk et al., 2017).

Among the existing engineering thermoplastics, polyamide (PA) is a promising candidate as a composite matrix, mainly due to its desirable properties, i.e., excellent thermal stability, high chemical resistance, low flammability, and favourable mechanical performances, as well as its low cost and easy handling (Botelho et al., 2003; Nie & Li, 2010; Grozdanov Bogoeva-Gaceva, 2010; Kuciel et al., 2012; Bahrami et al., 2024). Polyamides have the capacity to withstand temperatures of up to 250°C in settings with high humidity and up to 300°C in dry environments. Typical applications encompass components utilized in missiles and aircraft. Thermoplastic resins are often used in conjunction with thermosetting resins in the fabrication of composite structures. The materials encompassed in this category consist of nylon, polypropylene (PP), polyether ether ketone (PEEK), and polyphenylene sulphide (PPS).

The number of carbon atoms in the diamines in the polyamide structure has an important effect on the amide group amount and, consequently, on the properties of the polyamide. The most renowned bio-based polyamides are PA 11, PA 1010, and PA 610; these bio-based polyamides have lower density, lower water absorption, and lower melting temperature compared to PA 6 and PA 66, which are the most popular petro-based polyamides (Kuciel et al., 2012). The high melting temperature of plastics poses a challenge when they are mixed with thermally sensitive natural

fibres. Hence, the low melting point of the polymer matrix is an essential parameter in the processing and manufacturing of natural fibre-reinforced composites due to the low thermal stability of natural fibres (Botelho et al., 2003; Kuciel et al., 2012; Feldmann & Bledzki, 2014; Thakur et al., 2014). With an increase in the polyamide chain length, the intermolecular interactions, which mainly govern performance properties, including strength and stiffness, decrease (Kuciel et al., 2012; Endres & Siebert-Raths, 2011).

Adding reinforcing fibres into the polyamide matrix would further improve the mechanical and thermal properties of the matrix (Nie & Li, 2010; Kuciel et al., 2012; Feldmann & Bledzki, 2014; Bahrami et al., 2024). The functional end-groups and amide linkages allow for hydrogen bonding and good interfacial interaction with natural fibres in composite production. This gives biopolyamide the advantage of good processability and high mechanical and thermal properties.

Gigante et al. (2024) developed and optimized biocomposites based on bio-based polyamide 11 (PA11) reinforced with short basalt fibres, targeting improved mechanical and thermal performance for sustainable applications. A combination of 1D extrusion simulation (Ludovic® software) and experimental validation was used to optimize extrusion conditions, focusing on minimizing fibre breakage while maintaining processing stability. A design of experiments approach identified optimal screw speed and feed rate settings to reduce residence time and polymer degradation, while achieving good fibre dispersion and melt strength. Real fibre breakage measurements showed that even optimized processing resulted in a reduction of fibre length from the initial 6 mm to an average of 0.4 mm post-processing, lower than simulation predictions. Micro-CT and SEM analyses confirmed good fibre dispersion and interfacial adhesion, though higher fibre content (20 wt.%) led to increased fibre agglomeration and disrupted orientation during injection moulding.

Mechanical testing showed that incorporating basalt fibres increased the tensile modulus from 1.3 GPa (neat PA11) to 3 GPa (20 wt.% fibre) and improved the heat deflection temperature (HDT) by approximately 75%, reaching values suitable for applications below 160 °C. Flexural strength also improved with fibre addition, while impact strength decreased, particularly at higher fibre contents. Interfacial shear strength (IFSS) estimated using a modified Kelly–Tyson model reached 14.2 MPa, reflecting adequate fibre–matrix adhesion. The study demonstrated that by optimizing

extrusion and injection moulding parameters, bio-PA11/short basalt fibre biocomposites can achieve enhanced stiffness, thermal resistance, and structural performance, supporting their use in automotive and technical applications that require sustainable, lightweight materials.

2.3.1 Bio-based Polyamide

Biopolyamide is characterized by a long-chain polyamide group with repeating amides. Biopolyamides can be synthesized from (1) polycondensation of di-amines and bio-derived di-carboxylic acids with elimination of water (biopolyamides originated from bio-based acid and petro-based amine, such as PA 610, PA 410 and biopolyamides entirely originated from biomass, such as PA 1010, PA 510), (2) polycondensation reaction of amino carboxylic acids as bifunctional monomers, such as PA11, or (3) ring-opening polymerization of lactams, such as bio-based PA6, PA4 (at laboratory scale production) (Shen et al., 2010; Kuciel et al., 2012; Brehmer, 2014).

Some of the important commercial bio and petroleum-based polyamides and their key properties are shown in Table 1 (Brehmer, 2014), whereas the degree of bio-sourcing is illustrated in 1st column. (Kohan et al., 2003; Shen et al., 2010; Brehmer, 2014). Bio-sourcing refers to materials derived from renewable biomass sources (partially or entirely). Biomass refers to biological materials from living organisms, such as crops, trees, and castor beans. The carbon atom, the most important chemical element responsible for forming the backbones of materials, is always present in all fresh or fossilized organic or biosourced feedstocks. Bio-sourcing distinguishes between products originating from petroleum or renewable sources and is limited to available functional groups associated with biomaterials (Brehmer, 2014). Although most organic polymers contain varying proportions of H, C, and O, polyamides and bio-polyamides are essentially composed of nitrogen functional groups in the form of their amine bonds (Brehmer, 2014).

Due to longer-chain polymers, bio-based polyamides (PA610, PA1010, PA1012, and PA11) perform better in terms of moisture and chemical resistance than conventional shorter-chain polyamides, PA6 and PA66. On the other hand, compared to longer-chain PA12, bio-sourced polyamides exhibit superior thermal resistance and strength properties. Basically, lying between short and long-chain polyamides, bio-based polyamides can have either greater or lower performance depending on the preferred application compared to their petro-based relatives (Brehmer, 2014).

Table 1 Typical Properties of Fossil and Bio-based Polyamides (Kohan et al., 2003; Shen et al., 2010; Brehmer, 2014)

Polyamide Polymer	Bio-sourcing	Life Cycle Assessment	Temperature (°C)		Tensile (MPa)		Moisture Adsorption
	Carbon atom (%)	$kgCo_{2eq}/kg$	T_g*	T_m*	Strength	Modulus	Water Uptake (%)
PA6	0	9.1	47	218	80	3000	10.5
PA66	0	7.9	50	258	72	2500	8.2
PA610	63	4.6	48	206	61	2100	2.9
PA1010	100	4.0	37	191	54	1800	1.8
PA1012	45	5.2	49	181	40	1400	1.6
PA10T	50	6.9	125	285	73	2700	3.0
PA11	100	4.2	42	183	34	1100	1.9
PA12	0	6.9	138	176	45	1400	1.5

*T_g: Glass Transition; T_m: Melting-point temperature

2.3.2 Properties of Polyamides

Typically, PA6 and PA66 are implemented in cost-effective applications with high mechanical and thermal performances. However, they show quite low moisture resistance and insufficient dimensional stability. To overcome these obstacles while enhancing the mechanical properties of the polyamides for applications requiring elevated mechanical and thermal properties, they are usually strengthened with reinforcing fibres at a reasonable cost (Shen et al., 2010). A comprehensive comparison of the most common PAs used in the automotive industry with PA11 is represented in Table 2.

Table 2 A Comparison of the Most Significant Properties of PA11, PA6, and PA66

Category	PA11	PA6	PA66
Monomer	11-Aminoundecanoic acid (Arkema, 2023)	Caprolactam (Osswald & Menges, 2012)	Hexamethylene diamine + Adipic acid (Osswald & Menges, 2012)
Feedstock Origin	Bio-based (Castor oil) (Arkema, 2023; Gandini & Lacerda, 2015)	Fossil-based (Plastics Europe, 2020)	Fossil-based (Plastics Europe, 2020)
Bio-based Content	~100% (Arkema, 2023; Gandini & Lacerda, 2015)	0% (Plastics Europe, 2020)	0% (Plastics Europe, 2020)

Carbon Footprint	Low (~60% lower than PA6/PA66) (Shen et al., 2009; Arkema, 2023)	High (Shen et al., 2009)	High (Shen et al., 2009)
Melting Temperature	~190–200°C (Osswald & Menges, 2012)	~215–225°C (Osswald & Menges, 2012)	~255–265°C (Osswald & Menges, 2012)
Moisture Absorption	Low (~0.7%) (Côté et al., 2013)	High (~1.9%) (Côté et al., 2013)	Moderate (~1.3%) (Côté et al., 2013)
Water Resistance	Excellent (Osswald & Menges, 2012)	Moderate to poor (Osswald & Menges, 2012)	Moderate (Osswald & Menges, 2012)
Thermal Stability	Good (Osswald & Menges, 2012)	Moderate (Osswald & Menges, 2012)	High (Osswald & Menges, 2012)
Tensile Strength	Moderate to High (50–65 MPa) (Fakirov, 2010; Osswald & Menges, 2012)	High (75–85 MPa) (Osswald & Menges, 2012)	Higher (80–95 MPa) (Osswald & Menges, 2012)
Tensile Modulus	~1.2–1.6 GPa (Fakirov, 2010; Osswald & Menges, 2012)	~2.5 GPa (Osswald & Menges, 2012)	~3 GPa (Osswald & Menges, 2012)
Impact Resistance	Excellent (ductile, tough) (Osswald & Menges, 2012)	Moderate (Osswald & Menges, 2012)	Lower (Osswald & Menges, 2012)
Flexibility	High (ductile) (Osswald & Menges, 2012)	Lower (Osswald & Menges, 2012)	Lower (Osswald & Menges, 2012)
Abrasion Resistance	High (Osswald & Menges, 2012)	High (Osswald & Menges, 2012)	High (Osswald & Menges, 2012)
Chemical Resistance	Excellent (oils, fuels, bases) (Osswald & Menges, 2012)	Moderate (Osswald & Menges, 2012)	Moderate (Osswald & Menges, 2012)
UV Resistance	Good (with additives) (Fakirov, 2010)	Poor (Osswald & Menges, 2012)	Poor (Osswald & Menges, 2012)
Recyclability (Mechanical)	Good (Ellen MacArthur Foundation, 2021)	Good (Ellen MacArthur Foundation, 2021)	Good (Ellen MacArthur Foundation, 2021)
Recyclability (Chemical)	Limited (Eslami & Rabiee, 2018)	Yes (via depolymerization) (Eslami & Rabiee, 2018)	Limited (Eslami & Rabiee, 2018)
End-of-Life Options	Mechanical recycling, energy recovery (Ellen MacArthur Foundation, 2021)	Mechanical and chemical recycling (Eslami & Rabiee, 2018)	Mechanical recycling, energy recovery (Ellen MacArthur Foundation, 2021)
Applications	Automotive tubing, coatings, bio-composites (Arkema, 2023; Fakirov, 2010)	Fibres, packaging, consumer goods (Osswald & Menges, 2012)	Structural, automotive, electrical parts (Osswald & Menges, 2012)

Circularity Potential	High (Shen et al., 2009; Ellen MacArthur Foundation, 2021)	Moderate (Ellen MacArthur Foundation, 2021)	Moderate (Ellen MacArthur Foundation, 2021)
Industrial Maturity	Growing (Arkema, 2023; European Bioplastics, 2022)	Mature (Plastics Europe, 2020)	Mature (Plastics Europe, 2020)

2.3.3 Overview of Applications of Polyamides

Polyamides are widely used in industrial and structurally demanding applications due to their specific properties and negligible price pressure. Recently, the automotive industry has become the largest market for moulded polyamides, mainly due to their excellent resistance to petroleum products, high temperatures, and environmental conditions. In general, polyamides are mainly processed with injection moulding (76% of total) or extrusion (23% of total) methods. However, other processing methods are insignificant compared to these broad processing techniques (1% of the total) (Brehmer, 2014). Injection moulding is widely used in automotive, industrial machinery, electrical, hardware, furniture, appliance applications, etc. However, extrusion is mainly used in applications with simpler designs, such as films, tubing, pipes, wire, and cables (Brehmer, 2014). Biopolyamide 11 (100% bio-based) is utilized in various applications, including hydraulic hoses for vehicles, natural gas transportation and distribution pipes, oil pipes, electrical cables, medical and sports equipment, and plastic films for food packaging (Kohan et al., 2003; Shen et al., 2010). As mentioned earlier, PA610 (63% bio-based) has relatively low density, proper toughness, excellent dimensional stability, and high moisture resistance compared to PA6 and PA66 (petro-based polyamides) (Kohan et al., 2003; Shen et al., 2010; Brehmer, 2014). Polyamide 6 and 66 have been used widely in automotive applications (Kohan et al., 2003; Shen et al., 2010; Brehmer, 2014). Accordingly, PA610 has the potential to be substituted with PA6, especially in applications that require lightweight materials with higher moisture resistance. Adding reinforcing fibre would further increase the mechanical properties of the polymer, which can be highly beneficial in structurally demanding applications.

Gigante et al. (2024) presented an optimized processing and mechanical evaluation of bio-based polyamide 11 (PA11) composites reinforced with short basalt fibres, aiming to enhance their suitability for automotive applications. The study combined extrusion process simulation using

Ludovic® software with experimental validation to minimize fibre breakage and optimize mechanical performance. Biocomposites with 10%, 15%, and 20% basalt fibre content were produced through twin-screw extrusion followed by injection moulding. The optimized processing conditions resulted in improved fibre dispersion and minimized degradation, achieving a 38% increase in tensile strength, a 140% improvement in stiffness, and a 75% increase in heat deflection temperature (HDT) compared to neat PA11.

Morphological and micro-CT analyses confirmed good fibre distribution and alignment; however, higher fibre contents led to increased fibre breakage and a slight reduction in tensile strength due to agglomeration effects. The study also employed a modified Kelly–Tyson model to evaluate interfacial shear strength (IFSS), reporting a value of 14.2 MPa, indicating effective fibre–matrix adhesion. Despite a slight reduction in impact strength at higher fibre contents, the mechanical, thermal, and structural improvements demonstrated the potential of these optimized bio-PA11/basalt fibre composites as sustainable alternatives to conventional materials for lightweight automotive components.

2.3.4 Polyamides Reinforced with Natural Fibres

Polyamides have been recognized as a strong competitor to traditional matrix materials in the manufacture of advanced composite materials due to their excellent thermal stability, low dielectric constant, high mechanical strength, and chemical inertness (Saheb & Jog, 1999; George et al., 2001; Li et al., 2007; Ku et al., 2011; Faruk et al., 2012; Mohammed et al., 2015; Silva et al., 2017; Slamani & Châtelain, 2023; Bahrami et al., 2024). There is a growing trend in using natural fibres (biofibres) as reinforcing agents for composites, particularly in automotive-grade structural composites. As mentioned earlier, biopolyamides possess many desirable properties that can be utilized in various applications, and the addition of reinforcing fibres would further enhance the performance of the polyamide.

Natural fibres sourced from plants offer environmental benefits and advantages in lightweight, corrosion resistance, abrasion resistance, and biodegradability. Natural fibres, such as hemp, flax, sisal, and jute, have emerged as attractive alternatives to traditional glass and carbon fibres in polymer composites due to their low cost, renewable nature, and relatively low environmental

impact (Wool et al., 2002; Rouison et al., 2004; Sun et al., 2009; Mohammed et al., 2015; Lazarus et al., 2017; Khan et al., 2018; Sanjay et al., 2019; Billah et al., 2021).

In general, polymers are categorized into two main groups based on their origins: natural or bio-based and synthetic or petro-based (Singha & Thakur, 2010; Thakur et al., 2014). Contrary to the biodegradable nature of natural fibres, bio-based polymers can be categorized into either biodegradable or non-biodegradable groups, depending on the particular requirements of their applications (Panthapulakkal & Sain, 2006; Panthapulakkal & Sain, 2007a; Panthapulakkal & Sain, 2007b; Shen et al, 2010; Singha & Thakur, 2010; Thakur et al., 2014; Faruk et al., 2014). The balanced properties of natural fibres and biopolymers would accelerate future novel advances for sustainable and eco-friendly biocomposites (Shen et al., 2010; Thakur et al., 2014).

Adding natural fibres to the polyamide matrix can enhance their mechanical properties through various reinforcement mechanisms. One of the fundamental mechanisms is the load transfer from the matrix to the fibres, which improves the overall strength and stiffness of the composite material. The interfacial adhesion between the fibres and the matrix also plays a crucial role in determining the mechanical properties of the composites (Ku et al., 2011). In addition, the alignment and distribution of fibres within the matrix also contribute to the overall mechanical performance of the composites. It is well-documented that natural fibre reinforcement can significantly improve the tensile strength and modulus of polyamide composites (Rinberg et al., 2018). Moreover, natural fibres have been found to improve other properties of polyamide composites, such as impact resistance and thermal stability. These enhancements make natural fibre-reinforced polyamide composites attractive for a wide range of industrial applications.

The incorporation of natural fibre into biopolyamide results in bio-based composites that can potentially be employed in high-end applications. The functional end-groups and amide linkages of polyamide allow for hydrogen bonding and good interfacial interaction with natural fibres in composite production. This gives biopolyamide the added advantage of good processability, along with high mechanical and thermal performances (Shen et al., 2010; Kuciel et al., 2012).

Natural fibres are renewable, recyclable, inexpensive, lightweight, and non-abrasive to processing equipment (Panthapulakkal et al., 2005; Panthapulakkal & Sain, 2007a, 2007b; Faruk et al., 2014). However, natural fibres have some drawbacks, including their relatively low resistance to moisture

and heat, as well as high levels of instability in fibre properties correlated with their processing conditions (Panthapulakkal & Sain, 2007b). Natural fibres have a low tolerable processing temperature (around 200°C), above which the degradation of hemicellulose and lignin occurs. An Increase in thermal stability is required for structural applications with operating and processing temperatures above 200°C. Aromatic polyamides are usually challenging to fabricate with a resin matrix due to their immiscible properties (Nie & Li, 2010). Moreover, the polyamide matrix in thermoplastic composites absorbs moisture, leading to hydrolytic degradation of the material when exposed to water; this also impacts the mechanical performance of the composites over time. The moisture can potentially result in polymer plasticizing in a reversible physical process. In general, water penetrates through interfacial pathways from the exterior regions of the materials to the inner parts and attacks the polymer. Accordingly, the interface has a significant impact on the moisture absorption performance, especially in humid atmospheres. The moisture-related degradation mainly occurs when composites are reinforced with natural fibres (Khanna et al., 1988; Khanna et al., 1996).

De Arcaya et al. (2009) investigated the mechanical performance of natural fibre-reinforced polyamide (PA6 and PA66) composites below and above the glass transition temperature. Polyamide 6 and 66 composites required processing temperatures of approximately 230°C and 270°C, respectively. Isothermal analysis of fibres at 250°C indicated degradation of flax and jute fibres due to the presence of lignin and hemicellulose in their compositions. This fibre degradation resulted in deteriorating mechanical performances of the natural fibre composites compared to those of pure cellulose fibres. In addition, increasing fibre content augmented shear forces during melt-mixing and led to a decrease in fibre L/D ratio. This may also facilitate degradation at elevated temperatures, resulting in a decrease in tensile strength. On the other hand, interfacial bonding increases with increasing fibre content due to the high polarity of the polyamide matrix, causing an increase in flexural strength (De Arcaya et al., 2009).

As mentioned earlier, one of the major drawbacks associated with natural fibres used in structural applications is their hydrophilic nature, which is inherent to the organic components. This results in poor fibre distribution in the hydrophobic thermoplastic, insufficient adhesion between fibre and matrix, and high moisture absorption of the composites (Saheb et al., 1999). Another area of research is the optimization of processing methods for natural fibre-reinforced composites.

Various processing techniques have been thoroughly investigated to achieve better dispersion of the fibres in the matrix and improve the overall performance of the composites (Zhang & Horrocks, 2003; Holbery & Houston, 2006; Li et al., 2007; Monteiro et al., 2009; Pandey et al., 2010; Mohammed et al., 2015; Bhudolia et al., 2017; Sanjay et al., 2019; Rajak et al., 2019).

Feldmann and Bledzki (2014) investigated the performance characterization of man-made cellulose fibre (15-30 wt.%) reinforced biopolyamides (PA 610 and 1010). They reported that the addition of cellulose fibres significantly enhanced the properties of PA 1010 and PA 610 in terms of tensile properties (strength and stiffness), Charpy notched impact performance, energy absorption, and heat deflection temperature. They also reported that the heat deflection temperature of these biocomposites is effectively comparable to that of traditional glass fibre-reinforced polyamide composites, with the added advantage of energy absorption properties and lightweight potential (Feldmann & Bledzki, 2014).

Higher impact strength was reported for cellulose fibre-reinforced bio-based polyamide composites compared to those reinforced by glass fibres. This might be attributed to the greater fibre pull-outs and higher maximum displacement (elongation) at breakage of the cellulose fibres compared to the glass fibres. They compared the composites' properties produced by their newly developed single-step pultrusion process to those prepared in a conventional two-step pultrusion method (Feldmann & Bledzki, 2014). After compounding by pultrusion, specimens were subjected to the injection moulding process. Composites prepared via the new single-step pultrusion technique represented considerably greater mechanical performances (tensile and notched impact strength) compared to the composites manufactured from the two-step pultrusion technique. This might be correlated to the fibre length in the produced composites; the composites produced by the new single-step technique contain longer fibres due to the lower thermal and mechanical stresses applied to the fibres during their processing. However, glass fibres tend to break more in injection moulding processes compared to cellulose fibres, usually as a result of their greater stiffness, as well as lower elongation at breakage (Feldmann & Bledzki, 2014).

Kuciel et al. (2012) conducted a study on biocomposites composed of biopolyamides with glass, carbon, and flax fibres (10-20 wt%). They investigated the tensile properties of the composites (tensile strength, modulus, and maximum displacement at break) in both a conditioned state and

after water soaking. They reported that a significant enhancement in tensile performance of all the composites was achieved with the addition of the fibres; however, those composites reinforced with glass and flax fibres showed higher enhancement in terms of their elongation at breakage, as well as impact strength (Kuciel et al., 2012).

On the other hand, the composites reinforced with carbon fibre represented the highest tensile properties (strength and stiffness) but had the lowest elongation at breakage (the most brittle). The addition of flax fibres led to the manufacture of lightweight composites entirely derived from renewable resources with enhanced strength, stiffness, and toughness. The water absorption test of neat biopolyamide and its composites (1, 7, and 30 days of soaking) showed that flax fibre composites had the highest water absorption. In contrast, carbon and glass fibre composites did not experience any significant water absorption compared to the neat polyamide (Kuciel et al., 2012).

Hablot et al. (2010) synthesized dimer fatty acid-based polyamides (DAPA) by condensation polymerization. The synthesized biopolyamide was reinforced with cellulose fibres (5-20 wt%). They investigated the influence of adding these reinforcements on the thermal, rheological, and mechanical performances of the polymer matrix. They reported that the matrix fusion temperature did not change with the incorporation of cellulose fibres; however, chain mobility was improved by introducing the fibres, which decreased the crystallinity temperature and crystallinity content. Morphological examination represented an effective interfacial bonding between the fibres and DAPA. The biocomposites exhibited an augmentation in glass transition temperature (Tg); this might be attributed to partial interaction between the fibres and DAPA, resulting in the formation of micron-sized voids in the composites. The dynamic mechanical spectra showed an improvement in the thermal and mechanical stability of the biocomposites.

In terms of tensile properties, these biocomposites represented a significant increase in Young's modulus and yield stress, mainly as a result of effective fibre distribution and proper interfacial bonding between the fibres and the matrix. However, with an increase in fibre content, a considerable decrease in elongation at break was reported; this might be correlated with stress concentration areas, mainly found at the interface of fibres and matrix, which could be cracked under tensile loading (Hablot et al., 2010).

Feldmann et al. (2015) investigated the bio-based polyamide 1010 reinforced with short man-made cellulose fibres manufactured via a co-rotating twin-screw extruder with different screw configurations and temperature settings, followed by injection moulding. A single screw extruder was used as the reference process. In their study, the researchers used two different screw configurations to investigate the mechanical properties of the composites under varying shear strains. The screw configuration (SC_1), comprising kneading discs and mixing elements, was utilized for mixing and distributing the fibres after they passed through the feeding zone. However, the other screw configuration (SC_2) only consists of conveying elements after the fibre feeding zone. Figure 1 shows the different screw configurations for the twin screw extruder (Feldmann et al., 2015). The measured torque for the different screw configurations was reported to be 69.5% and 58.2% on average for the screw configurations SC_1 and SC_2, respectively, indicating that lower mechanical energy was applied to the materials by using conveying elements in the SC_2 configuration. They also investigated the effect of the processing temperature on the mechanical properties of the composites by using two different processing temperature settings (PT_1 and PT_2). Table 3 represents the different temperature settings in the melt-compounding process via twin screw extruder (Feldmann et al., 2015).

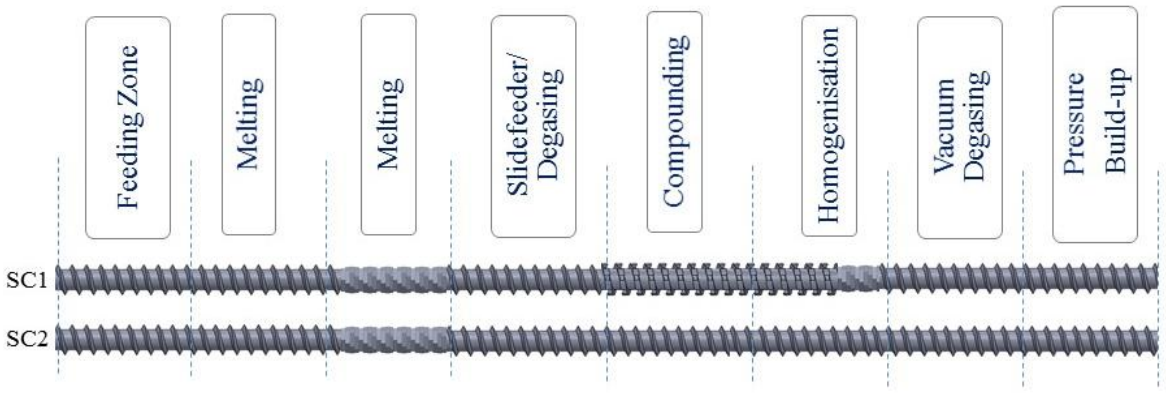

Figure 1 Two Different Twin Screw Configurations (SC1 and SC2)

Table 3 Different Temperature Settings in Melt-compounding Process by Twin-screw Extruder (Feldmann et al., 2015)

Processing Temperature	Zone1 (°C)	Zone2 (°C)	Zone3 (°C)	Zone4 (°C)	Zone5 (°C)	Zone6 (°C)	Zone7 (°C)	Extrusion Die (°C)	Melting Point (°C)

Setting PT_1	240	240	230	230	230	220	200	220	238
Setting PT_2	220	220	200	180	180	180	180	205	216

They reported that the reinforced biopolyamide (20 and 30 wt.% cellulosic fibres) increased notched impact strength and tensile performance. It was noted that the cellulose fibres could positively compete with conventional synthetic reinforcement fibres, such as glass fibres. Increasing the fibre content (from 20 to 30 wt.%) significantly enhanced the notched impact strength. Biocomposites reinforced with 30 wt.% cellulose fibres showed significantly higher impact properties than those reinforced with 30 wt.% glass fibres. They also observed that processing with different temperature and screw configuration settings of the twin-screw extruder did not significantly affect the morphology and mechanical properties of the biocomposites, mainly due to a similar fibre/matrix adhesion. A decrease in shear strain using the different screw configurations and temperature reduction during compounding did not significantly improve the composites' properties, regardless of the different fibre length distribution. Higher fibre length was reported for composites manufactured by the single-screw extruder and the gentle screw configuration on the twin-screw extruder (SC_2). This is due to the lower applied mechanical and thermal stresses on the cellulose fibres during the compounding process (Feldmann et al., 2015).

Liu et al. (2015) studied the effects of lignin-cellulose fibre (LCF) (a kind of cellulosic fibre, containing cellulose and lignin) on the thermomechanical and rheological performances of tall oil-based polyamide. The LCF was mixed with tall oil-based polyamides using a melt-compounding process. They reported that the incorporation of LCF did not significantly influence the glass transition temperature of the composites, and with increasing LCF content, the storage modulus at room temperature increased. In the temperature range of 250-400°C, the biocomposites' thermal stability was reduced by the addition of LCF fibres. However, it was significantly improved by increasing LCF content at a temperature range of 400-800°C. Increasing LCF content resulted in a significant increase in the dynamic viscosity and shear modulus. Tensile tests indicated that the Young's modulus and the yield strength improved with the incorporation of LCF; however, the elongation at breakage was decreased (Liu et al., 2015).

The potential of natural fibre-reinforced polyamide composites is significant; however, persistent challenges remain that require attention. A key hurdle lies in the variation of mechanical properties

among natural fibres, leading to inconsistent composite performance. Several studies have aimed to conquer this obstacle by optimizing fibre treatment methods and enhancing the adhesion between fibres and the matrix. Additionally, moisture absorption in natural fibres poses a challenge, causing dimensional instability and composite degradation. To address this issue, various approaches, including surface modification and chemical treatments, have been explored to minimize moisture absorption.

In order to enhance the properties and performance of natural fibre-reinforced polyamide composites, various modification techniques can be applied to the natural fibres. These modification techniques include chemical treatments, physical treatments, and hybridization with other types of reinforcing fibres. Chemical treatments involve the use of chemicals to modify the surface properties of natural fibres (Kalia et al., 2009; John & Anandjiwala, 2007; Ravi et al., 2018; Varghese & Mittal, 2018; Khalid et al., 2021).

Several chemical treatments have been explored to modify natural fibres and improve their adhesion to the polymer matrix, including alkali treatment, acetylation, the use of silane coupling agents, and grafting techniques. The purpose of applying chemical treatments is to enhance the bonding between fibres and the polyamide matrix. This is achieved by increasing the wettability and roughness of the fibres' surface and by adding functional groups that can react with the matrix. One major obstacle to overcome in this process is the high moisture absorption rate of natural fibres, which can negatively impact the mechanical properties of the resulting composites (Shalwan & Yousif, 2013; Mohammed et al., 2015; Karthi et al., 2020; Sathish et al., 2021; Khalid et al., 2021)

Alkali treatment has been shown to increase the surface roughness of natural fibres, resulting in better mechanical interlocking with the polymer matrix and improved bonding strength. Furthermore, alkali treatment can also remove impurities and hemicellulose from the natural fibres, leading to increased fibre-matrix adhesion (Yu et al., 2010; Yan et al., 2012; Mohammed et al., 2015). Silane treatment is another commonly used method for surface modification of natural fibres. Silane coupling agents can react with both the hydroxyl groups on the fibre surface and functional groups in the polymer matrix, forming covalent bonds that improve the interfacial

adhesion and mechanical properties of the composites (Oksman et al., 2003; Sgriccia et al., 2008; Kalia et al., 2009; Ku et al., 2011; Nassar et al., 2016; Ravi et al., 2018).

Physical treatments include mechanical processes such as grinding, milling, and surface roughening to improve the adhesion between the fibre and the polyamide matrix. Hybridization involves combining natural fibres with other types of reinforcing fibres, such as glass fibres or carbon fibres, to create composites with improved mechanical properties and performance.

In addition, research has shown that the mechanical properties of natural fibre-reinforced polyamide composites can be further enhanced by incorporating nanoparticles into the matrix. Nanoparticles, such as graphene oxide and clay nanoparticles, have been shown to improve the mechanical properties of these composites through mechanisms such as reinforcement by providing additional strength and stiffness, improving dispersion of fibres in the matrix, and creating a more efficient load transfer between the fibres and matrix (Li et al., 2007; Kalia et al., 2009; Gurunathan et al., 2015; Mohammed et al., 2015; Ramnath et al., 2018; Ravi et al., 2018; Sanjay et al., 2019; Atmakuri et al., 2020; Raju & Shanmugaraja, 2020).

Several methods have been investigated to reduce the moisture absorption of natural fibres, such as chemical treatments and coating techniques. For instance, studies have shown that the moisture absorption of natural fibre-reinforced composites can be significantly reduced by treating the fibres with hydrophobic agents or applying a protective coating on the fibres (Puglia et al., 2004; Goda et al., 2006; Holbery & Houston, 2006; Nirmal et al., 2015; Mohammed et al., 2015; Ravi et al., 2018; Wu et al., 2018; Sanjay et al., 2019).

In addition to enhancing the mechanical properties, studies have also been conducted on improving the thermal properties of natural fibre-reinforced polyamide composites for automotive applications (Das et al., 2021). One method that has been explored is the incorporation of fillers or additives to enhance the thermal stability and flame retardancy of the composites (Khalid et al., 2021). These additives, such as halogenated flame retardants or nano-clays, have shown promising results in improving the fire resistance and thermal stability of composites (Dahlke et al., 1998; Santos et al., 2007; Rodriguez-Castellanos et al., 2016; Guedes et al., 2016; Witayakran et al., 2017).

In a study conducted by Mundhe and Kandasubramanian (2024), the effectiveness of various chemical methods for enhancing the properties of natural fibres was thoroughly examined. Treatments such as alkali, acetylation, silane, potassium permanganate, and isocyanate were found to improve the physical characteristics, durability, and thermal stability of natural fibre composites by increasing their compatibility with polymer matrices. Notable developments include the incorporation of newly identified fibres like acai, guaruman, and corn straw, as well as novel treatments such as bromodecane, lime, and tannic acid.

Degradation mechanism of PA 11 and its natural fibre-reinforced composites during extrusion

Extrusion and injection moulding are two of the predominant methods used for the processing and manufacturing of polyamide in a wide range of products. Nevertheless, PA11 may undergo degradation during these procedures due to various parameters, including elevated temperatures, shear stress, and exposure to oxygen and moisture. The degradation of PA11 and natural fibre-reinforced PA11 during extrusion and injection moulding can lead to several adverse effects on the material's mechanical properties, including reduced strength and stiffness, decreased impact resistance, and increased brittleness. In addition, the degradation products of PA11 can also lead to discoloration, odour, and other visual issues.

The degradation of PA11 during extrusion involves various chemical reactions that can lead to the formation of shorter polymer chains, volatiles, and other by-products. The primary degradation mechanism is thermal decomposition, which occurs when the polymer is exposed to high temperatures for extended periods. PA11 contains (–CO–NH–) bonds in its backbone. During the extrusion process, the high processing temperatures and shear forces can cause the amide linkages to undergo hydrolysis and result in the formation of carboxylic acid and amine end groups (De Arcaya et al., 2009; Hablot et al., 2010; Kuciel et al., 2012; Ozen et al., 2013; Feldmann & Bledzki, 2014; Semba et al., 2014; Corrêa et al., 2014; Kiziltas et al., 2014; Feldmann et al., 2015; Liu et al., 2015; Peng et al., 2015; Aydemir et al., 2015).

The hydrolysis of the amide linkages in PA11 occurs via nucleophilic attack by water molecules on the carbonyl group of the amide bond, which leads to the formation of a tetrahedral intermediate. This intermediate then undergoes further hydrolysis, which results in the cleavage of the amide bond and the formation of carboxylic acid and amine end groups. The carboxylic acid

groups can react further with the polymer chain or other degradation products to form cyclic compounds (lactam). In contrast, the amine end groups can react with other amine end groups or with other degradation products to form oligomers or other low-molecular-weight species, which can affect its mechanical properties (De Arcaya et al., 2009; Hablot et al., 2010; Kuciel et al., 2012; Ozen et al., 2013; Semba et al., 2014; Corrêa et al., 2014; Kiziltas et al., 2014; Feldmann et al., 2015; Liu et al., 2015; Peng et al., 2015; Aydemir et al., 2015).

In addition to hydrolysis, PA11 can also undergo oxidative degradation during the extrusion process. This can occur due to the presence of oxygen or other reactive species, which can react with the polymer chain, resulting in the formation of carbonyl groups, hydroperoxides, and other oxidation products. These oxidation products can then react further with the polymer chain or with other degradation products to form cross-linked species, which can further degrade the material and reduce its mechanical properties (De Arcaya et al., 2009; Hablot et al., 2010; Kuciel et al., 2012; Ozen et al., 2013; Feldmann & Bledzki, 2014; Semba et al., 2014)

The degradation of PA11 during extrusion is a complex process involving multiple chemical reactions and pathways. The specific degradation products formed will depend on the processing conditions, the material's formulation, and the presence of any reactive species. To minimize the degradation of PA11 during extrusion and injection moulding, it is essential to carefully control the processing parameters and optimize the material's formulation. For instance, using lower processing temperatures, reducing shear stress, and minimizing residence time can all help reduce the degradation of PA11 during processing. Additionally, the use of additives such as antioxidants, stabilizers, and processing aids can also enhance the material's thermal stability and reduce the likelihood of degradation. Finally, proper storage and handling of the PA11 material prior to processing can also help to minimize the risk of degradation and ensure the optimal performance of the finished product (Hablot et al., 2010; Kuciel et al., 2012; Ozen et al., 2013; Feldmann & Bledzki, 2014; Semba et al., 2014; Corrêa et al., 2014; Kiziltas et al., 2014; Feldmann et al., 2015; Liu et al., 2015; Peng et al., 2015; Aydemir et al., 2015).

Falkenreck et al. (2025) investigated the hydrothermal degradation mechanisms of regenerated cellulose fibre (RCF)-reinforced bio-based polyamide 5.10 (PA5.10) composites, aiming to assess their suitability for automotive applications where moisture and elevated temperatures are prevalent. The study showed that both the polyamide matrix and RCF undergo significant

degradation when exposed to hydrothermal aging conditions, with moisture absorption leading to fibre swelling, loss of fibre–matrix adhesion and accelerated hydrolytic and thermo-oxidative chain scission in the PA5.10 matrix. Mechanical testing indicated that while RCF reinforcement initially enhanced tensile strength and impact resistance, these properties deteriorated substantially with prolonged exposure to high temperatures and humidity. The application of a carbodiimide-based hydrolysis stabilizer (P100) and a maleic anhydride-grafted polypropylene coupling agent (MAPP) improved moisture resistance, preserved fibre–matrix bonding, and mitigated mechanical degradation, particularly at moderate aging conditions. However, the protective effects diminished at extreme conditions (90°C). The findings emphasize the need for advanced stabilization strategies to extend the service life of natural fibre-reinforced biopolyamides in demanding environments, particularly in automotive applications that require long-term durability under fluctuating moisture and thermal loads.

2.4 Carbon Fibre Reinforced Composites

Carbon fibre (CF) is widely used as a reinforcing agent for polymer composites in various superior performance applications, i.e., automotive, aerospace, and wind turbines, due to its low weight, remarkable mechanical properties, excellent thermal and chemical stabilities, and low thermal expansion (Donnet & Bansal, 1990; Donnet et al., 1998; Morgan, 2005).

Carbon fibre is often selected as reinforcement for polymer matrices in advanced structural applications in the automotive sector due to its low weight and excellent mechanical properties (Donnet, 1998; Botelho et al., 2003; Morgan, 2005; Nie & Li, 2010; Karsli & Aytac, 2013). The properties of carbon fibre, such as high stiffness, proper tensile strength, good chemical resistance, high-temperature tolerance, and low thermal expansion, make it suitable for aerospace and automotive industries (Nie & Li, 2010; Nairn et al., 1994).

Carbon fibre has the most weight reduction potential and higher stiffness than glass fibres. Commercial-grade carbon fibres offer a modulus of 230 GPa, almost three times higher than E-glass fibres (70 GPa), with a specific gravity of 70% of E-glass fibres. Magniez et al. (2014) studied short carbon fibre-reinforced PA11 and reported that a small carbon fibre content (0.5-2%) could significantly improve the properties of PA11, including stiffness, elastic deformation before yield, and creep properties. However, carbon fibre is not renewable and is quite expensive compared to

other fibre types because of the high energy consumption in its manufacture. Using low-cost/recycled carbon fibre would be a cost-effective alternative for this, which has not been investigated in this study.

The inadequate adhesion or bonding between the resin matrix and the surface of the carbon fibres compromises the interfacial shear strength of reinforced composites with carbon fibres. The degree of the bonding is strongly associated with the surface properties of carbon fibres and their reactivity (Donnet & Bansal, 1990; Donnet et al., 1998; Morgan, 2005). A detailed study of carbon fibre surface structure is required to increase the interfacial shear strength between carbon fibre and matrix material by modification of carbon fibre surfaces (Donnet & Bansal, 1990; Nairn, 1994; Donnet et al., 1998; Morgan, 2005).

Sullivan (2006) critically examined the opportunities and challenges associated with integrating carbon fibre-reinforced polymers (CFRPs) into automotive applications, highlighting both the material's potential and the industrial barriers to its widespread adoption. While carbon fibre offers unparalleled weight reduction (up to 50% for structural components), its prohibitive cost, inconsistent supply chain, limited design data, and the lack of high-throughput manufacturing and recycling solutions have constrained its market penetration.

The U.S. Department of Energy's Freedom CAR program has prioritized overcoming these challenges by supporting the development of low-cost precursors, conversion technologies, and rapid manufacturing methods, with a target cost of $3–$5 per pound. Key advancements include exploring lignin-based precursors and plasma-assisted carbonization methods. Additionally, the study emphasizes that although aerospace and defence industries currently dominate carbon fibre demand, scaling up production through expanded applications in construction, consumer goods, and renewable energy could stabilize the market, reduce costs, and make CFRPs more viable for high-volume automotive manufacturing. Despite the technological promise, successful integration into automotive applications will require overcoming economic, technical, and recycling challenges to compete with established materials such as aluminum and magnesium.

2.4.1 Carbon fibre

Carbon fibres, often termed graphite fibres or carbon graphite, are mostly made of carbon atoms. They have been known for almost a century since Thomas Edison utilized them as filaments for incandescent lamps (Sitting, 1980; Delmonte, 1981; Donnet & Bansal, 1990; Donnet et al., 1998). The earliest carbon fibres were made by the carbonization of bamboo and rayon. Later, they were only made from rayon for thermal insulation applications. However, they could not compete with glass fibres at the time (Donnet & Bansal, 1990; Donnet et al., 1998). Carbon fibres are typically made from three precursors: rayon, polyacrylonitrile (PAN), and pitches (Morgan, 2005).

The production of carbon fibres involves the sequential processes of oxidation, carbonization, and controlled graphitization of pre-existing carbon-rich organic precursors in the form of fibres. Polyacrylonitrile (PAN) is often regarded as the predominant precursor due to its ability to yield fibres with superior characteristics. Nevertheless, fibres can also be derived from cellulose and pitch. The regulated graphitization method yields fibres exhibiting either high mechanical strength (at around 2600°C) or high elastic modulus (at approximately 3000°C), with various variations. After its formation, the carbon fibre undergoes a surface treatment to enhance its interaction with the matrix phase. Carbon fibres exhibit higher brittleness, characterized by reduced elongation at break, in comparison to both glass fibres and aramid. Similar to glass fibres, carbon fibres are readily accessible in various forms for commercial use, including continuous fibres, short fibres, and blankets (Donnet & Bansal, 1990; Morgan, 2005; Maia, 2017; Maia et al., 2019).

2.4.1.1 Classifications of Carbon Fibres

Carbon fibres can be classed into three main groups (Donnet & Bansal, 1990; Morgan, 2005):

1. Carbon fibres can be divided based on their final heat treatment temperature into high-heat-treatment carbon fibres (HTT), intermediate-heat-treatment carbon fibres (IHT), and low-heat-treatment carbon fibres (LHT).
2. Depending on their precursor fibre materials, carbon fibres can be classified into PAN-based carbon fibres, pitch-based carbon fibres, mesophase pitch-based carbon fibres, isotropic pitch-based carbon fibres, rayon-based carbon fibres, and gas-phase-grown carbon fibres.

3. Lastly, they can also be classified based on their properties into carbon fibres with ultra high modulus (UHM) for modulus higher than 450 GPa, high modulus (HM) for modulus between 350-450 GPa, intermediate modulus (IM) between 200-350 GPa, low modulus (<100 GPa) and high tensile carbon fibres (HT) for tensile strength between 3-4.5 GPa, and ultimately superhigh-tensile carbon fibre (SHT) for tensile strength higher than 4.5 GPa.

The IUPAC International Committee has indicated a tentative classification of carbon fibres into five classes based on their mechanical properties (Donnet & Bansal, 1990; Morgan, 2005):

1. UHM carbon fibres with a modulus of more than 500 GPa
2. HM carbon fibres with a modulus of more than 300 GPa and a ratio of tensile strength-to-tensile modulus of less than 1%
3. IM carbon fibres with a maximum modulus of 300 GPa and a ratio of tensile strength-to-tensile modulus of higher than 0.01
4. Low-modulus carbon fibres with modulus up to 100 GPa and low strength (isotropic structure)
5. HT-type carbon fibres have tensile strength higher than 300 MPa and a strength-to-stiffness ratio of 0.02-1.5.

2.4.1.2 Carbon Fibre Structure

The atomic structure of carbon fibre is similar to that of graphite, consisting of sheets of carbon atoms (graphene sheets) organized in a well-ordered hexagonal pattern. Their variations are mainly in their sheet's interconnection (Sitting, 1980; Delmonte, 1981; Morgan, 2005). Graphite is a crystalline material in which the sheets are oriented parallel to one another in a regular pattern. The intermolecular forces between the sheets are relatively weak Van der Waals forces, which give graphite its soft and brittle features (Bascom & Drzal, 1987; Donnet & Bansal, 1990; Krekel et al., 1994; Donnet et al., 1998; Morgan, 2005).

Depending on the fibre-forming precursor, carbon fibre may be turbostratic or graphitic or have both graphitic and turbostratic sections (hybrid structure) (Sitting, 1980). In turbostratic carbon fibre, the sheets of carbon atoms are randomly folded or crumpled. Typically, carbon fibres created

from polyacrylonitrile (PAN) are turbostratic, but carbon fibres derived from mesophase pitch are graphitic (heat treatment at temperatures above 2200 °C) (Bascom & Drzal, 1987; Donnet & Bansal, 1990; Donnet et al., 1998). Turbostratic carbon fibres exhibit high tensile strength, while heat-treated mesophase-pitch-derived carbon fibres have high Young's modulus (i.e., high stiffness or resistance to extension under load) and good thermal conductivity (Bascom & Drzal, 1987; Morgan, 2005; Maia, 2017; Maia et al., 2019).

The carbon fibre surface composition is largely determined during the graphitization of the fibre. The disintegration of the polyacrylonitrile polymer network and subsequent displacement of the carbon atoms into the hexagonal graphitic structure involve the creation and removal of volatile material from the carbon fibre interior and surface (Bascom & Drzal, 1987; Morgan, 2005). Theoretically, graphitization proceeds from the carbon fibre surface inward, and the escaping volatiles are continually transported through the forming surface, creating a disordered structure (Bascom & Drzal, 1987; Morgan, 2005). The skin-core structure observed in some carbon fibres implies two opposing processes: the consolidation of the outer layers and the simultaneous breakdown of the layers due to the release of volatiles from the inner layers. Therefore, virgin-produced carbon fibres, without any treatment, contain many flaws on their outer surfaces (Bascom & Drzal, 1987; Krekel et al., 1994; Maia et al., 2019).

2.4.1.3 Characteristics and Uses of Carbon Fibre

Carbon fibre is primarily used for strengthening composite materials, commonly known as carbon fibre-reinforced polymers. Applying a thin coating of carbon fibre greatly enhances the fire resistance of polymers or thermosets due to the efficient heat reflection of the dense carbon fibre layer (Morgan, 2005; Zhao & Gou, 2009; Maia et al., 2019).

Carbon fibres possess several key characteristics that contribute to their widespread use in various industries, including aerospace, civil engineering, military, motorsports, automotive, and wind turbine blade technologies. These properties include exceptional stiffness, high tensile strength, excellent chemical resistance, impressive temperature tolerance, low weight, and minimal thermal expansion (Sitting, 1980; Donnet, 1990; Morgan, 2005). Carbon fibres possess excellent heat resistance, allowing them to endure significantly elevated temperatures without melting.

Nevertheless, in comparison to other fibres, such as glass fibres or plastic fibres, they are somewhat costly (Morgan, 2005; Maia et al., 2019).

2.4.1.4 Recycling of Carbon Fibre

The growing demand for carbon fibre requires novel technologies for recovery and reuse. However, carbon fibre is non-renewable and relatively expensive compared to other conventional fibre types due to its high energy consumption during manufacture. The end-of-life carbon-containing materials usually end up in shredding, landfill, and incineration, which are not considered sustainable and environmentally friendly practices. On the other hand, inappropriate disposal of composites containing carbon fibre may cause severe environmental hazards. It has been reported that the energy requirement for virgin carbon fibre production is about 286 MJ/kg, which makes using recycled carbon fibre a cost-effective alternative (Suzuki &Takahashi, 2005; Szpieg et al., 2012; Thomas et al., 2016; Armioun et al., 2016a; Armioun et al., 2016b; Faruk et al., 2017; Maia et al., 2019; Xiong et al., 2021). Pimenta and Pinho (2011) reported that some of the carbon fibre recycling techniques require only about 10% of the energy needed for the manufacturing of virgin carbon fibre.

Additionally, it has been reported that recycled carbon fibre has the potential to compete with virgin carbon fibre in terms of mechanical performance, making it a cost-beneficial alternative compared to virgin carbon fibre (Pimenta & Pinho, 2011; Szpieg et al., 2012). Therefore, carbon fibres are considered extremely valuable and worthy of recovery and reuse in applications that require superior performance, where high strength and stiffness are essential. Carbon fibres sustain excellent properties, even when entrapped in other materials.

In general, carbon fibres are collected in two forms after recycling: as random short fibres from woven or non-woven products, or as woven fabric pieces. The size and shape of the recovered woven fabric pieces directly depend on their pretreatment processes. Sometimes, the recovered woven fabrics can maintain their woven structure and reinforcing level after recycling (Pimenta & Pinho, 2011; Oliveux et al., 2015; Rybicka et al., 2016; Xiong et al., 2021). Densely filled short fibre-reinforced thermoplastics have been receiving increasing attention in various industries due to their excellent specific mechanical properties, such as specific tensile strength and specific stiffness, compared to non-reinforced thermoplastics.

Reclaimed carbon fibres from performance-intensive applications may not exhibit similar properties compared to the original carbon fibres, which were recovered from and not necessarily reused for the same applications. Therefore, it is crucial to develop proper applications and specific standards to benefit from reusing recycled carbon fibres and their reinforcing potential (Oliveux et al., 2015; Rybicka et al., 2016; Maia, 2017; Maia et al., 2019).

The properties of the recycled carbon fibres are highly dependent on their length; longer fibres are usually more fragile and, consequently, more susceptible to damage and defects during the reclamation processes. Short and randomly distributed carbon fibres from thermochemical reclamation are not generally appropriate for reuse in structural applications, even if they were recovered from structural parts. These recycled carbon fibres are the best candidates to replace virgin carbon fibre and are reused in sheet moulding compound (SMC) and bulk moulding compound (BMC). However, long recycled carbon fibres can be reused in structural applications (Rybicka et al., 2016; Oliveux et al., 2015).

2.4.2 Polyamides Reinforced with Carbon Fibres

Due to their excellent mechanical properties, carbon fibre-reinforced polyamide composites have garnered significant attention in various industries, including the automotive and aerospace sectors. Carbon fibre-reinforced polyamide composites are composite materials that combine carbon fibres as reinforcement and polyamide as the matrix material. These composites exhibit enhanced mechanical properties, such as high tensile strength, flexural strength, and impact resistance, making them ideal for applications where lightweight yet strong materials are required (Botelho et al., 2003; Zhang et al., 2003; Karsli & Aytaç, 2013; Pathak et al., 2016).

Carbon fibre-reinforced polyamides are composite materials with exceptional strength, stiffness, versatility, and durability. Due to their remarkable properties and potential for lightweight applications, they have gained significant attention in multiple industries, particularly the automotive industry (Botelho et al., 2003; Liao et al., 2018; Kausar et al., 2019; Slamani & Châtelain, 2023).

The use of carbon fibre-reinforced polyamides offers several undeniable advantages, including high-specific strength and stiffness, lower density, and flexible design options. Carbon fibres are

ideal for structural composites due to their strength and stiffness, while polyamides provide excellent abrasion resistance, heat resistance, and high molecular weight that contribute to the overall mechanical properties (Botelho et al., 2003; Zhang et al., 2003; Karsli & Aytaç, 2013; Silva et al., 2017; Liao et al., 2018; Peng et al., 2018).

One of the critical reasons for the superior mechanical properties exhibited by carbon fibre-reinforced polyamide composites is the high strength and stiffness of carbon fibres combined with the toughness and flexibility of the polyamide matrix. Carbon fibre-reinforced polyamides are typically produced through a melt-compounding method. The manufacturing process involves dispersing the carbon fibres within the molten polyamide matrix, followed by solidification to form the composite (Botelho et al., 2003; Yao et al., 2018; Liao et al., 2018; Kausar et al., 2019; Ma et al., 2019; Ramezani-Dana et al., 2021).

Carbon fibre-reinforced polyamide composites have been the subject of extensive research and development due to their exceptional mechanical properties and potential for various applications. The mechanical properties of carbon fibre-reinforced polyamide composites have been extensively studied in the literature. (Liu et al., 2004; Koo et al., 2005; Jiang et al., 2008; Huang et al., 2009; Mei et al., 2011; Sharma et al., 2014; Zhang et al., 2017; Silva et al., 2017; Liao et al., 2018; Peng et al., 2019).

According to a study conducted by Goffin et al. (2012), carbon fibre-reinforced polyamide composites exhibited tensile strengths of up to 590 MPa, flexural strengths of up to 320 MPa, and impact strengths of up to 120 kJ/m². Furthermore, carbon fibre-reinforced polyamide composites have a high modulus value of approximately 20-25 GPa, indicating their ability to resist deformation under stress. Another study by Gupta et al. (2002) reported that carbon fibre-reinforced polyamide composites exhibited excellent interlaminar shear strength, ranging from 50 to 70 MPa. These studies highlight the superior mechanical properties of carbon fibre-reinforced polyamide composites, which can be attributed to the high strength and stiffness of carbon fibres combined with the toughness and flexibility of the polyamide matrix.

The properties of carbon fibre-reinforced polyamides are influenced by various factors, including the manufacturing process, the type and volume fraction of carbon fibres used, and the quality of

the interface between the fibres and the polymer matrix. Extensive research has been conducted on these materials for their mechanical, thermal, and physical properties under different conditions and loading scenarios and has confirmed their exceptional performance (Sui et al., 2013; Liu et al., 2017; Silva et al., 2017; Tseng et al., 2017; Liu et al., 2017; Silva et al., 2017; Liao et al., 2018; Peng et al., 2019; Peng et al., 2020). These studies emphasize the influence of various parameters on the properties of carbon fibre-reinforced polymers.

The mechanical properties of carbon fibre-reinforced polyamides, such as modulus, tensile strength, and flexural strength, are significantly influenced by the orientation of the carbon fibres within the composite (Tseng et al., 2017; Silva et al., 2017; Liao et al., 2018; Zhang et al., 2020). In a study by Chen et al. (2020), the effect of fibre orientation and content on the mechanical properties of carbon fibre-reinforced epoxy/polyamide composites has been investigated. Their findings highlighted the importance of optimizing fibre alignment and volume fraction to achieve the desired mechanical performance tailored for specific applications. One such study, by Li et al. (2011), utilized finite element analysis to investigate the effect of different fibre orientations on the mechanical properties of carbon fibre-reinforced polyamide composites. The study found that mechanical properties, such as tensile strength and modulus, highly depended on fibre orientation.

Furthermore, the fibre volume fraction and matrix type also significantly influence the mechanical properties of carbon fibre-reinforced polyamide composites (Botelho et al., 2003). Several studies found that increasing the fibre volume fraction increased the tensile strength and modulus of carbon fibre-reinforced polyamide composites. In addition to the fibre volume fraction, the type of matrix used in carbon fibre-reinforced polyamide composites can also affect their mechanical properties (Patel et al., 1992; Kausar, 2019; Kumar et al., 2007; Tibbetts et al., 2007; Bijwe & Rattan, 2007; Rattan & Bijwe, 2006; Zhou et al., 2006; Senthil et al., 2018; Kim et al., 2018). For instance, a study by Karsli & Aytaç (2013) demonstrated that carbon fibre-reinforced polyamide 6/6 composites exhibited higher tensile and flexural strengths compared to those reinforced with polyethylene.

Additionally, the mechanical properties of carbon fibre-reinforced polymer composites are highly influenced by the quality of the fibre-matrix interface (Gupta et al., 2002; Rattan et al., 2006; Bijwe et al., 2007; Padmavathi et al., 2008; Sharma et al., 2010; Rana et al., 2012; Rajmohan et al., 2013;

Adak et al., 2018; Kumar et al., 2020). The interface between the carbon fibres and polyamide matrix plays a crucial role in determining the overall mechanical properties of the composites. The interfacial adhesion between fibre and matrix can be improved through various methods, such as surface treatment of the carbon fibres. These surface treatments introduce chemically active groups on the fibre surfaces, enhancing both chemical reactivity with the matrix and surface roughness for improved mechanical interlocking between the fibres and the matrix.

Surface treatments, such as oxidation, coating, and grafting, are commonly used to modify the carbon fibre surface. One method of surface treatment that has shown promise is ozone (O_3) modification. Ozone modification involves exposing the carbon fibres to ozone gas, which chemically activates the fibre surface and enhances its reactivity with the polymer matrix. (Fu et al., 1998; Pittman et al., 1998; Yue et al., 1999; Park et al., 2003; Park et al., 2005; Jin et al., 2006; Zhang et al., 2007; Li et al., 2009). According to a study by Jiang et al. (2008), ozone modification of carbon fibres improved the interfacial adhesion properties of carbon fibre/polyamide composites. It resulted in stronger interfacial bonding between the fibres and the matrix.

In a study by Ma et al. (2019), various techniques, including surface treatment and chemical modification, have been employed to enhance the interfacial adhesion between carbon fibres and polyamide matrices. The results indicated that these methods improved the interfacial bonding, resulting in enhanced mechanical properties of the carbon fibre-reinforced polyamides. Moreover, the fabrication techniques used to produce carbon fibre-reinforced polyamide composites also play a crucial role in determining their mechanical properties. Interfacial polymerization and hot compression moulding techniques have been commonly used to fabricate carbon fibre-reinforced polyamide composites. The interfacial polymerization method involves passing and pulling the reinforcement (carbon fibres) across the polyamide reaction chamber, allowing for the impregnation of the fibres with the polymer matrix. Additionally, hot compression moulding involves impregnating the reinforcement with the polymer matrix under heating and pressure (Wan et al., 2000; Ma et al., 2003; Jang et al., 2005; Choi et al., 2006; Zhou et al., 2006; Jia et al., 2016; Tanaka et al., 2017; Lu et al., 2018; Peng et al., 2019).

In addition, valuable insights into improving fibre dispersion uniformity within the polyamide matrix have been provided (Zhang et al., 2003; Wang et al., 2004; Liu et al., 2004; Zhang et al.,

2017; Peng et al., 2019). Their study proposed advanced mixing technologies and processing parameters to achieve consistent and homogeneous dispersion of carbon fibres, ultimately leading to enhanced mechanical properties and overall performance of the composites.

Raushan et al. (2025) investigated the dynamic performance of carbon fibre-reinforced polyamide 66 (CF/PA66) composite drive shafts as a lightweight, high-strength alternative to conventional steel shafts for automotive applications. Using an analytical approach based on Hamilton's principle and the Wittrick-Williams' algorithm, the authors developed a dynamic stiffness matrix (DSM) to compute the natural frequencies and mode shapes of both two-piece and single-piece CF/PA66 hollow drive shafts. These results were validated using finite element analysis (FEA) in ANSYS and MATLAB programming, with close agreement observed between the analytical and numerical predictions. The findings showed that the single-piece CF/PA66 drive shaft, despite its increased length, maintained comparable or higher natural frequencies than the conventional two-piece steel shaft, while significantly reducing weight. The study concluded that CF/PA66 drive shafts offer improved vibration resistance and durability with potential benefits for long-term vehicle performance. However, it also noted that replacing short steel shafts with CF/PA66 shafts requires careful frequency and vibration analysis due to the different dynamic responses introduced by material and geometric changes.

Furthermore, the research conducted by Tanaka et al. (2020) addresses the challenge of impact resistance in carbon fibre reinforced polyamides. Their work explored novel techniques for enhancing the impact resistance of these materials, which is crucial for applications requiring high durability and toughness. Through the incorporation of toughening agents and optimization of the fibre-matrix interface, they were able to improve the impact resistance of carbon fibre-reinforced polyamides and enhance their ability to withstand sudden impacts and mechanical stresses (Tanaka et al., 2020).

In addition to mechanical properties, the characterization of the thermal behaviour of carbon fibre-reinforced polyamides has been a subject of interest in recent studies. The influence of fibre orientation on heat dissipation, thermal expansion, and resistance to temperature-induced degradation has been investigated to provide an understanding of the thermal performance of these materials. A study by Ren et al. (2020) provided an in-depth analysis of the thermal conductivity

of carbon fibre-reinforced polyamide 6 (PA6). The study revealed that the thermal conductivity of the composite can be further improved by optimizing the dispersion of carbon fibres within the polyamide matrix. By enhancing the uniform distribution of carbon fibres, the composite's ability to conduct heat was significantly enhanced, making it suitable for applications that require efficient heat dissipation. This finding highlights the versatility of these composite materials in terms of their mechanical performance and ability to regulate temperature effectively in various operational environments.

Several studies have investigated the effects of fibre volume fraction and matrix type on the mechanical properties of carbon fibre-reinforced polyamide composites. In general, an increase in carbon fibre content leads to improved mechanical properties, including higher elastic modulus, tensile strength, and compressive strength (Botelho et al., 2003; Jin et al., 2006; Tanaka et al., 2017; Athreya et al., 2011; Slamani & Châtelain, 2023; Silva et al., 2017; Veazey et al., 2016; Caba et al., 2007; Kim et al., 2018). In addition to the fibre content, the type of matrix used in carbon fibre-reinforced polyamide composites also influences their mechanical properties. (Botelho et al., 2001; Tibbetts et al., 2007; Bijwe & Rattan, 2007; Rattan & Bijwe, 2006; Wu et al., 2018; Ma et al., 2018; Chen et al., 2018; Senthil et al., 2018; Liao et al., 2018). In a study by Wang et al. (2004), the mechanical properties of PA 6 and PA 6/6 composites reinforced with fabric and unidirectional carbon fibres were compared. The study found that increasing the fibre volume fraction led to significant improvements in the tensile strength, modulus, and fracture toughness of both PA and PA 6/6 composites. These improvements were more pronounced in the composites reinforced with unidirectional carbon fibres than those reinforced with fabric.

In another study by Botelho et al. (2003), the mechanical properties of carbon fibre-reinforced polyamide composites were investigated with different matrix types, including PA 6 and PA 6/6. The study found that the matrix type had a significant influence on the mechanical properties, including tensile strength and modulus. For instance, the PA 6/6 composites exhibited higher tensile strength and modulus than the PA 6 composites. Furthermore, the study found that the matrix type also influenced the interlaminar shear strength of the composites. PA 6/6 composites exhibited higher interlaminar shear strength compared to PA 6 composites.

While the mechanical and thermal properties of carbon fibre-reinforced polyamides are of great significance, addressing the environmental impact of their production and use is crucial. Efforts to develop sustainable manufacturing processes, use recycled carbon fibres, and explore bio-based polyamide matrices are essential for reducing the environmental footprint of these materials while maintaining their structurally demanding characteristics. (Bhatt & Goe, 2017; Köhler et al., 2017; Yao et al., 2018; Rajak et al., 2019; Kausar et al., 2019; Alshammari et al., 2021; Wan & Takahashi, 2021) Moreover, the ability to recycle carbon fibre-reinforced polyamides at the end of their life cycle is an essential consideration for achieving environmental sustainability.

By implementing effective recycling strategies, such as pyrolysis or chemical processes, valuable carbon fibres can be recovered and reused in the production of new composites, minimizing waste and conserving resources (Allred et al., 2001; Connor et al., 2006; Howarth et al., 2009; Maia et al., 2019). Several studies have focused on improving the mechanical properties of carbon fibre-reinforced polyamide composites through various methods (Liu et al., 2004; Coleman et al., 2006; Jiang et al., 2008; Huang et al., 2009; Athreya et al., 2011; Sharma et al., 2014; Bhudolia et al., 2017). The studies have shown that carbon fibre-reinforced epoxy/polyamide composites exhibit higher mechanical properties compared to neat epoxy composites, attributing this strength to the presence of carbon fibres and their strong interfacial adhesion with the polyamide matrix (Allred et al., 2001; Wong et al., 2007a; Wong et al., 2007b).

Ajayi et al. (2025) advocate further integrating nanoscale characterization techniques and nanomaterials, such as graphene and carbon nanotubes, to improve interfacial properties and mechanical performance. The authors also highlight the emerging role of machine learning and physics-informed models in predicting composite behaviour and optimizing processing parameters, addressing limitations of empirical and experimental approaches. The review concludes by calling for more comprehensive lifecycle assessments, economic analyses, and recycling strategies to validate the environmental and commercial viability of NFRPCs. By providing a holistic view of material selection, processing technologies, and sustainability considerations, this work contributes to the advancement of bio-based composites as viable alternatives to synthetic materials in high-performance engineering applications.

2.5 Hybridization and Hybrid Composites

It has been reported in several studies that hybrid composites composed of natural and synthetic fibres can improve the thermo-mechanical properties of the composites by having the advantages of both fibre types in the composite (Panthapulakkal et al., 2005; Panthapulakkal & Sain, 2007a; Panthapulakkal & Sain, 2007b; KC et al., 2015; Hajiha & Sain, 2015; Pervaiz et al, 2016; Premnath et al., 2024). The behaviour of hybrid composites is a balance of the advantages and disadvantages of each component, in which the advantages of one type of fibre could compensate for the lack of the other. Figure 2 shows a simplified schematic of hybrid composites with randomly distributed short fibres in a polymer matrix.

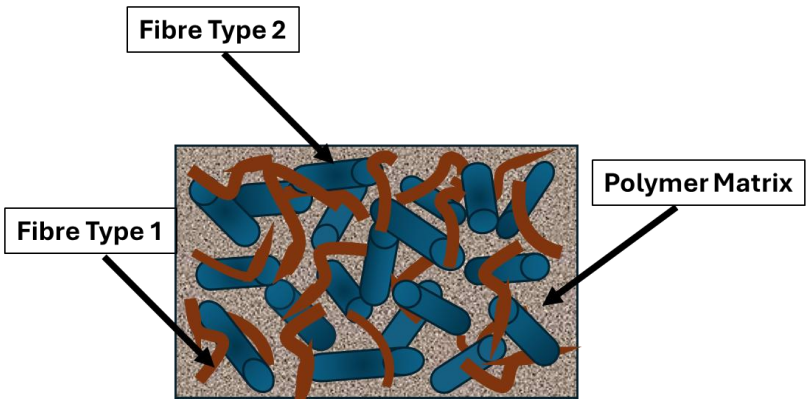

Figure 2 A Simplified Schematic of a Hybrid Composite, Composed of Two Fibre Types with Random Fibre Distribution in a Dual-fibre System

Swolfs et al. (2019) provided a comprehensive and critical review of fibre-hybrid composites, focusing on their ability to achieve mechanical performance beyond the linear combination of their constituents' properties. The authors classified fibre-hybrid composites into interlayer, intralayer, and intrayarn configurations, highlighting how the spatial distribution and interaction of distinct fibre types, such as high-strength carbon fibres and high-strain glass or natural fibres, can generate pseudo-ductile behaviour, improved impact resistance, and enhanced fatigue performance. These collaborations arise from controlled fibre fragmentation, suppression of catastrophic failure, progressive load sharing, and crack deflection at the fibre–matrix interface. The review particularly emphasized that the degree of fibre dispersion and alignment significantly influences these benefits. For instance, intrayarn hybrids offer superior cooperation due to their microscale mixing. However, they are more challenging to manufacture, while interlayer hybrids are easier to produce

but suffer from limited interaction across layers. Additionally, the authors discussed how hybrid composites enable the tailoring of other properties such as thermal stability, electrical conductivity, and vibration damping, making them attractive for advanced structural and multifunctional applications. The authors discussed recent technological advancements, including thin-ply technology, co-weaving, and aligned fibre deposition methods, which have enabled better control over fibre architecture and distribution in hybrid laminates. Successful applications in aerospace, automotive, wind energy, and sporting goods were highlighted as evidence of the growing industrial relevance of fibre-hybrid systems. However, the authors stressed that the fundamental mechanisms governing interlaminar toughness, translaminar crack growth, and progressive failure in hybrid composites remain insufficiently understood.

Chagas et al. (2022) developed and evaluated a hybrid green composite based on recycled polypropylene (rPP), dimension stone waste (Bege Bahia, BB), and coconut fibre aimed at sustainable automotive applications. Using melt processing and statistical optimization techniques, including multiple linear regression and response surface methodology, the study investigated how varying the proportions of rPP, BB, and coconut fibre affected mechanical properties such as impact resistance, hardness, and density. Results showed that the ternary composite with 70 wt% rPP, 10 wt% BB, and 20 wt% coconut fibre achieved mechanical performance closest to virgin PP, offering comparable impact resistance while incorporating 100% recycled and waste materials. SEM analysis revealed that while higher BB content introduced interfacial decohesion and increased water absorption, moderate coconut fibre content improved mechanical performance through fibre reinforcement and enhanced energy dissipation. The study concluded that coconut fibre content had a more significant positive influence on mechanical properties than stone waste. It recommended the optimized ternary formulation (70/10/20) as a promising eco-friendly material to replace virgin PP in non-structural automotive components, supporting fuel economy and emission reduction goals.

Benkhelladi et al. (2020) investigated the mechanical performance of epoxy-based polymer composites reinforced with flax, jute, and sisal fibres, individually and in hybrid combinations, aiming to optimize tensile and flexural properties through response surface methodology (RSM). Using statistical analyses including ANOVA, the study identified fibre volume fraction as the most influential parameter, followed by fibre type, while chemical treatments (NaOH and $NaHCO_3$) had

a relatively minor effect. Experimental results showed that jute fibre composites exhibited the highest tensile and flexural strengths compared to flax and sisal, with mechanical performance improving as fibre content increased from 10 wt% to 20 wt%. Sodium bicarbonate treatment yielded slightly better mechanical properties than NaOH treatment, attributed to improved fibre-matrix interfacial adhesion. Hybrid composites comprising 80% jute and 20% flax exhibited the best overall mechanical performance, surpassing those of single-fibre composites. The developed statistical models demonstrated good predictive accuracy, supporting the use of optimized natural fibre hybridization strategies to enhance the mechanical properties of sustainable polymer composites for engineering applications.

2.5.1 Hybrid natural/synthetic fibre-reinforced composites

Hybrid composites can be created by combining both natural and synthetic fibres within a single matrix. This combination enables a broader range of qualities that cannot be achieved with a single type of reinforcement (Khanam et al., 2009; Premnath et al., 2024). The subsequent sections examine the mechanical characteristics of hybrid composites of prevalent synthetic fibres (aramid, basalt, carbon, and glass) and natural fibres.

2.5.2 Hybrid aramid fibre-based composites

Rashid et al. (2011) examined the mechanical characteristics of epoxy composites reinforced with a combination of coir and Kevlar fibres. Kevlar is the proprietary name owned by the E.I. du Pont de Nemours and Company (often known as DuPont) for its para-aramid fibres. Kevlar exhibits a unique combination of exceptional strength, elevated modulus, resilience, and thermal stability.

Coconut or coir fibres are more commonly utilized as reinforcement materials because of their affordable price and favourable mechanical characteristics. The study revealed that the coir/woven Kevlar composites demonstrated the most significant impact strength, while their flexural strength was the lowest. The findings indicated that the hybrid composites consisting of woven coir yarn (warp) and Kevlar yarn (weft) exhibited a flexural strength of 16.7 MPa and an impact strength of 66.82 kJ/m^2. The findings indicate that coir fibres show great potential as reinforcements for applications requiring high-impact resistance, such as body armour.

Yahaya et al. (2016) investigated the effect of kenaf fibre orientation on the mechanical properties of hybrid aramid/kenaf-reinforced epoxy composites, focusing on their suitability for military applications. An investigation was conducted to analyze the impact of different kenaf structures, including woven, nonwoven, unidirectional (UD), and mat textiles. The simple weave structure of Aramid fabric, specifically Kevlar 129, was utilized. The nonwoven mat, kenaf/Kevlar hybrid composite, exhibited a comparatively low density due to its significant void contents. The tensile and Charpy impact strength capabilities of the woven kenaf/Kevlar composite exhibited superior performance to other hybrid composites. Conversely, the flexural strength of the hybrid composites containing the unidirectional (UD) kenaf was marginally more significant than that of the hybrid composite with woven kenaf. The scanning electron microscopy indicated that the mat kenaf hybrid composites displayed a greater void content than the woven and UD kenaf composites.

Zhong et al. (2011) investigated the effect of surface microfibrillation on the mechanical properties of phenolic composites reinforced with a combination of aramid and sisal fibres. The findings indicated that the mechanical properties of the hybrid aramid/sisal composites were significantly affected by the surface microfibrillation of the sisal fibres. The presence of microfibrils and aggregates on the surface of sisal fibres led to an increased contact area with the phenolic matrix, resulting in enhanced mechanical interlocking strength. Furthermore, the presence of microfibrils and aggregates effectively prevented the occurrence of spontaneous cracks in the composites. The hybrid composites exhibited considerable improvements in compression, tensile, and fibre/matrix interfacial bonding strengths, as well as wear resistance.

2.5.3 Hybrid basalt fibre-based composites

Petrucci et al. (2013) assessed the mechanical characteristics of composite laminates made from hybrid basalt fibres using the vacuum infusion method. Basalt fibres are derived from basalt, an igneous rock created through the solidification of volcanic lava. The basalt fibres and flax, hemp, or glass fibres were incorporated into the composites. The test findings indicated that the hybrid basalt/flax-glass composite had superior overall performance compared to all other composites studied. The hemp fibre hybrid composites exhibited a comparatively subpar layer-interface quality. Scanning electron microscopy (SEM) analysis of the hybrid composite laminates revealed

the widespread occurrence of fibre pull-out in both hemp and flax fibres. Additionally, all laminates displayed a brittle failure.

2.5.4 Hybrid carbon fibre-based composites

Nisini et al. (2016) examined the mechanical and impact characteristics of ternary hybrid composite laminates, including carbon, basalt, and flax fibres. All laminates were fabricated using the hand lay-up technique, followed by consolidation through the vacuum bagging process. Carbon-fibre layers were placed on the exterior surfaces, with basalt and flax fibre layers in between. The incorporation of flax fibre layers into basalt resulted in improved flexural and interlaminar strength. The impact performance of two laminates, which included varying arrangements of basalt and flax fibre layers, showed minimal enhancement.

Fiore et al. (2012) examined the mechanical properties of a hybrid carbon/flax/epoxy composite material intended for use in structural applications. The production of flax fabric-reinforced plastic (FFRP) laminates involved the use of two distinct bidirectional flax textiles through the vacuum bagging method. The test findings demonstrated a significant enhancement in the mechanical characteristics of the FFRP composites with the inclusion of a single external carbon-fibre layer. Hybrid carbon/flax composites are highly recommended for various applications, including the nautical and automobile industries.

In a study, Khanam et al. (2010) fabricated hybrid composites consisting of carbon/sisal fibres that were reinforced with an unsaturated polyester matrix. An assessment was conducted to determine the qualities of tensile strength, flexural strength, and chemical resistance. The tensile and flexural strength of the hybrid carbon/sisal composites exhibited a positive correlation with the carbon fibre loading as it increased. The hybrid composites with alkali-treated sisal fibres exhibited notable enhancements in their tensile and flexural properties. The chemical resistance test findings demonstrated that all hybrid composites exhibited robust resistance to all chemicals except for carbon tetrachloride (CCl_4).

Vengadesan et al. (2025) developed hybrid polylactic acid (PLA) composites reinforced with natural wood sawdust and graphite (5–20 wt.%) to improve mechanical performance and moisture resistance. Their results showed that adding 10 wt.% graphite significantly enhanced tensile,

flexural, and compressive strengths, reducing water absorption by up to 32.7% compared to sawdust-only composites. The improved performance was attributed to better filler dispersion, increased crystallinity, and enhanced interfacial bonding. However, higher graphite contents led to agglomeration and reduced impact strength. Thermal analysis confirmed improved thermal stability, a higher glass transition temperature, and higher melting temperatures with the addition of graphite. These findings position wood-graphite hybrid biocomposites as promising sustainable materials for structural and functional applications in automotive and consumer industries.

In a study by Bahrami et al. (2024), the tensile, impact, and damping performance of woven flax-carbon/PA11 hybrid biocomposites was compared to non-hybrid composites made of pure flax and pure carbon with a PA11 matrix. The findings revealed that the hybrid biocomposites demonstrated a positive hybridization effect, with higher tensile modulus and strength than pure flax, although still lower than pure carbon. It also exhibited impact resistance comparable to pure carbon, with greater displacement at maximum force, indicating increased ductility and fracture toughness. Micro-CT analysis showed that the hybrid composite experienced intermediate damage levels between the pure flax and carbon composites, allowing it to better withstand and dissipate impact energy. Moreover, the hybrid laminate displayed a 20% higher damping factor than the pure carbon composite, confirming its superior energy dissipation capacity.

2.5.5 Hybrid glass fibre-based composites

Venkatasubramanian and Raghuraman (2015) studied the mechanical properties of hybrid composites composed of abaca/banana and glass fibres reinforced with orthophthalic resins. The tensile strength of the hybrid banana-abaca/glass composites surpassed that of the abaca/glass and banana/glass composites. The banana/glass composites exhibited the maximum flexural strength, which can be attributed to the excellent adhesive capabilities of the banana fibre. The impact strength of the abaca/glass composites was the highest due to the superior strength and stiffness of the abaca fibre.

In a study by Liao et al. (2003), the long-term properties of composites made from bamboo fibres and polypropylene (BFRP) are examined, as well as those of composites made from a combination of bamboo and glass fibres with polypropylene (BGRP). The findings demonstrated that the tensile strength and tensile modulus of both BFRP and BGRP declined during prolonged exposure to

water at temperatures of 25°C and 75°C. The extent of the decrease in strength and stiffness was contingent upon the duration of exposure and the water temperature. BGRP specimens demonstrated superior resistance to the external environment in maintaining tensile strength and stiffness. The use of maleic anhydride polypropylene (MAPP) as a coupling agent in the polypropylene matrix improved the tensile strength and stiffness of the material, leading to greater interfacial bonding. Combining high-durable glass fibre and bamboo fibre was discovered to be a successful method for improving the durability of natural fibre composites when exposed to environmental aging. The fatigue performance of the hybrid glass/bamboo composites surpassed that of all composites reinforced only with bamboo fibres.

Jayabal et al. (2011) created hybrid composites by combining woven coir/glass fabric fibres that were pre-impregnated with a resin matrix. The resin matrix consisted of unsaturated orthophthalic polyester, cobalt octoate accelerator, and methyl ethyl ketone peroxide (MEKP) catalyst at a ratio of 1:0.015:0.015. Prior to being placed in the mould, a release agent consisting of polyvinyl acetate was applied to the surface of the laminates. The mechanical properties of the hybrid coir/glass composites were evaluated by considering various stacking sequences of different laminates. The glass/glass/coir and coir/glass/glass composites exhibited the highest levels of tensile, flexural, and impact strength. The hybrid composites, consisting of two plies of glass fibres, specifically the glass/glass/coir and coir/glass/glass composites, demonstrated superior breaking resistance compared to the coir/glass/coir composites, which only had a single glass ply. The coir fibres exhibited a higher rate of failure than the glass fibres, and including the glass woven fabric in the coir-fibre composites improved their mechanical characteristics. The glass fibres exhibited superior interfacial adhesion with the polyester matrix compared to the coir fibres.

The Curaua plants, scientifically known as Ananas erectifolius, are indigenous to the Brazilian Amazon region and are classified under the Bromeliaceae family. Curaua fibres possess exceptional characteristics, including favourable breaking elongation, elevated specific strength, and reduced density (Almeida et al., 2013). Almeida et al. (2012) investigated the thermal, mechanical, and dynamic mechanical properties of composites composed of a blend of curaua and glass. The findings indicated that the density of the hybrid curaua/glass composites increased in proportion to the increase in glass fibre content and the total fibre volume percentage. The addition of glass fibres to the curaua composites led to a substantial enhancement in both impact strength

and hardness. The observed phenomenon can be attributed to the inherent properties of the glass fibre, including its superior interfacial bond with the resin matrix and its greater ability to dissipate energy, as compared to the curaua fibre. The intermingled glass fibres increased the storage modulus, while the glass transition temperature remained unchanged. The study revealed that the hybrid composites containing 30% curaua fibres exhibited comparable characteristics to those reinforced solely with glass fibres.

2.6 Polymer Blends

Polymer blending is a common approach for improving the performance and properties of polymers used in various applications. It provides flexibility in combining two or more distinct individual polymers to create admixtures with varying properties. The composition, processing state, component interaction, and several other factors determine the characteristics of these blends (Park et al., 1990; Liang & Williams, 1992; Saheb et al., 1999; Piglowski et al., 2000; Thomas et al., 2006).

Polypropylene (PP) is a well-known, petroleum-based commodity polymer characterized by a simple chemical structure. The use of PP was motivated by its low cost, high availability, ease of processing, low density, hydrophobic nature, efficient recyclability, and proper chemical resistance (Saheb et al., 1999; Thomas et al., 2006). It is extensively used in high-shear processing, including extrusion and injection moulding, due to its excellent rheological properties (Saheb et al., 1999; Thomas et al., 2006; Anstey et al., 2018). PA11 has a processing temperature closest to PP among all the polyamides. (Park et al., 1990; Liang & Williams, 1992; Piglowski et al., 2000; Anstey et al., 2018). In general, blends of polyamides with polyolefins can potentially deliver a wide range of desirable characteristics, including proper chemical resistance, low water absorption, and reduced cost. Consequently, it is well-suited for an extensive range of industrial applications. PP (polypropylene), polyethylene (PE), and polyvinyl chloride (PVC) can be combined with PA11 to reduce moisture sensitivity and enhance processing efficiency. However, a low notched impact strength is a common shortcoming of these blends (Park et al., 1990; Liang & Williams, 1992; González-Montiel et al., 1995; Piglowski et al., 2000; Chow et al., 2003; Thomas et al., 2006; Jose et al., 2006; Liu et al., 2009; Battegazzore et al., 2016).

The blending of PP and PA11 can result in a material with improved tensile strength, stiffness, heat resistance, and resistance to abrasion and chemicals. This blend can also have improved thermal and mechanical properties compared to the individual polymers. The blend ratio between PP and PA11 can vary depending on the desired properties of the final material. Blending PP and PA11 can result in a material that combines the desirable properties of both polymers. The blending process can be conducted in several ways, such as melt blending, solution blending, or in situ polymerization. Melt blending is the most commonly used method, where the polymers are melted and mixed in a single or twin-screw extruder (Chow et al., 2003; Thomas et al., 2006; Jose et al., 2006; Liu et al., 2009; Battegazzore et al., 2016).

Although the use of polymer blends is known to improve the overall material properties, the chemical functionality of the polymer constituents and their relative viscosities also play essential roles in blend miscibility and compatibility (Thomas et al., 2006; Gadgeel & Mhaske, 2019). Proper performance of immiscible blends can be achieved once their components are effectively compatibilized, leading to decreased interfacial tension and increased adhesion between the two phases (Park et al., 1990; Liang & Williams, 1992; Piglowski et al., 2000; Gadgeel & Mhaske, 2019). This would result in a finer dispersed phase, better resistance to phase separation, and enhanced properties (Park et al., 1990; Liang & Williams, 1992; Piglowski et al., 2000).

Consistent dispersion in the mixture with homogeneous chain interaction is challenging due to the inherent insolubility of PA11 with commodity polymers. Many compatibilization procedures can improve the ineffective interaction between two polymers, but the reactive compatibilization process is the most widely used. Reactive compatibilization enhances the molecular interaction between polymer chains by forming a chemical bond. Reactive fillers, grafted polymers, ionomers, dynamic vulcanization, and other associated techniques are among the methods covered. All these techniques have a greater chance of enhancing the interaction for non-miscible polymers, such as polyamide and polypropylene (PP) (Piglowski et al., 2000; Gadgeel & Mhask, 2019).

Compatibilization of immiscible blends can be achieved by introducing a graft or block copolymer of a similar chemical structure (compatibilizer), which contains parts capable of specific interactions and/or chemical reactions with the blend components. These compatibilizers can be added as a third constituent in the polymer blend or generated in situ during the melt-compounding

process (Park et al., 1990; Liang & Williams, 1992; Piglowski et al., 2000; Liu et al., 2009; González-Montiel et al., 1995; Thomas et al., 2006). Polypropylene can be modified by grafting functional groups, enabling blending with polar polymers, such as polyamides (Endres & Siebert-Raths, 2011; Ozen et al., 2013). Blends of polyamide and polypropylene are commonly compatibilized by maleic and acrylic acid-grafted polypropylenes (Park et al., 1990; Liang & Williams, 1992; Piglowski et al., 2000; Liu et al., 2009; González-Montiel et al., 1995). Specifically, maleic anhydride polypropylene (MAPP) in PA/PP systems shows high compatibility between PA due to hydrogen bonding with amine and carboxyl end-groups and amide linkages and PP due to van der Waal forces between the carbon-carbon chains (Jose et al., 2006).

The consistent distribution of one polymeric phase within another is evident when various methods are combined. The kind of mechanism described by Kemmer et al. (1982), which comprises the entanglement mechanism, globule break-up mechanism, coalescence mechanism, and crosslinking mechanism, can improve the uniform distribution of immiscible liquids. Among these, globule rupture and coalescence are more significant since they are entirely focused on chain crystallization (Thomas et al., 2013). It is well known that the interfacial tension applied to one phase during the crystallization of distinct polymer phases in the mixture affects how the chains form globules, resulting in the globule splitting into smaller pieces. The size and form of those pieces are entirely determined by the pressure gradient surrounding the droplet, resulting from the neighbouring phase and the viscous force acting on it (Utracki & Shi, 1992).

Low viscous force and pressure levels cause less globule breakage, reducing the possibility of establishing a uniform distribution. The coalescence mechanism, which includes the collision of two phases at different speeds, is precisely the reverse. The melt mixing process utilized to join the two polymers has variable velocities. When molten polymers compress into one another under shear, they generate a coalescence structure. Vermant et al. (2004) employed this approach to enhance the compatibility between polydimethylsiloxane and polyisobutylene.

Elemans et al. (1990) state that more particles or chains become available for collision when the dispersed phase grows. As a result, there is less interfacial tension, reducing the size of the dispersed phase while increasing phase adhesion. Furthermore, they claim that the influence may be more precise when the compatibilizer is present.

Another strategy indicated in the state of the art is the employment of compatibilizers to introduce the stabilized co-continuous phase into blends, hence lowering interfacial tension inside the insoluble polymers (Huneault & Li, 2007; Wang et al., 2011). In the polymeric melt, the compatibilizer inhibited inter-droplet circulation and prevented the polymeric interface from moving, causing one phase to transition into another and form a co-continuous phase (Van Puyvelde et al., 2002).

According to Zanjanijam et al. (2016), the PP-g-MA compatibilizer causes the immiscible polymer chains to form an entangled structure during reactive compatibilization, enhancing the blend's miscibility. As a result, it is more challenging to achieve compatibilization if the dispersed phase is not evenly distributed throughout the structure. This is because the reaction depends on where the other polymeric phase reacts with it.

Liang and Williams (1992) studied the effect of compatibilization on the dynamic mechanical properties of the PA11/PP blend. They reported that the compatibilized blends exhibited an effectively dispersed morphology and proper adhesion between the two phases, especially when the components were proportioned in equal amounts. Liu et al. (2009) compared the conventional PP/PA6 flame retardant with their newly developed PP/PA11 flame retardant. They reported that the latter showed improved mechanical performances (tensile and Izod notched impact strength). In general, PA6 exhibits better mechanical properties compared to PA11 due to the presence of more amide groups in its chains. However, its poorer compatibility with PP might be responsible for this effect (Liu et al., 2009). Adding MAPP compatibilizer (5%) further enhanced the mechanical properties of both flame retardants (Liu et al., 2009). Compared to PA6, PA11 has longer alkyl segments in its chain unit, showing better compatibility with PP. In addition, PA11 has a lower melting point, similar to that of PP, which facilitates more effective blending with PP in the melt state and, consequently, better dispersion in the PP matrix (Liang & Williams, 1992; Liu et al., 2009). Jose et al. (2006) studied the morphology of a PA12/PP blend in the presence and absence of MAPP, reporting that the compatibilized blend showed a significant decrease in the diameter of the dispersed phase. Mechanical testing also showed increased stiffness and decreased elongation at breakage using compatibilizers (Jose et al., 2006).

2.7 Predictive Modelling of Hybrid Composites

This section presents an extensive overview of the most current modelling strategies used to investigate hybrid composites. A wide range of studies have explored the mechanical, thermal, and interfacial behaviour of these materials using analytical, numerical, micromechanical, and hybrid techniques.

Bakamal et al. (2021) examined the bending, vibration, and buckling responses of carbon–basalt hybrid laminates using a refined higher-order shear deformation theory. The model incorporated zig-zag functions to accurately simulate interlaminar stresses and captured the influence of fibre stacking sequences on mechanical performance. The study showed that hybridization enhances stiffness and cost-effectiveness, making it suitable for lightweight structural applications. However, the model assumed perfect bonding and linear elastic behaviour, neglecting interfacial degradation, progressive damage, and environmental effects.

Madan et al. (2025) developed a two-step methodology combining micromechanical modelling and finite element analysis (FEA) to predict the thermomechanical properties of hybrid metal matrix composites. The study focused on two-phase (Al–SiC) and three-phase (Al–SiC–B_4C) systems, evaluating their elastic modulus, coefficient of thermal expansion (CTE), thermal conductivity, and density. The modelling strategy involved generating representative volume elements (RVEs) with unidirectional and random particle geometries, applying periodic boundary conditions, and subjecting them to multi-loading simulations. The Halpin-Tsai model was employed analytically, while convergence and anisotropy were verified numerically. Results demonstrated the significant impact of ceramic volume fraction and particle configuration on effective properties. While the method offers high prediction accuracy, assumptions of isotropic inclusions and perfect interfaces reduce model fidelity in realistic systems featuring agglomeration or interfacial weakness.

Chichane et al. (2023) provided a detailed comparative analysis between analytical micromechanical models and finite element simulations for estimating the mechanical behaviour of hybrid composites of PP-based composites reinforced with alfa fibres and nano clay. The study evaluated three models (Rule of Mixtures, Halpin-Tsai, and Mori-Tanaka) against FEA results for different hybrid systems involving synthetic and natural fibres. The models were assessed for their

capability to predict tensile strength, stiffness, and modulus of elasticity. The research highlighted that while analytical models could approximate global behaviour trends, they often underestimated or overestimated stiffness and strength in hybrid systems with distinct constituent mismatches. While some analytical models performed adequately at low filler content, their accuracy deteriorated at higher loadings due to nonlinear filler interactions. The finite element method proved more reliable in capturing interfacial effects and fibre-matrix interactions. However, the study acknowledged computational complexity and mesh dependency as limitations of numerical methods, especially for anisotropic and random fibre orientations. The study highlighted the need to incorporate fibre orientation, dispersion, and interfacial debonding into predictive frameworks.

Liu and Wei (2021) introduced a dynamic hybrid shear-lag model to study stress transfer and damping in viscoelastic composites under transient loads. Their model deviated from traditional quasi-static shear-lag assumptions by incorporating dynamic stress distributions and viscoelastic matrix behaviour through a Kelvin–Voigt formulation. The hybrid system modelled consisted of two linear-elastic fibres with different stiffnesses but equal linear densities, alternately arranged and bonded by a thin viscoelastic matrix. The study concluded that pairing reinforcements of identical linear densities but contrasting stiffnesses could optimize energy dissipation while minimizing energy concentration within the matrix. This approach enhanced the understanding of impact behaviour and strain-rate sensitivity. Nevertheless, the model assumed perfect fibre–matrix bonding and linear viscoelasticity, ignoring interfacial failure, nonlinear friction, and matrix yielding.

Scheuring et al. (2024) investigated hybrid long fibre-reinforced thermoplastics composed of carbon fibre (CF) and glass fibre (GF) in a PA6 matrix using a combination of experimental characterization and multiscale homogenization. High-resolution micro-computed tomography (μCT) was employed to extract real fibre orientation tensors from representative sample regions. These orientation tensors were then used to inform multiscale mechanical property predictions through homogenization techniques. The study revealed significant variability in mechanical properties based on local fibre orientation and type, underscoring the limitations of assuming isotropic or ideal fibre distribution. This methodology bridges the gap between real microstructure and mechanical performance predictions. However, the approach is computationally intensive and

highly dependent on accurate μCT imaging and segmentation, which may not be feasible for large-scale or highly heterogeneous systems

Koutroumanis et al. (2024) investigated the interfacial performance of epoxy composites hybridized with carbon fibres and graphene nanoplatelets (GNPs). Raman spectroscopy and FEA showed that GNP alignment significantly enhanced interfacial shear strength and load transfer. This work offers a multiscale perspective on interface reinforcement, though it lacks consideration of fatigue, moisture effects, and real-world processing variability.

Miled et al. (2024) applied a viscoplastic constitutive model to flax–hemp fibre PP composites to evaluate strain-rate sensitivity. Experimental validation showed increased ductility and energy absorption in hybrid configurations. The model, however, treated the composite as homogeneous and did not account for fibre architecture, orientation, or interfacial degradation.

Meng and Wang (2014) developed a shear-lag-based micromechanical model for fibre debonding and pull-out in brittle matrix composites. The model accounted for different debonding stages but was limited by assumptions of perfectly aligned cylindrical fibres and brittle, non-yielding matrices. It did not capture interfacial friction, fibre entanglement, or matrix reinforcement, making it less suitable for modern thermoplastic hybrid systems.

Atmakuri et al. (2022) investigated the mechanical performance of flax–hemp hybrid composites using both epoxy and bio-based Eco Poxy matrices. The study combined experimental tensile, flexural, and impact testing with predictive modelling based on Halpin–Tsai equations and finite element analysis (FEA). Hybridization of the natural fibres demonstrated improvements in both strength and ductility, validating the synergistic potential of combining flax and hemp in a polymer matrix. While the study contributed valuable insights into matrix-dependent behaviour and the sustainability advantages of bio-resins, its modelling framework was limited in scope. Specifically, it did not incorporate microstructural details such as fibre orientation, dispersion, or interfacial bonding, reducing its capacity to predict fatigue behaviour or failure under complex loading conditions.

Sung et al. (2021) developed a micromechanical model to simulate the compressive failure behaviour of hybrid laminates composed of carbon fibre reinforced polymer (CFRP) and steel

layers. The model extended the classical shear-lag theory by integrating Weibull statistical functions to account for interfacial strength variability. The approach successfully predicted the onset of fracture and captured the effect of compressive transverse stress on load transfer across the interface. However, the model assumed perfect fibre alignment and brittle, non-degrading interfaces, failing to account for fibre waviness, long-term environmental effects, or fatigue behaviour. These oversights limit its reliability for durability prediction or crash performance in automotive or aerospace applications.

Han et al. (2023) proposed a virtual testing framework for aligned discontinuous fibre-reinforced composites, employing stochastic generation of representative volume elements (RVEs) to simulate the influence of fibre aspect ratio, orientation, and distribution on mechanical response. This computational approach enabled the exploration of statistical variability across composite samples and captured mesostructural heterogeneity more effectively than deterministic models. Nevertheless, the high computational cost associated with stochastic modelling and the absence of progressive damage or failure criteria constrain its practicality for early-stage material design or long-term performance prediction.

Chagas et al. (2022) studied hybrid composites based on recycled polypropylene (rPP) filled with coconut fibres and dimension stone waste, focusing on optimizing mechanical performance for sustainable automotive applications. Using regression analysis and response surface methodology (RSM), the study identified optimal filler proportions for maximizing tensile and flexural properties. While the research emphasized low-cost reinforcement strategies and circular economy principles, the modelling approach was purely statistical. It did not account for microstructural effects such as fibre–matrix adhesion, porosity, or moisture uptake, factors that are essential for predicting real-world durability and long-term mechanical integrity.

Hage (2024) combined self-consistent modelling with neural networks to predict modulus in porous ABS composites. They proposed a hybrid modelling approach that integrates a physics-based analytical homogenization model, the Generalized Stiffness Formulation (GSF), with a regression-type artificial neural network (ANN) to improve the predictive accuracy of the longitudinal elastic modulus in composite materials containing void inclusions. The study focused on ABS plastic composites with systematically varied inclusion volume fractions, shapes, and

orientations, which were fabricated via high-precision 3D printing and tested under uniaxial compression. While the GSF model analytically captured the influence of microstructural features, it exhibited notable discrepancies compared to experimental data. To address this, the ANN was trained on the error between the GSF predictions and experimental results and subsequently used to correct the theoretical outputs. This hybrid model significantly outperformed both the standalone ANN and GSF methods, achieving a mean squared error of 3.5 and an R^2 of 0.9988, substantially reducing predictive error across all test scenarios. The findings highlight the benefits of hybrid frameworks in composite modelling by combining the physical reliability of analytical methods with the pattern-recognition capabilities of data-driven tools, thereby improving the reliability of modulus predictions in heterogeneous materials. Although this hybrid model improved accuracy, it was data-dependent and lacked generalizability across materials and void morphologies.

Wang et al. (2024) investigated the dynamic mechanical behaviour of hybrid flax/basalt fibre-reinforced polymer composites (F/BFRP) under varying fibre ratios and loading frequencies. The study combined experimental characterization with two complementary predictive approaches: a fractional calculus-based viscoelastic model and a physics-informed neural network (PINN). The fractional calculus model provided a physically grounded framework that accurately captures the frequency-dependent storage modulus, loss modulus, and loss factor with minimal parameters, exhibiting excellent agreement with experimental data. A PINN model was developed to further improve prediction accuracy and reduce reliance on complex parameter fitting by integrating physical constraints derived from the fractional model into the neural network training process. The PINN demonstrated superior generalization and predictive performance, especially when trained on limited experimental datasets. Results highlighted the significant influence of both frequency and fibre composition on the anisotropic dynamic properties of F/BFRP, with basalt fibres enhancing stiffness and flax fibres improving damping behaviour. The use of PINNs also enabled data-efficient learning from limited experimental datasets. However, the fractional model's parameters lacked intuitive physical interpretation, and the absence of structural-scale failure analysis or damage modelling limited the method's applicability for structural design under complex loading scenarios.

Rajput and Jana (2025) proposed a multi-scale micromechanical modelling framework to predict the elastic behaviour of nano-coated carbon fibre-reinforced hybrid composites (NCRHC), accounting for both interfacial and agglomeration effects. By coupling a mean-field theory with a 3D mechanics of materials approach, the model captures the non-linear interactions between carbon nanotube (CNT) coatings, fibres, and the surrounding matrix. Unlike conventional micromechanical models, which often overestimate stiffness by neglecting critical phenomena such as CNT waviness, interfacial debonding, and agglomeration effects, this model integrates these phenomena through parametric descriptions of CNT aspect ratio, interface thickness, and agglomeration parameters. Validation against experimental data demonstrated improved prediction accuracy over traditional models such as Mori–Tanaka and finite element methods, particularly in capturing the optimal CNT concentration beyond which mechanical performance deteriorates due to poor dispersion and stress localization. The model highlighted that while increasing CNT content initially enhances stiffness, excessive concentrations lead to agglomeration-induced weakening, emphasizing the need for optimized nano-coating strategies. This multi-scale framework provides valuable insights into the design of hybrid composites with enhanced mechanical properties for structural applications, while underscoring the importance of considering coupled interfacial and dispersion effects, factors that are similarly overlooked in traditional analytical models, including classic shear-lag formulations.

Sathish et al. (2025) investigated the mechanical optimization of basalt/glass fibre-reinforced polymer composites enhanced with multi-walled carbon nanotubes and silicon dioxide (SiO_2) hybrid nanofillers. Using response surface methodology (RSM), the study systematically evaluated the effects of three processing parameters, filler weight (0–2 wt%), moulding pressure (5–15 MPa), and sonication time (10–30 minutes), on the tensile strength and elongation at break of the composites. Through a Box–Behnken design of experiments, predictive quadratic models were developed and validated, achieving high statistical significance with R^2 values exceeding 99%. The optimal mechanical performance was achieved with 1 wt% hybrid nanofiller, 15 MPa moulding pressure, and 30 minutes of sonication, resulting in a tensile strength of 267 MPa and an elongation at failure of 2.25%. Scanning electron microscopy (SEM) confirmed improved interfacial bonding and uniform nanofiller dispersion at optimal conditions. However, higher filler loadings (2 wt%) led to agglomeration and a reduction in mechanical performance. The study

highlights the importance of optimizing processing parameters and incorporating nanoscale reinforcement to improve stress transfer and interfacial adhesion in hybrid composites. It also demonstrates the utility of statistical modelling for material design, while implicitly revealing the limitations of such empirical approaches in providing physically generalized or mechanistically interpretable insights.

Tan et al. (2025) coupled cohesive zone and continuum damage modelling to simulate delamination in over-moulded glass-fibre PP hybrids. They investigated the mechanical behaviour of over-moulded hybrid thermoplastic composites, specifically an anti-collision beam made by over-moulding short glass fibre-reinforced polypropylene (SGFR-PP) onto a continuous glass fibre-reinforced polypropylene (CGFR-PP) laminate. Experimental characterization included tensile, bending, double cantilever beam (DCB), end-notched flexure (ENF), and single lap shear (SLS) tests to evaluate the material and interfacial properties. The measured Mode I (GIC) and Mode II (GIIC) fracture toughness values were 0.2023 kJ/m² and 0.4351 kJ/m², respectively. A continuum damage model based on the Tsai-Wu criterion and a cohesive zone model were implemented in Abaqus/Explicit to simulate damage initiation and propagation.

The finite element model accurately predicted the tensile and bending behaviour with an error of less than 5% in maximum load, demonstrating good agreement with the experimental results. The study highlighted that the interface failure occurred concurrently with matrix failure, confirming the effectiveness of the over-moulding process in achieving robust interfacial bonding. This combined experimental and numerical framework provides valuable insights for designing structurally integrated, lightweight thermoplastic composite components for automotive safety applications. The model captured crash-relevant failure but required complex parameter calibration and was limited to specific geometries and fibre configurations (Tan et al., 2025).

Ferdousi et al. (2023) developed and characterized 3D-printed lightweight hybrid composites made of a soft polydimethylsiloxane (PDMS) matrix reinforced with glass microfibres and hollow thin-shell microparticles. The composites were fabricated via direct ink writing and evaluated using a combined approach involving experimental testing, theoretical mechanics modelling, and image-driven convolutional neural network (CNN) machine learning. Statistical analysis using the Taguchi method and ANOVA identified printing direction (45.3% contribution) and fibre volume

fraction (57.7% contribution) as the most influential parameters on stiffness and strength, respectively. A hybrid mechanics model, integrating Weibull statistics with classical single-filler models, captured trends in mechanical performance but consistently overestimated experimental results due to idealized assumptions that neglected microstructural variability.

To overcome this, an image-driven CNN model was developed using 616 microstructural images, which enabled the prediction of mechanical properties with a 48.6% lower root mean square error compared to the theoretical model. The CNN model effectively captured local defects, geometric imperfections, and filler distributions directly from microscopy images, offering more accurate and robust predictions. Mechanical testing confirmed significant improvements in stiffness, strength, and impact performance of the hybrid composites compared to neat PDMS. Demonstration tests showed that the hybrid composites absorbed more impact energy and offered higher structural integrity under dynamic loading, highlighting their potential for protective and lightweight engineering applications (Ferdousi et al., 2023).

Shoja et al. (2021) employed statistical modelling and response surface methodology to optimize mechanical performance in starch–rice straw biocomposites. They applied hybrid mathematical modelling based on Response Surface Methodology (RSM) combined with Desirability Function Analysis (DFA) to model and optimize the mechanical performance of starch-based biocomposites reinforced with chemically modified rice straw fillers. The modelling effort involved constructing reduced quadratic and linear mixture regression models to predict four mechanical responses: Young's modulus, tensile strength, elongation at break, and absorbed energy. These models were based on D-optimal design of experiments, which allowed reducing the number of required experimental runs while maintaining high statistical reliability.

Each response was modeled as a polynomial function of the content of three fillers: benzylated rice straw, rice straw pulp, and benzylated rice straw pulp. The model equations included linear and interaction terms, capturing the influence of individual and combined filler effects. The model fitting was evaluated using ANOVA, yielding high R^2 values (up to 99%) for most responses, which validated the model's predictive capability. For multi-objective optimization, the Derringer-Suich desirability function was employed to convert multiple response surfaces into a single overall desirability index, allowing for the identification of optimal filler compositions that balance

stiffness, strength, ductility, and energy absorption. This approach provided a quantitative decision-making tool to guide the formulation of high-performance biodegradable composites from agricultural waste. While the approach improved tensile, flexural, and impact strength, it remained empirical, lacking mechanistic modelling of fibre–matrix interactions, debonding, or failure evolution.

A review by Swolfs et al. (2019) identified significant modelling and characterization gaps that hinder the full exploitation of hybrid composites in engineering applications. While conventional micromechanical models, including the rule of mixtures and shear-lag-based theories, provide baseline estimations of mechanical properties, they often fail to capture the non-linearities and interfacial complexities introduced by hybridization. Specifically, the assumption of perfect fibre–matrix bonding and uniform stress distribution limits their predictive accuracy, especially when dealing with natural fibres that exhibit inherent variability in geometry, surface chemistry, and mechanical properties. The authors noted that experimental deviations from theoretical predictions are often observed due to fibre clustering, agglomeration, and imperfect dispersion, which traditional models do not account for. Furthermore, although finite element analysis (FEA) and cohesive zone models have advanced the understanding of damage and failure mechanisms, these methods require extensive material characterization and high computational resources, making them less practical for early-stage design or material screening. This highlights the urgent need for refined semi-empirical models to bridge the gap between physical realism and practical applicability, particularly for hybrid composites that combine synthetic and bio-based reinforcements.

These studies illustrate the diversity of modelling techniques applied to hybrid composites and the need for more physically representative, multiscale, and interface-aware models, especially in systems involving short, discontinuous, and multi-axially aligned reinforcements. The development of multi-scale experimental datasets and validated predictive models has been emphasized as essential for advancing the design and broader implementation of hybrid composites in complex and demanding applications. This identified gap motivates this thesis, which aims to improve the predictive capability of shear-lag models by introducing semi-empirical and analytical modifications. These modifications better account for the multi-phase interactions,

interfacial stress transfer, and effective matrix behaviour in hybrid composites reinforced with cellulose microfibres and carbon fibres.

2.8 References

Adak, N C., Chhetri, S., Murmu, N C., Samanta, P., & Kuila, T. (2018). Effect of Thermally Reduced Graphene Oxide on Mechanical Properties of Woven Carbon Fibre/Epoxy Composite. Crystals, 8(3), 111–111.

Adelodun, A. A. (2021). Plastic recovery and utilization: From ocean pollution to green economy. *Frontiers in Environmental Science, 9*, 683403.

Afrinaldi, F., & Mat Saman, M. Z. (2008). The evaluation methods of disassemblability for automotive components - A review and agenda for future research. *Jurnal Mekanikal, 26*, 49-62.

Ajayi, O. O., Odeshi, A. G., & Szpunar, J. A. (2025). A comprehensive review of natural fibre reinforced polymer composites as emerging materials for sustainable applications. *Journal of Cleaner Production, 431*, 138969.

Alberti, C., Figueira, R., Hofmann, M., Koschke, S., & Enthaler, S. (2019). Chemical recycling of end-of-life polyamide 6 via ring closing depolymerization. *ChemistrySelect, 4*(43), 12638-12642.

Allred, R.E., Gosau, J.M., Shoemaker, JM, 2001. Recycling process for carbon/epoxy composites. In: SAMPE 2001 Symposium & Exhibition. SAMPE, Longbeach, CA, USA.

Allen, B., Connor, M., Heil, J., Cuomo, J., George, P. E., & Carberry, W. L. (2006). Recycled carbon fibre analysis: Morphological and chemical characterization. Paper presented at the International SAMPE Technical Conference

Alshammari, B A., Alsuhybani, M., Almushaikeh, A M., Alotaibi, B M., Alenad, A M., Alqahtani, N B., & Alharbi, A G. (2021). Comprehensive Review of the Properties and Modifications of Carbon Fibre-Reinforced Thermoplastic Composites. Polymers, 13(15), 2474-2474.

Akonda, M. H., Lawrence, C. A., & Weager, B. M. (2012). Recycled carbon fibre-reinforced polypropylene thermoplastic composites. Composites Part A, 43(1), 79-86.

Ahn, S., Yan, Y., & Jeon, H. -. (2020). Effect of maleic anhydride-grafted polypropylene on recycled carbon fibre reinforced polypropylene. Polymer (Korea), 44(1), 109-115. doi:10.7317/pk.2020.44.1.109

Anstey, A., Codou, A., Misra, M., & Mohanty, A. K. (2018). Novel compatibilized nylon-based ternary blends with polypropylene and poly (lactic acid): Fractionated crystallization phenomena and mechanical performance. *ACS Omega, 3*(3), 2845–2854.

Anthony, C., & Cheung, W. M. (2017). Cost evaluation in design for end-of-life of automotive components. *Journal of Remanufacturing, 7*(1), 97-111.

Arkema. (2023). *Rilsan® Polyamide 11: Sustainable and high-performance*. Retrieved from https://www.arkema.com

Arkema. (2024). *Virtucycle®: Sustainable PA11 and PA12 recycling program*. Retrieved from https://www.arkema.com

Armioun, S., Panthapulakkal, S., Scheel, J., Tjong, J., & Sain, M. (2016a). Biopolyamide hybrid composites for high performance applications. *Journal of Applied Polymer Science, 133*(27).

Armioun, S., Panthapulakkal, S., Scheel, J., Tjong, J., & Sain, M. (2016b). Sustainable and lightweight biopolyamide hybrid composites for greener auto parts. *Canadian Journal of Chemical Engineering, 94*(11), 2052-2060.

Armioun, S., Pervaiz, M., & Sain, M. (2017). Biopolyamides and high-performance natural fibre-reinforced biocomposites. In *Handbook of Composites from Renewable Materials* (pp. 253-270).

Arpitha, G.R., Sanjay, M.R., and Yogesha, B. (2014). Review on Comparative Evaluation of Fibre Reinforced Polymer Matrix Composites. Advanced Engineering and Applied Sciences An International Journal, 4, 44-47.

Athreya, S. R., Kalaitzidou, K., & Das, S. (2011). Mechanical and microstructural properties of Nylon-12/carbon black composites: Selective laser sintering versus melt compounding and injection moulding. *Composites Science and Technology, 71*(4), 506-510.

Anstey, A., Codou, A., Misra, M. & Mohanty, A. K. (2018). Novel Compatibilized Nylon-Based Ternary Blends with Polypropylene and Poly (lactic acid): Fractionated Crystallization Phenomena and Mechanical Performance. *ACS Omega, 3*(3), 2845–2854.

Atmakuri, A., Palevičius, A., Vilkauskas, A., & Janušas, G. (2020). Review of Hybrid Fibre Based Composites with Nano Particles—Material Properties and Applications. *Polymers., 14*(13), 2612.

Aydemir, D., Kiziltas, A., Erbas Kiziltas, E., Gardner, D. J., Gunduz, G., 2015. Heat-treated wood–nylon 6 composites. *Composites Part B,* 68, 414-423.

Bahrami, M., Butenegro, J.A., Mehdikhani, M., Swolfs, Y., Abenojar, J., Martinez, M.A. (2024). Tensile, impact, and the damping performance of woven flax-carbon hybrid polyamide biocomposites. *Polymer Composites*. 45(5): 3901–3917.

Bakamal, A., Ansari, R., & Hassanzadeh-Aghdam, M. K. (2021). Bending, free vibration, and buckling responses of chopped carbon fibre/graphene nanoplatelet-reinforced polymer hybrid composite plates: An inclusive microstructural assessment. *Proceedings of the Institution of Mechanical Engineers, 235*(8), 1455–1469.

Balla, V. K., Kate, K. H., Satyavolu, J., Singh, P., & Tadimeti, J. G. D. (2019). Additive manufacturing of natural fibre reinforced polymer composites: Processing and prospects. *Composites Part B: Engineering, 174*, 106956.

Bascom, W. D. (1987). In Drzal L. T. Drzal, Hercules Aerospace, Langley Research Center, and Michigan State University. (Eds.), The surface properties of carbon fibres and their adhesion to organic polymers. Hampton, Va: Langley Research Center.

Benkhelladi, A., Laouici, H., & Bouchoucha, A. (2020). Tensile and flexural properties of polymer composites reinforced by flax, jute and sisal fibres. *The International Journal of Advanced Manufacturing Technology, 108*(3-4), 895–916.

Bhatt, P., & Goe, A. (2017). Carbon Fibres: Production, Properties and Potential Use. Material Science Research India, 14(1), 52–57.

Bhudolia, S. K., Perrotey, P., & Joshi, S. C. (2017). Optimizing Polymer Infusion Process for Thin Ply Textile Composites with Novel Matrix System. *Materials, 10*(3), 293-293.

Bijwe, J., & Rattan, R. (2007a). Carbon fabric reinforced polyetherimide composites: Optimization of fabric content for best combination of strength and adhesive wear performance. *Wear, 262*(5-6), 749-758.

Bijwe, J., Rattan, R., & Fahim, M. (2007b). Abrasive wear performance of carbon fabric reinforced polyetherimide composites: Influence of content and orientation of fabric. *Tribology International, 40*(5), 844-854.

Bilym, P., Rogozin, A. D., Firsov, P., & Zolotov, S. (2021). Carbon fibre plastics for vehicles manufactured by resource-saving formation technology. IOP Conference Series: *Materials Science and Engineering, 1021*(1), 012034-012034.

Billah, M. M., Rabbi, M., & Hasan, A. (2021). A review on developments in manufacturing process and mechanical properties of natural fibre composites. *Journal of Engineering Advancements, 2*(01), 13–23.

Biswas, S., Satapathy, A., & Patnaik, A. (2010). A comparative study on wear properties of ferrous composites containing natural fibres. *Wear, 268*(11-12), 1355–1363.

Błędzki, A. K., Reihmane, S., & Gassan, J. (1996). Properties and modification methods for vegetable fibres for natural fibre composites. *Journal of Applied Polymer Science, 59*(8), 1329-1336.

Bledzki, A. K., Faruk, O., & Sperber, V. E. (2006). Cars from bio-fibres. *Macromolecular Materials and Engineering, 291*(5), 449–457.

Błędzki, A. K., Seidlitz, H., Gorący, K., Urbaniak, M., & Rösch, J. (2021). Recycling of Carbon Fibre Reinforced Composite Polymers—Review—Part 1: Volume of Production, Recycling Technologies, Legislative Aspects. Polymers, 13(2), 300-300.

Botelho, E C., Scherbakoff, N., Rezende, M C., Kawamoto, A M., & Sciamareli, J. (2001). Synthesis of Polyamide 6/6 by Interfacial Polycondensation with the Simultaneous Impregnation of Carbon Fibres. Macromolecules, 34(10), 3367-3375.

Botelho, E. C., Figiel, L, Rezende, M. C., & Lauke, B. (2003). Mechanical bahaviour of carbon fibre reinforced polyamide composites. *Composites Science and Technology, 63*(13), 1843-1855.

Brehmer, B., (2014). Polyamides from biomass derived monomers, in: *Bio-based plastics: Materials and Applications,* Kabasci, S. (1st Ed.), pp. 275-293, John Wiley & Sons Ltd, Marl.

Caba, A C., Loos, A C., & Batra, R. (2007). Fibre–fibre interactions in carbon mat thermoplastics. Composites Part A: Applied Science and Manufacturing, 38(2), 469-483.

Cabalova I, Ház A, Krilek J, Bubeníková T, Melicherčík J, Kuvik T. Recycling of Wastes Plastics and Tires from Automotive Industry. Polymers (Basel). 2021 Jul 3;13(13):2210.

Cai, J Y., McDonnell, J., Brackley, C., O'Brien, L J., Church, J S., Millington, K R., Smith, S., & Phair-Sorensen, N. (2016). Polyacrylonitrile-based precursors and carbon fibres derived from advanced RAFT technology and conventional methods – The 1st comparative study. Materials Today Communications, 9, 22-29.

Carbon fibres (1998). In Donnet J. (Ed.), (3rd ed., rev. and expanded. ed.). New York: Marcel Dekker.

Chagas, G. N., Barros, M. M., Leão, A. G., Tapanes, N. L. C. O., Ribeiro, R. C. C., & Bastos, D. C. (2022). A hybrid green composite for automotive industry. *Polímeros: Ciência e Tecnologia*, 32(2), e2022017.

Chagas, G. N., et al. (2022). A comprehensive review of natural fibre reinforced polymer composites as emerging materials for sustainable applications. *Polymer Composites, 43*(12), 5223–5245.

Chandekar, G. S., & Rathod, P. P. (2020). Characterization of natural fibre reinforced polymer composites: An overview. *Test Engineering and Management, 83*, 2249–2256.

Chen, C., & Chen-Chi, M. (1992). Pultruded fibre reinforced blocked polyurethane (PU) composites. I. Processability and mechanical properties. *Journal of Applied Polymer Science,* 46(6), 937–947.

Chen, H., Cai, Q., Wu, J., Xia, X., Liu, H., & Zhanjun, L. (2018). Interfacial enhancement of carbon fibre/nylon 12 composites by grafting nylon 6 to the surface of carbon fibre. *Applied Surface Science,* 441, 538–545.

Chichane, A., Boujmal, R., & El Barkany, A. (2023). A comparative study of analytical and numerical models of mechanical properties of composites and hybrid composites reinforced with natural reinforcements. *Polymers & Polymer Composites., 31*

Choi, Y., Sugimoto, K., Song, S., & Endo, M. (2006). Production and characterization of polycarbonate composite sheets reinforced with vapor-grown carbon fibre. *Composites Part A: Applied Science and Manufacturing*, 37(11), 1944-1951.

Coleman, J. N., Khan, U., & Gun'ko, Y. K. (2006). Mechanical Reinforcement of Polymers Using Carbon Nanotubes. Advanced Materials, 18(6), 689-706.

Connor, M., Allen, B., Heil, J., Cuomo, J., George, P. E., & Carberry, W. L. (2006). Recycled carbon fibre analysis: Mechanical properties. Paper presented at the International SAMPE Technical Conference

Corrêa, A. C., de Morais Teixeira, E., Carmona, V. B., Teodoro, K. B. R., Ribeiro, C., Mattoso, L. H. C., Marconcini, J. M., 2014. Obtaining nanocomposites of polyamide 6 and cellulose whiskers via extrusion and injection moulding. *Cellulose*, 21(1), 311-322.

Côté, J., Berthiaume, P., & Leduc, R. (2013). Moisture uptake in polyamides: A comparative study. *Polymer Testing, 32*(8), 1461–1472.

Das, O., Neisiany, R. E., Capezza, A. J., Hedenqvist, M. S., Försth, M., Sas, G., ... & Berto, F. (2020). The pursuit of greener composites: A review on the role of natural fibre reinforcement in polymer matrices for structural and non-structural applications. *Polymer Testing, 81*, 106283.

Das, P. P., Chaudhary, V., Ahmad, F., Manral, A., Gupta, S., & Gupta, P. (2021). Acoustic performance of natural fibre reinforced polymer composites: Influencing factors, future scope, challenges, and applications.

Dahlke, B., Larbig, H., Scherzer, H. D., & Poltrock, R. (1998). Natural Fibre Reinforced Foams Based on Renewable Resources for Automotive Interior Applications. Journal of Cellular Plastics, 34(4), 361-379.

De Arcaya, P. A., Retegi, A., Arbelaiz, A., Kenny, J. M., & Mondragon, I. (2009). Mechanical properties of natural fibres/polyamides composites. *Polymer Composites, 30*(3), 257–264.

Delmonte, J. (1981). Technology of carbon and graphite fibre composites. New York: Van Nostrand Reinhold.

Dhakal, H. N., Zhang, Z. Y., & Richardson, M. O. W. (2007). Effect of water absorption on the mechanical properties of hemp fibre reinforced unsaturated polyester composites. *Composites Science and Technology, 67*(7-8), 1674–1683.

Donnet, J. (1990). In Bansal R. C. (Ed.), Carbon fibres (2nd ed., rev. and expanded). New York: M. Dekker.

Duchoslav, J., Unterweger, C., Steinberger, R., Fürst, C., & Stifter, D. (2016). Investigation on the thermo-oxidative stability of carbon fibre sizings for application in thermoplastic composites. Polymer Degradation and Stability, 125, 33-42.

Dufresne, A. (2013). *Nanocellulose: From nature to high performance tailored materials*. De Gruyter.

Elemans, P. H. M., Janssen, J. M. H., & Meijer, H. E. H. (1990). The measurement of interfacial tension in polymer/polymer systems: The breaking thread method. *Journal of Rheology, 34*(8), 1311-1325.

Ellen MacArthur Foundation. (2021). *Circular economy for plastics: A strategy for rethinking the future*.

Endres H. J. and Siebert-Raths A., (2011). *Engineering biopolymers markets, manufacturing, properties and applications*. pp. 95-98, Carl Hanser Verlag, Munich.

Eslami, H., & Rabiee, M. (2018). Advances in polymer recycling technologies: A review. *Polymer Degradation and Stability, 147*, 4–20.

European Bioplastics. (2022). *Bio-based polyamide market overview*.

Fakirov, S. (Ed.). (2010). *Handbook of engineering biopolymers: Homopolymers, blends, and composites*. Munich: Hanser.

Falkenreck, C. K., Zarges, J.-C., Heim, H.-P., Seitz, M., & Bonten, C. (2025). Degradation of regenerated cellulose fibre-reinforced bio-polyamide in hydrothermal environment. *Composites Part A: Applied Science and Manufacturing, 188*, 108584.

Fan, H., Yang, W., Wang, B., Yan, Y., Fu, Q., Fang, D., & Zhuang, Z. (2006). Design and manufacturing of a composite lattice structure reinforced by continuous carbon fibres. Tsinghua Science & Technology, 11(5), 515-522.

Faruk, O., Bledzki, A. K., Fink, H., Sain, M. (2012). Biocomposites reinforced with natural fibres: 2000-2010. *Progress in Polymer Science.*, 37(11), 1552-1596.

Faruk, O., Bledzki, A. K., Fink, H., Sain, M., (2014). Progress report on natural fibre reinforced composites. *Macromol. Mater.* Eng., 299(1), 9-26.

Faruk, O., Tjong, J., Sain, M. (2017). Lightweight and Sustainable Materials for Automotive Applications - 6. Carbon Fibre Composite Materials. (pp. 204-238). CRC Press

Feldmann, M., & Bledzki, A. K. (2014). Bio-based polyamides reinforced with cellulosic fibres: Processing and properties. *Composites Science and Technology, 100*, 113–120.

Feldmann, M., Heim, H., & Zarges, J. (2015). Influence of the process parameters on the mechanical properties of engineering biocomposites using a twin-screw extruder. *Composites Part A: Applied Science and Manufacturing, 78*, 231–239.

Ferdousi, S., Advincula, R., Sokolov, A. P., Choi, W., & Jiang, Y. (2023). Investigation of 3D printed lightweight hybrid composites via theoretical modelling and machine learning. *Composites Part B: Engineering, 265*, 110958.

Franzen, B., Klason, C., Kubat, J., & Kitano, T. (1989). Fibre degradation during processing of short fibre reinforced thermoplastics. *Composites, 20*(1), 65–76.

Frye, E., & Rayner, R. (1972). Observations of Failure Modes in Carbon Composite Materials. Journal of Composite Materials, 6(2), 286–292.

Fu, X., Lü, W., & Chung, D. (1998). Ozone treatment of carbon fibre for reinforcing cement. Carbon, 36(9), 1337–1345.

Fukumori, K., Inaba, A., & Nakamura, H. (2003). Material recyclability of Japanese automobiles. *The International Journal of Life Cycle Assessment, 8*(4), 217–224.

Gadgeel, A. A. & Mhaske, S. T. (2019). Novel approach for the preparation of a compatibilized blend of nylon 11 and polypropylene with polyhydroxybutyrate: Mechanical, thermal, and barrier properties. *Applied Polymer Science*, *136*(43), 48152.

Gandini, A., & Lacerda, T. M. (2015). From monomers to polymers from renewable resources: Recent advances. *Progress in Polymer Science, 48*, 1–39.

George, J.S., Sreekala, M.S., & Thomas, S. (2001). A review on interface modification and characterization of natural fibre reinforced plastic composites. *Polymer Engineering and Science, 41*(9), 1471–1485.

Ghorbanian, M., Ferdousi, M. R., Cao, W., & Brinson, L. C. (2023). Investigation of 3D printed lightweight hybrid composites via theoretical modeling and machine learning. *Composites Part B: Engineering, 253*, 111743.

Ghosh, S., Maiti, S. N., & Jacobson, R. (2011). Mechanical properties of wood dust reinforced polymer composites. *Materials & Design, 32*(8-9), 4064–4071.

Gigante, V., Cartoni, F., Dal Pont, B., & Aliotta, L. (2024). Extrusion parameters optimization and mechanical properties of bio-polyamide 11-based biocomposites reinforced with short basalt fibres. *Polymers, 16*(21), 3092.

Go, T. F., Wahab, D. A., Rahman, M. N. A., Ramli, R., & Azhari, C. H. (2011). Disassemblability of end-of-life vehicle: A critical review of evaluation methods. *Journal of Cleaner Production, 19*(13), 1536-1546.

Goda, K., Sreekala, M. S., Gomes, A., Kaji, T., & Ohgi, J. (2006). Improvement of plant-based natural fibres for toughening green composites—Effect of load application during mercerization of ramie fibres. Composites Part A: Applied Science and Manufacturing, 37(12), 2213-2220.

Goffin, L., Zhao, Z., Raquez, J.M., Bailly, C. and Dubois, P. "Carbon fibre reinforced polyamide 6,6 composites: Influence of fibre length, fibre content and compounding method on properties." Composites Science and Technology, 72, pp. 1255-1262, 2012.

Gowda, T. Y., Sanjay, M. R., Bhat, K. S., Senthamaraikannan, P., & Yogesha, B. (2018). Polymer matrix-natural fibre composites: An overview. Cogent Engineering, 5(1), 1446667–1446667.

Grozdanov, A., and Bogoeva-Gaceva, G., 2010. Carbon fibres/polyamide 6 composites based on hybrid yarns. *J. Thermoplast. Compos. Mater.*, 23(1), 99-110.

Gu, F., Guo, J., Zhang, W., Summers, P. A., & Hall, P. (2017). From waste plastics to industrial raw materials: A life cycle assessment of mechanical plastic recycling practice based on a real-world case study. *Science of the Total Environment, 601-602*, 1192-1207.

Guedes, J. R., Florentino, W. M., & Mulinari, D. R. (2016). Thermoplastics Polymers Reinforced with Natural Fibres. Elsevier eBooks, 55-73.

Gupta, S. M., & Isaacs, J. A. (1997). Value analysis of disposal strategies for automobiles. *Computers and Industrial Engineering, 33*(1-2), 325-328.

Gupta, V., Anand, K., & Grape, J A. (1998). Failure of woven carbon–polyimide laminates under off-axis compression loading. Acta Materialia, 46(2), 711-718.

Gurunathan, T., Mohanty, S. and Nayak, S.K. (2015) A Review of the Recent Developments in Biocomposites Based on Natural Fibres and Their Application Perspectives. *Composites Part A*, 77, 1-25.

Hablot, E., Matadi, R., Ahzi, S., Avérous, L., 2010. Renewable biocomposites of dimer fatty acid-based polyamides with cellulose fibres: Thermal, physical and mechanical properties. *Compos. Sci. Technol.*, 70(3), 504-509.

Hage, I. S. (2024). A hybrid model for accurate prediction of composite longitudinal elastic modulus. *Computers & Mathematics with Applications., 174*, 287–297.

Haines, R C. (1986). Volume production with carbon fibre reinforced thermoplastics. *Composites,* 17(2), 168-168.

Han, Y., Hossain, M. S., & Chanda, T. (2023). A virtual testing framework for hybrid aligned discontinuous composites. *Composites Science and Technology, 241*, 109626.

Hashim, M. Y., Roslan, M. N., Amin, A. M., Zaidi, A. M. A., & Ariffin, S. (2012). Mercerization Treatment Parameter Effect on Natural Fibre Reinforced Polymer Matrix Composite: A Brief Review. World Academy of Science, Engineering, and Technology, 6(8), 778-784.

Hassan, E. A., Hassan, M. L., & Oksman, K. (2016). Improvement of the mechanical properties of natural fibre composite by lamination with glass fibre. *Journal of Composite Materials, 50*(9), 1243-1255.

Hao, M., Wu, H., Qiu, F., & Wang, X. (2018). Interface Bond Improvement of Sisal Fibre Reinforced Polylactide Composites with Added Epoxy Oligomer. Huang, X. (2009). Fabrication and Properties of Carbon Fibres. Materials, 2(4), 2369-2403.

Holbery, J., & Houston, D. (2006). Natural-fibre-reinforced polymer composites in automotive applications. *JOM*, *58*(11), 80–86

Huang, D., Wang, W., Tang, X., Zhu, P., & Zhao, X. (2025). A novel semi-empirical analytical method for stiffness prediction of unidirectional discontinuous-fibre composites. *Composites Science and Technology, 262*, 111087.

Huneault, M. A., & Li, H. (2007). Morphology and properties of compatibilized polylactide/thermoplastic starch blends. *Polymer, 48*(1), 270-280.

Ion, S. M., Tache, F., Mahu, R., & Opran, C. G. (2021). Advanced Polymeric Composite Product for Automotive Application. *Macromolecular Symposia,* 396(1).

Islam, M. S., Pickering, K. L., & Foreman, N. J. (2010). Influence of alkali treatment on the interfacial and physico-mechanical properties of industrial hemp fibre reinforced polylactic acid composites. *Composites Part A: Applied Science and Manufacturing, 41*(5), 596-603.

Jang, Y., Kim, S., Lee, S., Kim, D., & Um, M. (2005). Fabrication of carbon nano-sized fibre reinforced copper composite using liquid infiltration process. Composites Science and Technology.

Jia, M., Li, C X., Xue, P., Chen, K., & Chen, T H. (2016). Research on the melt impregnation of continuous carbon fibre reinforced nylon 66 composites. IOP Conference Series: Materials Science and Engineering, 137, 012053-012053.

Jiang, M., Wang, C., Zhu, B., Wang, Y., Gao, X., & Chen, W. (2008). Effects of preoxidation and carbonization technologies on tensile strength of PAN-based carbon fibre. Journal of Applied Polymer Science, 108(2), 1259-1264.

Jin, L., Fan, Q., Chen, Z., Huang, K., & Cheng, Y. (2006). Effect of electropolymer sizing of carbon fibre on mechanical properties of phenolic resin composites. Transactions of Nonferrous Metals Society of China, 16, s457-s461.

Jin, Z., Zhang, Z., & Lian, M. (2006). Effects of ozone method treating carbon fibres on mechanical properties of carbon/carbon composites. Materials Chemistry and Physics, 97(1), 167-172.

John, M. J., & Anandjiwala, R. D. (2007). Recent developments in chemical modification and characterization of natural fibre-reinforced composites. Polymer Composites, 29(2), 187-207.

Kalia, S., Kaith, B. S., & Kaur, I. (2009). Pretreatments of natural fibres and their application as reinforcing material in polymer composites—A review. Polymer Engineering & Science, 49(7), 1253-1272.

Kalia, S., Dufresne, A., Cherian, B. M., Kaith, B. S., Avérous, L., Njuguna, J., & Nassiopoulos, E. (2011). Cellulose-based bio- and nanocomposites: A review. *International Journal of Polymer Science, 2011*, 837875.

Karnani, R., Krishnan, M. R., & Narayan, R. (1997). Biofibre-reinforced polypropylene composites. Polymer Engineering and Science, 37(2), 476-483.

Karsli, N G., & Aytaç, A. (2013). Tensile and thermomechanical properties of short carbon fibre reinforced polyamide 6 composites. Composites Part B: Engineering, 51, 270-275.

Karthi, N., Kumaresan, K., Sathish, S., Gokulkumar, S., Prabhu, L., & Vigneshkumar, N. (2020). An overview: Natural fibre reinforced hybrid composites, chemical treatments and application areas. Materials Today: Proceedings, 27, 2828-2834.

Kausar, A. (2019). Advances in Carbon Fibre Reinforced Polyamide-Based Composite Materials. , 19(4), 67-82.

Kelkar, A D., Mohan, R., Bolick, R., & Shendokar, S. (2010). Effect of nanoparticles and nanofibres on Mode I fracture toughness of fibre glass reinforced polymeric matrix composites. Materials Science and Engineering: B, 168(1-3), 85-89.

Kemmer, H., Kryzewski, M., & Gateski, A. (1982). Adhesion between polymers. In E. Martuscelli (Ed.), *Polymer blends, processing, morphology and properties* (Vol. 4). Springer Science.

Khalid, M. Y., Imran, R., Arif, Z. U., Akram, N., Arshad, H., Rashid, A. A., & Márquez, F. P. G. (2021). Developments in Chemical Treatments, Manufacturing Techniques and Potential Applications of Natural-Fibres-Based Biodegradable Composites. Coatings, 11(3), 293-293.

Khan, M. Z., Srivastava, S. K., & Gupta, M. L. (2018). Tensile and flexural properties of natural fibre reinforced polymer composites: A review. Journal of Reinforced Plastics and Composites, 37(24), 1435-1455.

Khandekar, A., Mote, G., Vastre, N., Mosalgi, S., & Bhosale, S B. (2019). Study, Manufacturing and Analysis of Conveyor Chain Pin by using Composite Material. International journal of new technology and research, 5(4).

Khanna, Y. P., Reimschuessel, A. C., Banerjie, A., Altman, C., 1988. Memory effects in polymers. II. processing history vs. crystallization rate of nylon 6 - observation of phenomenon and product bahaviour. *Polym. Eng. Sci.,* 28(24), 1600-1606.

Khanna, Y.P., Han, P.K., Day, E.D., 1996. Memory effects in polymers. II.Processing history vs. cystallization rate of nylon 6—observation of phenomenon and product bahaviour. *Polym. Eng. Sci.*, 36, 1745–1751.

Kim, B., Cha, S., & Park, H W. (2018). Ultra-high-speed processing of nanomaterial-reinforced woven carbon fibre/polyamide 6 composites using reactive thermoplastic resin transfer moulding. , 143, 36-46.

Kim, B., Cha, S., Kong, K., Ji, W., & Park, H W. (2018). Synergistic interfacial reinforcement of carbon fibre/polyamide 6 composites using carbon-nanotube-modified silane coating on ZnO-nanorod-grown carbon fibre. Composites Science and Technology, 165, 362-372.

Kiziltas, A., Nazari, B., Gardner, D. J., Bousfield, D. W., 2014. Polyamide 6-cellulose composites: Effect of cellulose composition on melt rheology and crystallization bahaviour. *Polym. Eng. Sci.*, 54(4), 739-746.

Kodama, M., Karino, I., & Kobayashi, J. (1987). Interaction between the reinforcement and matrix in carbon-fibre-reinforced composite: Effect of forming the thin layer of polyimide resin on carbon fibre by in situ polymerization. Journal of Applied Polymer Science, 33(2), 361-373.

Kohan, M.I., Mestemacher, S.A., Pagilagan, R.U., Redmond, K., (7th Ed.), 2003. *Polyamides in Ullmann's encyclopaedia of Industrial Chemistry,* Wiley-VCH Verlag GmbH & Co. KGaA.

Köhler, T., Akdere, M., Röding, T., Gries, T., & Seide, G H. (2017). Cost efficient carbon fibre reinforced thermoplastics with in-situ polymerization of polyamide. IOP Conference Series: Materials Science and Engineering, 254, 042019-042019.

Kongar, E., & Gupta, S. M. (2006). Disassembly sequencing using genetic algorithm. *International Journal of Advanced Manufacturing Technology, 30*(5-6), 497–506.

Koo, J H., Pilato, L A., Wissler, G., Lee, A., & Abusafieh, A. (2005). Nanocomposites for Carbon Fibre-Reinforced Polymer Matrix Composites. 46th AIAA/ASME/ASCE/AHS/ASC Structures, Structural Dynamics and Materials Conference.

Koutroumanis, N., Manikas, A. C., Pappas, P. N., Anagnostopoulos, G., & Galiotis, C. (2024). Interfacial properties and mechanical performance of hybrid graphene/carbon fibre composites. *Materials Today Communications, 41*, 110458.

Krekel, G., Hüttinger, K. J., Hoffman, W. P., & Silver, D. S. (1994). The relevance of the surface structure and surface chemistry of carbon fibres in their adhesion to high-temperature thermoplastics. Journal of materials science, 29(11), 2968–2980.

Krilek J., Samešová D., Čabalová I., Potkany M., Dado M., Kučera M. Recycling and recovery of tires, rubber and plastics into the new products. In: Šooš Ľ., editor. The State and Vision of Waste Recovery from the Automotive Industry SR. 1st ed. Spektrum STU; Bratislava, Slovakia: 2020. p. 285.

Ku, H. S., Wang, H., Pattarachaiyakoop, N., & Trada, M. (2011). A review on the tensile properties of natural fibre reinforced polymer composites. *Composites Part B: Engineering*, 42(4), 856–873.

Kuciel, S., Kuzniar, P., Liber-Knec, A., 2012. Polyamides from renewable sources as matrices of short fibre reinforced biocomposites. Polimery/*polymers*, 57(9), 627-634.

Kumar, S., Rath, T., Mahaling, R N., Reddy, C S., Das, C K., Pandey, K N., Srivastava, R B., & Yadaw, S B. (2007). Study on mechanical, morphological and electrical properties of carbon nanofibre/polyetherimide composites. Materials Science and Engineering: B, 141(1-2), 61-70.

Kumar, R., Ul Haq, M. I., Raina, A., & Anand, A. (2020). A review of the mechanical and thermal properties of graphite and modified graphite reinforced polymer composites. *Materials Today: Proceedings, 21*, 1659–1672.

Kumar, G R., Vijayanandh, R., Venkatesan, K R., Ramesh, M., Kumar, M., & Balaji, S. (2020). Comparative Investigations on 1the Main Elements of Carbon Fibre Based Composites Using Computational Structural Simulations. *Journal of physics*, 1504(1), 012003-012003. La Mantia, F. P., Curto, D., & Scaffaro, R. (2002). Recycling of dry and wet polyamide 6. *Journal of Applied Polymer Science, 86*(8), 1899-1903.

Lazarus, S. B., Jamuna, E., Duraisivam, S., & Ravisankar, M. (2017). Experimental Investigation and Analysis of Ecofriendly Compression Molded Woven Plant Fibre Polyester Composite. *Applied Mechanics and Materials*, 867, 48-57.

Lee, J., & Kang, T J. (1997). Changes in physico-chemical and morphological properties of carbon fibre by surface treatment. *Carbon, 35*(2), 209-216.

Lee, S. G., Lye, S. W., & Khoo, M. K. (2001). A multi-objective methodology for evaluating product end-of-life options and disassembly. *International Journal of Advanced Manufacturing Technology, 18*(2), 148-156.

Li, X., Tabil, L. G., & Panigrahi, S. (2007). Chemical treatments of natural fibre for use in natural fibre-reinforced composites: A review. *Journal of Polymers and the Environment, 15*(1), 25-33.

Li, J., & Cai, C. L. (2011). The carbon fibre surface treatment and addition of PA6 on tensile properties of ABS composites. *Current Applied Physics, 11*(1), 50-54.

Li, M., Pu, Y., Thomas, V. M., Yoo, C. G., Ozcan, S., Deng, Y., Nelson, K., & Ragauskas, A. J. (2020). Recent advancements of plant-based natural fibre-reinforced composites and their applications. *Composites Part B: Engineering, 200*, 108254-108254.

Li, X., Tabil, L. G., & Panigrahi, S. (2020). The influence of fibre pretreatment on the properties of hemp–polypropylene composites. *Journal of Applied Polymer Science*, 138(10), 49891.

Liao, G., Li, Z., Cheng, Y., Xu, D., Zhu, D., Jiang, S., Guo, J., Chen, X., Xu, G., & Zhu, Y. (2018). Properties of oriented carbon fibre/polyamide 12 composite parts fabricated by fused deposition modelling. *Composites Part B: Engineering, 139*, 283–292.

Liu, T., Phang, I Y., Shen, L., Chow, S., & Zhang, W. (2004). Morphology and Mechanical Properties of Multiwalled Carbon Nanotubes Reinforced Nylon-6 Composites. Macromolecules, 37(19), 7214–7222.

Liu, K., Madbouly, S. A., Schrader, J. A., Kessler, M. R., Grewell, D., & Graves, W. R. (2015). Biorenewable polymer composites from tall oil-based polyamide and lignin–cellulose fibre. *Journal of Applied Polymer Science, 132*(48), 42739.

Liu, L., Wang, X., Hongrong, Z., Yu, M., & Xie, W. (2017). Optimizing synthesis parameters of short carbon fibre reinforced polysulfonamide composites by using response surface methodology. *Polymer Testing, 59*, 355–361.

Liu, J., & Wei, X. (2021). Enhancing the impact performance of reinforced composites through fibre hybridization—A hybrid dynamic shear-lag model. *Extreme Mechanics Letters, 47*, 101352.

Lu, C., Xu, N., Zheng, T., Zhang, X., Lv, H., Xiao, L., & Zhang, D. (2018). The Optimization of Process Parameters and Characterization of High-Performance CF/PEEK Composites Prepared by Flexible CF/PEEK Plain Weave Fabrics. *Polymers, 11*(1), 53-53.

Ma, H., Zeng, J., Realff, M L., Kumar, S., & Schiraldi, D A. (2003). Processing, structure, and properties of fibres from polyester/carbon nanofibre composites. *Composites Science and Technology, 63*(11), 1617–1628.

Ma, Y., Yan, C., Xu, H., Liu, D., Shi, P., Zhu, Y., & Liu, J. (2018). Enhanced interfacial properties of carbon fibre reinforced polyamide 6 composites by grafting graphene oxide onto fibre surface. *Applied Surface Science, 452,* 286–298.

Ma, L., Zhu, Y., Feng, P., Gao, S., Huang, Y., Liu, H., Zhang, J., Fan, J., Hou, H., & Guo, Z. (2019). Reinforcing carbon fibre epoxy composites with triazine derivatives functionalized graphene oxide modified sizing agent. Composites Part B: Engineering, 176, 107078-107078.

Madan, R., Khobragade, P., Mussada, E. K., Singh, M. K., Rangappa, S. M., Njim, E. K., & Siengchin, S. (2025). A novel two-step finite element approach to estimate the thermo-mechanical properties of two-phase and three-phase hybrid composites. *Composites Communications, 53*, 102213.

Maia, B. S., Tjong, J., & Sain, M. (2019). Material characterization of recycled and virgin carbon fibres for transportation composites lightweighting.

Marsh, G. (2008). Reclaiming value from post-use carbon composite. *Reinforced Plastics, 52*(7), 36–39. Mei, L., Li, Y., Wang, R., Wang, C., Peng, Q., & He, X. (2011). Multiscale carbon nanotube–carbon fibre reinforcement for advanced epoxy composites with high interfacial strength. *Journal of Reinforced Plastics and Composites, 30*(2–3), 107–112.

Meng, Q., & Wang, Z. (2015). Theoretical model of fibre debonding and pull-out in unidirectional hybrid-fibre-reinforced brittle-matrix composites. *Journal of Composite Materials., 49*(14), 1739–1751.

Meyer, L. O., Schulte, K., & Grove-Nielsen, E. (2009). CFRP-recycling following a pyrolysis route: Process optimization and potentials. Journal of Composite Materials, 43(9), 1121–1132.

Miled, B., Kammoun, S., Belyamani, I., & Cauret, L. (2024). Manufacturing, characterization, and macromechanical modeling of short flax/hemp fibre-hybrid reinforced polypropylene. *Forces in Mechanics., 15*, 100269.

Miller, L., Soulliere, K., Sawyer-Beaulieu, S., Tseng, S., & Tam, E. (2014). Challenges and alternatives to plastics recycling in the automotive sector. *Materials, 7*(8), 5883–5902. https://doi.org/10.3390/ma7085883

Mleziva, J., & Šňupárek, J. (2000). *Polymers—Production, structure, properties and utilization* (2nd ed.). Praha, Czech Republic: Sobotáles.

Mochane, M. J., Mokhena, T. C., Mokhothu, T. H., Mtibe, A., Sadiku, R., Ray, S. S., Ibrahim, I. L., & Daramola, O. O. (2019). Recent progress on natural fibre hybrid composites for advanced applications: A review. *Express Polymer Letters, 13*(2), 159–198. https://doi.org/10.3144/expresspolymlett.2019.14

Mohammed, L., Ansari, M. N. M., Pua, G., Jawaid, M., & Islam, M. S. (2015). A review on natural fibre reinforced polymer composite and its applications. *International Journal of Polymer Science, 2015*, Article 243947. https://doi.org/10.1155/2015/243947

Mohanty, A. K., Misra, M., & Drzal, L. T. (2001). Surface modifications of natural fibres and performance of the resulting biocomposites: An overview. *Composite Interfaces, 8*(5), 313–343.

Mohanty, A. K., Misra, M., & Drzal, L. T. (2002). Sustainable bio-composites from renewable resources: Opportunities and challenges in the green materials world. *Journal of Polymers and the Environment, 10*(1–2), 19–26.

Mondragon, G., Kortaberria, G., Mendiburu, E., González, N., Arbelaiz, A., & Peña-Rodriguez, C. (2020). Thermomechanical recycling of polyamide 6 from fishing nets waste. *Journal of Applied Polymer Science, 137*(10)10.

Monti, M., Perin, E., Conterosito, E., Romagnolli, U., Muscato, B., Girotto, M., Scrivani, M. T., & Gianotti, V. (2022). Development of an Advanced Extrusion Process for the Reduction of Volatile and Semi-volatile Organic Compounds of Recycled Hdpe from Fuel Tanks.

Monteiro, S. N., Lopes, F. P. D., Ferreira, A. S., & Nascimento, D. C. O. (2009). Natural-fibre polymer-matrix composites: Cheaper, tougher, and environmentally friendly. JOM, 61(1), 17-22.

Monteiro, S. N., Calado, V., Rodriguez, R. J. S., & Margem, F. M. (2012). Natural fibre polymer composites: A review. *Polímeros, 22*(3), 247-254.

Morgan, P. (2005). Carbon fibres and their composites. Boca Raton: Taylor & Francis.

Moritzer, E., & Heiderich, G. (2017). Fibre length reduction during shearing in polymer processing. Paper presented at the AIP Conference Proceedings, 1914

Mundhe, A., & Kandasubramanian, B. (2024). Advancements in natural fibre composites: Innovative chemical surface treatments, characterizaton techniques, environmental sustainability, and wide-ranging applications. *Hybrid Advances, 7*, 100282.

Mutlu, H. and Meier, M.A.R., 2010. Castor oil as a renewable resource for the chemical industry. *Euopean Journal Lipid Science Technology.*, 112, 10–30.

Nairn, J. A. (1994). In Bascom W. D., Harper S. I. and Langley Research Center. (Eds.), Effects of fibre, matrix, and interphase on carbon fibre composite compression strength. Hampton, Va: Langley Research Center.

Naito, K., Premala, V., Shimamura, Y., & Inoue, Y. (2014). Carbon Nanotubes/Carbon Fibre Polymer Matrix Hybrid Composites. Nihon Fukugō Zairyō Gakkaishi, 40(6), 275-282.

Nassar, M M A., Arunachalam, R M., & Alzebdeh, K I. (2016). MachiSaheblity of natural fibre reinforced composites: a review. The International Journal of Advanced Manufacturing Technology, 88(9-12), 2985-3004.

Nayak, S. Y., & Mohanty, S. (2010). Impact of alkali treatment on the surface and tensile properties of natural fibres. *Fibres and Polymers, 11*(8), 1146-1152.

Nie, W. Z., and Li, J. (2010). Effect of carbon fibre content on friction and wear properties of carbon fibre reinforced PA6 composites. *Plastic, Rubber Composites*, *39*(1), 10-15.

Nirmal, U., Hashim, J., & Ahmad, M. Z. (2015). A review on tribological performance of natural fibre polymeric composites. *Tribology International, 83*, 77-104.

Novotný M., Hipča H., Marušák V. Analysis of the process of old vehicles recycling. In: Šooš Ľ., editor. The State and Vision of Waste Recovery from the Automotive Industry SR. 1st ed. Spektrum STU; Bratislava, Slovakia: 2020. p. 285.

Ochi, S. (2008). Mechanical properties of kenaf fibres and kenaf/PLA composites. *Mechanics of Materials, 40*(4-5), pp. 446–452.

Ogunniyi, D.S., 2006. Castor oil: a vital industrial raw material. *Bioresource. Technology*, *97*, 1086–1091.

Oksman, K., Skrifvars, M., & Selin, J. (2003). Natural fibres as reinforcement in polylactic acid (PLA) composites. *Composites Science and Technology, 63*(9), 1317-1324.

Oksman Niska K. and Sain M. (Eds.), 2008. Wood-polymer composites. Woodhead Publishing, Cambridge.

Oliveux, G., Dandy, L. O., & Leeke, G. A. (2015). Current status of recycling of fibre reinforced polymers: Review of technologies, reuse and resulting properties. *Progress in Materials Science, 72*, 61–99.

Osswald, T. A., & Menges, G. (2012). *Material science of polymers for engineers* (3rd ed.). Cincinnati, OH: Hanser Publications.

Ozen, E., Kiziltas, A., Kiziltas, E. E., Gardner, D. J., 2013. Natural fibre blend - nylon 6 composites. *Polymer Composites*, *34*(4), 544-553.

Ozmen, S. C., Ozkoc, G., & Serhatli, E. (2019). Thermal, mechanical and physical properties of chain extended recycled polyamide 6 via reactive extrusion: Effect of chain extender types. *Polymer Degradation and Stability, 162*, 76-84.

Padmavathi, N., Subrahmanyam, J., Ray, K K., Mohanrao, R., Ghosal, P., & Kumari, S. (2008). Carbon fibre reinforced silicon carbide mini-composites-solution approach. Journal of Materials Processing Technology, 204(1-3), 434-439.

Palmer, J., Ghita, O.R., Savage, L., Evans, K.E., (2009). Successful closed-loop recycling of thermoset composites. Composites Part A, pp. 40, 490–498.

Pandey, J., Ahn, S., Lee, C. S., Mohanty, A. K., & Misra, M. (2010). Recent Advances in the Application of Natural Fibre Based Composites. Macromolecular Materials and Engineering, 295(11), 975–989.

Panthapulakkal, S., Law, S., Sain, M., 2005. Injection molded natural fibre hybrid composites for automobile applications - mechanical properties and flammability. *International SAMPE Technical Conference*, 2005.

Panthapulakkal, S., & Sain, M. (2006). Injection molded wheat straw and corn stem filled polypropylene composites. *Journal of Polymers and the Environment*, *14*(3), 265–272.

Panthapulakkal, S., & Sain, M. (2007a). Injection molded short hemp fibre/glass fibre-reinforced polypropylene hybrid composites—Mechanical, water absorption and thermal properties. *Journal of Applied Polymer Science*, *103*(4), 2432–2441.

Panthapulakkal, S., & Sain, M. (2007b). Studies on the water absorption properties of short hemp-glass fibre hybrid polypropylene composites. *Journal of Composite Materials*, *41*(15), 1871-1883.

Park, S., Seo, M., & Lee, J. (2003). Relationship between surface characteristics and interlaminar shear strength of oxyfluorinated carbon fibres in a composite system. *Journal of Colloid and Interface Science, 268*(1), 127-132.

Park, S., & Kim, B. (2005). Roles of acidic functional groups of carbon fibre surfaces in enhancing interfacial adhesion bahaviour. *Materials Science and Engineering: A, 408*(1-2), 269-273.

Patel, S R., & Patel, R G. (1992). Physicomechanical Properties of Carbon Fibre Reinforced Epoxy Composites. *Polymer-plastics Technology and Engineering, 31*(7-8), 705-712.

Pathak, A K., Borah, M., Gupta, A., Yokozeki, T., & Dhakate, S R. (2016). Improved mechanical properties of carbon fibre/graphene oxide-epoxy hybrid composites. *Composites Science and Technology, 135*, 28-38.

Peças, P., Carvalho, H., Salman, H., & Leite, M. (2018). Natural Fibre Composites and Their Applications: A Review. *Journal of Composites Science, 2*(4), 66-66.

Pejic, B. M., Kostic, M. M., Skundric, P. D., & Praskalo, J. Z. (2008). The effects of hemicelluloses and lignin removal on water uptake bahaviour of hemp fibres. *Bioresource Technology, 99*(15), 7152-7159.

Peng, Y., Gardner, D. J., Han, Y., (2015). Characterization of mechanical and morphological properties of cellulose reinforced polyamide 6 composites. *Cellulose*, *22*(5), 3199–3215.

Peng, Y., Wu, Y., Wang, K., Gao, G., & Ahzi, S. (2019). Synergistic reinforcement of polyamide-based composites by combination of short and continuous carbon fibres via fused filament fabrication. *Composite Structures, 207*, 232-239.

Peng, X., Zhang, M., Guo, Z., Sang, L., & Hou, W. (2020). Investigation of processing parameters on tensile performance for FDM-printed carbon fibre reinforced polyamide 6 composites. *Composites Communications, 22*, 100478-100478.

Pickering, S. J. (2006). Recycling technologies for thermoset composite materials—Current status. *Composites Part A: Applied Science and Manufacturing*, *37*(8), 1206–1215.

Pickering, S.J. (2009). Carbon fibre recycling technologies: what goes in and what comes out? In: Carbon Fibre Recycling and Reuse 2009 Conference, IntertechPira, Hamburg, Germany.

Pickering, S.J., Robinson, P., Pimenta, S., Pinho, S.T. (2010). Applications for recycled carbon fibre. In: Meeting of the Increasing SustaiSaheblity and Recycling Consortium (10 June 2010). BIS — UK Composites Strategy, London, UK.

Pickering, K. L., Efendy, M. G. A., & Le, T. M. (2016). A review of recent developments in natural fibre composites and their mechanical performance. *Composites Part A: Applied Science and Manufacturing, 83*, 98–112.

Pimenta, S., & Pinho, S. T. (2011). Recycling carbon fibre reinforced polymers for structural applications: Technology review and market outlook. *Waste Management, 31*(2), 378-392.

Pimenta, S., & Pinho, S. T. (2012). The effect of recycling on the mechanical response of carbon fibres and their composites. *Composite Structures, 94*(12), 3669-3684.

Piñero-Hernanz, R., Dodds, C., Hyde, J., García-Serna, J., Poliakoff, M., Lester, E., Cocero, M. J., Kingman, S., Pickering, S., & Wong, K. H. (2008). Chemical recycling of carbon fibre reinforced composites in near-critical and supercritical water. *Composites Part A: Applied Science and Manufacturing, 39*(3), 454–461.

Piñero-Hernanz, R., García-Serna, J., Dodds, C., Hyde, J., Poliakoff, M., Cocero, M. J., & Lester, E. (2008). Chemical recycling of carbon fibre composites using alcohols under subcritical and supercritical conditions. *Journal of Supercritical Fluids, 46*(1), 83–92.

Pittman, C U., Jiang, W., He, G., & Gardner, S D. (1998). Oxygen plasma and isobutylene plasma treatments of carbon fibres: Determination of surface functionality and effects on composite properties. *Carbon, 36*(1-2), 25-37.

Plastics Europe. (2020). *Polyamide market and technical overview*. Retrieved from https://plasticseurope.org

Premnath, K., Arunprasath, K., Sanjeevi, R. *et al.* (2024). Natural/synthetic fibre reinforced hybrid composites on their mechanical behaviours– a review. *Interactions 245*, 111.

Puglia, D., Biagiotti, J., & Kenny, J. M. (2004). A Review on Natural Fibre-Based Composites—Part II Application of Natural Reinforcements in Composite Materials for Automotive Industry. Journal of Natural Fibres, 1(3), 23-41.

Rabbi, M., Islam, T., & Islam, G M S. (2021). Injection-molded natural fibre-reinforced polymer composites–a review. International Journal of Mechanical and Materials Engineering, 16(1).

Rajak, D. K., Pagar, D. D., Menezes, P. L., & Linul, E. (2019). Fibre-Reinforced Polymer Composites: Manufacturing, Properties, and Applications. Polymers, 11(10), 1667-1667.

Rajmohan, T., Vignesh, G., Palanikumar, K., & Harish, G. (2013). Synthesis and characterization of nano filled carbon fibre reinforced composites.

Rajput, L., & Jana, P. (2025). Coupled nano-interfacial and agglomeration effects on elastic bahaviour of hybrid composites using multi-scale modelling. *International Journal of Mechanical Sciences., 296*, 110273.

Raju, A P A., & Shanmugaraja, M. (2020). Recent Researches In Polylactic Acid Reinforced With Natural Fibre Composites– A Literature Review., 988(1), 012025-012025.

Ramezani-Dana, H., Gomina, M., Bréard, J., & Orange, G. (2021). Experimental investigation of the mechanical bahaviour of glass fibre/high fluidity polyamide-based composites for automotive market.

Ramnath, B. V., Arvind, R., Dinesh, I., & Prasadh, M. H. (2018). Review on Natural Fibre Composites. IOP Conference Series: Materials Science and Engineering, 390, 012062-012062.

Rana, S., Alagirusamy, R., Fangueiro, R., & Joshi, M. (2012). Effect of carbon nanofibre functionalization on the in-plane mechanical properties of carbon/epoxy multiscale composites. Journal of Applied Polymer Science, 125(3), 1951-1958.

Rattan, R., & Bijwe, J. (2006). Carbon fabric reinforced polyetherimide composites: Influence of weave of fabric and processing parameters on performance properties and erosive wear. Materials Science and Engineering: A, 420(1-2), 342-350.

Raushan, R., Dhande, K. K., & Jamadar, N. I. (2025). Modal analysis of carbon fibre reinforced polyamide 66 drive shaft using analytical and finite element approach. *International Journal on Interactive Design and Manufacturing (IJIDeM), 19*, 2801–2816.

Rauwendaal, C. (2014). Polymer extrusion: Fifth edition. Polymer extrusion: Fifth edition (pp. 1-934).

Ravi, M., Dubey, R. R., Shome, A., Guha, S., & Kumar, C. R. (2018). Effect of surface treatment on natural fibres composite. Materials Science and Engineering, 376, 012053-012053.

Ravina, M. (2023). Hard-to-recycle plastics in the automotive sector: Economic, environmental and technical analyses of possible actions. *Journal of Cleaner Production.*, *394*.

Ren, Y., Ren, L., Li, J., Lv, R., Wei, L., An, D., Maqbool, M., Bai, S., & Wong, C. (2020). Enhanced thermal conductivity in polyamide 6 composites based on the compatibilization effect of polyether-grafted graphene. *Composites Science and Technology, 199*, 108340.

Rinberg, R., Hartmann, T., Nikiforov, A., Doynikov, A., Вольфсон, С И., & Kroll, L. (2018). Investigation of bio-based polyamide with short fibres for lightweight structures.

Rodriguez-Castellanos, W., & Rodrigue, D. (2016). Production and Characterization of Hybrid Polymer Composites Based on Natural Fibres. InTech eBooks.

Rosenau, B., (2007). *Polyamides (PA).* Kunststoffe International 10/2007

Rouison, D., Sain, M., & Couturier, M. F. (2004). Resin transfer moulding of natural fibre reinforced composites: cure simulation. Composites Science and Technology, 64(5), 629-644.

Ruffino, B., Panepinto, D., & Zanetti, M. (2021). A Circular Approach for Recovery and Recycling of Automobile Shredder Residues (ASRs): Material and Thermal Valorization. *Waste and Biomass Valorization, 12*(6), 3109-3123.

Rybicka, J., Tiwari, A., & Leeke, G. A. (2016). Technology readiness level assessment of composites recycling technologies. *Journal of Cleaner Production*, 112, 1001-1012.

Sadeghian, R B., Gangireddy, S., Minaie, B., & Hsiao, K. (2006). Manufacturing carbon nanofibres toughened polyester/glass fibre composites using vacuum assisted resin transfer moulding for enhancing the mode-I delamination resistance. *Composites Part A: Applied Science and Manufacturing*, 37(10), 1787-1795.

Saheb, D. N., & Jog, J. P. (1999). Natural fibre polymer composites: A review. *Advances in Polymer Technology*, 18(4), 351-363.

Sanjay, M. R., Siengchin, S., Jawaid, M., Pruncu, C. I., & Khan, A. (2019). A comprehensive review of techniques for natural fibres as reinforcement in composites: Preparation, processing and characterization. *Carbohydrate Polymers*, 207, 108-121.

Santos, P. A. M. D., Spinacé, M. A. S., Fermoselli, K. K., & Paoli, M. D. (2007). Polyamide-6/vegetal fibre composite prepared by extrusion and injection moulding. *Composites Part A: Applied Science and Manufacturing,* 38(12), 2404-2411.

Sarkis, J., González-Torre, P L., & Adenso-Díaz, B. (2009). Stakeholder pressure and the adoption of environmental practices: The mediating effect of training.

Sarkis, J., Helms, M M., & Hervani, A A. (2010). Reverse logistics and social sustaiSaheblity.

Sathish, S., Karthi, N., Prabhu, L., Gokulkumar, S., Balaji, D., Vigneshkumar, N., Farhan, T., AkilKumar, A., & Dinesh, V. (2021). A review of natural fibre composites: Extraction methods, chemical treatments and applications. *Materials Today*: Proceedings, 45, 8017-8023.

Sathish, T., Boobalan, V., Giri, J., Hourani, A. O., Santhosh, A. J., & Nasri, F. (2025). Optimization and Enhancement of Tensile Strength and Elongation at Failure in Basalt/Glass Fibre Polymer Composites With MWCNTs + SiO 2 Hybrid Nanofillers Using Response Surface Methodology. *Engineering Reports : Open Access., 7*(2).

Senthil, T., Divakaran, N., Wang, J., Wang, R., & Wu, L. (2018). Evolution of structural, electrical, and mechanical response of 3D robust network and conducting mechanically modified glass fabric-polyester composites with devisable 1D VGCNF. Composites Science and Technology, 163, 171–179.

Scheuring, B. M., Christ, N., Blarr, J., Liebig, W. V., Hohe, J. ö, Montesano, J., & Weidenmann, K. A. (2024). Experimental and homogenized orientation-dependent properties of hybrid long fibre-reinforced thermoplastics. *International Journal of Mechanical Sciences, 280*, 109470.

Scott, E., Peter, F., Sanders, J. (2007). Biomass in the manufacture of industrial products—the use of proteins and amino acids. *Applied Microbial Biotechnology*, 75(4), 751–762.

Semba, T., Ito, A., Kitagawa, K., Nakatani, T., Yano, H., Sato, A., 2014. Thermoplastic composites of polyamide-12 reinforced by cellulose nanofibres with cationic surface modification. *Journal of Applied Polymer Science*, 131(20).

Sgriccia, N., Hawley, M. C., & Misra, M. (2008). Characterization of natural fibre surfaces and natural fibre composites. Composites Part A: Applied Science and Manufacturing, 39(10), 1632–1637.

Shahzad, A. (2012). Hemp fibre and its composites - A review. *Journal of Composite Materials, 46*(8), 973–986.

Shalwan, A., & Yousif, B. F. (2013). In State of Art: Mechanical and tribological behaviour of polymeric composites based on natural fibres. Materials & Design, 48, 14-24.

Sharma, M., Gao, S., Mäder, E., Sharma, H., Wei, L Y., & Bijwe, J. (2014). Carbon fibre surfaces and composite interphases. Composites Science and Technology, 102, 35-50.

Sharma, S., & Lakkad, S. (2010). Compressive strength of carbon nanotubes grown on carbon fibre reinforced epoxy matrix multi-scale hybrid composites. *Surface & Coatings Technology, 205*(2), 350-355.

Shen, L., Haufe, J., & Patel, M. K. (2009). *Product overview and market projection of emerging bio-based plastics: PRO-BIP 2009*. Utrecht University.

Shen, L., Worrell, E., Patel, M., 2010. Present and future development in plastics from biomass. *Biofuels, Bioprod. Biorefin.*, 4(1), 25-40.

Shoja, M., Kazemi, R., Mohammadi-Roshandeh, J., Farizeh, T., Shadman, A., & Hemmati, F. (2021). Hybrid mathematical modelling and multi-objective optimization of mechanical properties of green composites based on starch and modified rice straw fillers. *Journal of Applied Polymer Science, 138*(36), e50915.

Silva, M., Pereira, A., Alves, N., Mateus, A., & Malça, C. (2017). A Hybrid Processing Approach to the Manufacturing of Polyamide Reinforced Parts with Carbon Fibres. Procedia Manufacturing, 12, 195-202.

Singha, A. S., Shama, A., & Thakur, V. K. (2008). Pressure induced graft co-polymerization of acrylonitrile onto *Saccharum cilliare* fibre and evaluation of some properties of grafted fibres. *Bulletin of Materials Science, 31*(1), 7–13.

Singha, A. S., and Thakura, V. K., (2008). Fabrication and study of lignocellulosic hibiscus sabdariffa fibre reinforced polymer composites. *Bioresources, 3*(4), 1173-1186.

Singha, A.S., Shama, A., Thakur, V.K., (2009). Graft copolymerization of acrylonitrile onto Saccaharum cilliare fibre. *E-Polymers*, 105, 1–12.

Singha, A. S., & Thakur, V. K. (2009a). Fabrication and characterization of *S. cilliare* fibre reinforced polymer composites. *Bulletin of Materials Science, 32*(1), 49–58.

Singha, A. S., & Thakur, V. K. (2009b). Fabrication and characterization of *H. sabdariffa* fibre reinforced polymer composites. *Polymer-Plastics Technology and Engineering, 48*(4), 482–487.

Singha, A. S., & Thakur, V. K. (2010). Mechanical, morphological, and thermal characterization of compression-molded polymer biocomposites. *International Journal of Polymer Analysis and Characterization, 15*(2), 87–97.

Sittig, M. (1980). Carbon and graphite fibres: Manufacture and applications. Park Ridge, N.J.: Noyes Data Corp.

Slamani, M., & Châtelain, J. (2023). A review on the machining of polymer composites reinforced with carbon (CFRP), glass (GFRP), and natural fibres (NFRP). *Discover Mechanical Engineering, 2*(1), Article 10.

Spreafico, C. (2021). Can modified components make cars greener? A life cycle assessment. *Journal of Cleaner Production, 307*, Article 127310.

Sugama, T., & Taylor, M J. (1994). Interfacial and mechanical bahaviour of fibre-reinforced calcium phosphate cement composites. , 16(2), 93-106.

Sui, G., Sun, F., Yang, X., Ji, J., & Zhong, W. (2013). Highly aligned polyacrylonitrile-based nano-scale carbon fibres with homogeneous structure and desirable properties. *Composites Science and Technology, 87*, 77-85.

Sullivan, R. A. (2006). Automotive carbon fibre: Opportunities and challenges. *JOM*, *58*(11), 77–79.

Sun, Z., Hai-shan, H., & Dai, G. (2009). Mechanical Properties of Injection-molded Natural Fibre-reinforced Polypropylene Composites: Formulation and Compounding Processes. *Journal of Reinforced Plastics and Composites*, 29(5), 637-650.

Sung, M., Ahn, H., Jang, J., Kwon, D., & Yu, W. (2021). A micromechanical model of carbon fibre-reinforced plastic and steel hybrid laminate composites. *Journal of Composite Materials., 55*(22), 3071–3086.

Sung, C. H., & Takashi, A. (2021). A micromechanical model of carbon fibre reinforced plastic and steel hybrid laminate composites. *Materials Today: Proceedings, 47*, 345–353.

Swolfs, Y., Gorbatikh, L., & Verpoest, I. (2019). Recent advances in fibre hybrid composites: Materials selection, design, and performance. *Composites Part B: Engineering, 183*, 107749.

Szpieg, M., Wysocki, M., & Asp, L. E. (2012). Mechanical performance and modelling of a fully recycled modified CF/PP composite. *Journal of Composite Materials,* 46(12), 1503-1517.

Tan, P., Zhai, Z., Liu, N., & Shi, W. (2025). Experimental and numerical investigations on the mechanical properties of overmolded hybrid fibre reinforced thermoplastic composites. *Journal of Polymer Engineering, 45*(2), 131–143.

Tanaka, K., Hosoo, N., & Katayama, T. (2017). Effects of temperature on the fibre matrix interfacial properties of carbon fibre reinforced highly heat resistant polyamide resin. *Journal of the Society of Materials Science, Japan, 66*(10), 746–751.

Tanaka, K., Yamada, K., & Katayama, T. (2020). Effect of copolyamide surface treatment on carbon fibre influencing the interfacial properties of carbon fibre and polyamide 12. *Journal of the Society of Materials Science, Japan, 69*(10), 740–745.

Tang, L., & Kardos, J L. (1997). A review of methods for improving the interfacial adhesion between carbon fibre and polymer matrix. *Polymer Composites*, 18(1), 100-113.

Tarrar, M., Despeisse, M., & Johansson, B. (2021). Driving vehicle dismantling forward - A combined literature and empirical study. *Journal of Cleaner Production, 295*10.1016.

Tekinalp, H., Kunc, V., Vélez-García, G M., Duty, C., Love, L J., Naskar, A K., Blue, C A., & Ozcan, S. (2014). Highly oriented carbon fibre–polymer composites via additive manufacturing. *Composites Science and Technology,* 105, 144-150.

Thakur, V. K., Thakur, M. K., & Raghavan, P. (2013). Processing and characterization of natural cellulose fibres/thermoset polymer composites. *Carbohydrate Polymers, 91*(2), 550-559.

Thakur, V. K., & Singha, A. S. (2010). Evaluation of *Grewia optiva* fibres as reinforcement in polymer biocomposites. *Polymer-Plastics Technology and Engineering, 49*(11), 1101–1107.

Thakur, V. K., Thakur, M. K., & Gupta, R. K. (2014a). Review: Raw Natural Fibre–Based Polymer Composites. International *Journal of Polymer Analysis and Characterization*, 19(3), 256-271.

Thakur, V. K., Thakur, M. K., Raghavan, P., Kessler, M. R., (2014b). Progress in green polymer composites from lignin for multifunctional applications: A review. *ACS Sustainable Chemical Engineering,* 2(5), 1072-1092.

Thomas, S., Grohens, Y., & Jyotishkumar, P. (2013). Thermodynamics and morphology and compatibilization of polymer blends. *Characterization of Polymer, 1*, 93.

Thomas, B. S., Gupta, R. C., & Panicker, V. J. (2016). Recycling of waste tire rubber as aggregate in concrete: Durability-related performance. *Journal of Cleaner Production, 112*, 504–513.

Thomason, J. L. (2002). The influence of fibre length and concentration on the properties of glass fibre reinforced polypropylene: 5. injection moulded long and short fibre PP. *Composites Part A: Applied Science and Manufacturing* (Incorporating Composites and Composites Manufacturing), 33(12), 1641-1652.

Thomason, J. L. (2005). The influence of fibre length and concentration on the properties of glass fibre reinforced polypropylene. 6. the properties of injection moulded long fibre PP at high fibre content. *Composites Part A*, 36(7), 995-1003.

Tibbetts, G G., Lake, M L., Strong, K L., & Rice, B P. (2007). A review of the fabrication and properties of vapor-grown carbon nanofibre/polymer composites. *Composites Science and Technology*, 67(7-8), 1709-1718.

Tseng, H., Chang, R., & Hsu, C. (2017). Numerical prediction of fibre orientation and mechanical performance for short/long glass and carbon fibre-reinforced composites. *Composites Science and Technology*, 144, 51-56.

Turner, D. A., Williams, I. D., & Kemp, S. (2015). Greenhouse gas emission factors for recycling of source-segregated waste materials. *Resources, Conservation and Recycling, 105*, 186–197.

Utracki, L. A., & Shi, Z. H. (1992). Development of polymer blend morphology during compounding in a twin-screw extruder. Part I: Droplet dispersion and coalescence—a review. *Polymer Engineering & Science, 32*(24), 1824-1833.

Vaidya, U., (2011). *Composites for automotive, truck and mass transit: Materials, design, manufacturing*. DEStech Publications.

Valadez-González, A., Cervantes-Uc, J. M., Olayo, R., & Herrera-Franco, P. J. (1999). Effect of fibre surface treatment on the fibre–matrix bond strength of natural fibre reinforced composites. *Composites Part B: Engineering,* 30(3), 309-320.

Van Puyvelde, P., Velankar, S., Mewis, J., Moldenaers, P., & Leuven, K. U. (2002). Effect of Marangoni stresses on the deformation and coalescence in compatibilized immiscible polymer blends. *Polymer Engineering and Science, 42*(10), 1956-1964.

Vanderreydt, I., Rommens, T., Tenhunen, A., Mortensen, L. F., & Tange, I. (2021). *Greenhouse gas emissions and natural capital implications of plastics (including biobased plastics)*. European Commission, DG Environment. Retrieved from https://environment.ec.europa.eu

Varghese, A., & Mittal, V. (2018). Surface modification of natural fibres. In V. Mittal (Ed.), *Surface modification of biodegradable and biocompatible polymers* (pp. 115–155). Elsevier.

Veazey, D., Hsu, T., & Gomez, E D. (2016). Next generation high-performance carbon fibre thermoplastic composites based on polyaryletherketones. *Journal of Applied Polymer Science*, 134(6). Vengadesan, E., Arunkumar, T., Muralidharan, S., Debnath, K., Dutta, H., & Kadirgama, K. (2025). Hybrid bio-composites reinforced with natural wood saw dust and eco-friendly graphite: Evaluation of physical, mechanical, and thermal properties. *Fibres and Polymers, 26*(3), 833–854.

Vermant, J., Cioccolo, G., Golapan Nair, K., & Moldenaers, P. (2004). Coalescence suppression in model immiscible polymer blends by nano-sized colloidal particles. *Rheologica Acta, 43*(5), 529–538.

Vogt, B. D., Stokes, K. K., & Kumar, S. K. (2021). Why is Recycling of Postconsumer Plastics so Challenging? *ACS Applied Polymer Materials, 3*(9), 4325–4346.

Volk, R., Stallkamp, C., Steins, J. J., Yogish, S. P., Müller, R. C., Stapf, D., & Schultmann, F. (2021). Techno-economic assessment and comparison of different plastic recycling pathways: A German case study. *Journal of Industrial Ecology, 25*(5), 1318-1337.

Wan, Y Z., Wang, Y., Luo, H., Dong, X., & Guo, C. (2000). Effects of fibre volume fraction, hot pressing parameters and alloying elements on tensile strength of carbon fibre reinforced copper matrix composite prepared by continuous three-step electrodeposition. *Materials Science and Engineering: A*, 288(1), 26-33.

Wan, Y., & Takahashi, J. (2021). Development of Carbon Fibre-Reinforced Thermoplastics for Mass-Produced Automotive Applications in Japan. *Journal of Composites Science*, 5(3), 86–86.

Wang, M.S. and Huang, J.C. (1994). Nylon 1010 properties and applications. *Journal of Polymer Engineering*, 13(2), 155–174.

Wang, S., Chen, Z., Ma, Q., Hu, H., & Zheng, W. (2005). Effect of fibre surface state on mechanical properties of Cf/Si–O–C composites. *Materials Science and Engineering: A*, 407(1-2), 245–249.

Wang, X., Chiang, M Y., & Snyder, C R. (2004). Monte-Carlo simulation for the fracture process and energy release rate of unidirectional carbon fibre-reinforced polymers at different temperatures. *Composites Part A: Applied Science and Manufacturing*, 35(11), 1277–1284.

Wang, D., Li, Y., Xie, X. -., & Guo, B. (2011). Compatibilization and morphology development of immiscible ternary polymer blends. *Polymer, 52*(1), 191-200.

Wang, X., Yang, T., Maeder, M., & Marburg, S. (2024). A novel fractional calculus modelling and physics-informed machine learning study on dynamic performance of hybrid flax/basalt fibre-reinforced composite. *Nonlinear Dynamics, 112*, 19917–19937.

Witayakran, S., Smitthipong, W., Wangpradid, R., Chollakup, R., & Clouston, P. L. (2017). Natural Fibre Composites: Review of Recent Automotive Trends. Elsevier eBooks, 166–174.

Wong, K. H., Pickering, S. J., & Brooks, R. (2007a). Recycled carbon fibre reinforced polypropylene composites: Effect of coupling agents on mechanical properties. In *Composites Innovation 2007 – Improved Sustainability and Environmental Performance*. NetComposites, Barcelona, Spain.

Wong, K. H., Pickering, S. J., Turner, T. A., & Warrior, N. A. (2007b). Preliminary feasibility study of reinforcing potential of recycled carbon fibre for flame-retardant grade epoxy composite. In *Composites Innovation 2007 – Improved Sustainability and Environmental Performance*. NetComposites, Barcelona, Spain.

Wong, K. H., Pickering, S. J., Turner, T. A., & Warrior, N. A. (2009a). Compression moulding of a recycled carbon fibre reinforced epoxy composite. Paper presented at the International SAMPE Symposium and Exhibition (Proceedings), 54, Baltimore, MD, USA.

Wong, K. H., Turner, T. A., Pickering, S. J., & Warrior, N. A. (2009b). The potential for fibre alignment in the manufacture of polymer composites from recycled carbon fibre. SAE Technical Papers, Seattle, Washington, USA.

Wong, D W., Lin, L., McGrail, P., Peijs, T., & Hogg, P. (2010). Improved fracture toughness of carbon fibre/epoxy composite laminates using dissolvable thermoplastic fibres. *Composites Part A: Applied Science and Manufacturing*, 41(6), 759-767.

Worrell, E., & Reuter, M. (Eds.). (2014). Handbook of Recycling: State-of-the-art for Practitioners, Analysts, and Scientists. Newnes.

Wool, R. P., Khot, S., LaScala, J., Bunker, S., Thielemans, W., Can, E., Morye, S., & Williams, G. T. (2002). Affordable Composites and Plastics from Renewable Resources: Part II: Manufacture of Composites. ACS Symposium Series, 205-224.

Wu, Q., Zhao, R., Ma, Q., & Zhu, J. (2018). Effects of degree of chemical interaction between carbon fibres and surface sizing on interfacial properties of epoxy composites. *Composites Science and Technology*, 163, 34-40.

Xiong, C., Li, Q., Lan, T., Li, H., Long, W., & Xing, F. (2021). Sustainable use of recycled carbon fibre reinforced polymer and crumb rubber in concrete: Mechanical properties and ecological evaluation. *Journal of Cleaner Production*, 279, 123624.

Xu, Y Y., Zhang, T., Lin, Z R., Zhou, S., & Xu, X. (2011). Advances in Research of Carbon Fibre Reinforced Composite Materials.

Yan, L., Chouw, N., & Yuan, X. (2012). Improving the mechanical properties of natural fibre fabric reinforced epoxy composites by alkali treatment. *Journal of Reinforced Plastics and Composites,* 31(6), 425-437.

Yao, S., Jin, F., Rhee, K Y., Hui, D., & Park, S. (2018). Recent advances in carbon-fibre-reinforced thermoplastic composites: A review. *Composites Part B: Engineering*, 142, 241-250.

Yue, Z., Jiang, W., Wang, L., Gardner, S D., & Pittman, C U. (1999). Surface characterization of electrochemically oxidized carbon fibres. *Carbon, 37*(11), 1785-1796.

Yu, T., Li, Y., & Ren, J. (2009). Preparation and properties of short natural fibre reinforced poly(lactic acid) composites. *Transactions of Nonferrous Metals Society of China, 19*(Supplement 2), s651–s655.

Yu, T., Ren, J., Li, S., Yuan, H., & Li, Y. (2010). Effect of fibre surface-treatments on the properties of poly(lactic acid)/ramie composites. *Composites Part A: Applied Science and Manufacturing,* 41(4), 499-505.

Yu, T., Ren, J., Li, S., Yuan, H., & Li, Y. (2011). Effect of fibre surface-treatment on the properties of poly (lactic acid)/ramie composites. *Composites Part A: Applied Science and Manufacturing, 42*(6), 649-658.

Zanjanijam, A. R., Hakim, S., & Azizi, H. (2016). Morphological, dynamic mechanical, rheological and impact strength properties of the PP/PVB blends: The effect of waste PVB as a toughener. *RSC Advances, 6*(50), 44673-44686.

Zhang, S., & Horrocks, A. R. (2003). A review of flame retardant polypropylene fibres. *Progress in Polymer Science*, 28

Zhang, W D., Shen, L., Phang, I Y., & Liu, T. (2003). Carbon Nanotubes Reinforced Nylon-6 Composite Prepared by Simple Melt-Compounding. *Macromolecules, 37*(2), 256-259.

Zhang, H., & Chen, M. (2014). Current recycling regulations and technologies for the typical plastic components of end-of-life passenger vehicles: A meaningful lesson for China. *Journal of Material Cycles and Waste Management, 16*(2), 187–200. https://doi.org/10.1007/s10163-013-0168-5

Zhang, W., Zhang, Y., Lu, C., & Zhou, Z. (2007). Study on the bio-tribological properties of a Mg-based alloy against different counterparts. *Wear, 262*(7–8), 819–825.

Zhang, X., Huang, Y., & Wang, T. (2007). Plasma activation of carbon fibres for polyarylacetylene composites. *Surface and Coatings Technology, 201*(9–11), 4965–4968.

Zhang, X. S., Yang, L., Liu, H. T., & Zu, M. (2017). A novel high-content CNT-reinforced SiC matrix composite-fibre by precursor infiltration and pyrolysis process. *RSC Advances, 7*(38), 23334–23341.

Zhang, H., Wu, Y., Wang, K., Peng, Y., Wang, D., Song, Y., & Wang, J. (2020). Materials selection of 3D-printed continuous carbon fibre reinforced composites considering multiple criteria. *Materials & Design, 196*, Article 109140.

Review on natural fibre reinforced polymer composites. (2013, January 27). *SpringerLink*. Retrieved from https://link.springer.com

Zhou, Y., Pervin, F., Rangari, V K., & Jeelani, S. (2006). Fabrication and evaluation of carbon nano fibre filled carbon/epoxy composite. *Materials Science and Engineering: A, 426*(1-2), 221-228.

Chapter 3 Materials and Experimental Methods

3.1 Materials

Rilsan© Polyamide 11 BMNO (density: 1.03 g/cm^3; Melt Flow Index @ 200°C: 18.9 g/10 min) was supplied by Arkema and polypropylene 3622 (density: 0.905 g/cm^3; Melt Flow Index @ 200°C: 7.3 g/10 min) was provided by Total Petrochemicals Inc. Cellulose microfibre or chemo-thermo mechanical pulp (CTMP), referred as WF in this manuscript, was supplied by Tembec (density: 1.4-1.5 g/cm^3) and was pelletized for easy handling and processing during extrusion. Carbon fibre (CF) was supplied by Zoltek (density: 1.81 g/cm^3). The length of cellulose microfibre used was 0.7-0.8 mm (diameter: 28 microns), whereas the length of carbon fibre used was 6 mm (diameter: 7 microns). Maleic anhydride grafted polypropylene (MAPP-G3003) was obtained from Eastman Chemical Company. Thermoplastic polyolefin (TPO CA 387 A) resin was provided by LyondellBasell Industries. A list of all raw materials with their most significant properties is represented in Table 4.

Table 4 List of Raw Materials and Their Most Significant Properties

Material & Manufacturer	Density (g/cm³)	MFI / Melt Flow (g/10 min @ Temp)	Tensile Modulus (GPa)	HDT (°C @246 Psi)	Key Properties	Applications / Roles
Rilsan® PA11 BMNO (Arkema)	1.03	18.9 @ 200 °C	1.6–2.2	~50–55	Low water uptake, high chemical resistance, biobased	Fuel lines, connectors, and overmoulding
Polypropylene 3622 (Total)	0.905	7.3 @ 200 °C	1.3–1.7	~55-65	Stiffness ~1.5 GPa, FDA compliant, moderate impact	Injection moulding, general purpose
TPO CA 387 A (LyondellBasell)	0.90–1.00	18.5 @ 230 °C	1.0–1.2	~110–120	Paintable, good impact and flow, Catalloy-based	Automotive fascia, durable weatherable parts
MAPP-G3003 (Eastman Chemical Co.)	~0.91	Not specified	~1.4 (est. PP base)	~90–110	Compatibilizer improves interfacial bonding	Coupling in PP/fibre composites
Cellulose Microfibre (CTMP)(Tembec)	1.40–1.50	N/A	10–30	Degrades ~250°C	Natural, high aspect ratio, high modulus	Biocomposites reinforcement

Carbon Fibre (Zoltek, chopped)	1.81	N/A	200–600	>300	Very high modulus and strength, chemically inert	Primary stiffener in composites

3.1.1 Polymer Blends and Composites Fabrication

Formulations used for the composite's preparation for different experimental approaches are presented in Table 5, Table 6, and Table 7. Two different polymer matrices were used to produce the composites: PA11 and a blend of PA11 and PP (76.5 wt% PA11, 13.5 wt% PP, and 10 wt% other additives). For the polymer blend composites, three different compositions of cellulose microfibre and carbon fibre were used in the experiment (WF30, WF20CF10, and WF10CF20), with a total fibre content of 30 wt% in each composite. All materials were oven-dried overnight at 65°C in a standard convection oven and then dried for 2 hours at 105°C prior to extrusion. The pre-dried materials were weighed to determine the weight percentage of each composition and were manually mixed prior to extrusion.

In composite manufacture, the polymer blend was not pre-processed and was mixed throughout the extrusion process in the presence of reinforcing fibres. The samples were extruded using a co-rotating twin screw extruder (Onyx model TEC, Canada) with a screw diameter of 25 mm, an L/D ratio of 40:1, and ten heating zones in the temperature range of 195-205°C. The pelletized extrudates were oven-dried for two hours at 105°C prior to injection moulding. Standard test specimens for tensile, flexural, and impact testing were injection moulded (Engel ES-28) according to ASTM D638, D790, and D256 specifications. Table 8 represents the temperature profile of the twin screw extruder, where carbon fibres were fed through the feeding hopper. Table 9 represents the temperature profile for twin screw extrusion for another set of composites in which carbon fibre feeding was done at the degassing zone. The injection moulding conditions were as follows: injection temperature, 204°C; injection time, 8 s; cooling time, 38 s; and mould opening time, 2 s.

Table 5 Composition of the extruded composite pellets

Extruded Pellets	Cellulose Microfibre	Carbon Fibre	PA11	MAPP

	(wt%)	(vol%)	(wt%)	(vol%)	(wt%)	(vol%)	(wt%)
WF10	10	7	-	-	86	93	4
WF20	20	15	-	-	76	85	4
WF30	30	23	-	-	66	77	4
WF20CF10	20	15	10	6	66	79	4
WF10CF20	10	8	20	13	66	79	4
CF30	-	-	30	20	66	80	4

Table 6 Composites Compositions with PA11 (PA) and Polymer Blend (PA+PP) Matrix

Extruded Pellets	Cellulose microfibre (wt%)	Carbon Fibre (wt%)	PA/PA+PP (wt%)	MAPP (wt%)
PA/PA+PP:WF30	30	-	66	4
PA/PA+PP:WF20CF10	20	10	66	4
PA/PA+PP:WF10CF20	10	20	66	4

Table 7 Composition of Modified Hybrid PA11 Composites

Extruded Pellets	Cellulose Microfibre		Carbon Fibre		PA11		MAPP
	(wt%)	(vol%)	(wt%)	(vol%)	(wt%)	(vol%)	(wt%)
PA11-WF10	10	7	-	-	86	93	4
PA11-WF10-CF2	10	7	2	1	84	92	4
PA11-WF10-CF5	10	7	5	3	81	90	4
PA11-WF10-CF10	10	7	10	6	76	86	4

Table 8 Extrusion Temperature Profile

Extrusion Zones	Zone 1	Zone 2	Zone 3	Zone 4	Zone 5	Zone 6	Zone 7	Zone 8	Zone 9	Zone 10
Temperature (°C)	190	195	195	200	200	200	200	200	200	200

Table 9 Modified Extrusion Temperature Profile

Extrusion Zones	Zone 1	Zone 2	Zone 3	Zone 4	Zone 5	Zone 6	Zone 7	Zone 8	Zone 9	Zone 10
Temperature (°C)	170	180	180	185	185	185	185	185	185	185

3.1.2 Material Characterization

3.1.2.1 Thermogravimetric Analysis

Thermal decomposition characterization of the polymers, fibres, and composites was carried out using thermogravimetric analysis (TGA). Approximately 10-15 mg of the samples were subjected to thermal degradation within a temperature range of ambient temperature to 800 °C in a thermogravimetric Analyzer (TA Instrument Q50, USA) at a heating rate of 10°C/min under a nitrogen gas flow.

3.1.2.2 Density

Densities of PA11, PP, the polymer blend, and the composites were measured using the ASTM D792 procedure at ambient temperature and were compared with their theoretical densities. The theoretical density of the composites was calculated using the following equations:

$$\rho_c = \rho_f V_f + \rho_m V_m \ ; \tag{1}$$

$$\mathrm{V_f} = \frac{\frac{\mathrm{w_f}}{\mathrm{\rho_f}}}{\frac{\mathrm{w_f}}{\mathrm{\rho_f}}+\frac{\mathrm{w_m}}{\mathrm{\rho_m}}} V_f \ = \frac{\frac{w_f}{\rho_f}}{\frac{w_f}{\rho_f}+\frac{w_m}{\rho_m}} ; \tag{2}$$

$$V_m = \frac{\frac{w_m}{\rho_m}}{\frac{w_f}{\rho_f}+\frac{w_m}{\rho_m}} \ ; \tag{3}$$

where ρ_c is the density of the composite, ρ_f and ρ_m are the densities of fibre and matrix, respectively. V_f, V_m, w_f, and w_m are the volume fraction and weight fraction for the fibre and matrix, respectively. The void content of the composites is defined as

$$\mathrm{V_v} = \frac{\rho_{ct} - \rho_{ce}}{\rho_{ct}} \ ; \tag{4}$$

where ρ_{ct} is the theoretical density and ρ_{ce} is the experimental density.

3.1.2.3 Melt Flow Index

Melt Flow Index (MFI) values of oven-dried PA, PA/PP blends, and the composites were measured using a melt index apparatus (Custom Scientific Instruments Inc.) by ASTM D1238 at 200 °C under a 2.16 kg load. Five replicates were performed for each sample.

3.2 Mechanical Properties

The static tensile and flexural properties of injection-moulded PA11, PA/PP blends, and their composites were measured using a universal testing machine (Instron 3367) according to ASTM standard test methods. Tensile tests were conducted according to ASTM D638, with a span length of 100 mm and a crosshead speed of 12.5 mm/min. Flexural tests were conducted according to ASTM D790 in a three-point loading model at a crosshead speed of 12.5 mm/min and a span width of 50 mm. Izod impact tests were conducted using a digital pendulum impact tester (Tinius Olsen 892) equipped with automatic correction for pendulum windage and pendulum bearing friction, as specified in ASTM D256. Six non-conditioned specimens were tested for each sample set in all mechanical tests.

3.3 Scanning Electron Microscopy

Scanning electron microscopy (SEM) (Hitachi S-2500, Tokyo, Japan) was used to observe the fracture surfaces of tensile samples under high magnification. Samples were cut carefully to preserve the fracture surfaces. The fracture surface was gold-sputtered to avoid electrostatic charge during the examination. Images were taken using an accelerating voltage of 15kV and a working distance of 10 mm.

3.4 Thermal Properties

3.4.1 Heat Deflection Temperature

A Heat Deflection Temperature (HDT) test was performed to study the behaviour of PA11, PA/PP blends, and the composites under stress at elevated temperatures. The tests were performed according to ASTM D648. Three injection-moulded samples for each specimen were used, with a heating rate of 2±0.2°C/min (CSI 107-M1-252). The temperature at a 0.25% deflection of the

sample bars under a constant load of 264 psi (1.82 MPa) was recorded as the HDT value. After each measurement, the apparatus was cooled by recirculating water until it reached a temperature of 20°C.

3.5 Water Absorption/Uptake

The water absorption test was conducted according to ASTM D570-98 (Two-hour Boiling Water Immersion). The percentage of water uptake was calculated using the following equation

$$Water\ Absorption\ (\%) = \frac{W_t - W_0}{W_0} \times 100\,, \tag{5}$$

Where W_t is the weight of the sample after boiling at time t, and W_0 is the initial weight of the sample at t=0.

Chapter 4 Results and Discussion

4.1 Cellulose Microfibre reinforced PA11 composites

4.1.1 Thermogravimetric analysis

The thermal degradation properties of PA11, cellulose microfibres, and carbon fibres were examined using TGA. Figure 3 shows the weight loss (%) with rising temperature from room temperature to 800°C for PA11 and the fibres. The graph shows no considerable weight change for PA11 and carbon fibres from ambient temperature to 200°C. In contrast, cellulose microfibre showed about 3% weight loss, indicating the presence of moisture in the cellulose microfibre. According to the TGA profiles, the onset degradation temperature for cellulose microfibre is around 200°C, followed by the maximum degradation temperature of around 300°C. Degradation of PA11 occurred between 350°C and 475°C. Carbon fibre exhibited a stable profile, with only around 4% decomposed materials, which is correlated with its sizing and coating materials. The important thermal characteristics captured by these plots, including temperatures at 25%, 50%, and 75% weight loss, maximum degradation, and residue at 800 °C, are extracted in Table 10. The findings indicated that cellulose microfibre exhibits lower thermal stability than polymer and carbon fibre. The residual amount of cellulose microfibre, approximately 18%, is likely attributable to the presence of lignin within the cellulose microfibres.

As presented in Figure 4a, samples WF10, WF20, and WF30 followed similar patterns with a two-stage decomposition profile. Compared to PA11, the weight of cellulose microfibre-reinforced composites decreased more rapidly with increased temperature. In the first stage, starting at around 200°C, a weight loss was observed, which was attributed to the degradation of cellulose microfibres in the composites. The second decomposition stage, correlated with PA11 degradation, began at approximately 350°C and was followed by the maximum decomposition at around 430 °C. However, it was observed that as the fibre content in the composite increased, the second decomposition temperature was slightly shifted to a higher temperature (Figure 14b). For example, a 50% loss was observed at approximately 424, 429, and 436°C, corresponding to the thermal stability of the composites WF10, WF20, and WF30, respectively. This trend can be attributed to the high thermal stability of lignin; as the cellulose microfibre content in the composites increased, so did the lignin content. Additionally, this observation may suggest a strong interaction between the cellulose microfibre and polyamide, enhancing the composites' thermal properties.

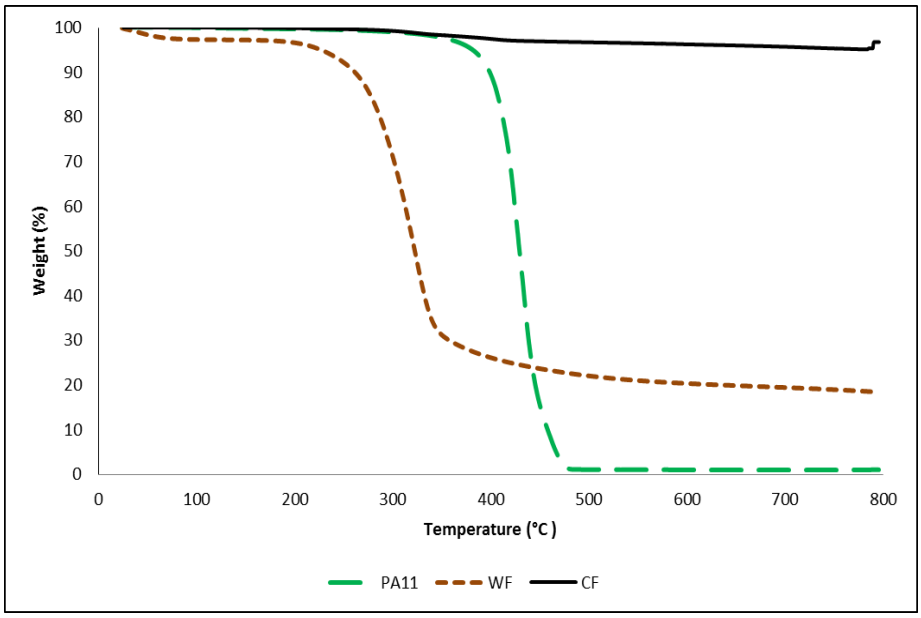

Figure 3 TGA Results for Neat PA11, Cellulose Microfibre (WF), and Carbon Fibre (CF)

Table 10 TGA Results Showing Degradation Temperatures for Neat PA11, Cellulose Microfibre, and Carbon Fibre

Base Materials	$T_{25\%}$ (°C)	$T_{50\%}$ (°C)	$T_{75\%}$ (°C)	T_{max} (°C)	Residue after 800°C (%)
Neat PA11	416	429	441	426	1
Cellulose microfibre (WF)	295	322	421	318	18
Carbon Fibre (CF)	-	-	-	-	96

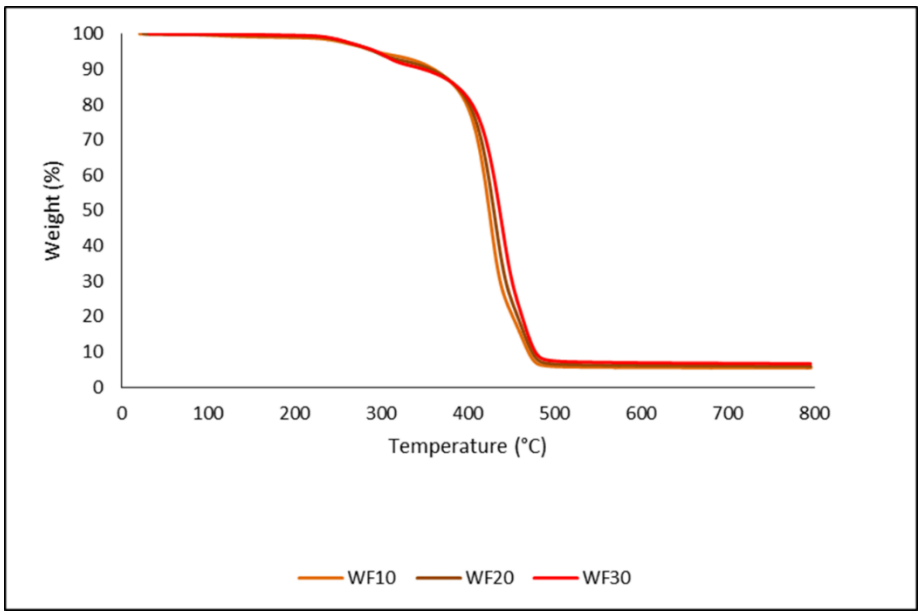

Figure 4a TGA Results for Cellulose Microfibre-reinforced Composites (WF10, WF20, and WF30)

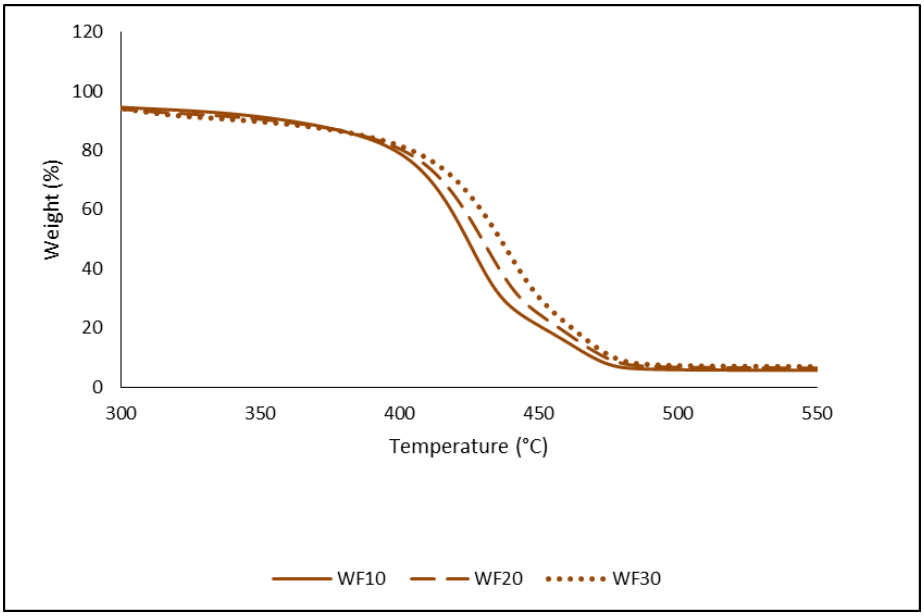

Figure 14 b Shift of the Second Decomposition Temperature of Cellulose Microfibre-reinforced Composites Towards Higher Temperature in Detail

4.1.2 Density

The density of a material is directly related to the weight of automotive components. It serves as an indicator of the potential for weight reduction through the use of hybrid biocomposites. Table

11 represents experimental and theoretical densities of the composites. As anticipated, the densities of the composites showed a slight increase with higher fibre content. All measured densities were lower than their theoretical counterparts, likely due to the presence of voids in the produced composites. The void content significantly affects the mechanical properties and fatigue strength of the composites, as it makes them more susceptible to moisture penetration (De Almeida et al., 1994). They act like defects, serving as stress concentrators and reducing stiffness, strength, and fatigue resistance.

The findings revealed that the void content in cellulose microfibre-reinforced composites (WF10, WF20, and WF30) increased with the rising fibre content. This may be due to inadequate interfacial bonding between the fibres and the matrix, resulting from a higher tendency of fibre agglomeration at increased fibre concentrations. Dhakal et al. (2007) reported similar outcomes in their study of hemp fibre-reinforced unsaturated polyester composites, noting that higher volume fractions of hemp fibre corresponded with increased void content.

Table 11 Experimental density vs. theoretical density of the Cellulose microfibre Composites

PA11 Composites	Experimental Density (g/ml)	Theoretical Density (g/ml)	Void Content (%)
WF10	1.04 ± 0.014	1.06	~1.9
WF20	1.07 ± 0.008	1.10	~2.7
WF30	1.08 ± 0.011	1.14	~5.3

4.1.3 Melt Flow Index

The Melt Flow Index (MFI) measures the ease with which a material flows through a die at a designated temperature and under a specified load. MFI is widely recognized as a key material property that indicates the processability of various materials, particularly in processes like injection moulding. The MFI results are presented in

Table *12*.

The MFI for neat PA11 was 18.9 ± 3.9 g/10 min. Compared to the neat polymer, the composites showed much lower MFI values, indicating that the presence of fibre reduced the mobility of the

polymer molecules under stress. As expected, an increase in fibre content reduced the MFI values. The presence of fibres in the polymer matrix interferes with the viscoelastic dynamics of the melt by limiting the mobility of molecular chains. As a result, this leads to lower MFI values, particularly pronounced in composites with higher fibre content (Ota et al., 2005).

Additionally, cellulose microfibres are structured as fibre bundles, which can be defibrillated into microfibrils during the compounding process. These microfibrils may remain on the fibre surface or disperse within the matrix (Sain et al., 2015). The formation of elementary microfibrils increases the surface area of the fibres, potentially leading to improved wetting of the fibres by the matrix, thereby increasing entanglement with the matrix. This further restricts the mobility of the polymer, contributing to the observed decrease in MFI.

Table 12 MFI for neat PA11 and the composites

Samples	MFI pellets from extrusion g/10 min
Neat PA11	18.9 ± 3.9
WF10	8.9 ± 1.6
WF20	4.8 ± 0.6
WF30	2.3 ± 0.3

4.1.4 Mechanical Properties

4.1.4.1 Tensile and Flexural Properties

Table 13 represents tensile and flexural strength and modulus for non-conditioned neat PA11 and cellulose microfibre-reinforced composites. The results showed that the tensile and flexural strength of the composites increased with the increase in fibre content. Compared to neat PA11, the tensile strength was improved from 10% to 22% with the addition of cellulose microfibre from 10 wt% to 30 wt%, while the flexural strength was enhanced by 15% to 30%. Moreover, compared to PA11, tensile and flexural modulus were improved from 37% to 71% and from 26% to 64%, respectively, with the addition of cellulose microfibre from 10 wt% to 30 wt% (Table 13). As expected, higher cellulose microfibre content resulted in higher tensile and flexural strength and modulus.

Table 13 Tensile and flexural strength and modulus, for neat PA11 and cellulose microfibre-reinforced composites (WF10, WF20, WF30)

Sample	Tensile Strength (MPa)	Tensile Modulus (GPa)	Flexural Strength (MPa)	Flexural Modulus (GPa)
Neat PA11	35.4 ± 0.8	1.04 ± 0.04	53.5 ± 0.9	1.10 ± 0.02
WF10	38.8 ± 0.5	1.41 ± 0.01	61.4 ± 0.7	1.39 ± 0.02
WF20	40.0 ± 1.2	1.61 ± 0.07	66.8 ± 0.7	1.64 ± 0.04
WF30	43.3 ± 0.5	1.78 ± 0.02	69.9 ± 0.8	1.80 ± 0.03

4.1.4.2 Impact Properties

Impact strength measures a material's capacity to withstand fracture under high-speed stress and is directly linked to its toughness as a composite. It indicates the energy needed for crack propagation through a notch or any deformation in the material (known as notched impact strength). This characteristic is often considered a significant weak point in natural fibre-reinforced composites (Panthapulakkal & Sain, 2007; Ranganathan et al., 2015). The impact strengths of neat PA11 and its composites were measured using both notched and unnotched Izod impact testing. Table 14 shows the notched and unnotched Izod impact strength for neat PA11 and cellulose microfibre-reinforced composites. Notched impact tests showed a strength of 73±12 J/m for neat PA11; however, adding cellulose microfibre significantly decreased the impact strength. The increase in cellulose microfibre content slightly improved the notched impact strength.

As shown in Table 14, the unnotched impact strengths of the cellulose microfibre composites are lower than those of neat PA11. The neat PA11 did not fracture during the unnotched impact test and exceeded the machine limit of 750 J/m. Composite WF10 exhibited a relatively high unnotched impact strength, which may be attributed to the low fibre content of the composite (10% WF). The low fibre content of the composite could result in matrix dilution, which makes the composite's performance quite similar to its matrix.

Table 14 Impact strength for neat PA11, and cellulose microfibre-reinforced composites (WF10, WF20, WF30)

Sample	Notched Impact Strength (J/m)	Unnotched Impact Strength (J/m)
Neat PA11	73.0 ± 12	>750

WF10	21.6 ± 0.83	430 ± 82
WF20	22.4 ± 0.75	227 ± 36
WF30	23.9 ± 0.91	228 ± 39

4.1.5 Scanning Electron Microscopy

The fracture surfaces of the impact test samples were observed by SEM (Figure 5). SEM is a valuable tool for investigating the fibre-matrix interaction and fracture behaviour of composites. Figure 5 shows effective fibre/matrix interfacial bonding, efficient component integration, and good fibre dispersion. Matrix cracking was not detected in any of the composite materials. The adequate interfacial bonding facilitated efficient stress transfer from the matrix to the fibres, and fibre fracture indicated that the applied stress exceeded the strength of the fibres. However, as the fibre content increased, voids emerged on the fracture surfaces. This may be attributed to inadequate interfacial bonding between the fibres and the matrix, due to a higher likelihood of fibre agglomeration at higher fibre concentrations. This is consistent with density test results, which show that the void content increased as the fibre content increased. Generally, fibre breakage/deformation and fibre-matrix interface degradation were likely the dominant failure mechanisms in cellulose microfibre composites.

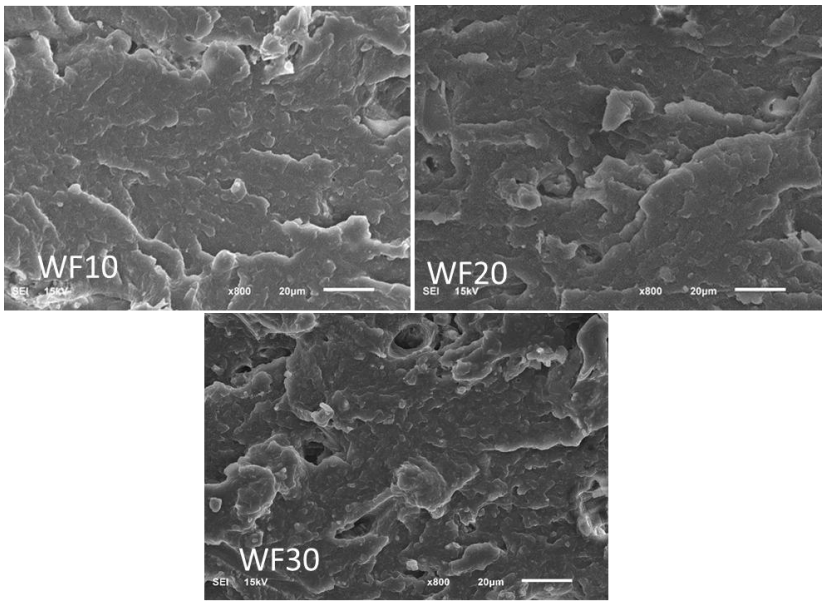

Figure 5 SEM Images of the Fracture Surface of the Composites WF10, WF20, and WF30 at 800X

4.1.6 Heat Deflection Temperature

Heat deflection temperature, also known as heat distortion temperature, measures the upper limit of dimensional stability for materials under a specific load at elevated temperatures. This thermomechanical property predicts the variation in stiffness of materials as temperatures rise and indicates the temperature at which a defined degree of deflection occurs under a given loading condition. It is a crucial material characteristic to consider when selecting materials for thermo-mechanically demanding applications.

The HDT values for neat PA11 and the composites are shown in Figure 6. The HDT for neat PA11 was 44°C, and no improvement was observed in the HDT of composite WF10. By increasing the cellulose microfibre content, a slight improvement in HDT was observed for composites WF20 and WF30. As illustrated in Figure 6, with the addition of 20% and 30% cellulose microfibre to the PA11 matrix, respectively, approximately 4.5% and 11% increases in HDT values were observed.

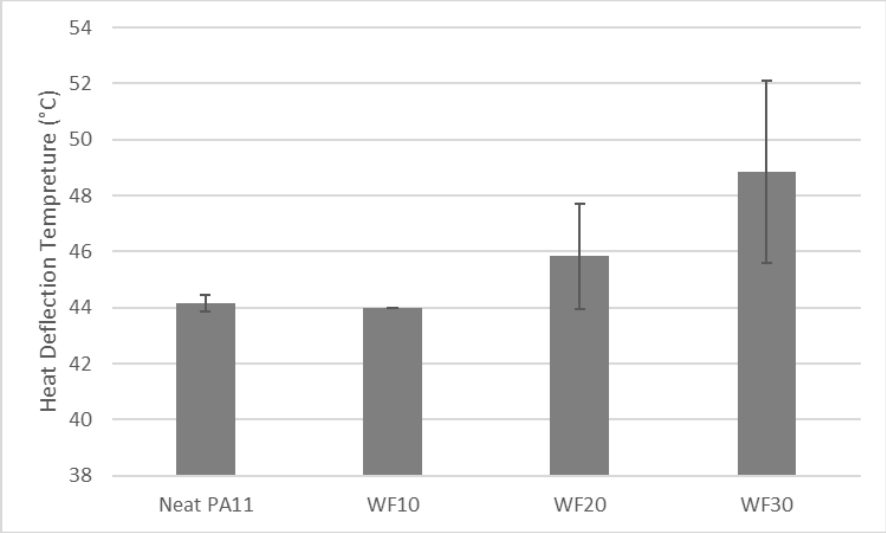

Figure 6 HDT for Composites: Cellulose Microfibre-reinforced (WF10, WF20, WF30) Composites

4.1.7 Water Absorption/Uptake

Water absorption in natural fibre-reinforced composites is a critical issue, primarily due to the moisture sensitivity of the natural fibre. This concern intensifies at elevated temperatures, where the rate of water uptake significantly accelerates. Such increased moisture exposure leads to a

marked reduction in mechanical properties, primarily due to the degradation of the fibre-matrix interface (Panthapulakkal & Sain, 2007; Dhakal et al., 2007).

Additionally, water absorption can cause swelling, resulting in dimensional instability and variation within the composites (Saheb & Jog, 1999). Notably, the extent of water uptake is further influenced by the fibre volume fraction; higher fractions typically result in increased void content, exacerbating moisture ingress.

Figure 7 represents water absorption for neat PA11 and the composites. The results indicate that adding cellulose microfibre increased the water absorption of the composites. As expected, with increasing cellulose microfibre content in the composites, water absorption also increased. The highest water absorption is detected for WF30, in which the water absorption was increased by 70% compared to neat PA11 (Figure 7). The water absorption of the PA11 was increased by approximately 28%, 57%, and 200% by increasing the cellulose microfibre by 10%, 20%, and 30%, respectively.

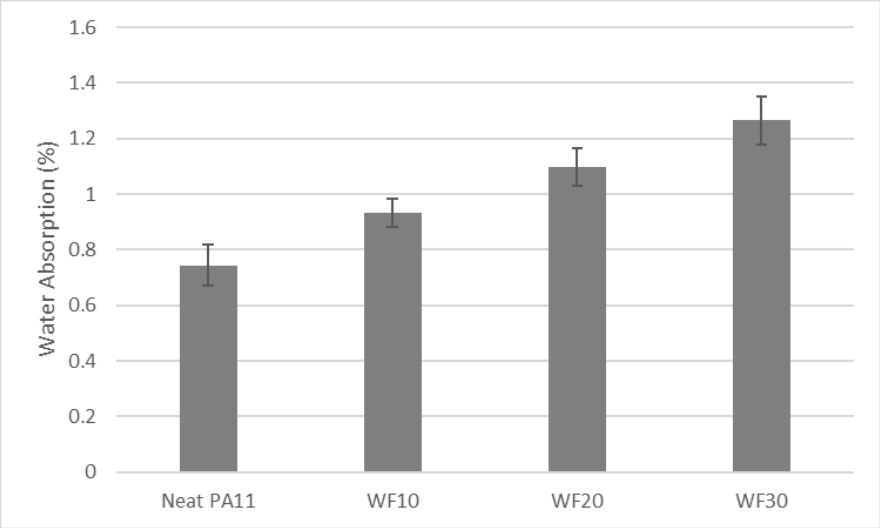

Figure 7 Water Absorption for Composites: Cellulose Microfibre-reinforced (WF10, WF20, WF30) Composites

4.2 Effect of Hybridization with Carbon Fibre on Cellulose Microfibre Reinforced PA11

4.2.1 Thermogravimetric Analysis

Figure 8 represents TGA profiles for composites with 30% reinforcements (WF30, WF20CF10, WF10CF20, and CF30). As shown in Figure 8, hybrid composites (WF20CF10 & WF10CF20)

exhibited a two-stage decomposition profile. The two-stage profile represented the decomposition of cellulose microfibre in the first stage at around 200 °C, followed by the decomposition of PA11 in the second stage at 350-430°C. Carbon fibre did not decompose in the decomposition profiles and increased the residue at the end. The incorporation of carbon fibre decreased the rate of decomposition and enhanced thermal stability. The degradation profile of hybrid composites indicates that they exhibit higher thermal stability than composites reinforced only by cellulose microfibres, showing that hybridization with carbon fibre enhances the composites' thermal performance. The weight percentages at 450°C were approximately 30%, 35%, and 40% for the cellulose microfibre composite (WF30), hybrid composites (WF20CF10 & WF10CF20), and carbon fibre composite (CF30), respectively. Composite CF30, however, showed a one-stage decomposition profile as a PA11 degradation profile, and almost all the initial carbon fibre content remained in the leftover, indicating that the carbon fibre did not decompose.

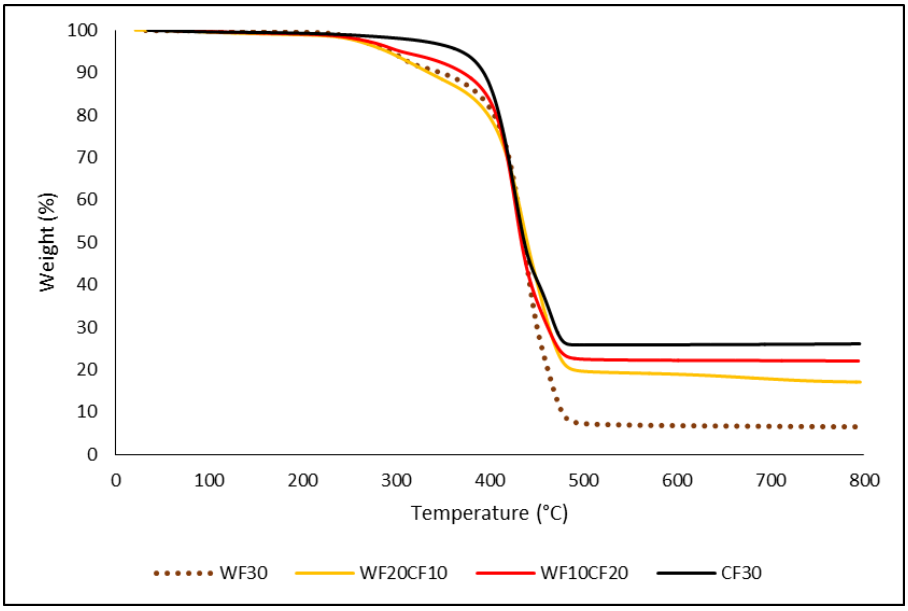

Figure 8 TGA Results for Composites with 30% Fibre Content: Cellulose Microfibre-reinforced (WF30), Hybrid (WF20CF10, WF10CF20), and Carbon Fibre-reinforced (CF30) Composites

4.2.2 Density

Hybridization with carbon fibre increased the density of the composites, and increasing the amount of carbon fibre led to higher densities. As shown in Table 15, among the 30 wt% reinforced

composites, the hybrid composite WF10CF20 exhibited the lowest void content, comparable to WF10. This suggests that the addition of carbon fibre partially alleviated the void content issue in the WF-reinforced composites. The reduced void content in the hybrid composites reflects better wettability of the fibres with the matrix and enhanced adhesion between the fibre and matrix.

The detrimental effect of void content is often more pronounced in natural fibre composites than in their synthetic counterparts. This is because natural fibres possess intrinsically lower strength and stiffness, and their mechanical performance is further affected by inherent variability in fibre dimensions, defects, and moisture content. Consequently, the presence of voids amplifies these weaknesses, leading to greater reductions in stiffness and strength compared to synthetic fibre-reinforced composites. Furthermore, natural fibres are generally more hydrophilic than synthetic fibres, which might result in challenges with achieving complete wetting of the fibres by the resin and a higher likelihood of void creation. This can lead to inadequate fibre interfacial bonding and insufficient resin flow during the manufacturing phase, resulting in voids within the composite material. Additionally, moisture present in the fibres can contribute to void formation during the curing stage.

Table 15 Experimental density vs. theoretical density of the composites

Samples	Experimental Density (g/ml)	Theoretical Density (g/ml)	Void Content (%)
WF30	1.08 ± 0.011	1.14	~5.3
WF20CF10	1.12 ± 0.005	1.15	~2.6
WF10CF20	1.15 ± 0.002	1.17	~1.7
CF30	1.15 ± 0.004	1.18	~2.5

4.2.3 Melt Flow Index

Compared to WF30, the incorporation of carbon fibre in the hybrid composite increased MFI by around 239% and 248% for WF20CF10 and WF10CF20, respectively (Table 16). This enhances the processability of the hybrid composites. However, CF30 exhibits a lower melt flow index (MFI) compared to the hybrid composites. This discrepancy may stem from differences in the compatibility between the fibres and the matrix. As previously noted, all composites contain the same amount of compatibilizer. In hybrid composites, the compatibilizer may facilitate stronger interactions between the cellulose microfibres and the polymer rather than enhancing the

interaction between the carbon fibres and the polymer matrix. Conversely, in CF30, the compatibilizer may reinforce the interaction between the carbon fibres and the matrix, which could hinder polymer flow relative to the hybrid composites. Additionally, a comparison of the SEM images reveals that the carbon fibres in the CF30 composites are more thoroughly coated with the polymer matrix than those in the hybrid composites, suggesting a more pronounced interaction of the carbon fibres within the CF30 composites than their hybrid counterparts. SEM images show voids and a strong interface between fibres and matrix for both hybrid and CF30 composites.

Table 16 MFI for neat PA11 and the composites

Sample	MFI pellets from extrusion (g/10 min)
WF30	2.3 ± 0.3
WF20CF10	7.8 ± 0.4
WF10CF20	8.0 ± 0.7
CF30	5.4 ± 0.9

4.2.4 Mechanical Properties

4.2.4.1 Tensile and Flexural Properties

Figure 9 and Figure 10 show tensile and flexural strength and modulus for composites with 30% reinforcement (WF30, WF20CF10, WF10CF20, and CF30), respectively. The results showed that incorporating carbon fibre increased the tensile strength of composites WF20CF10, WF10CF20, and CF30 by 36%, 65%, and 105%, respectively, compared to WF30 (Figure 9). Compared to WF30, the flexural strength was improved by 41% and 73% for hybrid composites WF20CF10 and WF10CF20, respectively, and by 103% for composite CF30 (Figure 9).

In hybrid composites, as the carbon fibre content increased, the tensile and flexural strength of the composites enhanced. A similar trend has been observed for the tensile and flexural modulus of the composites, which is due to the higher strength and modulus of carbon fibre. Tensile modulus for the hybrid composites WF20CF10 and WF10CF20 was improved by 79% and 168%, respectively (Figure 10). The flexural modulus for WF20CF10 and WF10CF20 was enhanced by 75% and 142%, respectively (Figure 10). Compared to WF30, tensile and flexural modulus of CF30 enhanced by 203% and 204%, respectively (Figure 10). The results showed that the incorporation of carbon fibre improved the tensile and flexural properties (strength and modulus)

of the composites, owing to its excellent mechanical properties. The results also represented a good fibre-matrix adhesion, resulting in a good transfer of the applied load from the matrix to the fibres. Similar outcomes have been reported by Magniez et al. (2014) for carbon fibre-reinforced PA11.

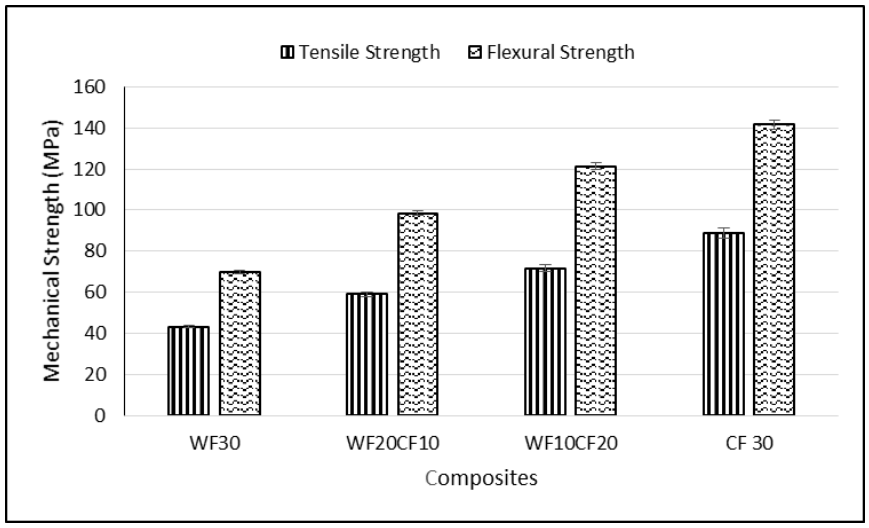

Figure 9 Tensile and Flexural Strength for Composites with 30% Fibre Content: Cellulose Microfibre-reinforced (WF30), Hybrid (WF20CF10, WF10CF20), and Carbon Fibre-reinforced (CF30) Composites

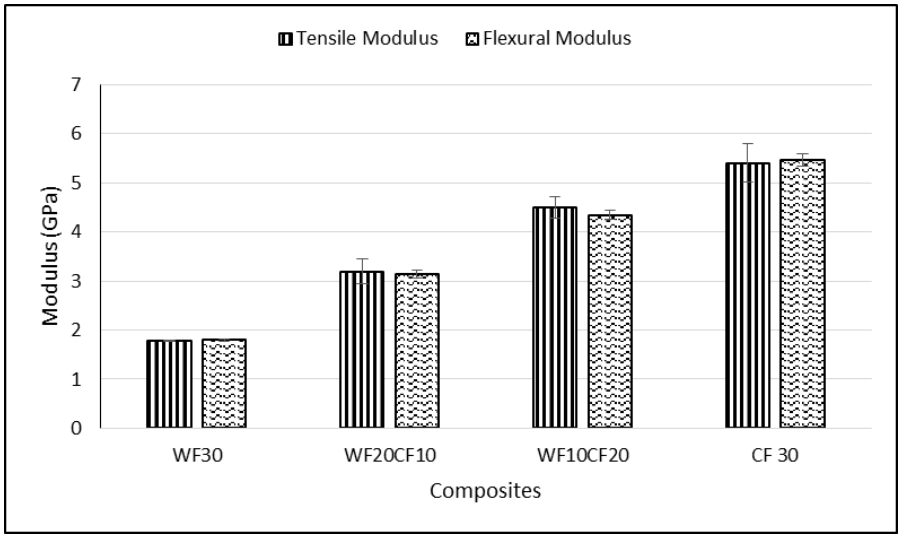

Figure 10 Tensile and Flexural Strength for Composites with 30% Fibre Content: Cellulose Microfibre-reinforced (WF30), Hybrid (WF20CF10, WF10CF20), and Carbon Fibre-reinforced (CF30) Composites

4.2.4.2 Impact Properties

Figure 11 represents the notched impact strength for composites with 30% reinforcement. As shown in Figure 11, incorporating carbon fibre in the composites improved notched impact strength to some extent. Composite CF30 represented the highest notched impact strength at 88.35±3 J/m, which was improved by about 20% compared to neat PA11. Compared to WF30, hybridization with carbon fibre increased the notched impact strength of the composite WF20CF10 and WF10CF20 by 9% and 88%, respectively (Figure 11).

Figure 12 represents the unnotched impact strength for composites with 30% reinforcement. Compared to WF30, hybridization with carbon fibre increased the unnotched impact strength of the composite WF20CF10 and WF10CF20 by 46% and 77%, respectively (Figure 12). Generally, the addition of carbon fibre increased the unnotched impact strength of the composites. Consequently, hybridization with carbon fibre improved both notched and unnotched impact strength. Proper interfacial strength between fibres and matrix may result in an increase in impact strength in hybrid biocomposites. However, the incorporation of two dissimilar fibres may also lead to a non-uniform distribution of fibres in the matrix. The impact strength requires further enhancement for use in mechanically robust structural applications.

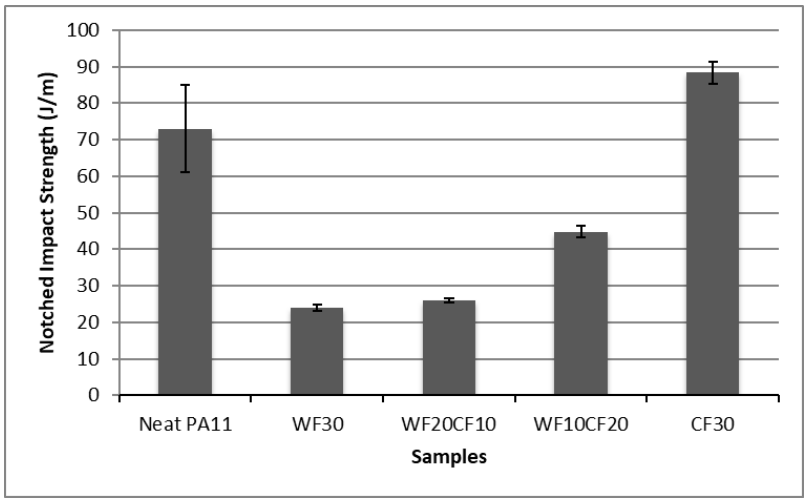

Figure 11 Notched Impact Strength for Composites with 30% Fibre Content: Cellulose Microfibre-reinforced (WF30), Hybrid (WF20CF10, WF10CF20), and Carbon Fibre-reinforced (CF30) Composites

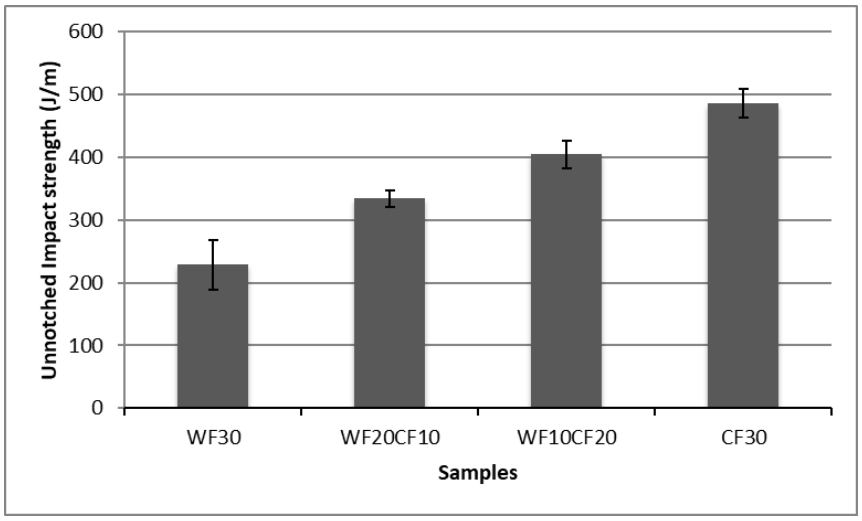

Figure 12 Unnotched Impact Strength for Composites with 30% Fibre Content: Cellulose Microfibre-reinforced (WF30), Hybrid (WF20CF10, WF10CF20), and Carbon Fibre-reinforced (CF30) Composites

4.2.5 Scanning Electron Microscopy

The SEM Figure 13 show effective fibre/matrix interfacial bonding with efficient component integration and good fibre dispersion. No instances of matrix cracking were observed in any of the composite materials analyzed. The establishment of proper interfacial bonding resulted in efficient stress transfer from the matrix to the fibres, with fibre fracture indicating that the applied stress exceeded the fibres' strength. As the fibre content increased, the presence of voids on the fracture surfaces became evident, which can be attributed to insufficient interfacial bonding between the fibres and the matrix. This observation is consistent with the density test results, which indicate that the void content increased with increasing fibre content. Furthermore, fibre pullout was notably more pronounced in composites reinforced with carbon fibre, specifically in the samples WF20CF10, WF10CF20, and CF30. In general, the mechanical behaviour of carbon fibre-reinforced and hybrid composites was governed by mechanisms related to both fibre pullout and fibre breakage.

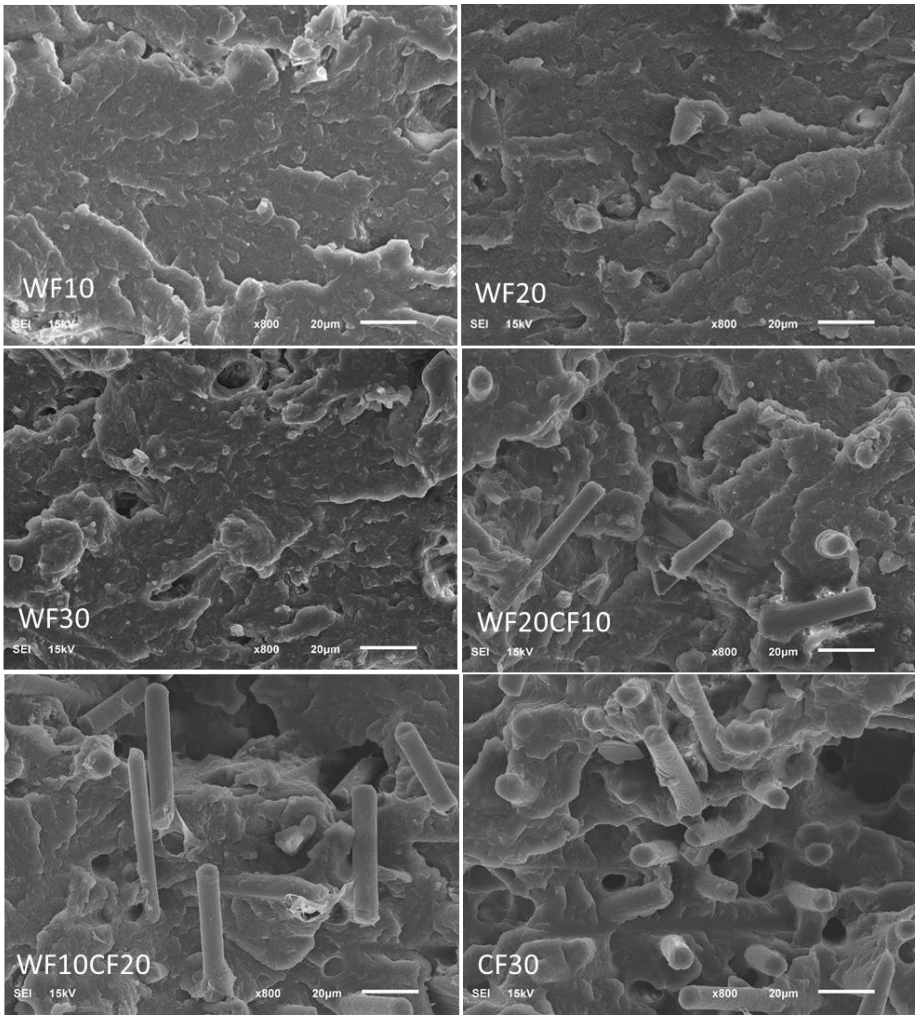

Figure 13 SEM Images of Fracture Surface of the Composites WF30, WF20CF10, WF10CF20, and CF30 at 800X

4.2.6 Heat Deflection Temperature

The HDT values for neat PA11 composites are shown in Figure 14. The incorporation of carbon fibre resulted in much higher HDT values. The highest HDT value was for the hybrid composite WF10CF20 at 123°C, which is significantly higher than the HDT of neat PA11 and cellulose microfibre-reinforced composites (WF10, WF20, and WF30), and lower than CF30 (142°C).

As shown in Figure 14, hybridization with carbon fibre improved the HDT values for the composites WF20CF10 and WF10CF20 by 106% and 159%, respectively, compared to WF30. This result suggests that these hybrid biocomposites have the potential to be applied where the maximum service temperature requirement is around 120°C.

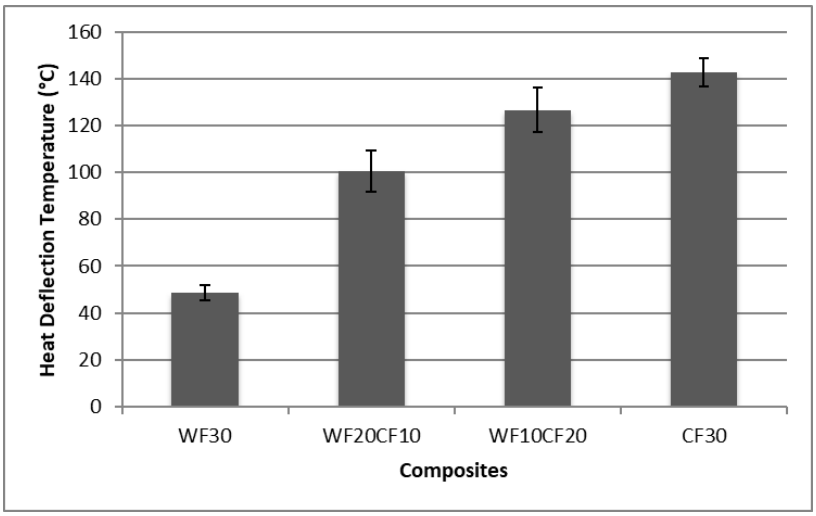

Figure 14 HDT for Composites: Cellulose Microfibre-reinforced (WF30), Hybrid (WF20CF10, WF10CF20), and Carbon Fibre-reinforced (CF30) Composites

4.2.7 Water Absorption/Uptake

The reported values in Figure 15 indicated that the incorporation of carbon fibre in cellulose microfibre composites decreased their water absorption. Compared to WF30, the water uptake for WF20CF10 and WF10CF20 was reduced by 18% and 52%, respectively (Figure 15). Reducing cellulose microfibre content from 20 wt% to 10 wt% in hybrid composites (WF20CF10 to WF10CF20) resulted in lower water uptake. The lowest water absorption was observed for CF30 due to the absence of cellulose microfibre in the composites.

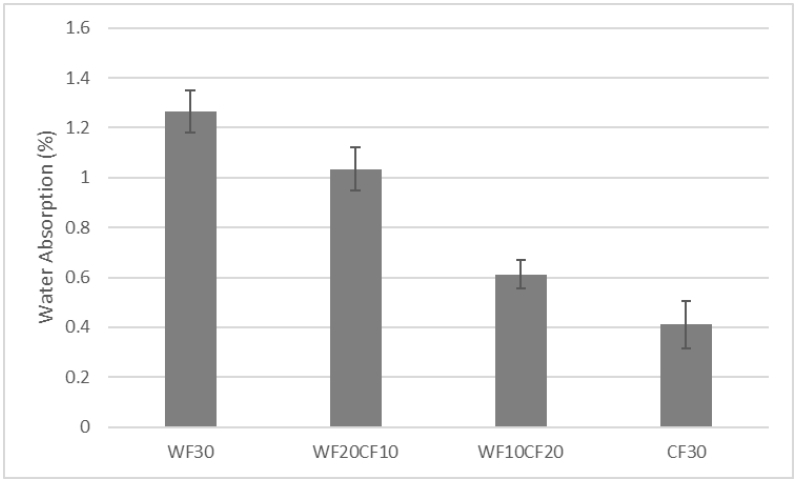

Figure 15 Water Absorption for Composites: Cellulose Microfibre-reinforced (WF30), Hybrid (WF20CF10&WF10CF20), and Carbon Fibre-reinforced (CF30) Composites4.3 Effect of Polymer Blending on the Hybrid Composites

4.3 Polymer Blends (PA/PP) Compositions

Bio-polyamide 11 underwent a slight degradation at elevated temperatures during processing in the earlier observations of the study on developing cellulose microfibre-reinforced bio-polyamide composites. Therefore, to overcome thermal degradation and enhance the processability of the composites at elevated temperatures, a thermoplastic matrix blend of bio-polyamide 11 and polypropylene was used, combining the advantageous properties of each while reducing costs to some extent.

Various formulations were tested for the polymer blends of PA and PP. Different blend compositions with their most important properties are presented in Table 17. Our selected polymer blend, composed of 76.5 wt% PA11, 13.5 wt% PP, and 10 wt% copolymer and MAPP, exhibited a balance of properties, including notched impact strength and MFI. It is expected that tensile and flexural properties, as well as HDT, increase with the addition of reinforcing fibres. However, adding fibre usually decreases the impact strength and MFI; therefore, the polymer blend with the highest impact strength and moderate MFI was selected for further study. The HDT values were quite similar for most of the polymer blends.

Table 17 Different Polymer Blend (PA/PP) Compositions with Some Important Properties

Blend Composition (Wt%)		Tensile Strength (MPa)	Tensile Modulus (GPa)	Flexural Strength (MPa)	Flexural Modulus (GPa)	Notched Impact Strength (J/m)	MFI (g/10min)	HDT (°C)
PA	100	35.4±0.8	1.0±0.04	53.4±0.9	1.1±0.01	73±12	18.9±3.9	44±0.5
PP	0							
TPO	0							
MAPP	0							
PA	81	35.8±0.2	1.2±0.03	49.5±0.9	1.1±0.02	54±2	8.5±0.3	45±0.5
PP	9							
TPO	7							

MAPP	3							
PA	76.5	32.2±0.4	1.2±0.03	49.1±0.5	1.1±0.01	66±4	8.1±0.2	45±0.4
PP	13.5							
TPO	7							
MAPP	3							
PA	68	31.5±0.4	1.2±0.03	47.4±1.3	1.1±0.04	61±3	7.0±0.3	45±0.7
PP	17							
TPO	10							
MAPP	5							
PA	60	32.8±0.4	1.2±0.02	49.7±1.9	1.2±0.1	58±3	6.6±0.2	47±0.6
PP	25							
TPO	10							
MAPP	5							

4.3.1 Material Characterization

4.3.1.1 Thermogravimetric Analysis

Figure 16 shows the weight loss (%) with rising temperature from room temperature to 800°C for the polymers and the fibres. The graph shows no considerable weight change for the polymers and carbon fibres in the ambient temperature range of 200°C, whereas cellulose microfibre showed about 3% weight loss, representing the moisture uptake of the fibre. According to the TGA profiles, the onset degradation temperature for cellulose microfibre is approximately 200°C, followed by a maximum degradation temperature of around 300°C. Degradation of PA11 and the polymer blend mainly occurred between 350°C and 500°C. Carbon fibre showed a stable profile with only 4% decomposed materials, which is more likely correlated to its sizing and coating materials. The results presented the lower thermal stability of the cellulose microfibre compared to the polymers and carbon fibre. Cellulose microfibre residue (about 18%) could be from the lignin existing in the cellulose microfibres.

As presented in Figure 17, the hybrid composites exhibited quite similar patterns with a two-stage decomposition profile. In the first stage, starting at around 200°C, a weight loss was observed, which was attributed to the degradation of cellulose microfibres in the composites. The second decomposition stage, correlated with the degradation of the polymers, began at approximately 350°C and was followed by the maximum decomposition at around 430 °C.

Carbon fibre did not decompose in the decomposition profiles and only increased the residue at the end. However, it was observed that as the carbon fibre content in the composite increased, the second decomposition temperature was slightly shifted to a higher temperature. Incorporating carbon fibre decreased the decomposition rate and enhanced thermal stability. The degradation profile of hybrid composites indicates their higher thermal stability compared to composites reinforced only by cellulose microfibres, showing that hybridization with carbon fibre enhances the composites' thermal performance.

As shown in Figure 18, PA: WF30 exhibited a slightly higher thermal degradation temperature and, consequently, higher thermal stability compared to PA+PP: WF30. However, hybrid composites of PA and polymer blend showed almost similar patterns. For instance, at the temperature of around 400°C, in which plastic decomposition occurred, the weight loss was about 74% and 72% for PA: WF30 and PA+PP: WF30, respectively; however, that was around 79% for both PA: WF20CF10 and PA+PP: WF20CF10, and approximately around 83% and 85% for PA: WF10CF20 and PA+PP: WF10CF20, respectively. In general, PA and polymer blend composites showed similar decomposition patterns and thermal stabilities.

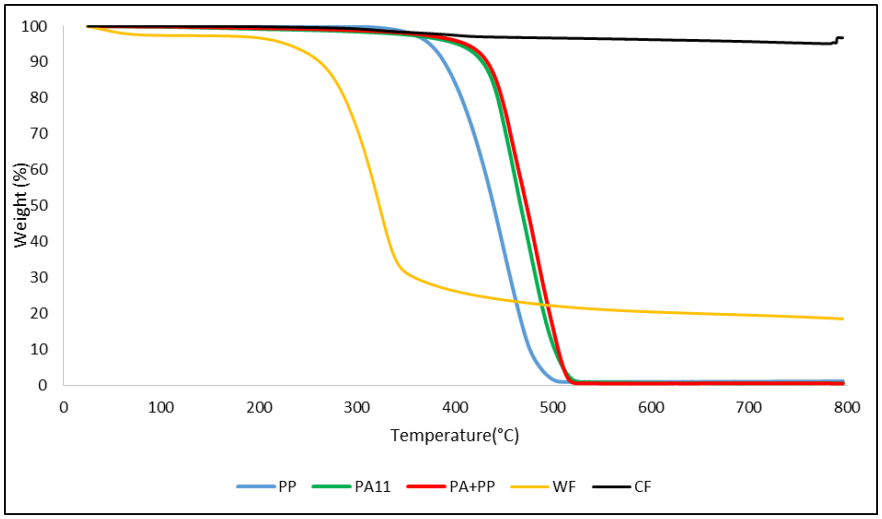

Figure 16 Thermogravimetric Analysis for Base Materials

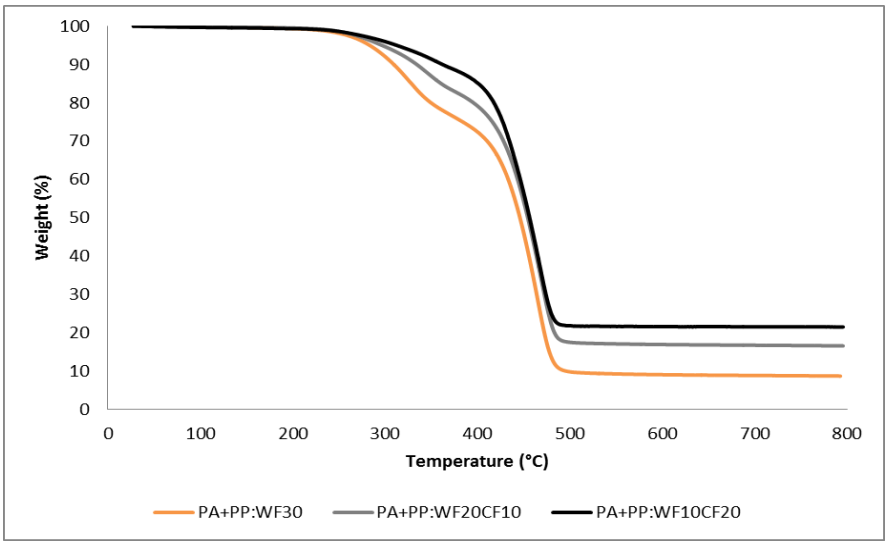

Figure 17 Thermogravimetric Analysis for Polymer Blend Composites

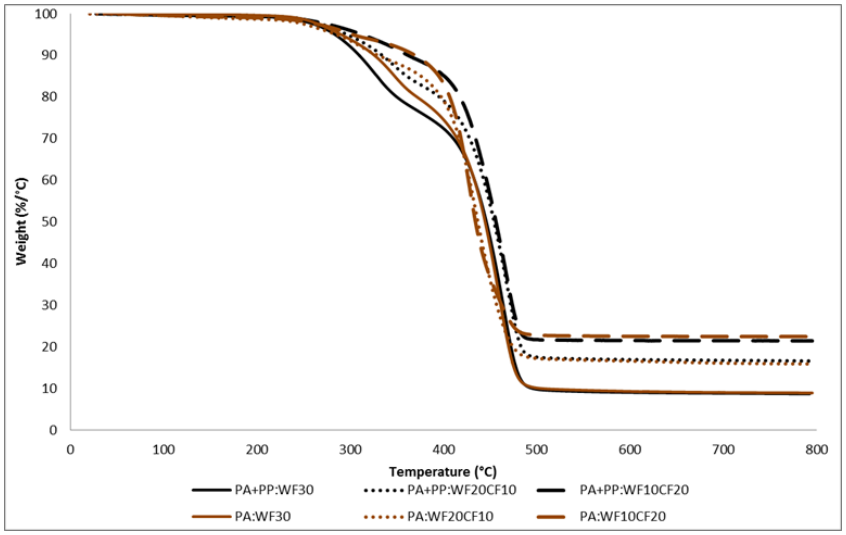

Figure 18 Comparison of Thermogravimetric Analysis for PA11 Composites with Polymer Blend Composites

4.3.1.2 Density

As noted earlier, the density of the material is directly correlated with the weight of the automotive part and provides a measure of the potential for weight reduction. Table 18 represents experimental and theoretical densities of the composites along with their void contents. In general, PA composites had greater densities than the blend composites, due to the higher density of PA11 compared to the polymer blend. As expected, since carbon fibre has a higher density compared to cellulose microfibre, hybridizing with carbon fibre slightly increased the density of the composites.

The experimental densities had lower values than the theoretical ones, which could be attributed to voids in the manufactured composites, poor fibre-matrix adhesion, and increased microstructural defects. The void content significantly influences the composites' mechanical properties by increasing their susceptibility to moisture penetration and other environmental conditions (De Almeida & Neto, 1994).

The results indicated that void content exhibited a similar trend for the polymer blend composites and the PA composites. In both scenarios, adding reinforcing fibres increased void content compared to the polymers, and incorporating carbon fibre slightly decreased void content. The densities of the hybrid composites with polymer blend matrices were relatively lower than those of existing materials used in some auto parts, such as battery trays (KC et al., 2015).

A void may arise in the production process due to causes such as insufficient resin flow, trapped air bubbles, incomplete fibre wetting, and inadequate reinforcing impregnation. Increased void content may result in reduced strength, stiffness, and durability of the composite material, as well as greater susceptibility to damage and failure under applied loads.

Voids in composites lead to stress concentrations, which are crucial in causing adverse effects on the material's characteristics. When an external force is exerted on a composite material containing voids, the stress intensifies at the boundaries of these voids, making them vulnerable as weak points within the material. These factors can lead to premature malfunction, reduced load-bearing capacity, and limited longevity of the composite material. Voids not only impact the mechanical qualities but also influence the overall quality and look of the composite. Excessive void content can lead to an irregular or uneven surface texture, increasing the difficulty of machining or bonding the material to other components.

The existence of voids in a composite material can exert many unfavourable impacts on its mechanical properties, including:

1. Reduced Strength and Rigidity: Voids can act as stress concentration points within the material, leading to premature failure and a decrease in overall strength and rigidity.
2. Decreased Durability: Voids can increase the material's susceptibility to fatigue and mechanical degradation over time.
3. Impaired Thermal and Electrical Conductivity: Voids may compromise the material's thermal and electrical conductivity, limiting its usability in specific applications.

Table 18 Experimental Density vs. Theoretical Density of the Composites

Sample	Experimental Density $(^{g}/_{cm^3})$	Theoretical Density $(^{g}/_{cm^3})$	Void content (%)
PA11	1.04 ± 0.01	1.03	~-0.1
PA+PP	1.00 ± 0.01	1.00	~0
PA+PP:WF30	1.08 ± 0.01	1.13	~5
PA+PP:WF20CF10	1.11 ± 0.01	1.14	~3
PA+PP:WF10CF20	1.11 ± 0.00	1.15	~3

PA:WF30	1.08 ± 0.01	1.14	~5
PA:WF20CF10	1.12 ± 0.01	1.15	~3
PA:WF10CF20	1.15 ± 0.00	1.17	~2

4.3.1.3 Melt Flow Index

The MFI results are presented in Table 19. The polymer blend had a lower MFI value than PA11 due to the intermolecular bonding of the polymers, which restricts the movement of the polymer chain and reduces the MFI. A similar pattern has been observed for the composites, i.e., the polymer blend composites had lower MFI values than PA composites. This is consistent with the results of the study by Chow et al. (2001) that reported the MFI value of PA 6/PP blend decreased in the presence of MAPP compatibilizer, which might be related to the higher reactivity of maleic anhydride, resulting in the formation of a graft copolymer (PA-g-PP) in the polymer blend.

As expected, compared to the polymers, the composites showed much lower MFI values, indicating that the fibre restricts the mobility of the polymer molecules under stress. The fibres present in the polymer matrix disturb the dynamics of the viscoelasticity of the melt by restricting the mobility of molecular chains, leading to lower MFI values (Ota et al., 2005).

The MFI values were lower for polymer blend composites compared to PA11 composites. One reason could be that the polymer blend had a lower MFI value than PA11. However, this is slightly inconsistent with the processing observations of the composites. Compared to the polymer blend composites, the PA11 composites presented many more processing difficulties, characterized by a slow flow rate and high shear, as indicated by a voltmeter measuring the power required for extrusion. Moreover, during injection moulding, PA11 composites showed a low flow rate at set processing temperatures.

The decreasing impact on MFI was more pronounced for cellulose microfibre-reinforced composites, which could be attributed to the difference in the microstructure of the two fibres, as well as the lower volume fraction of carbon fibres compared to cellulose microfibres at the same weight fraction. Cellulose microfibres exist as fibre bundles, which become defibrillated into microfibrils during the compounding process. These microfibrils may remain on the fibre surface

or be dispersed in the matrix (Sain et al., 2015). The generation of these elementary microfibrils during compounding increases the surface area of the cellulose microfibres. It causes further entanglement with the matrix, restricting the mobility of the polymer. This effect does not exist in the carbon fibres, as synthetic fibres, such as carbon fibres, remain as single fibrils (Sain et al., 2015). The MFI values were increased by hybridization with carbon fibre, which would be beneficial for the composites' processing.

Table 19 MFI for Polymers and Composites

Sample	MFI (g/10 min)
PA11	18.9 ± 3.9
PA+PP	8.1 ± 0.2
PA+PP:WF30	0.2 ± 0.01
PA+PP:WF20CF10	1.0 ± 0.1
PA+PP:WF10CF20	1.9 ± 0.3
PA:WF30	2.0 ± 0.3
PA:WF20CF10	7.8 ± 0.4
PA:WF10CF20	8.0 ± 0.7

4.3.1.4 Mechanical Properties

Tensile and Flexural Properties

Figure 19 shows the tensile strength for PA11, the polymer blend, and their composites. One-way ANOVA statistical analysis (95% confidence interval) revealed no significant difference between the tensile strength of the polymer blend and that of PA (P-value > 0.05). However, the polymer blend composites showed higher tensile properties than the PA composites. Compared to PA: WF30, the tensile strength of PA+PP: WF30 was improved by 28%. Compared to cellulose microfibre composite WF30, the incorporation of carbon fibre in the hybrid composite WF10CF20 increased tensile strength by 46% and 65% for polymer blend composites and PA composites, respectively. The tensile strength for PA+PP: WF10CF20 was 13% higher than that of PA: WF10CF20. The results indicated good fibre-matrix adhesion, resulting in a satisfactory transfer of the applied load from the matrix to the fibres. As mentioned earlier, the fibres act as load carriers

in the fibre-reinforced composites; thereby, the stress is transferred from the matrix to the fibres, leading to a uniform stress distribution.

The higher tensile properties of the polymer blend composites can be correlated with the processing observations, i.e., the polymer blend composites exhibited better processability during composite preparation and experienced less thermal degradation during the process. Thermal degradation of natural fibres reinforced PA11 under high shear processing at elevated temperatures may be responsible for the lower tensile properties of the PA composites. Degradation of polyamide is primarily a thermal-oxidative mechanism in humid conditions, resulting in a severe decrease in tensile strength (Khanna et al., 1988; Khanna et al., 1996; Bernstein et al., 2005; Gonçalves et al., 2007). Using a polymer blend consisting of PA and PP instead of neat PA, and incorporating carbon fibre, increased the tensile properties of the hybrid composites.

Figure 20 represents the tensile modulus of the PA and polymer blend composites. One-way ANOVA statistical analysis (95% confidence interval) revealed no significant difference between the tensile modulus of the polymer blend and that of PA (P-value > 0.05). Tensile modulus showed a similar trend to that of tensile strength. The polymer blend composites had a higher tensile modulus compared to the PA composites. The higher stiffness of polymer blend composites can be attributed to their lower MFI values. In other words, the higher stiffness of the polymer blend composites may be correlated with a higher energy requirement to align the polymers. The tensile modulus of the polymer blend composite PA+PP: WF30 was improved by 53% compared to PA: WF30. In addition, hybridization with carbon fibre increased the tensile modulus of the composites. The incorporation of carbon fibre improved the tensile modulus of the hybrid composites WF10CF20 by 114% and 169% for the polymer blend and PA composites, respectively. The polymer blend composites generally showed higher tensile properties than the PA composites. The tensile strength results for the hybrid composites with both matrices are relatively similar to the automotive application requirements for some structural under-the-hood parts, such as battery trays (KC et al., 2015).

Elongation at breakage or failure under strain indicates the plastic deformation of the material. Figure 21 illustrates the elongation at break for the composites. The polymers did not break at the set crosshead limit of 50.8 mm. Fillers or reinforcing fibres usually prohibit the plastic deformation

of the matrix in reinforced composites and consequently reduce the elongation at breakage. Results showed that elongation at breakage is generally higher for PA composites. As shown, the incorporation of carbon fibre decreased the elongation at breakage for PA composites, indicating that adding carbon fibre resulted in more brittle composites due to the brittle nature of carbon fibre compared to the natural fibres; however, polymer blend composites showed quite a consistent elongation at breakage, irrespective of the carbon fibre content of the composites.

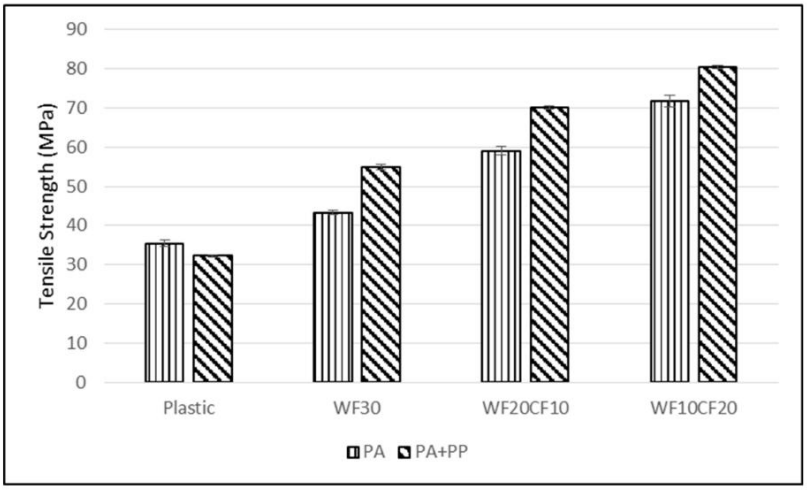

Figure 19 Tensile Strength for PA and Polymer Blend Composites

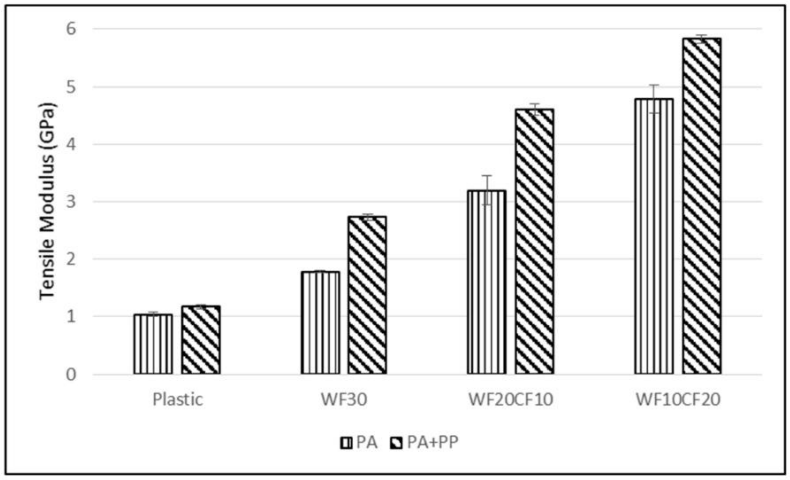

Figure 20 Tensile Modulus for PA and Polymer Blend Composites

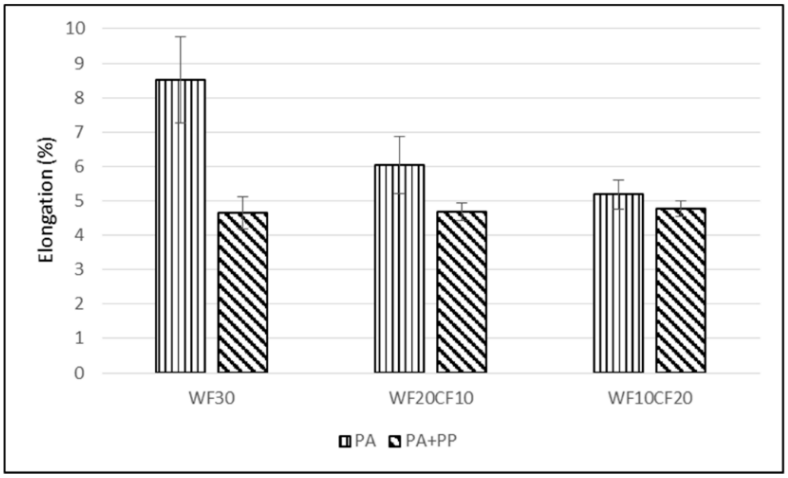

Figure 21 Elongation at Breakage for PA and Polymer Blend Composites

Figure 22 and Figure 23 represent the flexural strength and modulus of the PA and polymer blend composites, respectively. One-way ANOVA statistical analysis (95% confidence interval) revealed no significant difference between the flexural strength and modulus of the polymer blend and the PA (P-value > 0.05). Polymer blend composites generally showed higher flexural properties. Flexural strength and modulus were enhanced by 24% and 47%, respectively, for the

polymer blend composite PA+PP: WF30, compared to those of PA: WF30. In addition, hybridization with carbon fibre increased the flexural strength and modulus of the composites in both scenarios. Hybridization with carbon fibre improved the flexural strength of the hybrid composites WF10CF20 by 52% and 73% for polymer blend composites and PA composites, respectively. The results also demonstrated a good fibre-matrix adhesion, resulting in a satisfactory transfer of the applied load from the matrix to the fibres. The mechanical properties of the composites, such as tensile and flexural properties, are often governed by the interfacial bonding of fibres and matrix. The underperformance of the composites due to the lack of proper interfacial bonding has been investigated in the literature (Magniez et al., 2014).

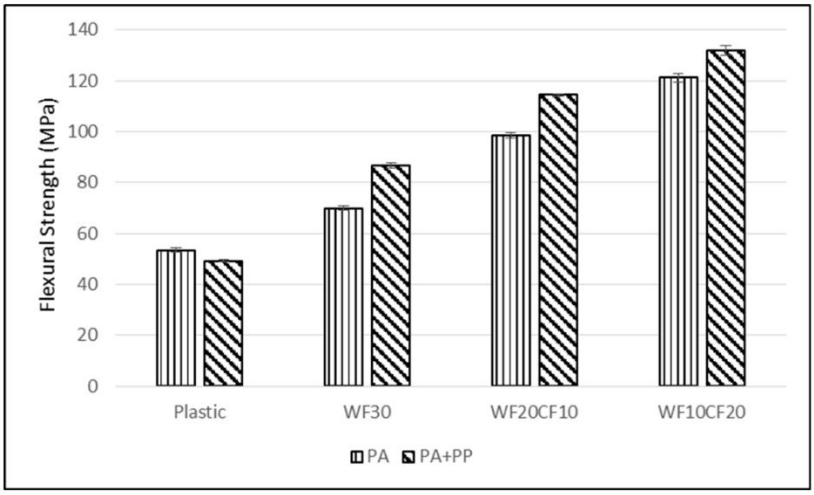

Figure 22 Flexural Strength for PA and Polymer Blend Composites

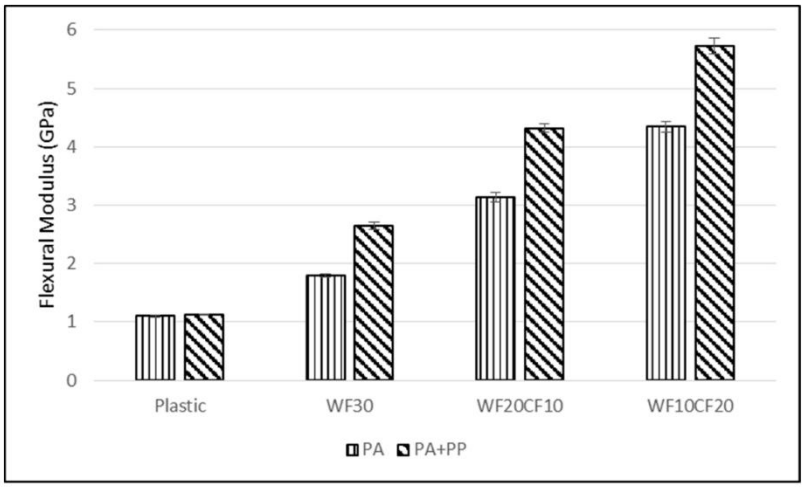

Figure 23 Flexural Modulus for PA and Polymer Blend Composites

Impact Strength

Figure 24 shows notched Izod impact strength for the plastics and composites. The notched impact strength of the composites exhibited a relatively decreasing trend compared to the polymers, indicating that adding fibres reduced the impact strength. However, hybridization with carbon fibre and increasing fibre loading significantly increased the notched impact strength due to energy dissipation when the fibres are pulled out. Polyamide had a higher notched Izod impact strength compared to the polymer blend. However, the polymer blend composites generally showed higher notched impact strengths. The notched impact strength increased by 58% and 30% for PA+PP: WF20CF10 and PA+PP: WF10CF20 hybrid composites, respectively, compared to the hybrid PA composites with the same fibre composition. The higher notched impact strength for polymer blend composites could be attributed to their lower MFI values, showing that greater energy was required to align the polymer blend in the composites.

Unnotched impact strength results are presented in Figure 25. The neat polyamide and polymer blend did not break at the unnotched impact test and exceeded the machine limit of 750 J/m. Contrary to the notched impact strength, the unnotched impact strength was generally higher for the PA composites. Adding carbon fibre to the composites increased both notched and unnotched impact strengths. For the polymer blend hybrid composite PA+PP: WF10CF20, the notched and unnotched impact strengths increased by 87% and 49%, respectively, and for the PA hybrid

composite PA: WF10CF20, the notched and unnotched impact strengths increased by 87% and 77%, respectively, compared to their corresponding cellulose microfibre composites (PA+PP: WF30 and PA: WF30). Lower impact strength typically indicates a strong fibre-matrix interfacial bonding, as well as fewer fibre pullouts (Feldmann & Bledzki, 2014). This suggests that cellulose microfibre composites (PA: WF30 and PA+PP: WF30) had better fibre-matrix interfacial bonding compared to the hybrid composites and showed lower impact strengths. The impact strength values for the hybrid composites with the polymer blend matrix surpassed the impact strength requirements for some auto parts for under-the-hood applications, such as battery trays (KC et al., 2015).

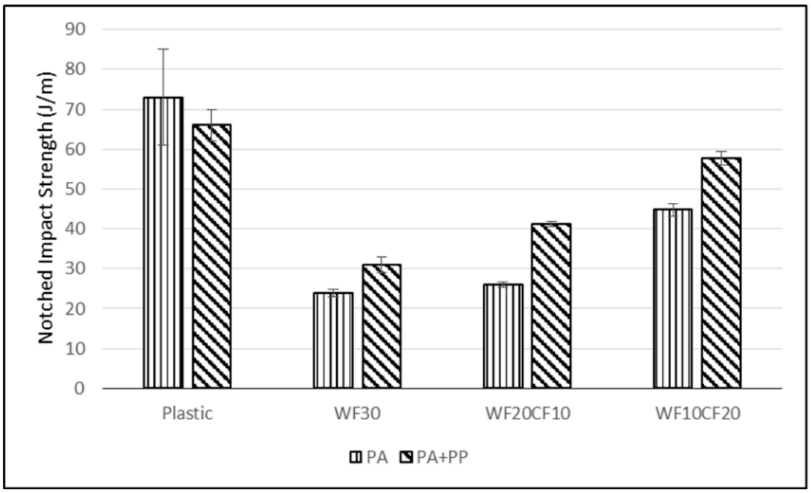

Figure 24 Notched Impact Strength for PA and Polymer Blend Composites

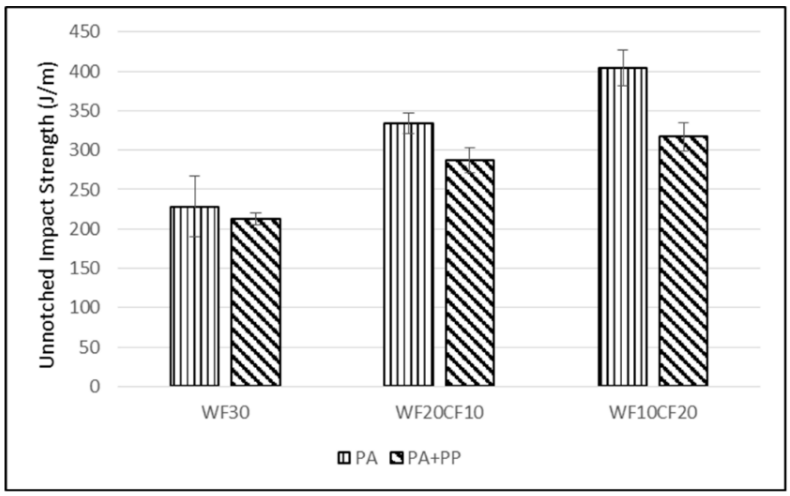

Figure 25 Unnotched Impact Strength for PA and Polymer Blend Composites

4.3.1.5 Scanning Electron Microscope

The fracture surfaces of the tensile test samples were observed by SEM (Figure 25). The figures show effective fibre-matrix interfacial bonding with efficient component integration and good fibre dispersion. None of the composites showed matrix cracking. In some cases, voids were observed on the fracture surfaces due to the lack of a proper interfacial bonding between fibre and matrix. Fibre pullout was more pronounced in hybrid composites (PA/PA+PP: WF20CF10, PA/PA+PP: WF10CF20), which is consistent with impact strength results. Cellulose microfibre composites had better fibre-matrix adhesion compared to the hybrid composites. In general, fibre breakage and fibre-matrix interface decomposition were the dominant failure mechanisms in cellulose microfibre composites, whereas the failure mechanisms of hybrid composites were governed by fibre pullout and fibre breakage.

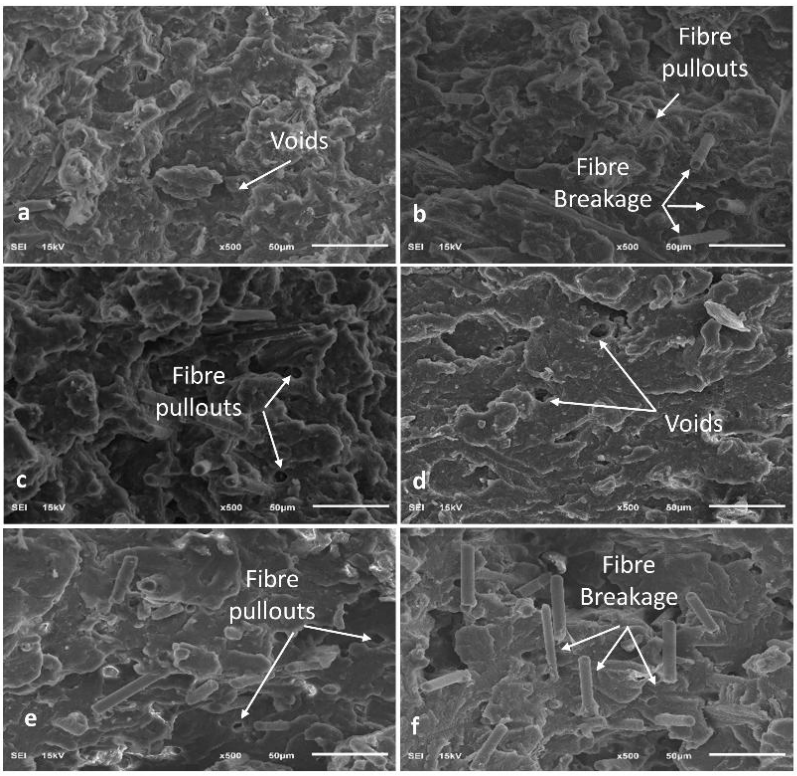

Figure 26 Scanning Electron Microscopy for a) PA+PP: WF30; b) PA+PP: WF20CF10; C) PA+PP: WF10CF20; d) PA: WF30; e) PA: WF20CF10; f) PA: WF10CF20

4.3.1.6 Thermal Properties

Heat Deflection Temperature

The HDT value of the fibre-reinforced composites depends on the base polymer and the reinforcing agents, as the HDT value of the glass fibre/carbon fibre-reinforced engineering polymers often approaches the melting point of the polymer matrix. It is an important material property to consider when choosing materials for thermo-mechanically demanding applications. The HDT test results provide valuable information about the relative service temperature for a material used in load-bearing parts. However, the HDT test is a short-term test that does not account for the duration of exposure to elevated temperature, the rate of temperature increase, or the geometry of the parts.

The HDT values for the polymers and the composites are shown in Table 20. The HDT for PA11 was approximately 44°C, which was slightly improved by incorporating 30% cellulose microfibre. However, hybridization with carbon fibre increased the HDT value up to 127°C in the PA: WF10CF20 composite due to the high thermal stability of synthetic carbon fibre. This

improvement is directly associated with the increase in the modulus of the hybrid composites along with the interfacial interactions between the matrix and fibres. The high heat resistance may also be due to carbon fibres preventing the deformation of the composites.

The HDT value for the polymer blend was approximately 45°C, and one-way ANOVA statistical analysis (95% confidence interval) revealed no significant difference between the HDT of the polymer blend and that of PA (P-value > 0.05). However, the incorporation of 30% cellulose microfibre increased the HDT value of the polymer blend composites up to 100°C. This may be attributed to the hydrolysis of PA11 in the presence of higher cellulose microfibre content when exposed to the environment. In contrast to the PA+PP: WF30 system, the significantly lower HDT observed for PA: WF30 may be attributed to matrix degradation initiated by moisture uptake and hydrolysis. This significant difference may be attributed to the susceptibility of PA11 to hydrolytic degradation, particularly in the presence of high cellulose microfibre content (WF30). The hydrophilic nature of cellulose promotes moisture absorption, which can accelerate hydrolysis of the polyamide matrix during environmental exposure or thermal cycling. This results in plasticization, reduced intermolecular hydrogen bonding, and an eventual decline in thermal stability, thereby lowering the HDT of PA: WF30 composites.

The incorporation of carbon fibre further increased the HDT value of the polymer blend composites up to 143°C for the PA+PP: WF10CF20 composite. Compared to PA11 composites, polymer blend composites represented higher HDT values. Replacing the polymer blend with PA11, along with hybridization, significantly improved the HDT values. The results suggest that these hybrid biocomposites have the potential to be applied where the maximum service temperature requirement is around 143°C. The HDT values for the hybrid composites PA+PP: WF20CF10 and PA+PP: WF10CF20 meet the automotive requirements for some parts, such as the battery tray (KC et al., 2015).

Table 20 Heat Deflection Temperature for Polymers and Composites

Sample	HDT (°C)
PA	44 ± 0.3
PA+PP	45 ± 0.4
PA+PP: WF30	100 ± 4

PA+PP:WF20CF10	131 ± 4
PA+PP: WF10CF20	143 ± 2
PA: WF30	49 ± 3
PA: WF20CF10	101 ± 9
PA: WF10CF20	127 ± 9

Upon careful analysis of the Heat Deflection Temperature (HDT) data, two significant issues were addressed:

1. Low HDT values for PA11 and PA11/PP polymer blends:

The experimental HDT values recorded for neat PA11 and PA11/PP blends consistently ranged between approximately 44°C and 47°C (Table 17). Although these values might seem relatively low compared to typical expectations, the consistency observed across different compositions validates their reliability under the applied experimental processing conditions. Multiple polymer blend compositions, with varying PA11/PP ratios, yielded remarkably similar HDT outcomes, reinforcing the robustness of these experimental measurements.

To further verify these results, comparisons were made with relevant literature. Literature sources generally report HDT values for neat PA11 and similar PA11/PP polymer blends within the approximate 40–55°C range, closely matching the measured range in this study (Table 4). Thus, the obtained values align well with the literature, indicating that these results accurately reflect the material characteristics under the specific processing conditions.

2. Significant HDT difference between PA11 and PA11/PP blends reinforced with cellulose microfibres:

An intriguing discrepancy appeared when comparing PA11 composites reinforced with cellulose microfibres to similar composites using a polymer blend matrix of PA11 and PP. Specifically, PA11 reinforced with 30 wt% cellulose microfibre (PA: WF30) presented an HDT value of approximately 49°C, whereas the PA11/PP blend reinforced with the identical fibre loading (PA+PP: WF30) demonstrated substantially higher HDT values around 100°C (Table 20).

Since all processing conditions (e.g., mixing, compounding, moulding temperature, and cooling rate) were strictly maintained for both sets of composites, the significant difference in HDT values

strongly suggests a notable matrix degradation initiated by moisture uptake and hydrolysis. Polyamide 11 is known for its hygroscopic nature, and the addition of 30 wt% cellulose microfibre, an inherently hydrophilic reinforcement, likely promotes further water absorption. Over time, absorbed moisture can induce chain scission through hydrolysis, leading to reduced molecular weight, chain mobility, and compromised thermal resistance. These effects, coupled with potential fibre agglomeration and inadequate stress transfer at high fibre content, may contribute to early deflection under thermal load.

This interpretation aligns with established evidence regarding the thermal sensitivity of PA11 reinforced with natural fibres, highlighting the importance of optimal thermal management during processing to maintain fibre integrity and enhance mechanical performance.

4.3.1.7 Water Absorption/Uptake

Polyamides, in general, are more susceptible than most other polymers to absorbing moisture from the air. This impacts processability, dimensional stability, and physical qualities. As a plasticizer, moisture lowers tensile strength and stiffness while raising elongation. While absorbed moisture reduces several qualities, the plasticizing effect of moisture is partly responsible for polyamides' tenacity. Increases in impact strength and general energy absorption properties are noticeable when the moisture content rises.

Water absorption is an undesirable problem in natural fibre-reinforced composites due to the moisture sensitivity of the natural fibres. Water uptake behaviour is significantly accelerated at elevated temperatures, resulting in a significant decrease in mechanical properties related to the degradation of the fibre-matrix interface (Panthapulakkal & Sain, 2007a; Panthapulakkal &Sain, 2007b; Dhakal et al., 2007). Additionally, water absorption can cause swelling, resulting in dimensional variations in the composites (Saheb & Jog, 1999). Water uptake increases with rising fibre volume fraction due to increased void contents.

Figure 27 represents water absorption for the neat plastics and the composites. The results indicate that adding cellulose microfibre increased the water absorption of the composites. As expected, with a decrease in cellulose microfibre content and hybridization with carbon fibre, water absorption is also reduced. The highest water absorption was observed in WF30 composites, where

the water absorption increased by 70% and 140% compared to PA11 and the polymer blend, respectively. The reported values in Figure 14 indicate that incorporating carbon fibre in cellulose microfibre composites decreased their water absorption. Reducing cellulose microfibre content from 20 wt% to 10 wt% in hybrid composites (WF20CF10 to WF10CF20) resulted in lower water uptake.

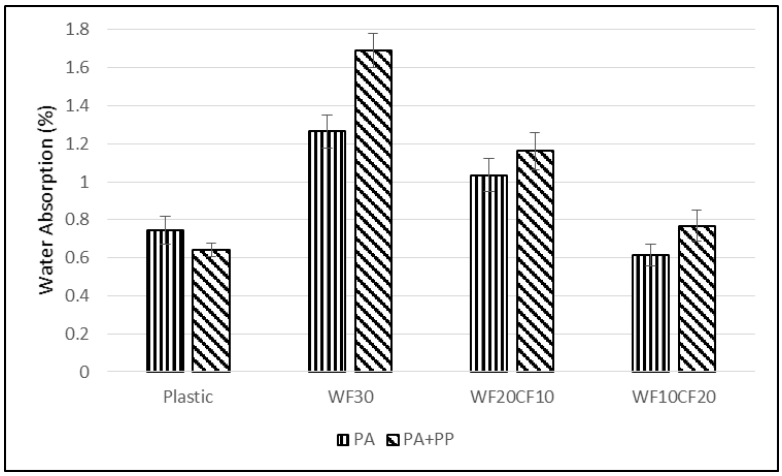

Figure 27 Water Absorption of Polymers and Composites

While PP is hydrophobic, its blend with PA11 may reduce crystallinity or cause interfacial voids, especially at high WF content (like WF30), creating more pathways for water ingress. This explains why PA+PP:WF30 absorbs more water (~1.7%) than PA:WF30 (~1.3%), despite PP being less hygroscopic than PA11.

While the PA+PP matrix demonstrated lower water absorption than neat PA11 in its unreinforced form, this trend was reversed in the fibre-reinforced systems, particularly at high wood fibre content. The PA+PP: WF30 composite exhibited higher moisture uptake (~1.7%) compared to PA: WF30 (~1.3%), despite the blend matrix being less hygroscopic. This counterintuitive result is best explained by interfacial morphology rather than bulk matrix polarity. The non-polar nature of PP reduces chemical compatibility with hydrophilic cellulose microfibres, leading to weaker fibre–matrix adhesion, void formation, and capillary pathways for moisture ingress, especially at high fibre loadings. Interestingly, PA+PP: WF30 also displayed significantly higher tensile modulus and HDT than PA: WF30, despite its greater water absorption. This apparent contradiction can be understood by examining their Melt Flow Index (MFI). The PA+PP: WF30 formulation had an extremely low MFI (0.2 g/10 min), indicating high melt viscosity during processing. Although low

MFI can hinder fibre dispersion, it may also result in tightly packed fibre networks, which limit polymer chain mobility and thereby enhance both stiffness and thermal resistance. Furthermore, the presence of PP in the blend likely improved initial fibre wetting and mixing during compounding, facilitating more effective stress transfer despite the presence of interfacial defects. Therefore, the superior mechanical and thermal performance of PA+PP: WF30 arises not from lower moisture sensitivity, but from the complex interplay between processing viscosity, fibre packing, and interfacial morphology. These findings highlight that material performance in hybrid composites is governed not solely by chemical composition, but also by rheological behaviour and microstructural development during processing.

The bond between carbon fibres and cellulose microfibrils in hybrid composites is typically dominated by non-covalent interactions, primarily hydrogen bonding and van der Waals forces. However, the specific nature of the bonding can vary depending on the surface treatments and modifications of the fibres.

- Hydrogen Bonding

Cellulose microfibrils contain hydroxyl groups (–OH) along their molecular chains, which can bond to hydrogen with compatible functional groups on the carbon fibre surface. However, carbon fibres themselves are chemically inert and hydrophobic due to their graphitic structure. Therefore, direct hydrogen bonding between untreated carbon fibres and cellulose is limited unless the surface is chemically treated (e.g., through oxidation).

- Van der Waals Forces

In the absence of strong chemical bonding, van der Waals forces play a significant role in the interaction between carbon fibres and cellulose microfibrils. Although weaker than hydrogen bonds, these forces contribute to the adhesion between the two phases by developing close surface proximity.

- Surface Energy and Surface Treatment

Surface energy affects the adhesion between carbon fibres and cellulose microfibrils. Carbon fibres typically have low surface energy due to their hydrophobic nature. To improve adhesion, carbon fibres often undergo surface treatments like oxidation, plasma treatment, or functionalization with

polar groups, which increases their surface energy and enhances compatibility with cellulosic fibres.

By increasing surface energy, these treatments can create functional groups, such as carboxyl or hydroxyl groups, on the carbon fibre surface, promoting better interfacial bonding through hydrogen bonding with the cellulose microfibrils. Additionally, higher surface energy increases the wettability of the carbon fibres, ensuring better dispersion and mechanical interaction with the cellulose microfibrils, thereby improving stress transfer within the composite.

- Interfacial Adhesion and Mechanical Performance

The strong interfacial adhesion between carbon fibres and cellulose microfibrils is crucial for efficient stress transfer and overall composite performance. A weak interface would result in poor load sharing between the two phases, leading to suboptimal mechanical properties such as reduced tensile strength and modulus.

Surface treatments that enhance surface energy and introduce reactive groups can significantly improve interfacial bonding, leading to better mechanical synergy between carbon fibres and cellulose microfibrils. While van der Waals forces primarily govern the inherent bond between untreated carbon fibres and cellulose microfibrils, surface modifications can enable hydrogen bonding, increase surface energy, and improve the overall interfacial adhesion between these two phases in hybrid composites.

4.4 Effect of relocating carbon fibre feeding and modifying the extrusion profile on the mechanical characteristics of composites

This section examines an alternative material composition with a lower fibre concentration compared to the previous sections. The primary objective is to preserve carbon fibre length and decrease both the cost and the use of synthetic fibres in the final composites, as shown in Table 7. Due to the significant impact of carbon fibre on the mechanical and thermal properties of composites, its feeding point has been relocated to the degassing zone, while it was initially introduced through a feeding hopper along with other components. This allows the fibre to maintain its length as it experiences considerably reduced shearing stresses throughout the extrusion procedures. In addition, the temperature profile of the extruder zones has been slightly decreased to minimize the chance of degradation of PA11 and natural fibres during the extrusion

process, as indicated in Table 9. To prevent any ambiguity with the earlier composites of the study, the composites created in this section are referred to as the "modified PA11 composites". Carbon fibres were extracted by incinerating the composites from both sections to measure their post-processed lengths.

4.4.1 Mechanical Performance of the Modified PA11 Composites

4.4.1.1 Tensile and Flexural Characteristics of the Composites

Figure 28 and Figure 29 show tensile strength and modulus of PA11 composites, respectively. The addition and increase in carbon fibre content resulted in the expected enhancement of tensile strength and modulus. Figure 30 represents elongation at breakage of the composites. The incorporation and augmentation of carbon fibre resulted in a lower elongation at the point of fracture in the composites. These results are in good agreement with the findings of the previous sections of this study.

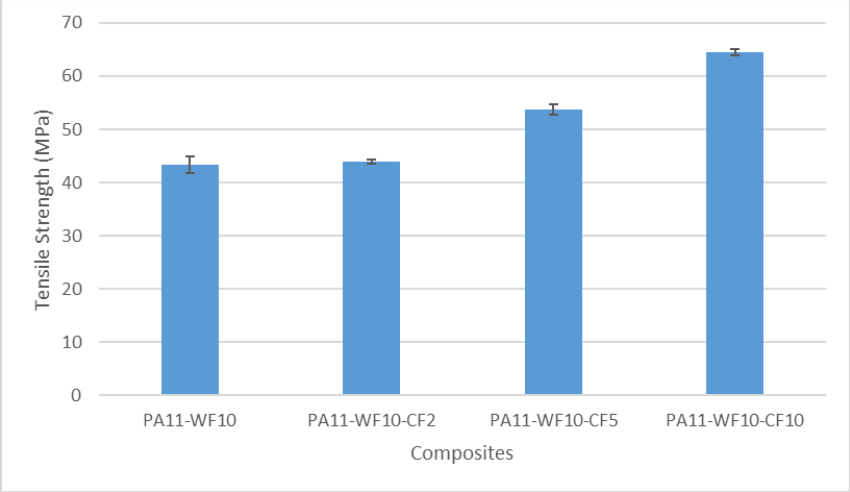

Figure 28 Tensile Strength of the Modified PA11 Composites

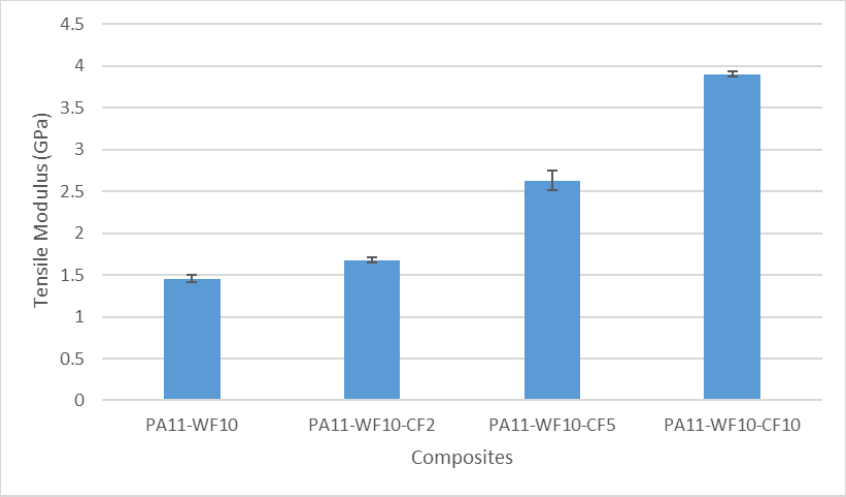

Figure 29 Tensile Modulus of the Modified PA11 Composites

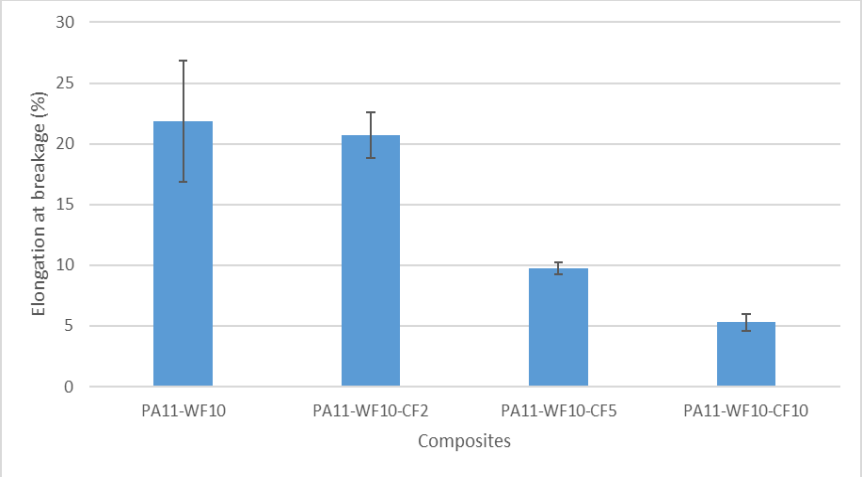

Figure 30 Elongation at Breakage of the Modified PA11 Composites

Figure 31 and Figure 32 represent the flexural strength and modulus of the modified PA11 composites, respectively. The flexural strength and modulus results align with the findings of previously produced composites in the current study. As expected, the inclusion and augmentation of carbon fibre resulted in a notable enhancement of both the flexural strength and modulus of the composites.

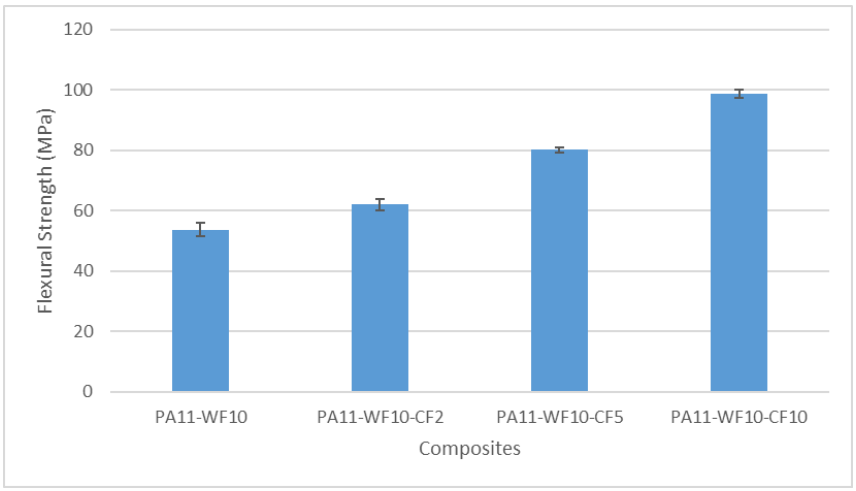

Figure 31 Flexural Strength of the Modified PA11 Composites

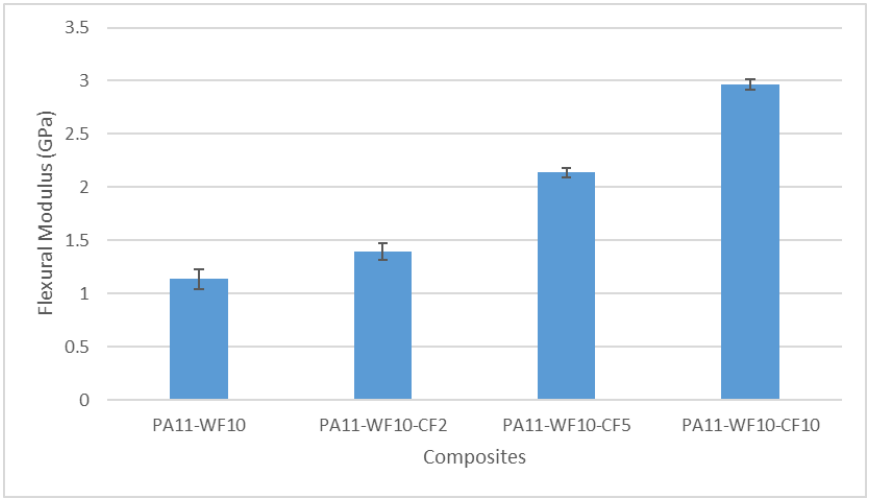

Figure 32 Flexural Modulus of the Modified PA11 Composites

4.4.1.2 Impact Performance of the Composites

The notched and unnotched impacts were shown in Figure 33 and Figure 34, respectively. The findings of the impact analysis show that the incorporation and increasing the amount of carbon fibre enhanced the notched impact strength of the composites.

As previously mentioned in this study, the unnotched impact results differ from the notched impact results. During the unnotched impact test, the PA11-WF10 remained fracture-free and surpassed the machine limit of 750 J/m. The composite PA11-WF10-CF2 exhibited a notable unnotched impact strength value, potentially attributable to its low fibre content of 2% CF and 10% WF.

These results are consistent with those of the present study's previous findings, which reported a high unnotched impact strength value for WF10 composites. As stated earlier, the composite's performance is essentially the same as that of its matrix due to matrix dilution caused by the low fibre content.

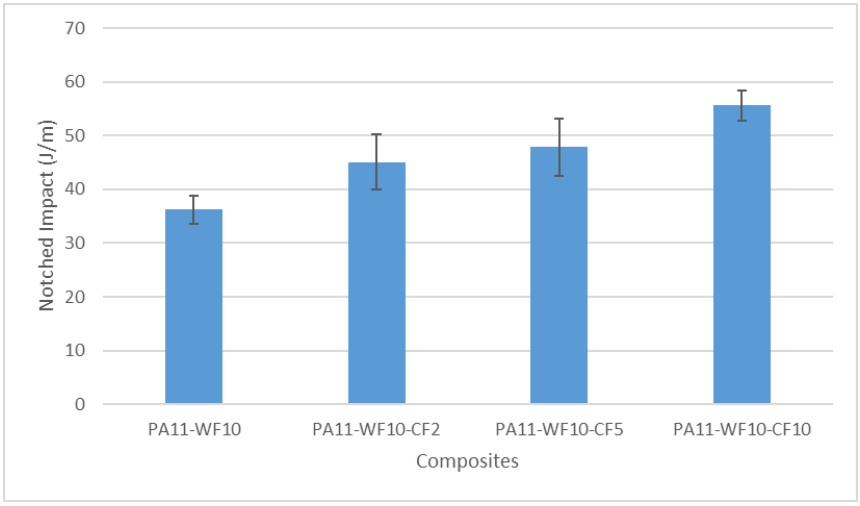

Figure 33 Notched Impact for the Modified PA11 Composites

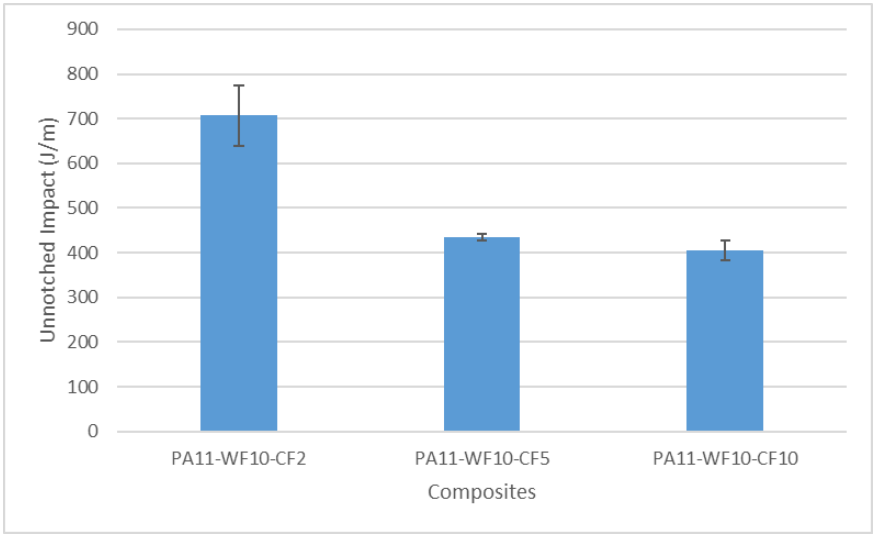

Figure 34 Unnotched Impact for the Modified PA11

In extrusion processing of hybrid fibre composites, shear rate and residence time play interdependent yet often opposing roles in determining final composite quality. High shear rates, typically associated with higher screw speeds, are beneficial for breaking up fibre agglomerates and improving dispersion, particularly for fibrillated cellulose microfibres. However, this comes

at the cost of increased mechanical degradation of stiffer, brittle fibres, such as short carbon fibres, whose reinforcement efficiency strongly depends on maintaining their aspect ratio. Conversely, longer residence times, achieved by lowering screw speed or feed rate, allow more time for matrix-fibre wetting, interfacial diffusion, and network formation, particularly between bio-based fibres and the polymer melt. However, this extended thermal exposure can increase the risk of degradation for thermally sensitive components.

In the context of this study, the improved extrusion configuration, wherein PA11 and cellulose microfibres are first compounded to form a well-dispersed matrix, and carbon fibres are subsequently added via the degassing port, strikes a critical balance. By reducing screw speed and feed rate, the process enhances residence time for cellulose microfibre–polymer interaction while minimizing the shear exposure of carbon fibres. This staged feeding strategy not only preserves carbon fibre length but also allows them to be physically anchored within a pre-formed cellulose microfibre–PA11 matrix. This optimized approach aligns with the pseudo-unified hybrid system hypothesis, wherein the cellulose-reinforced matrix serves as an effective medium for embedding and transferring stress to carbon fibres. As a result, the process achieves improved fibre integrity and interfacial architecture, ultimately leading to superior mechanical performance in the hybrid composite.

This study evaluates a series of hybrid biocomposites based on PA11 and PA11+PP matrices reinforced with cellulose microfibre and carbon fibre. The hybrid systems are benchmarked against Ford Motor Company specifications for engine beauty covers, considering variations in carbon fibre length, matrix type, and hybrid fibre loading.

A summary of the most important properties of the developed hybrid composites is compared with Ford Motor Company's specifications for the engine beauty cover, shown in Table 21.

1. **Influence of Carbon Fibre Length (400 µm vs. 215 µm)**

The carbon fibre length significantly affects the load transfer capability, stress localization, and ultimately, the mechanical performance of the composite.

Hybrid composites with carbon fibre length of 400 µm (WF10CF5 and WF10CF10):

- These samples demonstrate higher impact resistance and greater ductility while maintaining strong mechanical performance.
- The longer carbon fibres are more effective in bridging microcracks and facilitating fibre–matrix stress transfer, which enhances tensile and flexural strength.

Hybrid composites with carbon fibre length of 215 μm (WF20CF10 and WF10CF20):

Shorter carbon fibres (due to higher shear during processing) exhibit reduced stress transfer efficiency. However, the matrix composition plays a decisive role in compensating for this loss.

2. Role of Matrix Type: PA11 vs. PA11+PP (Polymer Blend)

At a constant fibre formulation (WF20CF10 and WF10CF20), the comparison between PA11-only and PA11+PP blend matrices highlights the significance of the matrix in defining composite performance when carbon fibre length is suboptimal (215 μm).

PA11-Only Matrix Systems (WF20CF10 and WF10CF20):

- Tensile strength is still respectable (59.1 MPa and 71.73 MPa, respectively), with flexural strength ranging from 98.49 MPa to 121.27 MPa.
- Moduli are moderate (3.19 GPa to 4.79 GPa), likely limited by reduced fibre length and possible entanglement-induced stress shielding.
- Impact strength declines significantly, especially in WF20CF10 (26.07 J/m), where higher fibre content (20% cellulose microfibre) likely led to fibre–fibre interactions and reduced energy absorption.
- While stiffness and strength values are acceptable, poor impact performance disqualifies these for use in engine covers, which are exposed to frequent handling and minor impacts during maintenance.

PA11+PP Blend Matrix Systems (PA+PP:WF20CF10 and PA+PP:WF10CF20):

- PA+PP: WF10CF20 is the only 215 μm fibre-based system that fully satisfies the engine beauty cover requirements.

- PP improves toughness and processability, mitigating the embrittlement caused by shorter carbon fibres.
- The blend matrix likely enhances fibre dispersion, reduces fibre-fibre agglomeration, decreases fibre degradation, and introduces morphological flexibility, allowing better stress redistribution.
- The result is a synergistic improvement, where the matrix compensates for the mechanical disadvantages of reduced fibre length while promoting overall structural efficiency.

Table 21 Comparison of the Properties of the Developed Hybrid Composites with Ford Motor Company Specifications for the Engine Beauty Cover

Properties	Developed Hybrid Composites						Engine Beauty Cover Requirements (Ford Motor Company Specifications)
	PA: WF10CF5	PA: WF10CF10	PA: WF20CF10	PA: WF10CF20	PA+PP: WF20CF10	PA+PP: WF10CF20	
Tensile Strength (MPa)	53.70±0.94	64.50±0.54	59.1±1.00	71.73±1.51	70.20±0.42	80.33±0.43	60
Flexural Strength (MPa)	80.23±0.81	98.75±1.26	98.49±1.12	121.27±1.15	114.41±0.53	131.98±2.04	80
Tensile Modulus (GPa)	2.63±0.12	3.90±0.03	3.19±0.26	4.79±0.25	4.60±0.09	5.83±0.74	3.5
Impact Strength (J/m)	47.84±5.34	55.59±2.84	26.07±0.59	44.80±1.50	41.16±0.63	57.63±1.69	50
HDT (°C)	111 ± 5	139 ± 3	101 ± 9	127±9	131±4	143±2	120
Carbon Fibre	400	400	215	215	215	215	-

Length (µm) after Processing							
Shear Rate (rpm)	100	100	120	120	120	120	-

Engine beauty covers are non-load-bearing but functionally demanding components in automotive applications. While they do not contribute to the structural integrity of the vehicle, they must satisfy specific mechanical, thermal, and impact resistance criteria to ensure long-term performance under hood conditions.

4.4.1.3 Effect of Aspect Ratio on Mechanical Performance

As described in the preceding section, the carbon fibre post-processing length was approximately 215 µm, while it was about 400 µm for the modified composites. The subsequent findings demonstrate the importance of fibre length in determining the mechanical characteristics of the composites. The aspect ratio (length-to-diameter ratio) of fibres plays a crucial role in determining the effectiveness of fibre reinforcement in composite materials. A higher fibre aspect ratio improves stress transfer from the matrix to the fibre, enhancing the composite's mechanical performance. This is because a longer fibre-to-diameter ratio provides a greater surface area for interfacial bonding with the surrounding matrix, facilitating more efficient load distribution across the composite. Furthermore, fibres with a higher aspect ratio exhibit stronger resistance to pullout under stress, which contributes to increased tensile strength and enhances the overall reinforcement efficacy of the composite material.

Critical fibre length is closely related to the aspect ratio and defines the minimum fibre length necessary for efficient stress transfer between the fibre and matrix. If the fibre is shorter than this critical length, it may not contribute effectively to reinforcement and could act as a filler instead. The critical fibre length depends on several factors, including the fibre's tensile strength, the matrix's interfacial shear strength, and the fibre diameter.

The aspect ratio must typically be sufficiently high for fibre reinforcement to enhance mechanical properties such as tensile strength, stiffness, and impact resistance. Typically, an aspect ratio of

10:1 is considered the minimum for fibres to contribute to reinforcement in composites. Most effective fibre reinforcement usually occurs with an aspect ratio between 20:1 and 100:1 or higher. The specific ratio depends on fibre type, matrix material, and desired mechanical properties.

The carbon fibres employed in the first extrusion feeding setup of this study exhibited an aspect ratio of approximately 31:1, while the fibres in the second extrusion setup reached an aspect ratio of around 57:1. The variation in aspect ratios had a pronounced influence on the mechanical properties of the resulting composite material. Specifically, the higher aspect ratio in the second setup led to more efficient stress transfer and improved reinforcement, owing to the increased fibre length relative to its diameter. This enhanced fibre-matrix interaction likely contributed to the superior mechanical performance observed in the composites processed with higher aspect ratio fibres.

The findings align with micromechanical reinforcement theories, which predict that fibres with higher aspect ratios provide superior reinforcement due to better interfacial bonding and load-bearing capacity. The second extrusion setup, with its longer post-process carbon fibres, supported these theoretical predictions, showcasing enhanced composite performance as a function of fibre geometry. This confirms the critical role of aspect ratio in determining the structural integrity and mechanical properties of fibre-reinforced composites.

These findings highlight the importance of optimizing fibre aspect ratio in the design and fabrication of fibre-reinforced composites for composites engineered for critical structural performance. The enhanced mechanical properties observed in the composites with higher aspect ratios suggest that tailoring fibre dimensions could be an essential strategy for improving the durability and functionality of composite materials in various engineering applications.

4.5 Conclusion

The developed cellulose microfibre/carbon fibre hybrid biocomposites have a balance between thermal stability, tensile, flexural, impact, heat deflection, and flow properties required for composites engineered for critical structural performance, such as automotive applications. The incorporation of carbon fibre in cellulose microfibre composites improved their mechanical and thermal properties. Tensile and flexural strength and modulus, as well as heat deflection temperature and thermal stability of the composites, were enhanced by replacing a fraction of

cellulose microfibre with carbon fibre. Compared to neat PA11, impact strength was generally reduced in the composites reinforced with cellulose microfibre; however, it was considerably improved by hybridization with carbon fibre. The moisture uptake was also decreased by incorporating carbon fibre in the hybrid composites. This study demonstrates that the hybridization of synthetic fibres, such as carbon fibre, makes natural fibre composites more suitable for lightweight structural components in transportation systems.

Since PA11 and its composites experienced some level of degradation and hydrolysis during extrusion processing, a polymer blend consisting of PA11 and PP was employed to improve the processability of the composites. Neat PA11 and the polymer blend of PA11 and PP were compared as polymer matrices of the composites. The polymer blend composites showed enhanced performance properties compared to PA11 composites, except that the unnotched Izod impact strength was higher for PA11 composites. For both PA11 and polymer blend composites, hybridization with synthetic carbon fibre enhanced the thermo-mechanical properties of the composites, including tensile, flexural, impact, and heat deflection, which are essential for applications requiring superior mechanical strength and stiffness. However, it had no significant effect on elongation at break for polymer blend composites. Image analysis revealed effective fibre-matrix interfacial bonding, efficient component integration, and good fibre dispersion. In addition, HDT values showed a significant improvement for hybrid polymer blend composites.

By switching the carbon fibre input from the feeding hopper to the degassing zone, the length of the carbon fibre was preserved to a certain degree, resulting in improved mechanical performance. The aspect ratio of the carbon fibres employed in the two extrusion feeding setups varied significantly, with the first setup yielding fibres with an aspect ratio of approximately 31:1, while the second setup produced fibres with an aspect ratio of around 57:1. This variation in fibre geometry plays a critical role in the mechanical behaviour of the composite, as a higher aspect ratio leads to enhanced stress transfer between the fibre and matrix, which improves the reinforcement efficiency of the composite material. This can reduce the quantity of carbon fibre used in the hybrid system, resulting in cost savings and the use of a smaller proportion of synthetic fibres in our final product, while still meeting the requirements for structural applications.

This study demonstrates that blending synthetic fibres with natural fibres in a polyamide and polypropylene matrix significantly enhances the performance properties of the natural fibre polyamide composites while reducing their cost. The developed hybrid composites with enhanced thermo-mechanical properties have the potential to be used in automotive applications.

4.6 References

Aydemir, D., Kiziltas, A., Erbas Kiziltas, E., Gardner, D. J., & Gunduz, G. (2015). Heat treated wood–nylon 6 composites. *Composites Part B: Engineering, 68*, 414–423. https://doi.org/10.1016/j.compositesb.2014.08.034

Battegazzore, D., Salvetti, O., Frache, A., Peduto, N., De Sio, A., & Marino, F. (2016). Thermo-mechanical properties enhancement of bio-polyamides (PA10.10 and PA6.10) by using rice husk ash and nanoclay. *Composites Part A: Applied Science and Manufacturing, 81*, 193–201. https://doi.org/10.1016/j.compositesa.2015.11.027

Bernstein, R., Derzon, D. K., & Gillen, K. T. (2005). Nylon 6.6 accelerated aging studies: Thermal-oxidative degradation and its interaction with hydrolysis. *Polymer Degradation and Stability, 88*(3), 480–488. https://doi.org/10.1016/j.polymdegradstab.2004.11.007

Bledzki, A. K., Faruk, O., & Sperber, V. E. (2006). Cars from bio-fibres. *Macromolecular Materials and Engineering, 291*(5), 449–457. https://doi.org/10.1002/mame.200500378

Botelho, E. C., Figiel, Ł., Rezende, M. C., & Lauke, B. (2003). Mechanical behaviour of carbon fibre reinforced polyamide composites. *Composites Science and Technology, 63*(13), 1843–1855. https://doi.org/10.1016/S0266-3538(03)00186-1

Brehmer, B. (2014). Polyamides from biomass derived monomers. In S. Kabasci (Ed.), *Bio-based plastics: Materials and applications* (pp. 275–293). John Wiley & Sons Ltd.

Corrêa, A. C., Teixeira, E. M., Carmona, V. B., Teodoro, K. B. R., Ribeiro, C., Mattoso, L. H. C., & Marconcini, J. M. (2014). Obtaining nanocomposites of polyamide 6 and cellulose whiskers via extrusion and injection moulding. *Cellulose, 21*(1), 311–322. https://doi.org/10.1007/s10570-013-0124-5

De Almeida, S. F. M., & Neto, Z. d. S. N. (1994). Effect of void content on the strength of composite laminates. *Composite Structures, 28*(2), 139–148. https://doi.org/10.1016/0263-8223(94)90052-3

De Arcaya, P. A., Retegi, A., Arbelaiz, A., Kenny, J. M., & Mondragon, I. (2009). Mechanical properties of natural fibres/polyamides composites. *Polymer Composites, 30*(3), 257–264. https://doi.org/10.1002/pc.20606

Dhakal, H. N., Zhang, Z. Y., & Richardson, M. O. W. (2007). Effect of water absorption on the mechanical properties of hemp fibre reinforced unsaturated polyester composites. *Composites Science and Technology, 67*(7–8), 1674–1683. https://doi.org/10.1016/j.compscitech.2006.06.019

Du, Y., Yan, N., & Kortschot, M. T. (2012). Investigation of unsaturated polyester composites reinforced by aspen high-yield pulp fibres. *Polymer Composites, 33*(2), 169–177. https://doi.org/10.1002/pc.22133

Du, Y., Wu, T., Yan, N., Kortschot, M. T., & Farnood, R. (2013). Pulp fibre-reinforced thermoset polymer composites: Effects of the pulp fibres and polymer. *Composites Part B: Engineering, 48*, 10–17. https://doi.org/10.1016/j.compositesb.2012.12.010

Du, Y., Yan, N., & Kortschot, M. T. (2014). The use of ramie fibres as reinforcements in composites. In K. Oksman Niska & M. Sain (Eds.), *Biofibre reinforcements in composite materials* (pp. 104–137). Woodhead Publishing. https://doi.org/10.1533/9780857099228.2.104

Endres, H. J., & Siebert-Raths, A. (2011). *Engineering biopolymers: Markets, manufacturing, properties and applications* (pp. 95–98). Carl Hanser Verlag.

Faruk, O., Bledzki, A. K., Fink, H. P., & Sain, M. (2012). Biocomposites reinforced with natural fibres: 2000–2010. *Progress in Polymer Science, 37*(11), 1552–1596. https://doi.org/10.1016/j.progpolymsci.2012.04.003

Faruk, O., Bledzki, A. K., Fink, H. P., & Sain, M. (2014). Progress report on natural fibre reinforced composites. *Macromolecular Materials and Engineering, 299*(1), 9–26. https://doi.org/10.1002/mame.201300008

Feldmann, M., & Bledzki, A. K. (2014). Bio-based polyamides reinforced with cellulosic fibres: Processing and properties. *Composites Science and Technology, 100*, 113–120. https://doi.org/10.1016/j.compscitech.2014.06.010

Feldmann, M., Heim, H., & Zarges, J. (2015). Influence of the process parameters on the mechanical properties of engineering biocomposites using a twin-screw extruder. *Composites Part A: Applied Science and Manufacturing, 76*, 28–35. https://doi.org/10.1016/j.compositesa.2015.05.002

Gonçalves, E. S., Poulsen, L., & Ogilby, P. R. (2007). Mechanism of the temperature-dependent degradation of polyamide 66 films exposed to water. *Polymer Degradation and Stability, 92*(10), 1977–1985. https://doi.org/10.1016/j.polymdegradstab.2007.08.011

Grozdanov, A., & Bogoeva-Gaceva, G. (2010). Carbon fibres/polyamide 6 composites based on hybrid yarns. *Journal of Thermoplastic Composite Materials, 23*(1), 99–110. https://doi.org/10.1177/0892705709335586

Hablot, E., Matadi, R., Ahzi, S., & Avérous, L. (2010). Renewable biocomposites of dimer fatty acid-based polyamides with cellulose fibres: Thermal, physical and mechanical properties. *Composites Science and Technology, 70*(3), 504–509. https://doi.org/10.1016/j.compscitech.2009.11.003

Hajiha, H., & Sain, M. (2015). High toughness hybrid biocomposite process optimization. *Composites Science and Technology, 111*, 44–49. https://doi.org/10.1016/j.compscitech.2015.03.009

Holbery, J., & Houston, D. (2006). Natural-fibre-reinforced polymer composites in automotive applications. *JOM, 58*(11), 80–86. https://doi.org/10.1007/s11837-006-0234-2

KC, B., Panthapulakkal, S., Kronka, A., Agnelli, J. A. M., Tjong, J., & Sain, M. (2015). Cellulose reinforced PA6,6 composites: Physicomechanical, morphological, and thermal properties. *Journal of Applied Polymer Science, 132*(10). https://doi.org/10.1002/app.41663

Khanna, Y. P., Reimschuessel, A. C., Banerjie, A., & Altman, C. (1988). Memory effects in polymers. II. Processing history vs. crystallization rate of nylon 6: Observation of phenomenon and product behavior. *Polymer Engineering & Science, 28*(24), 1600–1606. https://doi.org/10.1002/pen.760282403

Khanna, Y. P., Han, P. K., & Day, E. D. (1996). Memory effects in polymers. II. Processing history vs. crystallization rate of nylon 6—Observation of phenomenon and product behavior. *Polymer Engineering & Science, 36*(13), 1745–1751. https://doi.org/10.1002/pen.10680

Kiziltas, A., Nazari, B., Gardner, D. J., & Bousfield, D. W. (2014). Polyamide 6–cellulose composites: Effect of cellulose composition on melt rheology and crystallization behavior. *Polymer Engineering & Science, 54*(4), 739–746. https://doi.org/10.1002/pen.23636

Kohan, M. I., Mestemacher, S. A., Pagilagan, R. U., & Redmond, K. (2003). Polyamides. In *Ullmann's Encyclopedia of Industrial Chemistry* (7th ed.). Wiley-VCH Verlag GmbH & Co. KGaA. https://doi.org/10.1002/14356007.a21_717

Kuciel, S., Kuźniar, P., & Liber-Kneć, A. (2012). Polyamides from renewable sources as matrices of short fibre reinforced biocomposites [Poliamidy ze źródeł odnawialnych jako osnowy biokompozytów wzmacnianych krótkimi włóknami]. *Polimery, 57*(9), 627–634.

Liu, K., Madbouly, S. A., Schrader, J. A., Kessler, M. R., Grewell, D., & Graves, W. R. (2015). Biorenewable polymer composites from tall oil-based polyamide and lignin–cellulose fibre. *Journal of Applied Polymer Science, 132*(48). https://doi.org/10.1002/app.42711

Magniez, K., Iftikhar, R., & Fox, B. L. (2015). Properties of bio-based polymer nylon 11 reinforced with short carbon fibre composites. *Polymer Composites, 36*(4), 668–674. https://doi.org/10.1002/pc.23093

Mohanty, A. K., Misra, M., & Drzal, L. T. (2002). Sustainable bio-composites from renewable resources: Opportunities and challenges in the green materials world. *Journal of Polymers and the Environment, 10*(1–2), 19–26. https://doi.org/10.1023/A:1021013921916

Mutlu, H., & Meier, M. A. R. (2010). Castor oil as a renewable resource for the chemical industry. *European Journal of Lipid Science and Technology, 112*(1), 10–30. https://doi.org/10.1002/ejlt.200900138

Nie, W. Z., & Li, J. (2010). Effect of carbon fibre content on friction and wear properties of carbon fibre reinforced PA6 composites. *Plastics, Rubber and Composites, 39*(1), 10–15. https://doi.org/10.1179/174328910X12584689990804

Saheb, D. N., & Jog, J. P. (1999). Natural fibre polymer composites: A review. *Advances in Polymer Technology, 18*(4), 351–363. https://doi.org/10.1002/(SICI)1098-2329(199924)18:4<351::AID-ADV6>3.0.CO;2-X

Ogunniyi, D. S. (2006). Castor oil: A vital industrial raw material. *Bioresource Technology, 97*(9), 1086–1091. https://doi.org/10.1016/j.biortech.2005.03.028

Oksman Niska, K., & Sain, M. (Eds.). (2008). *Wood–polymer composites*. Woodhead Publishing.

Ota, W. N., Amico, S. C., & Satyanarayana, K. G. (2005). Studies on the combined effect of injection temperature and fibre content on the properties of polypropylene–glass fibre composites. *Composites Science and Technology, 65*(6), 873–881. https://doi.org/10.1016/j.compscitech.2004.10.009

Ozen, E., Kiziltas, A., Kiziltas, E. E., & Gardner, D. J. (2013). Natural fibre blend–nylon 6 composites. *Polymer Composites, 34*(4), 544–553. https://doi.org/10.1002/pc.22470

Panthapulakkal, S., Law, S., & Sain, M. (2005). Injection molded natural fibre hybrid composites for automobile applications—Mechanical properties and flammability. *International SAMPE Technical Conference, 37*, 1–11.

Panthapulakkal, S., & Sain, M. (2006). Injection molded wheat straw and corn stem filled polypropylene composites. *Journal of Polymers and the Environment, 14*(3), 265–272. https://doi.org/10.1007/s10924-006-0014-4

Panthapulakkal, S., & Sain, M. (2007a). Injection-molded short hemp fibre/glass fibre-reinforced polypropylene hybrid composites—Mechanical, water absorption and thermal properties. *Journal of Applied Polymer Science, 103*(4), 2432–2441. https://doi.org/10.1002/app.25234

Panthapulakkal, S., & Sain, M. (2007b). Studies on the water absorption properties of short hemp–glass fibre hybrid polypropylene composites. *Journal of Composite Materials, 41*(15), 1871–1883. https://doi.org/10.1177/0021998306069877

Peng, Y., Gardner, D. J., & Han, Y. (2015). Characterization of mechanical and morphological properties of cellulose reinforced polyamide 6 composites. *Cellulose, 22*(5), 3199–3215. https://doi.org/10.1007/s10570-015-0738-1

Rosenau, B. (2007). Polyamides (PA). *Kunststoffe International, 10*, 58–60.

Sain, M., Panthapulakkal, S., & Law, S. (2015). U.S. Patent No. 8940132. U.S. Patent and Trademark Office.

Scott, E., Peter, F., & Sanders, J. (2007). Biomass in the manufacture of industrial products—the use of proteins and amino acids. *Applied Microbiology and Biotechnology, 75*(4), 751–762. https://doi.org/10.1007/s00253-007-0932-6

Semba, T., Ito, A., Kitagawa, K., Nakatani, T., Yano, H., & Sato, A. (2014). Thermoplastic composites of polyamide-12 reinforced by cellulose nanofibres with cationic surface modification. *Journal of Applied Polymer Science, 131*(20). https://doi.org/10.1002/app.40718

Shen, L., Worrell, E., & Patel, M. K. (2010). Present and future development in plastics from biomass. *Biofuels, Bioproducts and Biorefining, 4*(1), 25–40. https://doi.org/10.1002/bbb.189

Singha, A. S., Shama, A., & Thakur, V. K. (2008). Pressure induced graft co-polymerization of acrylonitrile onto *Saccharum cilliare* fibre and evaluation of some properties of grafted fibres. *Bulletin of Materials Science, 31*(1), 7–13. https://doi.org/10.1007/s12034-008-0013-4

Singha, A. S., & Thakur, V. K. (2008). Fabrication and study of lignocellulosic *Hibiscus sabdariffa* fibre reinforced polymer composites. *Bioresources, 3*(4), 1173–1186.

Singha, A. S., Shama, A., & Thakur, V. K. (2009). Graft copolymerization of acrylonitrile onto *Saccharum cilliare* fibre. *e-Polymers, 2009*(105), 1–12. https://doi.org/10.1515/epoly.2009.9.1.464

Singha, A. S., & Thakur, V. K. (2009a). Fabrication and characterization of *S. cilliare* fibre reinforced polymer composites. *Bulletin of Materials Science, 32*(1), 49–58. https://doi.org/10.1007/s12034-009-0009-z

Singha, A. S., & Thakur, V. K. (2009b). Fabrication and characterization of *H. sabdariffa* fibre reinforced polymer composites. *Polymer-Plastics Technology and Engineering, 48*(4), 482–487. https://doi.org/10.1080/03602550902717363

Singha, A. S., & Thakur, V. K. (2010). Mechanical, morphological, and thermal characterization of compression-molded polymer biocomposites. *International Journal of Polymer Analysis and Characterization, 15*(2), 87–97. https://doi.org/10.1080/10236660903575301

Thakur, V. K., & Singha, A. S. (2010). Evaluation of *Grewia optiva* fibres as reinforcement in polymer biocomposites. *Polymer-Plastics Technology and Engineering, 49*(11), 1101–1107. https://doi.org/10.1080/03602551003778769

Thakur, V. K., Thakur, M. K., & Gupta, R. K. (2014a). Review: Raw natural fibre-based polymer composites. *International Journal of Polymer Analysis and Characterization, 19*(3), 256–271. https://doi.org/10.1080/1023666X.2014.880016

Thakur, V. K., Thakur, M. K., Raghavan, P., & Kessler, M. R. (2014b). Progress in green polymer composites from lignin for multifunctional applications: A review. *ACS Sustainable Chemistry & Engineering, 2*(5), 1072–1092. https://doi.org/10.1021/sc500087x

Vaidya, U. (2011). *Composites for automotive, truck and mass transit: Materials, design, manufacturing*. DEStech Publications.

Wang, M. S., & Huang, J. C. (1994). Nylon 1010 properties and applications. *Journal of Polymer Engineering, 13*(2), 155–174. https://doi.org/10.1515/polyeng.1994.13.2.155

Chapter 5 Theoretical Analysis of the Hybrid Polyamide 11 Composites

5.1 Introduction and Background

Hybrid composites are engineered materials composed of different types of fibres, providing a combination of properties not achievable by using a single material. Hybrid composites have gained substantial attention due to their superior mechanical, thermal, and physical properties derived from their multi-constituent structure (Facca et al., 2006b; Facca et al., 2007; Kc et al., 2015; Panthapulakkal et al., 2017; Armioun et al., 2016a; Armioun et al., 2016 b). However, predicting the performance of hybrid composites under diverse loading and environmental conditions is fundamentally complex due to the complexity of their internal structure and the variability of properties among their constituents.

This challenge has inspired the development of a range of theoretical models, each with its unique methodologies and scope of applicability (Facca et al., 2006b; Banerjee & Sankar, 2014). The use of theoretical models has become an integral part of understanding the behaviour and properties of hybrid composites. These models enable the evaluation of various microstructures and their performance under service conditions, providing valuable insights into the potential of different approaches to optimize material properties for specific applications.

In terms of durability, natural fibres are generally more prone to environmental degradation than synthetic fibres. They are susceptible to moisture absorption, UV radiation, and biological degradation. However, this can be accounted for using durability models, which consider these environmental exposure factors, allowing for the prediction and addressing of these effects. An important aspect of using natural fibres is their lower environmental impact compared to synthetic fibres (Facca et al., 2006a; Armioun et al., 2017; Kc et al., 2016). Anisotropy is another critical factor in the study of both natural and synthetic fibres. The composite models must account for this, which can be accomplished using various models, such as the Rule of Mixtures, the Inverse Rule of Mixtures, or more complex anisotropy models (Facca et al., 2006b). Natural fibres typically exhibit lower strength and modulus compared to synthetic fibres, which can potentially affect the composite's overall strength. However, this can be significantly mitigated by consciously organizing or aligning the fibres to optimize the composite structure, thereby enhancing its mechanical properties (Kc et al., 2016; Armioun et al., 2016a; Banerjee & Sankar, 2014). By

coordinating all these factors, a comprehensive theoretical model for hybrid composites can be created. Such a model not only predicts composite properties but also provides valuable information in the material and structural design processes. Furthermore, it can help optimize the balance between mechanical performance and the environmental impact of hybrid composites (Banerjee & Sankar, 2014).

In the study of hybrid composites that include both synthetic and natural fibres, a mix of challenges and opportunities arises due to the unique attributes of these fibres. When theoretical models are created for these materials, a comprehensive examination of the characteristics of each fibre type is required. The result of a composite's performance often lies at the interface, also referred to as the interaction between the fibres and the matrix material. In the case of hybrid composites, it is critical to understand how natural and synthetic fibres behave at this interface. Theoretical models have been developed to predict the mechanical behaviour of these composites based on their constituent materials and geometries. The accurate prediction of the mechanical behaviour of hybrid composites under various conditions is challenging due to the natural heterogeneity and anisotropy of these materials.

In recent years, micromechanical models have proven to be effective tools in understanding and predicting the complex behaviour of hybrid composites. The theoretical models used to describe the mechanical behaviour of hybrid composites can be broadly categorized into micromechanical and macromechanical models. Micromechanical models are based on the analysis of the behaviour of individual reinforcing fibres within the composite. They aim to predict the overall mechanical properties of the composite based on the properties of the constituent fibres and the matrix material. Examples of micromechanical models include the rule of mixtures, the Halpin-Tsai model, and the shear lag model. Micromechanical models describe the mechanical behaviour of composites at the microscale, considering individual constituents (matrix and fibres) and their interactions. These models can be divided into two broad categories: analytical models (like the Rule of Mixtures or the shear lag model) and numerical methods (like the Finite Element Method). By employing these models, the properties of the composite can be predicted based on the properties and behaviour of its constituents.

Macromechanical models, on the other hand, are based on the analysis of the overall behaviour of the composite as a whole. They consider the composite as a single entity with effective mechanical

properties that are different from those of the individual fibres and matrix material. Examples of macromechanical models include the classical lamination theory and the finite element method. In addition to these models, some hybrid models combine micromechanical and macromechanical approaches. These models aim to capture both the microstructural details and the overall behaviour of the composite. Examples of hybrid models include the multi-scale finite element method and the bridging scale method (Banerjee & Sankar, 2014).

5.1.1 Micromechanical models for prediction of the tensile modulus of single fibre reinforced composites

Linear elastic models, first introduced by Jones (1975), are fundamental for the initial understanding of hybrid composites. These models treat the composite constituents as homogeneous, isotropic, and linearly elastic entities, thereby simplifying the prediction of properties. Although their computational efficiency is invaluable during the early design stages, these assumptions often do not adequately capture the intrinsic complexity of hybrid composites. As a result, the precision of these models may be compromised when applied to composites with anisotropic or heterogeneous characteristics.

Linear elastic models postulate that the strain experienced by a material is directly proportional to the applied stress, a relationship described by Hooke's Law. In these models, the stress-strain relationship remains linear until the material reaches its elastic limit. Beyond this point, the material may deform plastically or even fail, which linear elastic models do not account for (Jones, 1975). They have a limited range of applicability and operate under the assumption of material linearity and elasticity, which is often unrealistic in real-world applications where materials can undergo plastic deformation or failure. They cannot accurately model the viscoelastic behaviour (time-dependent deformation) exhibited by many materials when subjected to long-term loading conditions. Linear elastic models cannot accurately model damage progression, a crucial aspect when evaluating the lifecycle of composites.

5.1.1.1 Rule of Mixtures (ROM)

The rule of mixtures (ROM) is the simplest model for predicting the properties of composites based on the properties of the fibre and matrix and their corresponding volume fractions. The ROM model was initially defined for single-fibre-reinforced composites. In the model, it has been

assumed that fibres are aligned and oriented in the direction of the applied load. To calculate any composite's property, the following formula can be applied:

Equation 1

$$P_c = P_f V_f + P_m V_m$$

Where P_c represents any composite's property, V_f and V_m are volume fractions of fibre and matrix, respectively. It should be noted that $V_f + V_m = 1$, assuming no void is present in the composite's structure.

The rule of mixtures (ROM) is the most basic model used to predict the elastic characteristics of a composite material. Voigt assumed that both the matrix and fibre undergo the same amount of strain (ε_1), as seen in Figure 35, in order to determine the elastic modulus of the composite material in the 1-direction (E_1). This strain is the result of applying a uniform stress (σ_1) over a uniform cross-sectional area (A) (Tucker & Liang, 1999; Banerjee & Sankar, 2014). Since it is assumed that each element deforms elastically and that the strain in both the fibre and the matrix is identical (i.e., $\varepsilon_f = \varepsilon_m = \varepsilon_1$), the stress on each element is computed as follows:

Equation 2

$$\sigma_f = E_f \varepsilon_1$$

Equation 3

$$\sigma_m = E_m \varepsilon_1$$

Equation 4

$$\sigma_1 = E_1 \varepsilon_1$$

The sum of the forces acting on the fibre and the matrix is equal to the total force (F_t) acting in the direction of application and acting on the cross-sectional area A:

Equation 5

$$F_t = \sigma_1 A = \sigma_f A_f + \sigma_m A_m$$

The ROM equation for the apparent Young's modulus in the fibre direction will be found by substituting Equation 2 through Equation 4 into Equation 5 and solving for E_1 (Jones, 1975):

Equation 6

$$E_1 = E_f V_f + E_m V_m$$

where V_f and V_m are the volume fractions of the fibre and the matrix, respectively.

Equation 7

$$V_f = \frac{A_f}{A}$$

Equation 8

$$V_m = \frac{A_m}{A}$$

Young's modulus in the principal fibre direction will always be smaller than the values anticipated by ROM (Equation 6) for all composites with well-bonded reinforcements.

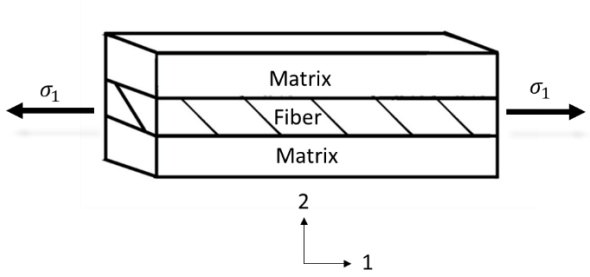

Figure 35 Simplified Representation of A Fibre-reinforced Matrix Stressed in the 1-direction

5.1.1.2 Inverse rule of mixtures (IROM)

According to Reuss's assumption, the applied transverse stress (σ_2) must be identical in both the fibre and the matrix to compute the elastic modulus of the composite in the 2-direction (E_2), as illustrated in Figure 36 (Tucker & Liang, 1999). Therefore, the strains in the matrix (ε_m) and the fibre (ε_f) are determined as follows:

Equation 9

$$\varepsilon_f = \frac{\sigma_2}{E_f}$$

Equation 10

$$\varepsilon_m = \frac{\sigma_2}{E_m}$$

The sum of the average strains in the fibre and matrix, as given by Equation 11, results in the total strain experienced in the 2-direction (ε_2) as a result of 2-direction stress (σ_2).

Equation 11

$$\varepsilon_2 = V_f \varepsilon_f + V_m \varepsilon_m$$

Equation 11 is obtained by combining Equation 9 and Equation 10, which results in the following equation:

Equation 12

$$\varepsilon_2 = V_f \frac{\sigma_2}{E_f} + V_m \frac{\sigma_2}{E_m}$$

The elastic modulus of the composites in the 2-direction (E_2) is found by dividing the total stress (σ_2) by the total strain (ε_2). Consequently, E_2 is calculated by an inverse rule of mixtures equation known as (Jones, 1975):

Equation 13

$$E_2 = \frac{E_f E_m}{V_m E_f + V_f E_m} \qquad \text{or} \qquad \frac{1}{E_2} = \frac{V_m}{E_m} + \frac{V_f}{E_f}$$

In general, Young's modulus in the leading direction of all well-bonded reinforced composites is higher than the values predicted by the IROM (Equation 13).

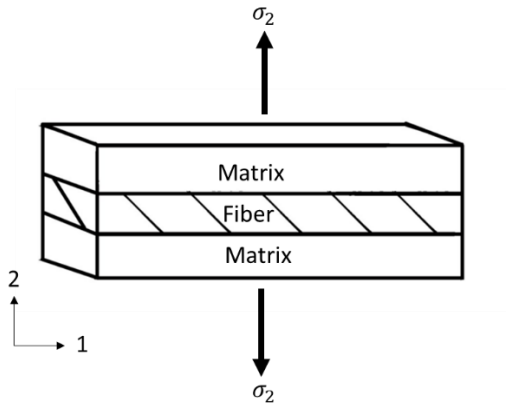

Figure 36 Simplified Representation of A Fibre-reinforced Matrix Stressed in the 2-direction

These foundational models, with their principle rooted in the direct proportionality of composite properties to their constituents' volume fraction, offer a simplistic yet quick estimation of composite properties. However, its underlying simplifications overlook the complex interactions between fibres and matrix, as well as the effects of fibre distribution within the composite, which can lead to potential discrepancies between estimated and actual properties.

5.1.1.3 Halpin-Tsai Model

Developed by Jack A. Halpin and J. Pagano Tsai in the late 1960s, the Halpin-Tsai model extends the rule of mixtures by incorporating the effects of fibre orientation, thereby accounting for anisotropic behaviour. The Halpin-Tsai model is initially an empirical model designed to predict the elastic moduli of single fibre-reinforced composite materials. This model considers the influence of the aspect ratio and volume fraction of the fibres, offering a semi-empirical relationship between the composite properties and those of its constituents (Halpin & Tsai, 1969). Although this model enhances accuracy for composites with oriented fibres, it still assumes perfect bonding and uniform fibre distribution. These assumptions might not always hold, especially for hybrid composites with complex fibre-matrix interactions and irregular fibre distribution.

Semi-empirical equations developed by Halpin and Tsai are commonly used to predict the elastic performance of single-fibre-reinforced composites (Halpin & Kardos, 1976). The Halpin-Tsai equation is expressed in its general form as follows (Halpin & Tsai, 1969):

Equation 14

$$\frac{\Omega}{\Omega_m} = \frac{1 + \xi\eta V_f}{1 - \eta V_f}$$

Where η is expressed as (Halpin & Tsai, 1969):

Equation 15

$$\eta = \frac{\left(\Omega_f / \Omega_m\right) - 1}{\left(\Omega_f / \Omega_m\right) + \xi}$$

In the above equations, the parameter Ω represents a range of properties, i.e., the longitudinal modulus (E_1), the transverse modulus (E_2) or the longitudinal shear modulus (G_{12}). Like the ROM equations, the subscripts *f* and *m* imply the specific properties of the fibre (Ω_f) and matrix (Ω_m), respectively. The parameter ξ is defined to fit the Equation 14 to experimental data. This parameter considers both the packing arrangement and the geometry of the reinforcing fibres (Halpin-Tsai, 1969; Tucker & Liang, 1999). Accordingly, a considerable value of ξ indicates the good effectiveness of fibres in enhancing the composite's stiffness (Halpin & Tsai, 1969). A summary of analytical equations available in the literature to predict ξ is shown in Table 22. The equations listed in Table 22 for ξ depends on the shape of the particles as well as the predicted modulus (i.e., longitudinal, transverse, shear) (Halpin & Kardos, 1976).

In this study, the longitudinal tensile modulus of fibre-reinforced composites is defined using the following form of Equation 14 (Halpin & Kardos, 1976):

Below is the Halpin-Tsai equation for modulus presented:

Equation 16

$$E_c = E_m \left(\frac{1 + \xi\eta V_f}{1 - \eta V_f}\right)$$

In Equation 16 the parameter η is given as (Halpin & Kardos, 1976):

Equation 17

$$\eta = \frac{\left(E_f / E_m\right) - 1}{\left(E_f / E_m\right) + \xi}$$

Table 22 Halpin-Tsai Parameters (Halpin & Kardos, 1976; Tucker & Liang, 1999)

Composite Property	Fibre Property Ω_f	Matrix Property Ω_m	ξ
Bulk modulus of aligned fibres, k_{23}	k_f	K_m	$\xi = \frac{1 - \nu_m - 2\nu_m^2}{1 + \nu_m}$
Transverse shear modulus of aligned fibres, G_{23}	G_f	G_m	$\xi = \frac{1 + \nu_m}{3 - \nu_m - 4\nu_m^2}$
Longitudinal shear modulus of aligned fibres, G_{12}	G_f	G_m	1
Bulk modulus of particulates, K	K_f	K_m	$\xi = \frac{2 - 4\nu_m}{1 + \nu_m}$
Shear modulus of particulates, G	G_f	G_m	$\xi = \frac{7 - 5\nu_m}{8 - 10\nu_m}$
Longitudinal modulus of SFRT, E_1	E_f	E_m	$\xi=2(\frac{l}{d})$
Transverse modulus of SFRT, E_2	E_f	E_m	2
Longitudinal shear modulus SFRT, G	G_f	G_m	1

SFRT: Single Fibre Reinforced Thermoplastic

For rectangular and circular fibres, ξ is given by the following equations (Halpin & Kardos, 1976):

Equation 18

$$\xi = 2\left(\frac{l}{d}\right)$$

Where l represents the length of a fibre in the 1-direction and t or d represents the thickness or diameter of the fibre.

In Equation 16, as L→0, ξ→0, and Halpin-Tsai equation becomes the IROM (Inverse Rule of Mixture) equation (Equation 13). On the other hand, as L→∞, ξ→∞ , and the Halpin-Tsai equation become the ROM (Rule of Mixture) equation (Equation 6).

The Halpin-Tsai equations are well recognized for predicting the stiffness of composite materials at low fibre volume fractions (Tucker & Liang, 1999). However, high levels of variations have been reported at high fibre volume fractions (Halpin & Tsai, 1969; Tucker & Liang, 1999; Ingber & Papathanasiou, 1997).

Hewitt and Malherbe reported that the Halpin-Tsai equation could underestimate composites' shear modulus (G_{12}) at a fibre volume fraction of 0.5 by around 30% (Halpin & Tsai, 1969; Hewitt & Malherbe, 1970). Accordingly, it was suggested that once the parameter ξ is presented as a function of the fibre volume fraction (V_f), the Halpin-Tsai equation would represent better consistency with experimental results as follows (Halpin & Tsai, 1969; Hewitt & Malherbe, 1970; Tucker & Liang, 1999):

Equation 19

$$\xi = 1 + 40V_f^{10}$$

The basic Halpin-Tsai equation was enhanced by Lewis and Nielsen by incorporating the effect of fibre packing as well as the aspect ratio of fibre (Lewis & Nielsen, 1970; Ingber & Papathanasiou, 1997; Tucker & Liang, 1999). In this format of the Halpin-Tsai equation, a maximum volume fraction for a bed of particles ($V_{f,\,max}$) has been introduced (Lewis & Nielsen, 1970). It has been reported through several experiments that a bed of randomly filled sphere particulates will approximately yield $V_{f,\,max}$ = 0.64. The modified Halpin-Tsai equation is given as (Lewis & Nielsen, 1970; Tucker & Liang, 1999):

Equation 20

$$\frac{\Omega}{\Omega_m} = \frac{1 + \xi\eta V_f}{1 - \mu(V_f)\eta V_f}$$

where the higher fibre volume fraction limit $\mu\,(V_f)$ is described as:

Equation 21

$$\mu(V_f) = 1 + \left(\frac{1 - V_{f,max}}{V_{f,max}^2}\right)V_f$$

The lower fibre volume fraction limit $\mu\,(V_f)$ is described as:

Equation 22

$$\mu(V_f) = \frac{1}{V_f}\left[1 - \exp\left(\frac{-V_f}{1 - \frac{V_f}{V_{f,max}}}\right)\right]$$

Initially, Nielsen and Lewis's (1970) model was employed to modify the longitudinal shear modulus (G_{12}); however, it was later reported by Ingber and Papathanasiou (1997) that this model presents better predictions of the properties listed in Table 22 compared to the original Halpin-Tsai equation (Lewis & Nielsen, 1970; Ingber & Papathanasiou, 1997).

While the Halpin-Tsai model provides a good approximation, it may not capture the exact mechanical behaviour of hybrid composites, particularly those with complex geometric or compositional arrangements. The model overlooks the interaction between fibres and the matrix, a critical factor in composite performance. It also assumes the composite is homogeneous and isotropic, which may not apply to hybrid composites.

5.1.1.4 Halpin-Tsai model for randomly oriented fibres

The Halpin-Tsai model equations take the form of Equation 23 for composites reinforced with randomly oriented short fibres (Halpin & Kardos, 1976; Banerjee & Sankar, 2014; Loos, 2015):

Equation 23

$$E_c^{ran} = E_m\left[\frac{3}{8}\left(\frac{1 + \xi\eta_L V_f}{1 - \eta_L V_f}\right) + \frac{5}{8}\left(\frac{1 + 2\eta_T V_f}{1 - \eta_T V_f}\right)\right]$$

Equation 24

$$\eta_L = \frac{\left(\frac{E_f}{E_m}\right) - 1}{\left(\frac{E_f}{E_m}\right) + \xi}$$

Equation 25

$$\eta_T = \frac{\left(\frac{E_f}{E_m}\right) - 1}{\left(\frac{E_f}{E_m}\right) + 2}$$

When

$$\xi = 2\left(\frac{l}{d}\right)$$

Where η_L and η_T are in longitudinal and transverse directions, respectively.

Semi-empirical models such as Halpin-Tsai do not consider the interactions between fibres. Therefore, analytical models were employed to better understand the effects of fibre interactions on the stiffness of the composites. Some of the analytical models available in the literature are shown below.

5.1.1.5 Cox's shear-lag model

Introduced by Cox (1952), shear-lag models represent a significant advancement by accommodating the stress transfer between the matrix and fibres. Cox introduced one of the earliest mathematical models to explain the reinforcing impact that fibres have on the strength characteristics of composite materials. The shear-lag model is an analytical model that analyzes the process of stress transfer in single-fibre composites that are subjected to an applied load. The model is commonly used for unidirectional fibre-reinforced composites. In this model, it is assumed that the fibres within the composite material are perfectly aligned and evenly distributed. These models incorporate the influence of fibre length, orientation, and the quality of the interfacial bond, making them particularly suited for scenarios where these factors significantly influence composite behaviour (Cox, 1952).

According to traditional shear-lag theory, the reinforcing fibres must be both oriented and packed in an ordered fashion. The fundamental equations are determined using a unit cell composed of a single fibre embedded in a matrix cylinder, with the cylinder's exterior surface subjected to a uniform strain comparable to the remote strain on the composite. In addition, both fibres and matrix are assumed to be elastic and isotropic, with no yielding or sliding between them. However, the complexity of these models and the need for detailed input data often result in computationally intensive procedures, limiting their use in time-sensitive or resource-constrained situations (Facca et al., 2007; Liu et al., 2014; Azeko et al., 2023; Hou & Panesar, 2023).

In the shear-lag theory, the load is transmitted from the matrix to the fibre by interfacial shear stresses. The tensile tension at the ends of each fibre is assumed to be zero. Therefore, the maximum tensile stress ($\sigma_{f,\,max}$) happens at the middle of the fibre, whilst the maximum shear stress ($\tau_{f,\,max}$) happens at the end of the fibre. Shear-lag equations for the axial tensile modulus of composites are derived using second-order differential equations as follows (Cox, 1952):

Equation 26

$$\frac{d\sigma_f^2}{d^2x} = \frac{2E_m\left(\frac{\sigma_f - \varepsilon_1 E_f}{E_f}\right)}{r^2 \ln\left(\frac{P_f}{V_f}\right)(1+\nu_m)}$$

Where ν_m represents Poisson's ratio of the matrix, and P_f refers to the packing factor of the fibres that are assumed to be cylindrical with a radius of r. The packing factor value varies depending on the assumed packing. Simple square or hexagonal packings are the most typical types, where P_f =π for square packing and p_f=2π/$\sqrt{3}$ for hexagonal packing.

Applying boundary conditions of either x=L/2 or x=-L/2 (at which the tensile strength of the fibre is zero (σ_f=0)) in the integration of Equation 26 results in the general format of Cox's shear lag model (Equation 27) as presented below:

Equation 27

$$E_c = V_f E_f \left(1 - \frac{\tanh(\eta s)}{\eta s}\right) + V_m E_m$$

Where η is given as:

Equation 28

$$\eta = \left(\frac{2E_m}{E_f(1+\nu_m)\ln\left(\frac{1}{V_f}\right)}\right)^{0.5}$$

Once the aspect ratio (L/r) approaches infinity in Equation 23, the shear-lag equation transforms to the ROM equation.

5.1.2 Micromechanical models for prediction of the tensile modulus of hybrid composites

5.1.2.1 Rule of mixture for hybrid composites

The hybrid rule of mixtures (HROM) equation is derived from the rule of mixtures (ROM) equation and is one of the simplest equations to be used to predict the tensile modulus of hybrid fibre-reinforced thermoplastics. The composite's components are assumed to be continuous and parallel, experiencing the same strain (Jones, 1975). The HROM equation is presented as follows:

Equation 29

$$E_c = E_{f1}V_{f1} + E_{f2}V_{f2} + E_mV_m$$

where E_C, E_{f1}, E_{f2}, and E_m represent the moduli of the hybrid composite, fibre 1 and 2, and the matrix, respectively, and V_{f1}, V_{f2}, and V_m represent the volume fractions of fibre 1, fibre 2, and the matrix, respectively. This equation predicts the maximum theoretical tensile modulus of a hybrid composite reinforced perfectly with short fibres with the provided volumetric composition of fibres and plastic.

There is also an alternative form of the HROM equation, in which the matrix material is separated into two subsystems, each containing one of the reinforcing fibres as presented in the following equation (Fu & Lauke, 1998; Fu et al., 2001):

Equation 30

$$E_{1h} = E_{s1}V_1 + E_{s2}V_2$$

where E_{S1} and E_{S2} represent the tensile moduli of system 1 and system 2, respectively, and V_1 and V_2 represent the volume fraction of each subsystem, respectively.

An illustration indicating the two subsystems in Equation 30 is shown in Figure 37. For instance, a hybrid composite reinforced by hemp and carbon fibres in a polypropylene matrix can be divided into two subsystems, where one system contains hemp fibre-reinforced polypropylene, and the other is carbon fibre-reinforced polypropylene. It should be noted that the hybrid volume fractions must be equal to unity. Considering each subsystem experiences the same strain, the interactions between the different reinforcing fibres are not taken into account in Equation 30.

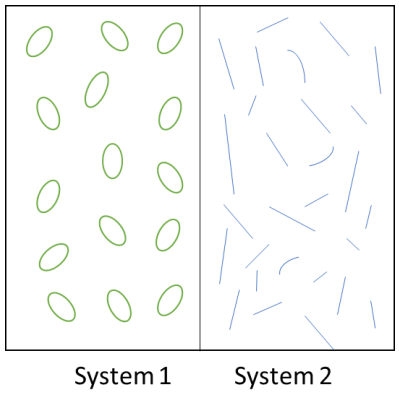

Figure 37 Illustration of Two Subsystems Containing Different Fibres in the Hybrid Rule of Mixtures Equation (Equation 30)

A hybrid effect is a term defined by the deviation from the HROM equation. A positive deviation from the HROM equation is considered a synergistic effect. It should be noted that a positive hybrid effect for a specific mechanical property does not necessarily result in a positive effect on all other mechanical properties (Fu et al., 2001; Facca et al., 2007).

A matrix partition coefficient (α_m) is defined to divide the matrix into its subsystems in Equation 30. Considering the matrix partition coefficient, V_1 and V_2 are determined as follows:

Equation 31

$$V_1 = \frac{\emptyset_{f1} + \alpha_m(\emptyset_m + \emptyset_v)}{\emptyset_{f1} + \emptyset_{f2} + \emptyset_m + \emptyset_v} = V_{f1} + \alpha_m(V_m + V_v)$$

Equation 32

$$V_2 = \frac{\emptyset_{f2} + (1 - \alpha_m)(\emptyset_m + \emptyset_v)}{\emptyset_{f1} + \emptyset_{f2} + \emptyset_m + \emptyset_v} = V_{f2} + (1 - \alpha_m)(V_m + V_v)$$

Where Φ_{f1}, Φ_{f2}, $\Phi_{v,}$ and Φ_m represent the volume fraction of fibre 1, fibre 2, voids, and the polymer matrix, respectively. The matrix partition coefficient (α_m) is described as the relative volume fraction of fibres as follows:

Equation 33

$$\alpha_m = \frac{\emptyset_{f1}}{\emptyset_{f2} + \emptyset_{f2}} = \frac{V_{f1}}{V_{f1} + V_{f2}}$$

Tensile moduli E_{S1} and E_{S2} (of the two subsystems) can be calculated using different micromechanical models available in the literature, such as Cox's shear-lag theory. The volume fraction of fibres and matrix in each subsystem (Figure 37) is calculated as follows:

System 1

Equation 34

$$V_{f1}^{*} = \frac{V_{f1}}{V_{f1} + \alpha_m (V_m + V_v)}$$

Equation 35

$$V_{m1}^{*} = \frac{\alpha_m V_m}{V_{f1} + \alpha_m (V_m + V_v)}$$

System 2

Equation 36

$$V_{f2}^{*} = \frac{V_{f2}}{V_{f2} + (1 - \alpha_m)(V_m + V_v)}$$

Equation 37

$$V_{m2}^{*} = \frac{(1 - \alpha_m) V_m}{V_{f2} + (1 - \alpha_m)(V_m + V_v)}$$

where V^{*}_{f1}, V^{*}_{f2}, V^{*}_{m1}, and V^{*}_{m2} represent the volume fraction of fibres and matrix in each subsystem, respectively.

5.1.2.2 Modified HROM equation

In multiple studies conducted by Fecca et al. (2006a, 2006b, 2007), a simple empirical approach is employed to predict the tensile properties of single-fibre-reinforced and hybrid composites, using modified ROM and HROM equations, respectively. For a composite reinforced with a single short fibre, the ROM equation is modified as follows:

Equation 38

$$E_1 = \chi E_f V_f + E_m V_m$$

Considering the effect of fibre length and all imperfections in fibre orientation and adhesion, the parameter χ multiplied by the fibre modulus may be referred to as the effective fibre modulus. In the literature, the parameter χ has been stated as the product of two variables η_l and η_θ (Thomason & Vlug, 1996), representing modifying factors for fibre length and orientation, respectively. In addition, in the HROM equation, another modifying component is introduced, which applies the best-fit value of χ obtained from corresponding single fibre-reinforced systems (Equation 38) (Facca et al., 2006b, 2007).

5.1.2.3 The Least Squares method for forecasting the parameters of mathematical models

The least squares method, also called the secant method, is a statistical technique used to estimate the parameters of a mathematical model by minimizing the sum of the squares of the differences between the observed data and the model's predicted values. In the least squares method, the goal is to find the values of the model parameters that minimize the sum of the squares of the differences between the observed data and the model's predicted values.

The least square method is employed to calculate the best-fit value of χ (as defined in Equation 39) between the ROM and the empirical data. The best-fit value of χ was assessed independently for each fibre and included in the updated HROM equation (Facca et al., 2006a, 2006b). The least square method used to assess the accuracy of the ROM model predicted the tensile modulus of each of the composites, given as follows:

Equation 39

$$\text{Sum of squared error } \sum_i^N \left(X_{p,i} - X_{m,i}\right)^2$$

where N, $X_{p,i}$ and $X_{m,i}$ represent the number of data points, the estimated values of the micromechanical model, and the empirically observed values, respectively (i.e., tensile modulus or strength).

Equation 40

$$Ec = \chi_1 E_{f1} V_{f1} + \chi_2 E_{f2} V_{f2} + E_m V_m$$

The variables χ_1 and χ_2 denote the best-fit χ values for fibres 1 and 2, respectively, in the hybrid system, which have been determined by experimental analysis conducted on single-fibre systems (Facca et al., 2006a, 2006b).

While Equation 40 may appear to be straightforward, it is important to determine if the best-fit values of χ from single-fibre systems, namely χ_1 and χ_2 in the hybrid systems, can be directly employed to predict the stiffness of hybrid systems. In this case, it is viable to estimate the performance of various hybrid compositions by utilizing a small set of characteristics obtained by single-fibre systems. One benefit of utilizing Equation 40 is the elimination of the need for an independent allocation of matrix material among the reinforcing elements. Consequently, employing a more straightforward methodology for forecasting the rigidity of hybrid systems becomes feasible.

5.1.2.4 The Halpin-Tsai model for hybrid composites

The semi-empirical Halpin-Tsai model for hybrid composites was proposed by Banerjee and Sankar (2014) using finite element method-based micromechanics, presented as follows:

Equation 41

$$E_c = E_m \left[\frac{1 + \xi\left(\eta_1 V_{f1} + \eta_2 V_{f2}\right)}{1 - \left(\eta_1 V_{f1} + \eta_2 V_{f2}\right)} \right]$$

Equation 42

$$\eta_1 = \frac{\left(\frac{E_{f1}}{E_m}\right) - 1}{\left(\frac{E_{f1}}{E_m}\right) + \xi}$$

Equation 43

$$\eta_2 = \frac{\left(\frac{E_{f2}}{E_m}\right) - 1}{\left(\frac{E_{f2}}{E_m}\right) + \xi}$$

In the presented equation, ξ is a curve-fitting parameter associated with the fibre packaging configuration.

5.1.3 Effective matrix approach in hybrid composites

One significant shortcoming associated with the simple HROM equations (Equation 29 and Equation 30) is that it does not consider the fibres' interactions in each subsystem, as illustrated in

Figure 37. Besides, an improper selection of the partition coefficient (i.e., α_M) could lead to a highly deviated estimation of the composite modulus.

Fu et al. (2002) introduced another approach for predicting the tensile modulus of hybrid fibre-reinforced composites, known as the "effective matrix" approach. Figure 38 demonstrates a graphical illustration of the effective matrix approach. In this approach, it is assumed that one type of fibre is embedded in an "effective matrix" that has already been reinforced by the other fibre type (Fu et al., 2002). This means that the effective matrix has the properties of a composite reinforced by another fibre.

The tensile modulus of the effective matrix is evaluated by shear-lag theory, where one set of fibres and the polymer matrix are applied. The volume fractions of fibre (V_{f1}) and matrix (V_{m1}) required to determine the properties of an effective matrix are as follows:

Equation 44

$$V_{f1} = \frac{\emptyset_{f1}}{\emptyset_{f2} + \emptyset_m + \emptyset_v}$$

Equation 45

$$V_{m1} = \frac{\emptyset_m}{\emptyset_{f1} + \emptyset_m + \emptyset_v}$$

The shear modulus of the effective matrix is calculated to apply the shear-lag theory for the second stage. This can be evaluated using the IROM equation as follows:

Equation 46

$$\frac{1}{G_m} = \frac{V_{f1}}{G_{f1}} + \frac{V_{m1}}{G_{m1}}$$

Where G_{f1}, G_{m1}, and G_m are the shear modulus of fibre type 1, the polymer matrix, and the effective matrix, respectively.

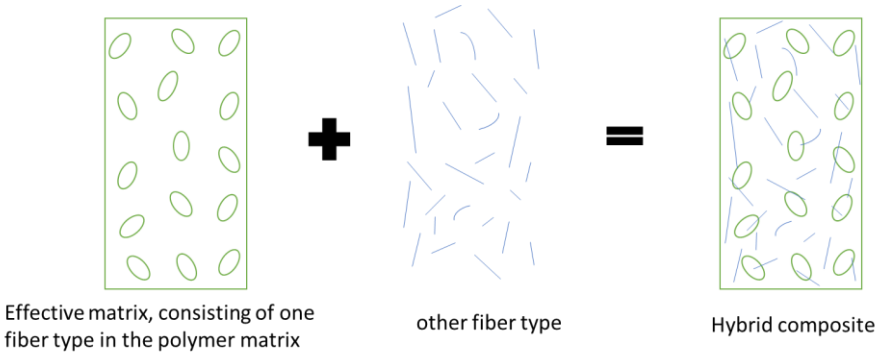

Figure 38 Effective Matrix Approach to Predict the Tensile Modulus of Hybrid Composites (Fu et al., 2002)

Once again, the shear-lag theory is applied to evaluate the tensile modulus of the other fibre set embedded in the effective matrix. The volume fractions of the second set of fibre (V_{f2}) and matrix (V_{m2}) employed in the shear-lag equation are as follows:

Equation 47

$$V_{f2} = \frac{\emptyset_{f2}}{\emptyset_{f1} + \emptyset_{f2} + \emptyset_m + \emptyset_v}$$

Equation 48

$$V_{m2} = \frac{\emptyset_{f1} + \emptyset_m + \emptyset_v}{\emptyset_{f1} + \emptyset_{f2} + \emptyset_m + \emptyset_v}$$

This effective matrix approach was used for composites containing synthetic particles and short fibres, not ones containing natural fibres (Fue et al., 2002). It is also unclear to what extent fibre order affects the predicted results or whether the approach is applicable to systems comprised of fibres rather than particulates. Besides, it is unclear how much the limitation of other micromechanical models applied to single fibre-reinforced composites would impact the predicted results of the hybrid composites.

5.2 Semi-empirical Approach to Predict the Tensile Modulus of Hybrid Composites

5.2.1 Modification of micromechanical models to predict the tensile modulus of single fibre-reinforced composites

As mentioned earlier, analytical micromechanical models can predict the stress development in fibre reinforcement composites. However, these models often require detailed information on fibre and matrix interactions, as well as their complex morphologies and properties, during and after

composite fabrication. Assuming that the effect of fibre alignment on the composite modulus is negligible and the moisture content of the natural fibres after composite processing is zero, the volume fraction and tensile modulus of the natural fibres used in the micromechanical models were computed on a cell wall basis.

Since natural fibres such as cellulose microfibres are orthotropic materials, their mechanical properties vary in different directions (longitudinal, radial, and tangential). This study uses the longitudinal tensile properties in the micromechanical models since they are the highest in the longitudinal direction. The fibre grains usually run parallel along their length; however, the fibres may be chopped or separated during the process. In this case, their maximum tensile properties occur at an angle of θ ($0 \leq \theta \leq \pi/2$) from the longitudinal direction of the fibre. A Hankinson-type formula can be used to predict the elastic properties of fibres in such situations, stated as follows (Facca et al., 2006b):

Equation 49

$$E_f = \frac{E_l \, E_p}{E_l \, sin^2\theta + E_p \, cos^2\theta}$$

Where E_l and E_p represent tensile modulus parallel and perpendicular to the grain, respectively.

In this study, it is assumed that the direction of the fibre grains is parallel along the fibre lengths; therefore, the longitudinal tensile modulus can be used in the micromechanical models without any modification.

5.2.1.1 Modification of ROM for single fibre reinforced composites

For this document, it is necessary to conduct individual theoretical analyses of the cellulose microfibre-reinforced composites in order to work in conjunction with the effective matrix approach in the theoretical modelling of hybrid composites. As mentioned earlier, the ROM and IROM equations represent the upper and lower bounds for the tensile properties of the composites, respectively. The modified ROM (Equation 38) was employed in this study for a single fibre system. The best-fit χ_f for a single-fibre system containing cellulose microfibres was calculated by minimizing the residual error between the model and the single-fibre data. In order to maintain consistency with the other micromechanical models that have been adjusted in this study, the modified ROM (Equation 38) has been revised to Equation 50, as demonstrated below:

Equation 50

$$E = \chi_f E_f V_f + E_m V_m$$

A list of modifying components for each micromechanical model given in this study is found in Table 23.

5.2.1.2 Modification of Halpin-Tsai equation for single fibre reinforced composites

As mentioned earlier, the Halpin-Tsai model is a widely utilized micromechanical method for estimating the effective stiffness of unidirectional fibre-reinforced composite materials. While the model has valuable attributes, it remains subject to specific limitations. The Halpin-Tsai model assumes that the matrix and fibres in a composite material have linear elastic behaviour. This assumption may not be valid for composites that incorporate matrix materials with nonlinear or time-dependent properties or for fibres that demonstrate nonlinear behaviour under high stress or strain conditions. The created model is specifically designed for unidirectional fibre composites, characterized by the alignment of fibres in a singular direction. The applicability of the discussed approach may not extend directly to composites featuring complex fibre structures, such as those characterized by woven or randomly aligned fibres. Furthermore, the model fails to account for potential interactions or interfacial phenomena between the composite material's individual fibres. The mechanical behaviour of fibre composites, particularly those that are densely packed or greatly aligned, can be significantly influenced by interactions between the fibres.

The Halpin-Tsai model tends to overestimate the effective stiffness qualities when the fibre volume percentages are high. This is due to the assumption made by the model that a linear correlation exists between the volume fraction and the effective characteristics. However, it is important to note that this assumption may not be valid when the fibre volume percentage reaches or exceeds a specific threshold. Moreover, the model does not explicitly account for the mechanisms involved in stress transfer between the fibres and the matrix. The assumption in this context is that the fibres exhibit perfect bonding with the matrix, disregarding the potential occurrence of fibre-matrix debonding or sliding. It is important to note that such debonding or sliding phenomena might substantially impact the composite material's mechanical properties. Furthermore, it is assumed that the fibres exhibit a notably high aspect ratio, referring to their length-to-diameter proportion.

When the fibres deviate significantly from this assumption, as observed in short fibre or chopped fibre composites, the model's predictions may not align with the empirical data.

Despite these limitations, the Halpin-Tsai model can still provide reasonable estimates of the effective stiffness properties for certain fibre-reinforced composite systems, particularly when the model's assumptions are satisfied and the fibre volume fractions are moderate. However, more sophisticated micromechanical models or experimental characterization techniques may be required for more complex or non-ideal composite configurations. This study presents a semi-empirical modification of the Halpin-Tsai model for predicting potential errors in cellulose microfibre-reinforced composites.

The modified Halpin-Tsai equation for single fibre-reinforced composites is defined in this study as follows:

Equation 51

$$E_c = E_m\left(\frac{1+\xi\eta_{eff}V_f}{1-\eta_{eff}V_f}\right)$$

Equation 52

$$\eta_{eff} = \frac{\left(\frac{\lambda_{f,eff}E_f}{E_m}\right)-1}{\left(\frac{\lambda_{f,eff}E_f}{E_m}\right)+\xi}$$

Where $\lambda_{f,\,eff}$ represents the best-fit modification component for effective fibre modulus, calculated by minimizing the residual error between the model and the single fibre data. Accordingly, η_{eff} is calculated by equation 86 using the corresponding $\lambda_{f,\,eff}$.

5.2.1.3 Modification of Halpin-Tsai equation for randomly fibre distributed single fibre reinforced composites

The refined Halpin-Tsai equations for randomly distributed fibres in single fibre reinforced composites are presented as follows:

Equation 53

$$E_c^{ran} = E_m\left[\lambda_L\left(\frac{1+\xi\eta_L V_f}{1-\eta_L V_f}\right)+\lambda_T\left(\frac{1+2\eta_T V_f}{1-\eta_T V_f}\right)\right]$$

$$\eta_L = \frac{\left(\frac{E_f}{E_m}\right) - 1}{\left(\frac{E_f}{E_m}\right) + \xi}$$

$$\eta_T = \frac{\left(\frac{E_f}{E_m}\right) - 1}{\left(\frac{E_f}{E_m}\right) + 2}$$

When

$$\xi = 2\left(\frac{l}{d}\right)$$

Where η_L and η_T are in longitudinal and transverse directions, respectively, and $\lambda_L$and λ_T are the modifying fitting parameters defined in this study in longitudinal and transverse directions, respectively.

5.2.1.4 Modification to shear-lag equation for single fibre reinforced composites

Despite its simplicity and practicality, the shear-lag model has limitations in estimating stress distribution in unidirectional fibre-reinforced composites. The model assumes that the fibres are uniformly packed and ideally aligned, which is not necessarily the case in composite materials found in real life. Furthermore, the model does not account for the effects of transverse stresses, which may be necessary in certain composite constructions.

The Cox's shear lag hypothesis assumes uniform stress along the fibre length and perfect bonding between the fibre and matrix. However, stress concentrations can occur at fibre ends or due to varied fibre-matrix interactions, and the interface bonding may not be perfect. These assumptions limit the model's ability to accurately represent actual stress transfer behaviour. Furthermore, the theory presupposes that the matrix and fibre will behave linearly elastic. However, nonlinear behaviour is sometimes displayed by composite materials, particularly at high pressures or when the matrix experiences plastic deformation. Under such circumstances, the model might not adequately capture stress transfer behaviour.

The Cox's shear lag hypothesis does not explicitly consider interfacial debonding or sliding between the fibre and matrix. Interfacial debonding and sliding can occur in real-life scenarios for various reasons, including mechanical loading, moisture absorption, and thermal cycling. These events, which are not considered by Cox's shear lag theory, can substantially impact the composite's overall mechanical behaviour and stress transfer.

Additionally, unidirectional fibre composites are the main application for Cox's shear lag hypothesis. For composites with more complex fibre architectures, such as woven or braided composites, where the stress transfer mechanisms can be more complex and difficult to calculate precisely, this might not be immediately relevant. According to Cox's shear lag theory, the fibres' geometry is continuous and uniform down their length. For fibres with differences in diameter, curvature, or other geometric abnormalities, it might not adequately represent stress transfer behaviour. Variations in fibre shape can cause the load distribution to change or create localized stress concentrations that are not accounted for by the theory.

While stress transfer analysis is another area of emphasis for the theory, it does not directly show how composite failure may occur. Failure processes, including matrix cracking, fibre fracture, and delamination, are not taken into consideration. Additional failure analysis methods or models are needed to supplement the stress transfer analysis given by Cox's shear lag theory. When applying Cox's shear lag theory to the stress transfer analysis in fibre-reinforced composites, it is crucial to consider these restrictions and related special assumptions. More sophisticated models or experimental characterization techniques might be required for a more accurate analysis when the restrictions are substantial or the assumptions are not appropriately implemented. The modified shear lag for the prediction of single-fibre reinforced composites is defined in this study as follows:

Equation 54

$$E_c = \chi_f \, V_f \, E_f \left(1 - \frac{\tanh(\eta s)}{\eta s}\right) + V_m E_m$$

Where χ_f represents the modification component for the elastic modulus of the fibre in a single fibre-reinforced system, the best-fit value of χ_f is calculated by minimizing the residual error between the model and experimental data.

5.2.2 Modification of micromechanical models to predict the tensile modulus of hybrid composites

5.2.2.1 HROM modification using the effective matrix approach for hybrid composites

This study proposes a further modification to the HROM equation using the effective matrix approach. The modified HROM equation in this study incorporates cellulose microfibre-reinforced polymer as the effective matrix, with the addition of carbon fibre as a reinforcing agent to the effective matrix. The choice of a cellulose microfibre-reinforced polymer as the effective matrix is attributed to the production of a homogeneous, well-dispersed microfibrillated polymer, with negligible variation in the volume fraction of the natural fibre utilized in this investigation, in contrast to the volume fraction variability of carbon fibres. The modified HROM equation is presented as follows:

Equation 55

$$E_C = \lambda_{m,eff} E_{m,eff} V_{m,eff} + \chi_2 E_{f2} V_{f2}$$

Where $\lambda_{m,\,eff}$, $E_{m,\,eff}$, and $V_{m,\,eff}$ represent the modifying component for the effective matrix, modulus of the effective matrix, and volume fraction of the effective matrix, respectively. Furthermore, χ_2 represents the modifying component for carbon fibre. The least square method is employed to determine the best-fit values for $\lambda_{m,\,eff}$, and χ_2, which serve to minimize the sum of squared errors (as defined in Equation 39) between the HROM and the empirical data.

While the rule of mixture provides a quick estimation of composite properties, it has limitations in capturing complex microstructural interactions, interfacial effects, and stress transfer mechanisms. More advanced micromechanical models or computational methods are often required to accurately predict the properties of composite materials with more complex configurations and behaviour.

5.2.2.2 Halpin-Tsai models modification using the effective matrix approach for hybrid composites

In this study, the modifications for the Halpin-Tsai equation, employing the effective matrix approach, are presented as follows:

Equation 56

$$E_c = E_{m,eff}\left(\frac{1+\xi\eta_{eff}V_f}{1-\eta_{eff}V_f}\right)$$

Equation 57

$$\eta_{eff} = \frac{\left(\frac{\lambda_{f,eff}E_f}{\lambda_{m,eff}E_{m,eff}}\right)-1}{\left(\frac{\lambda_{f,eff}E_f}{\lambda_{m,eff}E_{m,eff}}\right)+\xi}$$

Where $E_{m,\ eff}$ represents the modulus of the effective matrix, and $\lambda_{\ f,\ eff}$ represents the modifying component for fibre modulus. The least square method is employed to determine the best-fit values for $\lambda_{\ f,\ eff}$, which serves to minimize the sum of squared errors (as defined in Equation 39) between the Halpin-Tsai and the empirical data.

5.2.2.3 Halpin-Tsai models modification for random fibre distribution for hybrid composites

The Halpin-Tsai model for randomly distributed fibres was refined for hybrid composites, as follows:

Equation 58

$$E_c^{ran} = \lambda_{m,eff}E_{m,eff}\left[\lambda_L\left(\frac{1+\xi\eta_L V_f}{1-\eta_L V_f}\right)+\lambda_T\left(\frac{1+2\eta_T V_f}{1-\eta_T V_f}\right)\right]$$

$$\eta_L = \frac{\left(\frac{E_f}{E_m}\right)-1}{\left(\frac{E_f}{E_m}\right)+\xi}$$

$$\eta_T = \frac{\left(\frac{E_f}{E_m}\right)-1}{\left(\frac{E_f}{E_m}\right)+2}$$

When

$$\xi = 2\left(\frac{l}{d}\right)$$

Where $E_{m,\ eff}$ represents the modulus of the effective matrix, η_L and η_T are in longitudinal and transverse directions, respectively, and $\lambda_{m,\ eff}$, $\lambda_{L,}$ and λ_T are the modifying components defined in

this study for the effective matrix and fibres orientations in longitudinal and transverse directions, respectively.

5.2.2.4 Shear-lag model using the effective matrix approach for hybrid composites

The modified shear lag theory, applying the effective matrix approach, is presented as follows:

Equation 59

$$E_c = \chi_f V_f E_f \left(1 - \frac{\tanh(\eta s)}{\eta s}\right) + \lambda_{m,eff} V_{m,eff} E_{m,eff}$$

Where χ_f and $\lambda_{m,\,eff}$ represent the modifying components for carbon fibre and effective matrix, respectively, which are calculated using the least square method.

5.3 Results and Discussion

It was unknown which theoretical model would be the most accurate at predicting the outcomes because none of the previous theoretical models had been used to analyze hybrid composites made of natural and synthetic fibres. The experimental moduli of cellulose microfibre-reinforced PA11 were compared to the predicted values in this study, employing some of the most commonly used literature models, including the ROM, IROM, Halpin-Tsai, and Shear lag models. The following graphs compare the expected values from the above semi-empirically modified micromechanical models with the experimental results.

5.3.1 Prediction of Modulus Using Literature Models for Single-Fibre System

5.3.1.1 ROM model

As presented in Figure 39, the empirical data and predicted values from the ROM model follow a similar pattern; however, as expected, the ROM equation overestimates modulus values for cellulose microfibre composites. The ROM equation represents the perfect yet unrealistic fibre reinforcement, in which all the fibres are distributed along the composite longitudinal direction, having a perfect bonding with the matrix for load transferring. This is the main reason for the discrepancies observed between the experimental results and the ROM equation. As noted earlier, while the ROM theory provides a quick approximation of modulus, it has certain limitations. The ROM equation assumes that the properties of the composite material are a linear combination of the properties of its constituent phases. However, in many cases, the interactions between the

phases are not strictly linear. The presence of interfaces or interphases can lead to non-linear behaviour, which is not accurately captured by the rule of mixture.

Besides, it does not consider the influence of microstructural factors, such as the size, shape, and distribution of the phases within the composite. These factors can significantly affect the overall properties of the composite material, especially when the phases have different volume fractions or orientations. Additionally, the equation assumes perfect bonding or no interaction between the phases. However, the presence of interfaces between the phases can have a profound effect on the overall properties of the composite. Interfacial phenomena, such as interfacial bonding, debonding, or sliding, can significantly impact the mechanical behaviour and failure mechanisms of the composite material.

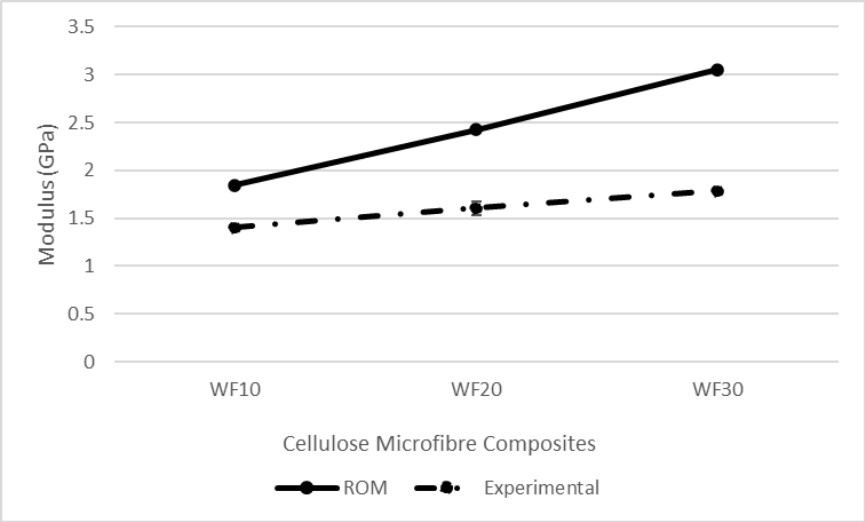

Figure 39 Comparison of Predicted Modulus Using the ROM Model with Experimental Data for the Single-fibre System

It also does not explicitly consider the mechanisms of stress transfer between the phases within the composite. It assumes uniform stress distribution across the phases, neglecting the possibility of stress concentration, local deformation, or load transfer mechanisms. This limitation becomes more critical when the phases have significant differences in stiffness or when the composite undergoes complex loading conditions. Moreover, the equation is less accurate for composites with complex designs, such as fibre-reinforced composites with non-unidirectional or random fibre orientations, woven or braided composites, or composites with hierarchical structures. These complex architectures introduce additional interactions and complexities that the simple linear additive assumption of the rule of mixture cannot adequately capture. Furthermore, the ROM

equation assumes that the composite consists of two distinct phases with known volume fractions. However, when the volume fractions of the phases are close or when multiple phases exist in significant amounts, the accuracy of the rule of mixture decreases. The ROM model tends to be more accurate when there is a substantial difference in volume fractions between the phases.

As mentioned earlier, the ROM model often offers the upper limit values for composite properties. In this study, the modifying component for the ROM equation (χ_f) calculated for a single fibre system is about 0.375 (presented in Table 23), signifying that only about 37.5% of the system follows the ideal bonding and unidirectional fibre orientation (longitudinal direction) in the studied system.

5.3.1.2 IROM model

As shown in Figure 40, the values of the cellulose microfibre-reinforced PA11 were undervalued when employing the IROM equation. As previously stated, the ROM and IROM equations serve to define the upper and lower bounds of the fibre-reinforced composites' properties, respectively. This statement aligns with the empirical data of this study, as the experimental data fall within the range of expected values generated by the two equations. The IROM equations assume a linear relationship between the volume fraction of the constituent phase and the overall properties of the composite. However, this assumption may not be valid for all composite systems, especially when there are non-linear interactions or complex microstructural arrangements. Deviations from linearity can reduce the accuracy of the estimated volume fraction. This study has excluded the IROM equation modification since it displays values that are lower than the experimental values.

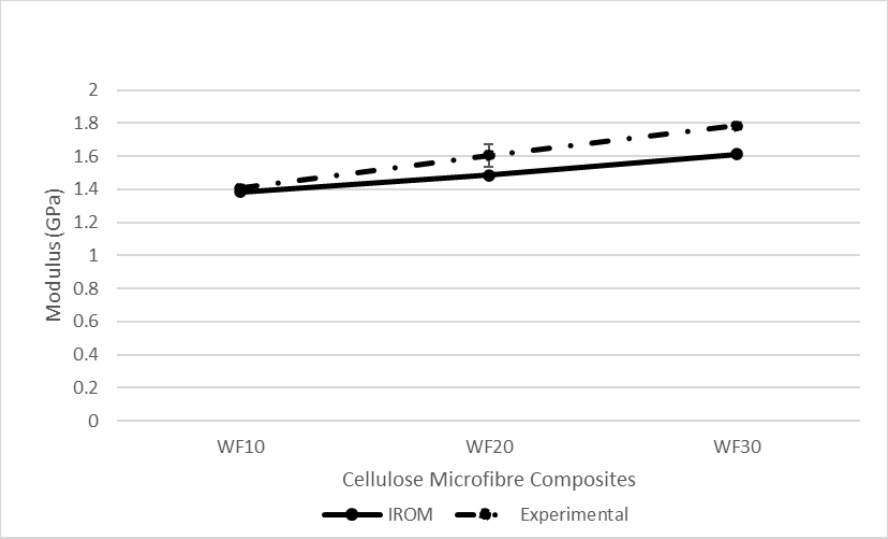

Figure 40 Comparison of Predicted Modulus Using the IROM Model with Experimental Data for the Single-fibre System

5.3.1.3 Halpin-Tsai model

According to the data presented in Figure 41, the predicted values for modulus, as determined by the Halpin-Tsai model, exhibited a higher magnitude compared to the corresponding experimental findings. Nevertheless, as demonstrated in Figure 8, the modified Halpin-Tsai model proposed by Halpin and Kardos (1976) for randomly dispersed fibres (Equation 23) exhibited a better agreement with the experimental data. As presented in Table 23, the best-fit value for modifying components for the Halpin-Tsai model ($\lambda_{f,\,eff}$) is 0.380, implying that only about 38% of the system in the present study aligns with the original Halpin-Tsai equations in single-fibre systems. As previously stated, the Halpin-Tsai equations are widely employed in the field of composite materials to predict the mechanical properties of composite materials. However, predictions derived from the Halpin-Tsai equations rely on a set of assumptions that may not consistently align with real-world circumstances. Their applicability may be limited in cases where these assumptions are not met or when dealing with complex composite structures. Therefore, it is important to consider these limitations and potential deviations from the assumptions when using the Halpin-Tsai equations to predict composite properties.

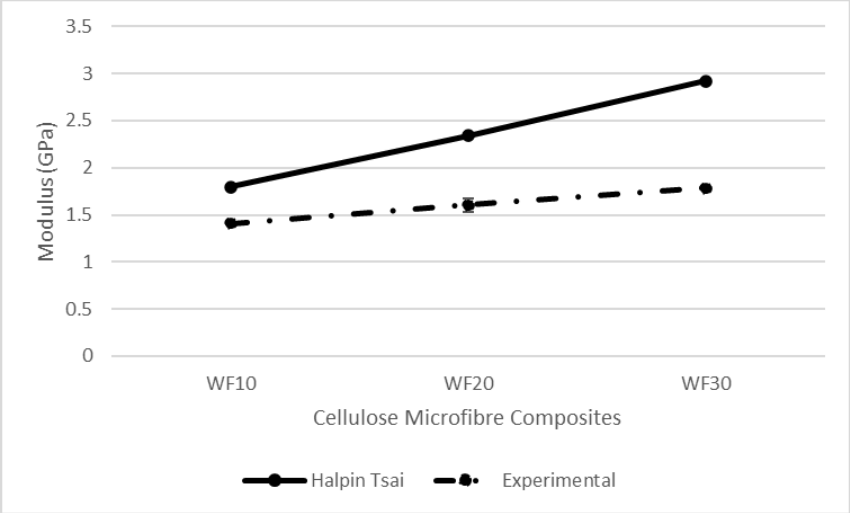

Figure 41 Comparison of predicted modulus using the Halpin-Tsai model with experimental data for the single-fibre system

An underlying assumption within the Halpin-Tsai equation is the homogeneous dispersion of fibres and matrix constituents throughout the composite material. In practice, achieving a state of thoroughly uniform distribution presents challenges, and any deviation from uniformity may have an impact on the accuracy of predictions. Another assumption is the existence of a perfect bonding interaction between the fibres and the matrix. However, it should be noted that the adhesion between the fibres and matrix may not be ideal in real-life situations, as observed in the present study. The imperfections in the fibre-matrix interface bond can arise due to the deterioration of natural fibres during the melt compounding process. The imperfection in the interfacial bonding has the potential to result in stress concentration, hence increasing the likelihood of delamination or debonding. These phenomena can have a substantial impact on the mechanical characteristics of the composite material (Armioun et al., 2016a, 2016b).

Furthermore, it is assumed by the Halpin-Tsai equation that the fibres have a long and slender morphology, free of any curvature. The validity of this assumption may be questionable when considering various types of fibres, particularly those of natural form. For instance, the cellulose microfibre used in this study exhibits natural curvature or an unequal aspect ratio, both of which have the potential to influence the stress distribution within the composite material and thus alter its mechanical response (Armioun et al., 2016a, 2016b).

Moreover, it should be noted that the assumption of a small volume fraction of fibres could not be valid for composites with high fibre volume fractions. In such cases, the interaction between fibres

becomes extensive, leading to deviations in the composite behaviour from the predicted values by the Halpin-Tsai equations. The Halpin-Tsai equation assumes that the material's response follows linear elasticity and that the composite is performing within the linear elastic regime. However, it is essential to note that in real-world circumstances, composites have the potential to exhibit non-linear characteristics and undergo plastic deformation when subjected to specific loading conditions. For example, the equation is primarily intended for aligned fibre composites and may not accurately predict the properties of composites with randomly oriented fibres or other types of reinforcements.

The equations assume a specific configuration and alignment of the fibres, which may not be suitable for composites where the fibres are randomly oriented or have different shapes. Additionally, it is assumed that the composite material exhibits homogeneity, implying that its qualities remain consistent in all directions. However, this assumption is not valid in practical scenarios, particularly when natural fibres are involved. It should be noted that the Halpin-Tsai equation functions under the assumption that the composite material is defect-free and void-free. Nonetheless, the present research (Armioun et al., 2016a, 2016b) has observed the existence of voids at certain levels.

5.3.1.4 Modified Halpin-Tsai Model for Randomly Oriented Fibres

According to the Halpin-Tsai model modified by Halpin and Kardos (1976), about 37.5% of the fibres are oriented in the longitudinal direction (λ_L), whereas 62.5% of the fibres are aligned in the transverse direction (λ_T) of the strain. However, as shown in Table 23, the best-fit values for λ_L and λ_T in the present study were calculated to be 0.420 and 0.559, respectively, which are in close agreement with the original Halpin–Kardos predictions, although not an exact match. It may be inferred from these values that approximately 42% and 56% of the fibres in this study are oriented in the longitudinal and transverse directions of the applied stress, respectively, and the remaining fibres are oriented in directions other than longitudinal and transverse in the single-fibre system.

As illustrated in Figure 42, the Halpin-Tsai model for randomly oriented fibres shows better agreement with the experimental findings of the study, compared to the classical Halpin-Tsai model. When utilizing the Halpin-Tsai equations for property prediction, it is essential to thoroughly acknowledge and consider the associated limitations. In some cases, it may be essential

to explore other models or modify the equations to achieve more accurate predictions of composite properties.

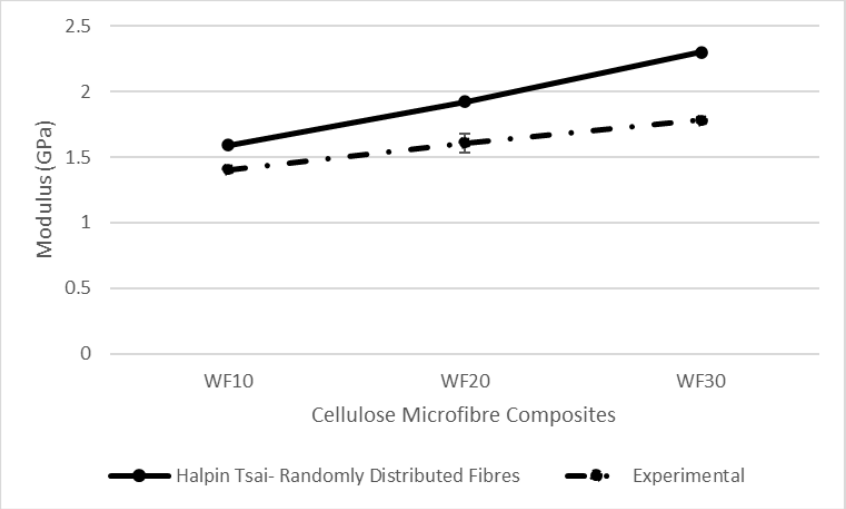

Figure 42 Comparison of Predicted Modulus Using the Halpin-Tsai Model for Randomly Oriented Fibres with Experimental Data for the Single-fibre System

As mentioned earlier, empirical models such as Halpin-Tsai do not consider the interactions between fibres. Therefore, analytical models were employed to better understand the effects of fibre interactions on the composites' stiffness.

5.3.1.5 Shear-lag model

As illustrated in Figure 43, the shear lag theory predicted that tensile modulus values are greater than the experimental values. The modifying component for the shear-lag theory (χ_f) was 0.414 (Table 23), which signifies that about 41% of the fibres in the single fibre system of the current work align with the Shear-lag theory's assumptions. The discrepancies observed between the experimental data and predicted values derived by the shear-lag theory can be acknowledged by two fundamental assumptions made by the model: Initially, it is assumed that the main role of the fibre in a composite material in a single fibre system is to predominantly sustain axial loading, hence serving as the primary carrier of tensile loads. Additionally, it assumes that the matrix is primarily responsible for transmitting shear loading. Nevertheless, it is worth noting that in certain situations, the shear-lag theory might undervalue the stiffness of composites containing short fibres. Several studies have shown that the primary shortcoming of the Shear-lag theory is its

failure to consider the stresses at the ends of the fibres, which may result in miscalculating the predictions (Facca et al., 2007; Liu et al., 2014; Azeko et al., 2023; Hou & Panesar, 2023).

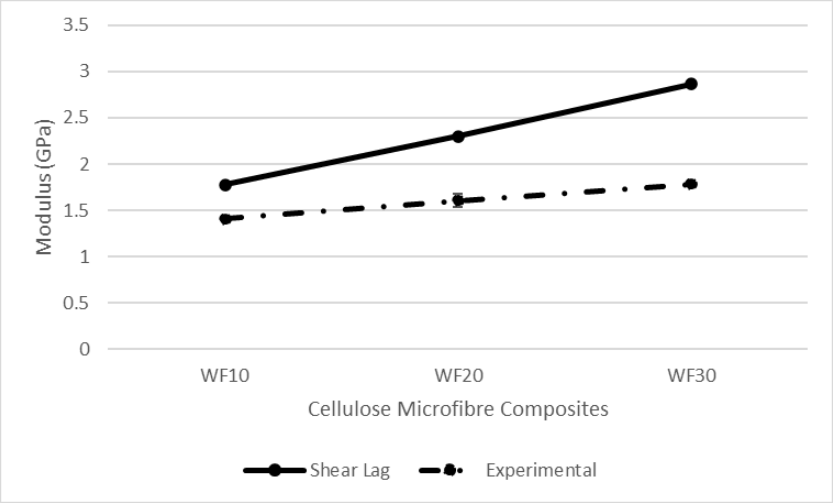

Figure 43 Comparison of Predicted Modulus Using the Shear-Lag Model with Experimental Data for the Single-Fibre System

Among the previously mentioned models, the modified Halpin-Tsai model developed by Halpin and Kardos (1976) for randomly oriented fibres demonstrated the most favourable correspondence with the empirical data for single-fibre-reinforced composites. It is noteworthy to mention that the theoretical models discussed here were initially developed and applied to composites reinforced with synthetic fibres. The inherent features of natural fibres, in contrast to synthetic fibres, including increased susceptibility to environmental conditions, reduced chemical resistance, and decreased stiffness, can have a considerable impact on the degree of consistency observed in composite models.

5.3.2 Comparison of the predicted modulus using modified models with experimental data for a single-fibre system

The experimental data were compared to the predicted modulus values using the modified models, employing the modifying components presented in Table 23 for single-fibre systems as follows:

5.3.2.1 Modified ROM

Figure 44 represents the comparison between the experimental modulus of the cellulose microfibre composites and the predicted modulus using the modified ROM equation in this study. The experimental and predicted modulus exhibits perfect alignment.

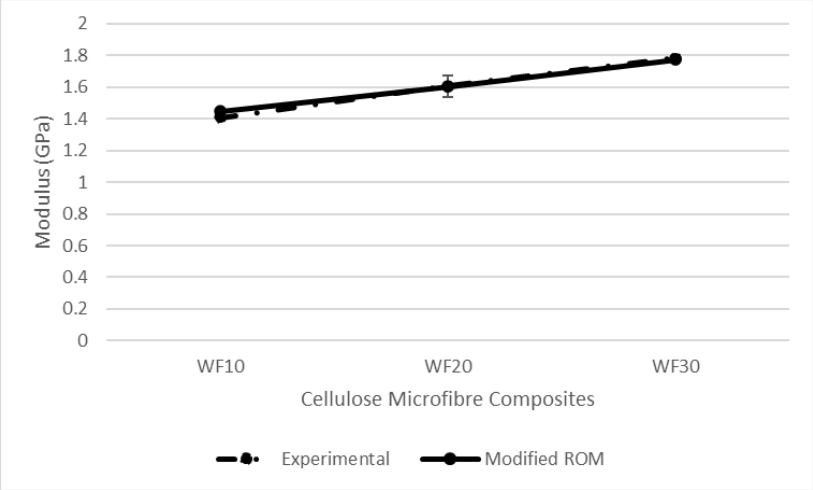

Figure 44 Comparison of Modified ROM with Experimental Data for the Single-fibre System

5.3.2.2 Modified Halpin-Tsai

Figure 45 represents the comparison between moduli from experimental analysis and the predicted moduli with the modified Halpin-Tsai model in this study. The predicted moduli are in good agreement with the experimental moduli.

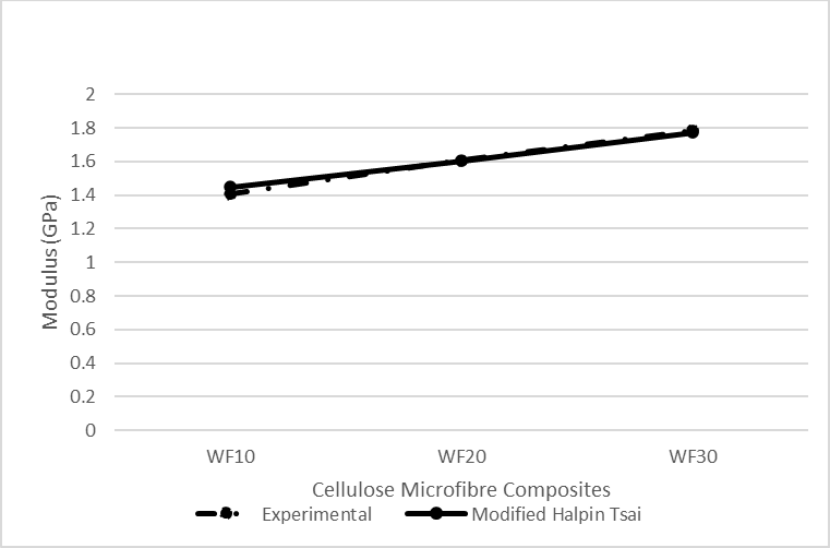

Figure 45 Comparison of Modified Halpin-Tsai with Experimental Data for the Single-fibre System

5.3.2.3 Halpin-Tsai for Randomly Oriented Fibres

Figure 46 exhibits the comparison between experimental moduli of the cellulose microfibre composites and the predicted moduli using the modified Halpin-Tsai model for randomly oriented fibres. The experimental and predicted modulus show perfect alignment.

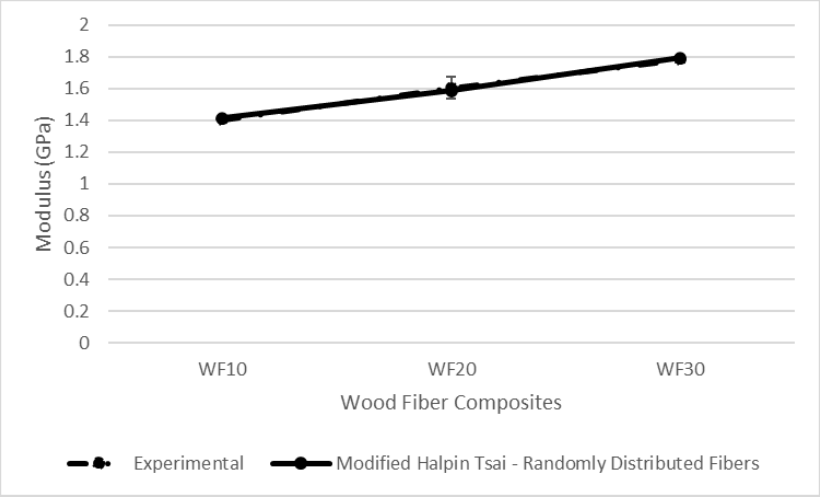

Figure 46 Comparison of Halpin-Tsai for Randomly Oriented Fibres with Experimental Data for The Single-fibre System

5.3.2.4 Modified Shear Lag

Figure 47 represents the comparison between moduli from experimental analysis and the predicted moduli with the modified Shear-lag model in this study. The predicted moduli are in good agreement with the experimental moduli.

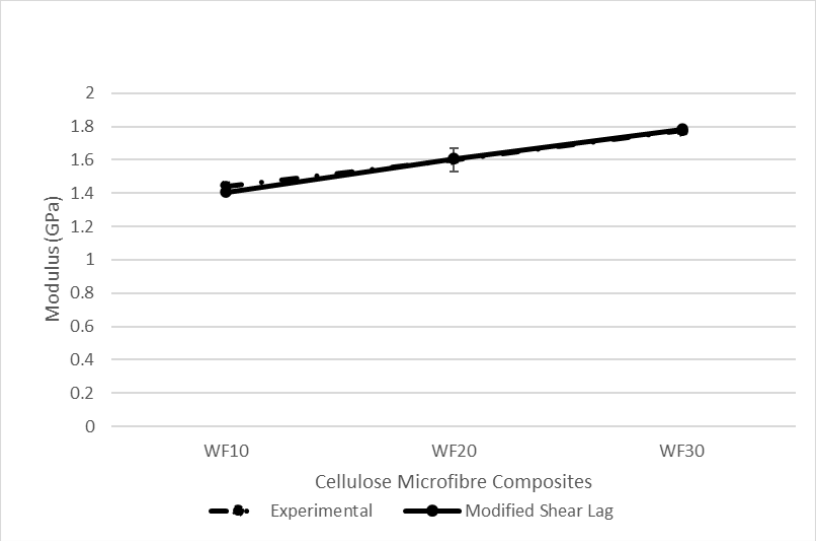

Figure 47 Comparison of the Modified Shear Lag Model with Experimental Data for The Single-Fibre System

Table 23 presents the evaluated best-fit values of the modifying components for multiple micromechanical models of single-fibre systems. The figures above demonstrate that utilizing the best-fit values of the modifying components listed in Table 23 can produce an excellent prediction of the experimental modulus for the single-fibre system for various volume fractions.

Table 23 The Best-Fit Values for Modification Components for The Single-fibre System

Modified Models	Modification component	Best-fit values
ROM	χ_f	0.375
Halpin-Tsai	$\lambda_{f,eff}$	0.380
Halpin-Tsai-Randomly distributed fibres	λ_L	0.420
	λ_T	0.559
Shear-lag	χ_f	0.414

5.3.3 Predicted modulus using literature models for the hybrid system

The moduli of the hybrid composites were first calculated using some of the available micromechanical models in the literature. The evaluated moduli were presented and compared with the experimental results in the graphs below. In this study, the effective matrix approach has been employed to predict the moduli of hybrid composites, utilizing Halpin-Tsai and Shear-lag

models for single-fibre systems. The calculation of the modifying component for the effective matrix approach for those micromechanical models can be performed using the formulae previously presented for single-fibre systems.

5.3.3.1 HROM Model

Figure 48 illustrates the comparison between the predicted moduli using the HROM model (Equation 29) and the experimental data for the hybrid system. Although the experimental and predicted moduli by the HROM equation exhibit a similar pattern, a growing discrepancy between the two is observed as the volume fraction of synthetic fibre increases. It is crucial to consider the HROM method's presumptions and restrictions.

As described earlier, the additivity rule, which assumes that a composite material's qualities are linearly dependent on the volume or percentage of its constituent parts, is one of the underlying presumptions of the hybrid rule of mixture. Moreover, the HROM method assumes that there is no interaction between the components of the composite material or the two systems, which can result in imprecise predictions. The introduced modifying components in Equation 50 for carbon fibre (χ_2) and the effective matrix ($\lambda_{m,\ eff}$) are calculated as 0.177 and 0.727, respectively, as presented in Table 24. Additionally, the accuracy of predictions made using the HROM may vary depending on the specific properties being estimated and the complexity of the composite material structure.

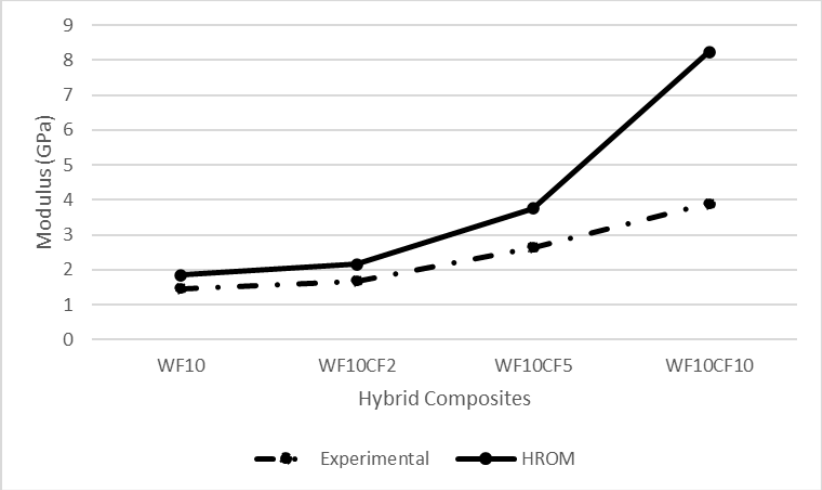

Figure 48 Comparison of Predicted Modulus Using the HROM Model with Experimental Data for the Hybrid System

5.3.3.2 Halpin-Tsai Model Using Effective Matrix Approach

Figure 49 shows the predicted moduli for the hybrid system by the Halpin-Tsai equation using the effective matrix approach. The predicted values and experimental results follow similar patterns. However, the differences between the values increase as the volume fraction of the synthetic fibres increases. Among the limitations highlighted earlier for Halpin-Tsai models, another underlying reason for the deviations of predicted values from empirical data may be attributed to the use of the effective matrix approach, which introduces an additional source of inaccuracy to the equation. The introduced modifying components in Equation 56 and Equation 57 for fibre ($\lambda_{f,\,eff}$) and the effective matrix ($\lambda_{m,\,eff}$) are evaluated at 1.101 and 5.078, respectively.

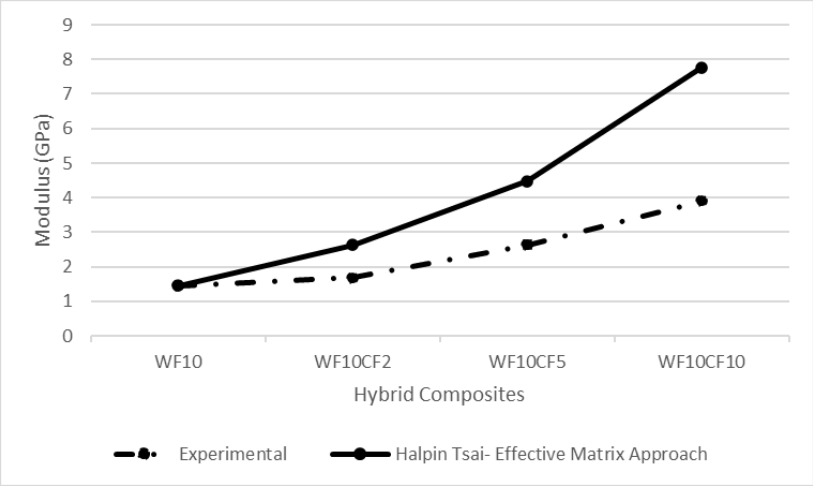

Figure 49 Comparison of Predicted Modulus Using the Halpin-Tsai Model with Experimental Data for The Hybrid System Using the Effective Matrix Approach

5.3.3.3 Halpin-Tsai Model for Hybrid Composites

Figure 50 illustrates the comparison between the empirical data and the predicted moduli for hybrid composites, employing Equation 41 as proposed by Banerjee and Sankar (2014). The Halpin-Tsai equation demonstrates a strong correlation with the empirical data obtained in the present study, particularly when considering the augmentation in the volume fraction of the secondary fibre. In this study, the curve fitting parameter (ξ) was computed to be 25.00.

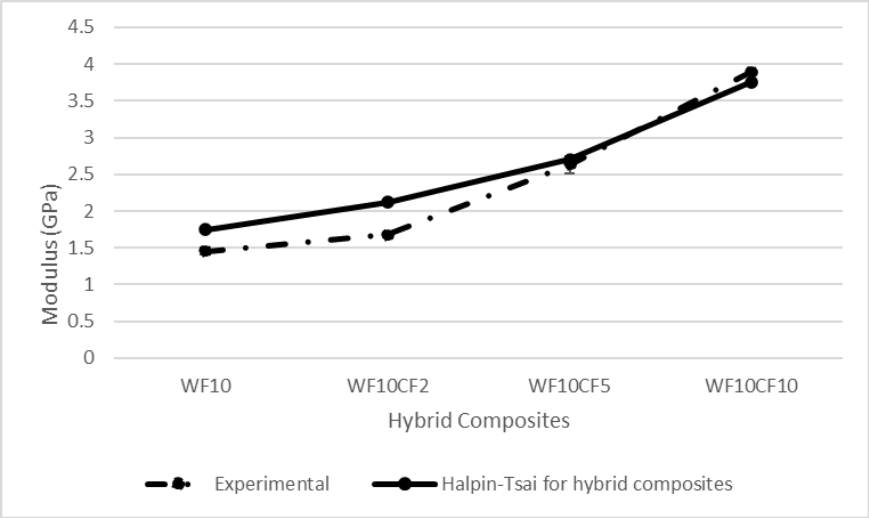

Figure 50 Comparison of Experimental Data with Halpin-Tsai for Hybrid Composites

5.3.3.4 Halpin-Tsai Model for Random Fibre Orientation

Figure 51 illustrates the comparison of the predicted moduli obtained from the use of the Halpin-Tsai model for a randomly dispersed fibre (Equation 23), utilizing the effective matrix approach. The figure demonstrates a strong correlation between the predicted values obtained by the effective matrix approach in the Halpin-Tsai equation for random fibre distribution in the composites and the experimental data collected in this study. According to the Halpin-Tsai model modified by Halpin and Kardos (1976), about 37.5% of the fibres are oriented in the longitudinal direction (λ_L), whereas 62.5% of the fibres are aligned in the transverse direction (λ_T) of the strain. Nonetheless, the study's best-fit values for λ_L and λ_T were determined to be 48.1% and 73.6%, respectively.

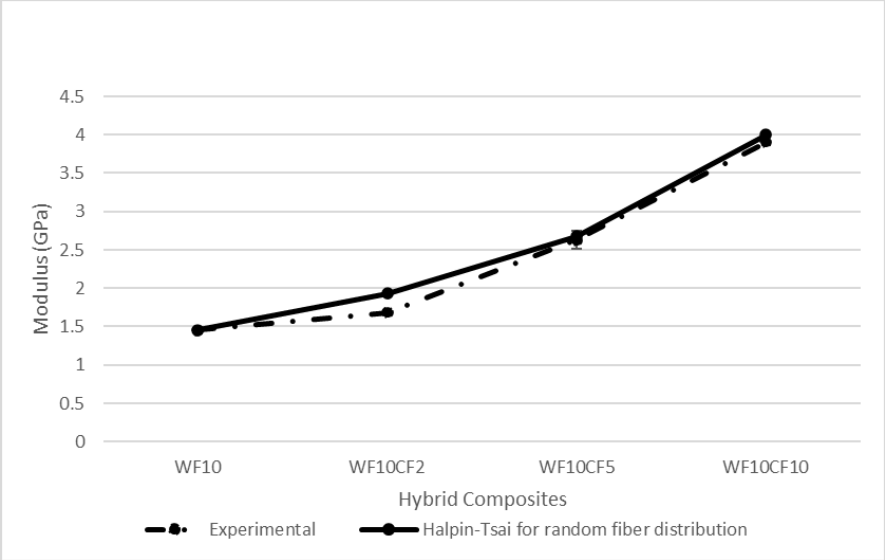

Figure 51 Comparison of Experimental Data with Halpin-Tsai for Randomly Distributed Fibres, Using the Effective Matrix Approach for Hybrid Systems

5.3.3.5 Shear-Lag Model

Figure 52 illustrates the comparison of the predicted moduli obtained by the shear-lag model (Equation 27) using the effective matrix approach. The figure illustrates that the predicted values obtained by the shear-lag theory, employing the effective matrix approach, exhibit comparable patterns to the experimental data reported in the study. The modifying components computed for the fibre (χ_f) and the effective matrix ($\lambda_{m,\,eff}$) for the shear-lag theory were 0.243 and 0.947, respectively.

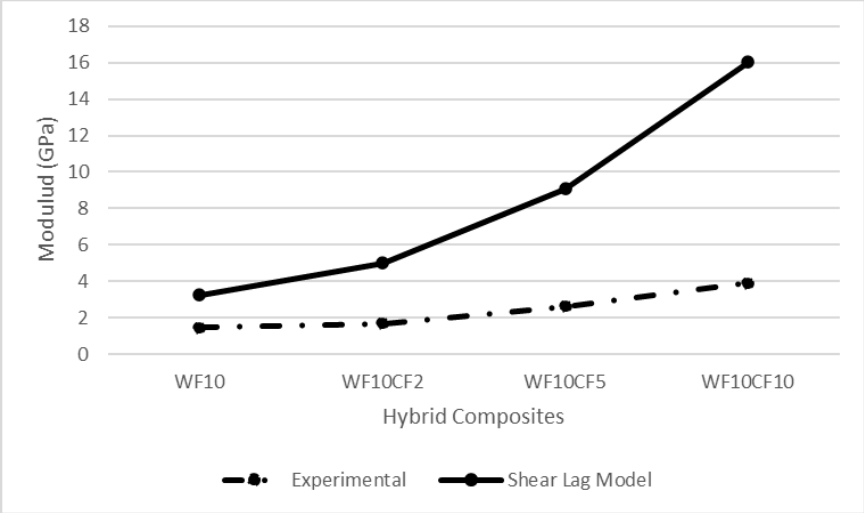

Figure 52 Comparison of Experimental Data with the Shear-Lag Model, Using the Effective Matrix Approach for the Hybrid System

As depicted in the figures above, the experimental data exhibit a comparable trend to the hybrid composite models documented in the existing literature. However, as expected, the values predicted by the models were greater than the observed experimental values. In this study, various literature models were employed to analyze hybrid composites. However, it was shown that the Halpin-Tsai model for randomly dispersed short fibres, using the effective matrix approach, exhibited the most accurate alignment with the experimental results.

The best-fit values for modification components in various micromechanical models were computed using the least-squares method, as was done for single-fibre-reinforced composites. Table 24 shows the best-fit values for modification components for hybrid composites for various models.

Table 24 The Best-Fit Values for Modification Components for Hybrid Composites

Modified Models	Modification component	Best-fit values
HROM	x_2	0.177
	$\lambda_{m,eff}$	0.727
Halpin-Tsai	$\lambda_{f,eff}$	1.101
	$\lambda_{m,eff}$	5.078

Halpin-Tsai for Hybrid composites	ξ	25.00
Halpin-Tsai-Randomly distributed fibres	$\lambda_{m,eff}$	0.773
	λ_L	0.481
	λ_T	0.736
Shear Lag	χ_f	0.243
	$\lambda_{m,eff}$	0.947

Note: λ_L and λ_T are components introduced in the Halpin-Tsai model for randomly distributed fibres, and their best-fit values for the present study are reported in this table.

5.3.4 Comparison of the predicted moduli using the proposed semi-empirically calibrated models for the Hybrid system with the experimental data

The modified micromechanical models developed in this study for hybrid composites have been demonstrated and compared with the experimental data as follows:

5.3.4.1 Semi-Empirically Modified HROM Model

Figure 53 exhibit the comparison between the modulus values predicted using the modified HROM model and the experimental results for the hybrid composites of this study. The predicted values are in great accordance with the experimental findings of the study.

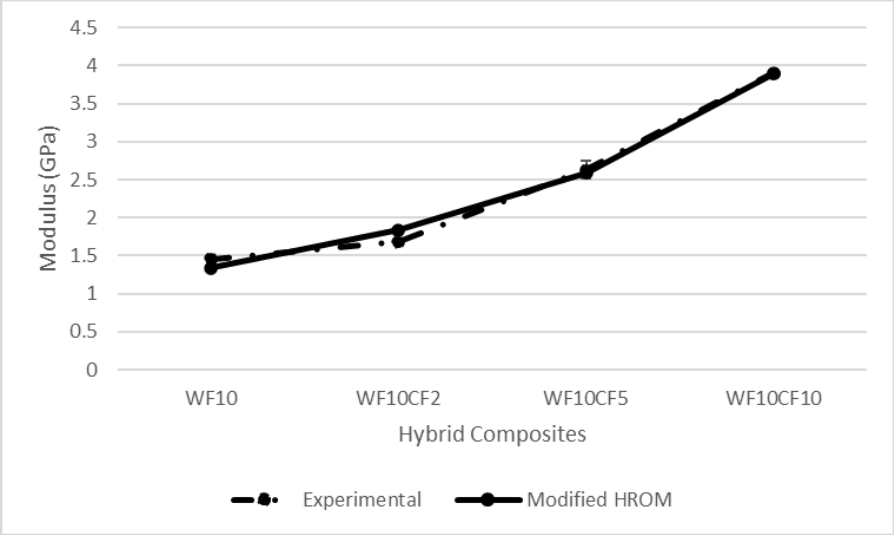

Figure 53 Comparison of the Proposed Modified HROM Model with the Experimental Data

5.3.4.2 Semi-Empirically Modified Halpin-Tsai Models

As shown in Figure 54, the predicted moduli using modified Halpin-Tsai models have been illustrated and compared with the experimental findings of this study. All the predicted values were consistent with the experimental findings for hybrid systems.

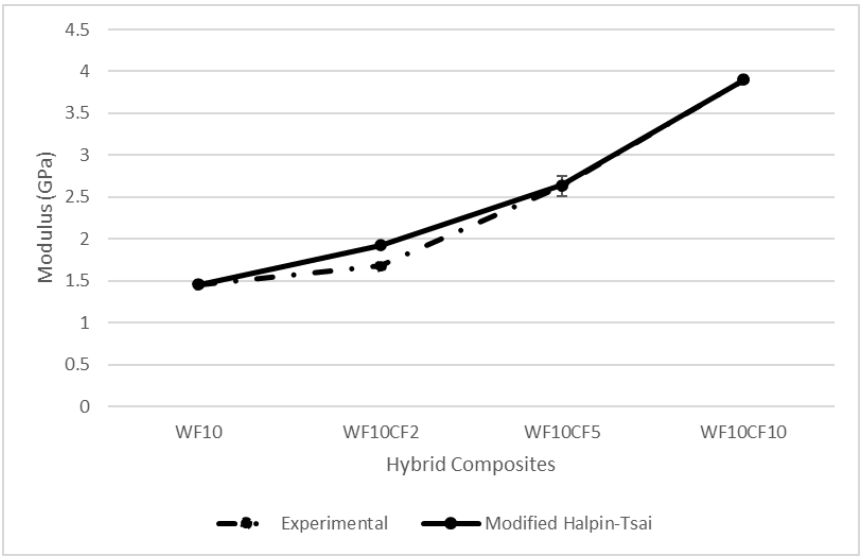

Figure 54 Comparison of the Proposed Modified Halpin-Tsai Model with the Experimental Data

5.3.4.3 Modified Halpin-Tsai Model for Random Fibre Orientation

Figure 55 illustrates the comparison of the modified Halpin-Tsai for randomly oriented fibres with the experimental data. The predicted values are in perfect accordance with the experimental findings of the study for the hybrid system.

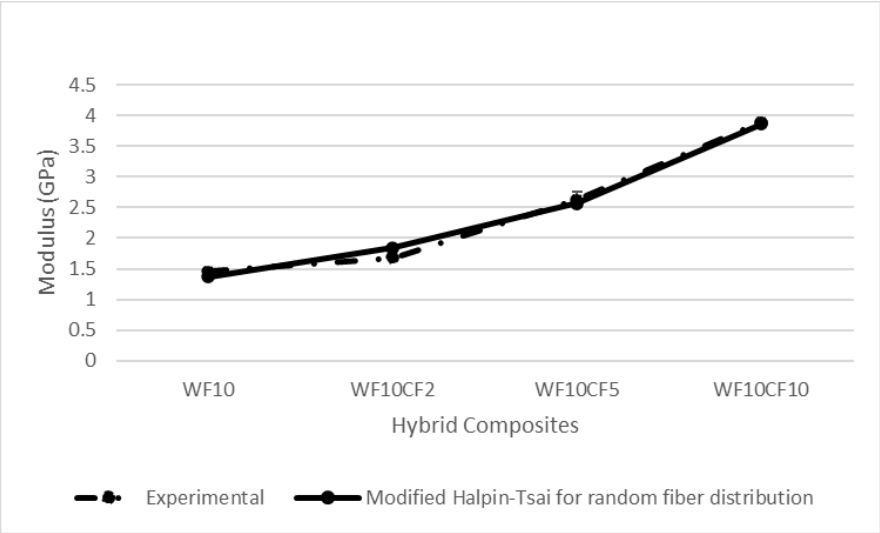

Figure 55 Comparison of the Proposed Semi-empirically Modified Halpin-Tsai for Randomly Oriented Fibres with the Experimental Data

5.3.4.4 Semi-Empirically Calibrated Shear-Lag Model

As illustrated in Figure 56, a good agreement is found between the experimental moduli and those predicted by the modified Shear-lag models of the present study.

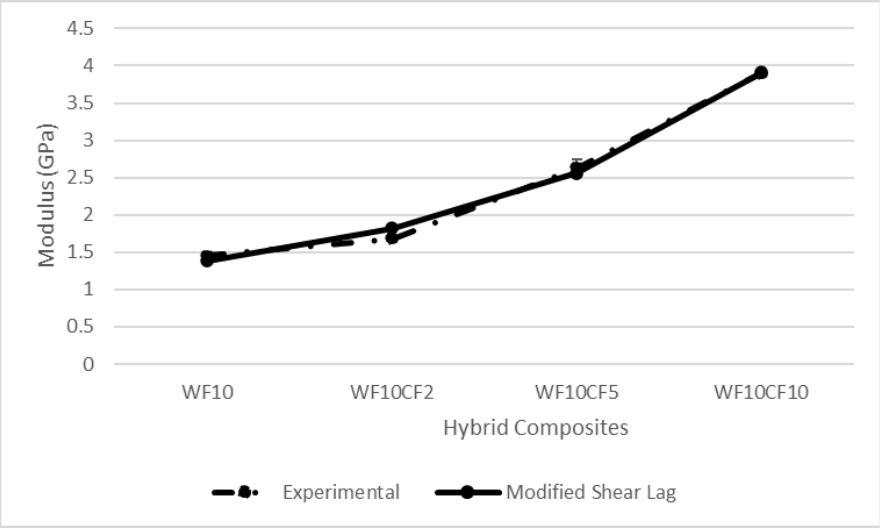

Figure 56 Comparison of the Proposed Semi-empirically Modified Shear-Lag Model with the Experimental Data

The assumption of perfect fibre-matrix interfacial bonding, which would lead many micromechanical models to overestimate the tensile modulus of the composites, is an essential source of inconsistencies between experimental findings and model predictions. On the other hand, in hybrid composites, including hydrophilic natural fibres and hydrophobic polymer matrices along with synthetic fibres, poor adhesion and the subsequent slip at the interface can be a common issue, which lowers the average stress transferred to the fibres. A coupling agent that enhances chemical compatibility at the fibre-matrix interface can be applied to overcome poor adhesion (Armioun et al., 2016a, 2016b). As commonly employed in most micromechanical models, the assumption of ideal adhesion between the fibre and matrix at their interface is only valid for simulating the modulus at extremely low stresses.

Considering the micromechanical models outlined in this investigation, it is evident that the stiffness of hybrid composites has the potential to be enhanced through several means. These include augmenting the volume fraction of fibres with greater modulus within the composite (i.e., carbon fibres in this study). Additionally, utilizing fibres with greater moduli and aspect ratios and subjecting natural fibres to a drying process prior to composite fabrication can effectively strengthen their stiffness. The fibre-matrix adhesion plays a crucial role in conveying the load from the matrix to the fibres within the composites, and enhancing the adhesion between the phases can significantly improve the overall stiffness of the hybrid composites.

While incorporating additional variables, such as the angle and distribution of fibres, into the micromechanical model has the potential to improve the accuracy of the model's predictions, this study assumes that the fibres exhibit steady alignment and have a constant length and aspect ratio. In practical application, the alignment demonstrates an acceptable level of accuracy. However, it is important to note a notable variation in length and aspect ratio throughout the processing phase. The methodology employed in this work involves using upfront micromechanical models to provide a rationale for the observed experimental patterns while avoiding unnecessary complexity.

5.4 Conclusion

Hybrid composites of PA11, reinforced with natural and carbon fibres, present a novel pathway towards sustainable and lightweight structural component materials. The experimental findings of this study were in close agreement with several micromechanical models documented in the literature, such as the Halpin-Tsai model for randomly distributed short fibres and the Halpin-Tsai model for hybrid composites.

Furthermore, certain existing micromechanical models for single fibre-reinforced composites (ROM, Halpin-Tsai, Halpin-Tsai for randomly dispersed fibres, and shear-lag theory) alongside hybrid composites (HROM, Halpin-Tsai, Halpin-Tsai for randomly dispersed fibres, Halpin-Tsai for hybrid composites, and shear-lag theory) have been effectively modified to properly correspond with the experimental findings of the study. The predicted moduli using modified micromechanical models have been compared with the experimental findings of this study. All the predicted values were consistent with the experimental findings for both single-fibre and hybrid systems. The modifying components introduced to the equations involve numerous factors, such as imperfections in fibre alignment, inadequate interactions between fibres and the matrix, fibre breakage that occurs during the processing and manufacture of the composites, degradation of natural fibres during their processing, and moisture absorption in natural fibre-reinforced composites, etc.

5.5 References

Aranguren, M. I., & Mosiewicki, M. A. (2018). A review on the use of natural fibres in composites. *Polymer Reviews, 58*(1), 1–33. https://doi.org/10.1080/15583724.2017.1336980

Armioun, S., Panthapulakkal, S., Scheel, J., Tjong, J., & Sain, M. (2016a). Biopolyamide hybrid composites for high performance applications. *Journal of Applied Polymer Science, 133*(27), 43595. https://doi.org/10.1002/app.43595

Armioun, S., Panthapulakkal, S., Scheel, J., Tjong, J., & Sain, M. (2016b). Sustainable and lightweight biopolyamide hybrid composites for greener auto parts. *Canadian Journal of Chemical Engineering, 94*(11), 2052–2060. https://doi.org/10.1002/cjce.22609

Armioun, S., Pervaiz, M., & Sain, M. (2017). Biopolyamides and high-performance natural fibre-reinforced biocomposites. In V. K. Thakur & M. K. Thakur (Eds.), *Handbook of composites from renewable materials* (pp. 253–270). Wiley. https://doi.org/10.1002/9781119441632.ch49

Azeko, S. T., Mensah, J. K., Arthur, E. K., Abiwu, N., Flomo, M. K., Boadu, J. A., Yamba, P., Larson, E. A., Akayeti, A., Satankar, R. K., & Annan, E. (2023). Eco-friendly green composites reinforced with recycled polyethylene for engineering applications. *Journal of Material Cycles and Waste Management, 25*, 2431–2441. https://doi.org/10.1007/s10163-023-01701-z

Banerjee, S., & Sankar, B. V. (2014). Mechanical properties of hybrid composites using finite element method based micromechanics. *Composites Part B: Engineering, 58*, 318–327. https://doi.org/10.1016/j.compositesb.2013.10.065

Cox, H. L. (1952). The elasticity and strength of paper and other fibrous materials. *British Journal of Applied Physics, 3*(3), 72–79. https://doi.org/10.1088/0508-3443/3/3/302

De Almeida, S. F. M., & Neto, Z. d. S. N. (1994). Effect of void content on the strength of composite laminates. *Composite Structures, 28*(2), 139–148. https://doi.org/10.1016/0263-8223(94)90044-2

Eshelby, J. D. (1957). The determination of the elastic field of an ellipsoidal inclusion and related problems. *Proceedings of the Royal Society of London. Series A: Mathematical and Physical Sciences, 241*(1226), 376–396. https://doi.org/10.1098/rspa.1957.0133

Eshelby, J. D. (1961). Elastic inclusions and inhomogeneities. In J. Sneddon & R. Hill (Eds.), *Progress in solid mechanics* (Vol. 2, pp. 89–140). North-Holland Publishing.

Facca, A. G., Kortschot, M. T., & Yan, N. (2006a). Predicting the elastic modulus of hybrid fibre reinforced thermoplastics. *Polymers and Polymer Composites, 14*(3), 239–250. https://doi.org/10.1177/096739110601400308

Facca, A. G., Kortschot, M. T., & Yan, N. (2006b). Predicting the elastic modulus of natural fibre reinforced thermoplastics. *Composites Part A: Applied Science and Manufacturing, 37*(10), 1660–1671. https://doi.org/10.1016/j.compositesa.2005.10.006

Facca, A. G., Kortschot, M. T., & Yan, N. (2007). Predicting the tensile strength of natural fibre reinforced thermoplastics. *Composites Science and Technology, 67*(11–12), 2454–2466. https://doi.org/10.1016/j.compscitech.2006.12.015

Forest Products Laboratory. (1999). *Wood handbook: Wood as an engineering material*. U.S. Department of Agriculture, Forest Service, Forest Products Laboratory.

Fu, S. Y., & Lauke, B. (1998). Characterization of tensile behaviour of hybrid short glass fibre/calcite particle/ABS composites. *Composites Part A: Applied Science and Manufacturing, 29*(5–6), 575–583. https://doi.org/10.1016/S1359-835X(97)00143-7

Fu, S. Y., Lauke, B., Mäder, E., Hu, X., Yue, C. Y., & Mai, Y. W. (2001). Hybrid effects on the tensile properties of hybrid short glass fibre and short carbon fibre reinforced polypropylene composites. *Journal of Materials Science, 36*(5), 1243–1251. https://doi.org/10.1023/A:1004817505886

Fu, S. Y., Xu, G. S., & Mai, Y. W. (2002). On the elastic modulus of hybrid particle/short fibre/polymer composites. *Composites Part B: Engineering, 33*(4), 291–299. https://doi.org/10.1016/S1359-8368(02)00018-8

Guedes, J. M., & Kikuchi, N. (1990). Preprocessing and postprocessing for materials based on the homogenization method with adaptive finite element methods. *Computer Methods in Applied Mechanics and Engineering, 83*(2), 143–198. https://doi.org/10.1016/0045-7825(90)90148-F

Halpin, J. C., & Kardos, J. L. (1976). The Halpin–Tsai equations: A review. *Polymer Engineering and Science, 16*(5), 344–352. https://doi.org/10.1002/pen.760160512

Halpin, J. C., & Tsai, S. W. (1969). Effects of environmental factors on composite materials. *AFML-TR*, 67–423.

Hewitt, R. L., & Malherbe, M. C. (1970). An approximation for the longitudinal shear modulus of continuous fibre composites. *Journal of Composite Materials, 4*(2), 280–282. https://doi.org/10.1177/002199837000400210

Hill, R. (1963). Elastic properties of reinforced solids: Some theoretical principles. *Journal of the Mechanics and Physics of Solids, 11*(5), 357–372. https://doi.org/10.1016/0022-5096(63)90036-X

Hou, Y., & Panesar, A. (2023). Effect of manufacture-induced interfaces on the tensile properties of 3D printed polyamide and short carbon fibre-reinforced polyamide composites. *Polymers, 15*(3), 773. https://doi.org/10.3390/polym15030773

Ingber, M. S., & Papathanasiou, T. D. (1997). A parallel-supercomputing investigation of the stiffness of aligned, short-fibre reinforced composites using the boundary element method. *International Journal for Numerical Methods in Engineering, 40*(18), 3477–3491. https://doi.org/10.1002/(SICI)1097-0207(19970930)40:18<3477::AID-NME202>3.0.CO;2-P

Jayaraman, K., & Kortschot, M. T. (1996). Correction to the Fukuda–Kawata Young's modulus theory and the Fukuda–Chou strength theory for short-fibre reinforced composite materials. *Journal of Materials Science, 31*(8), 2059–2064. https://doi.org/10.1007/BF00352862

Jones, R. M. (1975). *Mechanics of composite materials*. McGraw-Hill.

Kc, B., Faruk, O., Agnelli, J. A. M., Leao, A. L., Tjong, J., & Sain, M. (2016). Sisal–glass fibre hybrid biocomposite: Optimization of injection moulding parameters using Taguchi method for reducing shrinkage. *Composites Part A: Applied Science and Manufacturing, 83*, 152–159. https://doi.org/10.1016/j.compositesa.2015.05.030

Kc, B., Panthapulakkal, S., Kronka, A., Agnelli, J. A. M., Tjong, J., & Sain, M. (2015). Hybrid biocomposites with enhanced thermal and mechanical properties for structural applications. *Journal of Applied Polymer Science, 132*(39), 42565. https://doi.org/10.1002/app.42565

Kc, B., Tjong, J., Jaffer, S. A., & Sain, M. (2018). Thermal and dimensional stability of injection-molded sisal–glass fibre hybrid PP biocomposites. *Journal of Polymers and the Environment, 26*(3), 1279–1289. https://doi.org/10.1007/s10924-017-1044-5

Krenchel, H. (1964). *Fibre reinforcement*. Akademisk Forlag.

Lewis, T. B., & Nielsen, L. E. (1970). Dynamic mechanical properties of particulate-filled composites. *Journal of Applied Polymer Science, 14*(6), 1449–1471. https://doi.org/10.1002/app.1970.070140604

Li, T. Q., & Wolcott, M. P. (2005). Rheology of wood–plastics melt. Part 1: Capillary rheometry of HDPE filled with maple. *Polymer Engineering and Science, 45*(4), 549–559. https://doi.org/10.1002/pen.20294

Liu, C., Wang, X., & Wang, Y. (2014). Analysis on the process of stress transferring in single fibre composite and Monte Carlo simulation on the process of single-fibre fragmentation. *Journal of Reinforced Plastics and Composites, 33*(12), 1105–1119. https://doi.org/10.1177/0731684414525675

Liu, X., Zhang, Q., Lu, C., & Chung, D. D. L. (2017). Electrical and thermal conduction in carbon fibre reinforced polyamide-11. *Composites Part A: Applied Science and Manufacturing, 95*, 229–238. https://doi.org/10.1016/j.compositesa.2017.01.016

Loos, M. (2015). Fundamentals of polymer matrix composites containing CNTs. In M. Loos (Ed.), *Carbon nanotube reinforced composites* (pp. 125–170). William Andrew Publishing. https://doi.org/10.1016/B978-1-4557-3195-4.00005-9

Magniez, K., Iftikhar, R., & Fox, B. L. (2014). Properties of bio-based polymer nylon 11 reinforced with short carbon fibre composites. *Polymer Composites, 35*(10), 1966–1974. https://doi.org/10.1002/pc.22876

Mori, T., & Tanaka, K. (1973). Average stress in matrix and average elastic energy of materials with misfitting inclusions. *Acta Metallurgica, 21*(5), 571–574. https://doi.org/10.1016/0001-6160(73)90064-3

Oliver-Ortega, H. (2019). Research on the use of lignocellulosic fibres reinforced bio-polyamide 11 with composites for automotive parts: Car door handle case study. *Journal of Cleaner Production, 226*, 64–73. https://doi.org/10.1016/j.jclepro.2019.03.301

Panthapulakkal, S., Raghunanan, L., Sain, M., Kc, B., & Tjong, J. (2017). Natural fibre and hybrid fibre thermoplastic composites: Advancements in lightweighting applications. In C. Baillie, R. Subramanian, & L. V. D. Ven (Eds.), *Green composites: Waste and nature-based materials for a sustainable future* (2nd ed., pp. 39–72). CRC Press.

Rowell, R. M., Sanadi, A. R., Caulfield, D. F., & Jacobson, R. E. (1997). Utilization of natural fibres in plastic composites: Problems and opportunities. In *Lignocellulosic–plastics composites* (pp. 1–51). U.S. Department of Agriculture, Forest Service.

Sun, C. T., & Chen, J. L. (1989). A simple flow rule for characterizing nonlinear behaviour of fibre composites. *Journal of Composite Materials, 23*(11), 1009–1020. https://doi.org/10.1177/002199838902301105

Thomason, J. L., & Vlug, M. A. (1996). Influence of fibre length and concentration on the properties of glass fibre reinforced polypropylene: 1. Tensile and flexural modulus. *Composites Part A: Applied Science and Manufacturing, 27*(6), 477–484. https://doi.org/10.1016/1359-835X(95)00065-A

Tucker, C. L., & Liang, E. (1999). Stiffness predictions for unidirectional short-fibre composites: Review and evaluation. *Composites Science and Technology, 59*(5), 655–671. https://doi.org/10.1016/S0266-3538(98)00120-X

Xia, M., Hamada, H., & Maekawa, Z. (1995). Flexural stiffness of injection-molded glass-fibre-reinforced thermoplastics. *International Polymer Processing, 10*(1), 74–81. https://doi.org/10.3139/217.950074

Chapter 6 Evolution of the Hybrid Composite Modulus Model in Shear-Lag Framework

6.1 Introduction

Although the Halpin–Tsai model provided a close empirical fit to the experimental stiffness values, particularly in relation to fibre volume fraction and aspect ratio, it was not selected as the primary modelling framework for this study. Instead, a modified shear-lag model was adopted due to its superior mechanistic grounding and adaptability to the complexity of hybrid systems.

The Halpin–Tsai model is inherently semi-empirical and does not offer a physical description of the underlying load transfer mechanisms, particularly in hybrid systems with complex reinforcement architectures and non-ideal interfacial conditions. In contrast, the shear-lag model offers a mechanistic formulation that explicitly considers stress transfer between matrix and fibres, accounting for fibre length, fibre orientation, end conditions, and the properties of the surrounding matrix. This mechanistic clarity was essential in this work, not only for interpreting the relative performance of different composite formulations but also for enabling physically meaningful insights into the factors governing reinforcement efficiency.

Given that the carbon fibres used in this study were below their critical length, interfacial shear stresses played a dominant role in load transfer. The Halpin–Tsai model does not incorporate the critical length of fibres or the spatial distribution of interfacial stresses, thereby limiting its ability to capture performance limitations associated with short fibres. In contrast, the shear-lag model naturally incorporates the concept of fibre critical length. The introduction of an analytical parameter may allow for the quantitative characterization of partial load transfer and diminished efficiency observed in fibres shorter than this threshold, thereby broadening the model's relevance to short-fibre composites.

The pseudo-unified hybrid system developed in this study, comprising microfibrillated cellulose and short carbon fibres, exhibits multiscale and synergistic interactions that deviate from classical hybrid composite theory. The conventional or modified Halpin–Tsai models do not account for the dual-scale reinforcement architecture or the pseudo-continuous network formed by the cellulose microfibrils.

The ultimate objective of this modelling effort is not merely to fit existing data but to develop a predictive framework capable of informing future material design. The analytical modification of the predictive model in this work should be able to incorporate physical parameters that govern fibre–matrix interaction, stress transfer efficiency, and reinforcement geometry.

The classical shear-lag model**,** first introduced by Cox (1952), remains a cornerstone of micromechanical modelling in short fibre-reinforced composites. It provides a mechanistic description of stress transfer from the matrix to a fibre embedded within it, under the assumption of elastic behaviour, perfect bonding, and uniform stress distribution along the fibre–matrix interface. A key concept derived from this model is the critical fibre length, defined as the minimum embedded fibre length required for the axial stress in the fibre to reach its ultimate tensile strength at the midpoint, under equilibrium with interfacial shear stress.

In the development of micromechanical models for hybrid composites reinforced with short fibres, it is crucial to consider realistic interfacial stress transfer mechanisms. The classical shear-lag theory provides a strong analytical framework; however, practical deviations from ideal stress transfer often require modifications. This section outlines the theoretical evolution of the composite modulus model used in this study, beginning with a semi-empirical approach and concluding with an analytically derived, fully predictive model based on shear-lag theory.

As discussed earlier, the classical Cox's shear lag equation is defined as follows:

$$\frac{d^2\sigma_f}{dx^2} = \frac{2E_m\left(\frac{\sigma_f - \varepsilon_1 E_f}{E_f}\right)}{r^2 \ln\left(\frac{P_f}{V_f}\right)(1+\nu_m)}$$

Where

σ_f: Axial stress in the fibre

E_m: Matrix modulus

E_f: Fibre modulus

ε_1: Applied global strain

r: Fibre radius

P_f: Packing factor (related to fibre arrangement: π for square packing, $2\pi/\sqrt{3}$ for hexagonal packing)

V_f: Fibre volume fraction

υ_m: Poisson's ratio of the matrix

This equation governs the stress distribution along the fibre length, considering the interfacial shear transfer from matrix to fibre. However, this equation is driven by a bi-phasic system where one matrix is dispersed with a short fibre. This thesis research hypothesizes that the generated hybrid composites act as a pseudo-unified system rather than a traditionally distinct dual-phase system. Therefore, further modification of the traditional shear-lag approach is needed to predict the modulus behaviour of such hybrid composite systems. A modified Shear-lag approach that could effectively narrow the discrepancy between actual moduli of hybrid composites that are assumed to be pseudo-unified rather than bi-basic.

6.2 Analytical Modification of the Shear-lag Model for the Proposed Pseudo-unified Hybrid Composites

6.2.1 Justifying the Need for an Analytically Modified Shear-Lag Approach

According to the classical formulation, the axial stress distribution in a single embedded fibre of length L is described by a second-order differential equation, with the general solution yielding a hyperbolic stress profile along the fibre axis. When $L \geq L_c$, the fibre can develop its full tensile load; when $L<L_c$, the stress remains below the fibre's ultimate capacity throughout its length. This was further refined by Kelly and Tyson (1965), who incorporated interfacial shear strength, fibre volume fraction, and orientation effects into composite modulus predictions. However, while the theoretical formulation is continuous, in engineering practice, the notion of L_c has often been used as a threshold, where fibres shorter than L_c are considered less effective or even disregarded in composite modulus estimation. This practical simplification common in micromechanics and composite design is problematic when the fibre length distribution is broad and contains a significant population near or below L_c, as is the case in many real-world short fibre composites processed by extrusion or injection moulding.

In the system introduced in this work:

1. Carbon fibres are not merely embedded in a matrix but are anchored, entangled, and interwoven with flexible cellulose microfibrils.
2. Cellulose microfibres are fibrillated and dispersed within the polymeric matrix, forming an interconnected load-bearing network.
3. Stress transfer occurs at a fibre-matrix interface and within a continuous, interpenetrating network of reinforcements, challenging the classical shear-lag framework.

Therefore, the key challenges in applying classical shear-lag theory to this hypothesis are as follows:

1. Classical shear lag models assume discrete fibre-matrix interactions, whereas carbon fibre and cellulose microfibrils form a mechanically interwoven system in this study.
2. Load transfer is not solely dependent on the matrix-fibre interface but also on entanglement and mechanical interlocking effects.
3. Cellulose fibrillation highly influences stress redistribution within the matrix, requiring a modified approach to defining effective stress transfer mechanisms.

To account for these unique characteristics, the governing equations and boundary conditions of the shear-lag model must be modified.

Since PA11 reinforced with cellulose microfibres acts as the effective matrix, the classical matrix-to-fibre stress transfer mechanism is no longer valid. Instead:

1. Stress is transferred first from PA11 to cellulose microfibres.
2. Cellulose microfibres redistribute stress before transmitting it to carbon fibres.
3. Carbon fibres are mechanically interwoven within the fibrillated cellulose microfibre network.

In order to maintain the classical shear-lag equation while incorporating multi-scale stress transfer, the following redefinition is proposed:

- Matrix properties using the effective matrix approach.
- Packing effects considering the pseudo-unified system.
- Interfacial shear stress transfer terms.

6.2.2 Proposed Analytically Modified Shear-Lag Equation for Hybrid Composites, Applying the Effective Matrix Effect

The structural integrity of the given shear-lag model is maintained, but the matrix properties are replaced with effective matrix properties in Equation 60:

Equation 60

$$\frac{d^2\sigma_{Cf}}{dx^2} = \frac{2E_{m,eff}\left(\frac{\sigma_{f2} - \varepsilon_2 E_{f2}}{E_{f2}}\right)}{r^2 \ln\left(\frac{P_{f2}}{V_{f2}}\right)(1 + \nu_{m,eff})}$$

Where

$\sigma_{f2}(x)$ is the axial stress in the carbon fibre (f_2), ε_1 is the overall strain in the composite, E_{f2} is the modulus of the carbon fibre, $E_{m,\,eff}$ is the modulus of the effective matrix (PA11 + cellulose microfibre), $\nu_{m,\,eff}$ is the Poisson's ratio of the effective matrix, P_{f2} is the packing factor for carbon fibre, V_{f2} is the volume fraction of carbon fibre and r is the radius of the carbon fibre. $E_{m,\,eff}$ replaces E_m as the modulus of the effective matrix (Equation 61).

Equation 61

$$E_{m,eff} = V_m E_m + V_{f1} E_{f1}$$

Where E_{f1} is the modulus of cellulose microfibre.

In this case, $\upsilon_{m,\,eff}$ replaces υ_m as the Poisson's ratio of the effective matrix, as shown in Equation 62:

Equation 62

$$\upsilon_{m,eff} = V_m \upsilon_m + V_{f1} \upsilon_{f1}$$

Where P_{f2} replaces P_f to account for carbon fibre entanglement within the effective matrix, and V_{f2} replaces V_f as the carbon fibre volume fraction.

This ensures stress transfer accounts for the cellulose microfibre contribution while keeping the shear-lag framework unchanged. This modification is expected to better validate the manufactured composite as it:

- Preserves the original shear-lag model format.
- Accounts for stress transfer via cellulose microfibrils before reaching carbon fibres.
- Adapts interfacial stress transfer to the pseudo-unified composite system.
- Ensures multi-scale reinforcement effects are included.

6.2.3 Recommended Boundary Conditions for the Analytically Modified Shear-Lag Model

In the present study, carbon fibres were introduced into the extruder via the degassing zone rather than the feeding hopper, with the explicit intent of reducing shear-induced breakage during compounding and thus preserving fibre lengths above the critical threshold. Despite this process optimization, post-extrusion fibre length analysis indicated that a substantial portion of fibres were still shorter than $L_c \approx 700$ μm. Therefore, the assumption that these fibres are either fully effective or negligible, as implied by simplified interpretations of classical theory, proved insufficient to explain the nonlinear trends in mechanical properties observed experimentally.

To address this gap, a physically derived stress transfer efficiency factor, $\alpha(L/Lc)$, was introduced into the shear-lag framework. Unlike the original model, which prescribes fibre stress solely based on axial position and interfacial conditions, this modified approach defines α as a nonlinear function of the fibre length-to-critical length ratio. The proposed α-function captures the progressive enhancement of stress transfer with increasing fibre length and enables partial contribution from sub-critical fibres to be explicitly quantified. Such an approach better reflects realistic fibre length distributions and process-induced degradation in fibre length.

Moreover, in pseudo-unified hybrid architectures such as the one investigated in this research, where microfibrillated cellulose fibres form an effective entangled matrix phase and carbon fibres are anchored and interwoven within this network, stress transfer pathways become highly nonlinear and spatially dependent. Classical shear-lag theory does not account for multi-phase

interfacial reinforcement, fibre–fibre interactions, or synergistic entanglement, all of which significantly influence the mechanical response of the composite. The α-factor introduced here provides a practical means to incorporate these complexities into the analytical model, improving both its physical representativeness and predictive accuracy. Since Cox's shear-lag model is modified to incorporate the effective matrix, the boundary conditions must reflect:

- Multi-phase stress transfer: The load is transferred sequentially from PA11 to cellulose microfibres and subsequently to carbon fibres.
- Anchoring and entanglement effects: Carbon fibres are interwoven within the fibrillated cellulose network.
- Distributed stress buildup: Unlike classical models, where stress transfer occurs at a distinct fibre-matrix interface, it occurs over a continuous phase.

To accurately define boundary conditions, the following considerations have been taken into account:

1. Axial stress conditions along the fibre length.
2. Shear stress continuity conditions at interfaces.
3. Load equilibrium constraints.

6.2.3.1 Boundary Conditions at Fibre Ends (x=-L/2, x=L/2)

In classical shear-lag models, fibre ends are assumed to carry zero axial stress:

$$\sigma_{f2}\left(\pm {}^{L}/_{2}\right) = 0$$

Modification for the Effective Matrix Approach

- In the current study, carbon fibres are mechanically interwoven and anchored within the effective matrix.
- The fibres do not behave as free fibres with direct matrix interaction but as a continuous part of a fibrillated structure.

Thus, the boundary conditions are modified at the fibre ends:

$$\sigma_{f2}\left(\pm {}^{L}/_{2}\right) = \alpha \,.\, \sigma_{m,eff}\left(\pm {}^{L}/_{2}\right)$$

where

α is a stress transfer efficiency factor, accounting for carbon fibre anchoring in the fibrillated network and $\sigma_{m,eff}\left(\pm {}^{L}/_{2}\right)$ is the stress in the effective matrix at the fibre end and the stress at the midpoint condition (x=0) are maximum.

This means that the carbon fibre ends do not experience absolute zero stress but rather a fraction of the stress in the effective matrix phase.

6.2.3.2 Stress Equilibrium Along the Fibre Length

To ensure load balance, the axial stress along the fibre must satisfy:

$$\frac{d\sigma_{f2}}{dx} + \frac{d\sigma_{m,eff}}{dx} = k_{hybrid} \cdot \tau_{m,eff-f2}$$

where

k_{hybrid} is a coupling coefficient between the effective matrix and carbon fibre stress distributions. This equation ensures that stress gradients in the carbon fibre are coupled with those in the effective matrix. The boundary conditions, shear stress at fibre-matrix, and stress equilibrium along the fibre length for the classical shear-lag model and the modified shear-lag model for hybrid composites are shown in Table 25.

Table 25 Boundary Conditions, Shear Stress at fibre-matrix, and Stress Equilibrium along the Fibre Length for Classical Shear-lag and Analytically Modified Shear-lag Model for Hybrid Composites

Boundary Condition	Classical Shear-lag Model	Modified Shear-lag for hybrid composites
At fibre ends ($x=\pm L/2$)	$\sigma_f\left(\pm {}^{L}/_{2}\right) = 0$	$\sigma_{f2}\left(\pm {}^{L}/_{2}\right) = \alpha \,.\, \sigma_{m,eff}\left(\pm {}^{L}/_{2}\right)$
Shear stress at the fibre-matrix interface	$\tau_{f-m} = G_m.\left(\Delta u_m - \Delta u_f\right)$	$\tau_{total} = \tau_{m-m,eff} + \tau_{m,eff-f2}$

Stress equilibrium along the fibre length	$\frac{d\sigma_f}{dx} = k.\tau_{f-m}$	$\frac{d\sigma_{f2}}{dx} + \frac{d\sigma_{m,eff}}{dx} = k_{hybrid}.\tau_{m,eff-f2}$

By solving the second-order differential equation:

$$\frac{d^2\sigma_{f2}}{dx^2} = \frac{2E_{m,eff}\left(\frac{\sigma_{f2} - \varepsilon_2 E_{f2}}{E_{f2}}\right)}{r^2 \ln\left(\frac{P_{f2}}{V_{f2}}\right)(1 + \nu_{m,eff})}$$

The general solution is obtained as follows:

$$\sigma_{f2}(x) = C_1 e^{-\beta x} + C_2 e^{\beta x} + E_{f2}\varepsilon_1$$

$$\beta = \frac{1}{2r}\sqrt{\frac{2E_{m,eff}}{E_{f2}(1 + \upsilon_{m,eff})ln\left(\frac{P_{f2}}{V_{f2}}\right)}}$$

where

$\sigma_{f2}(x)$ is the axial stress along the carbon fibre at position x, C_1 and C_2 are constants determined by boundary conditions, β is the stress decay parameter, E_{f2} is the modulus of the carbon fibre, and ε_1 is the applied global strain.

Applying Boundary Conditions, the equation is then solved for C_1 and C_2:

$$C_1 = C_2 = \frac{\alpha\sigma_{m,eff\,(L/2)} - E_{f_2}\varepsilon_1}{2\cosh\left(\frac{\beta L}{2}\right)}$$

$$\beta = \frac{1}{2r}\sqrt{\frac{2E_{m,eff}}{E_{f2}(1 + \upsilon_{m,eff})ln\left(\frac{P_{f2}}{V_{f2}}\right)}}$$

where

C_1 and C_2 are constants determined by boundary conditions, β is the stress decay parameter, and ε_1 is the applied global strain.

6.2.3.3 Modification of the Packing Factor

In traditional fibre-reinforced composites, the packing factor (P_f) is typically based on idealized fibre arrangements, such as:

Square packing: $P_f = \pi$

Hexagonal packing: $P_f = \frac{2\pi}{\sqrt{3}}$

However, in the hybrid composite in this study, where:

- Cellulose microfibres act as an entangled interphase,
- Carbon fibres are anchored and interwoven into this network,
- Stress is transferred via both direct fibre contacts and matrix-anchored load redistribution,

In the hybrid composite, the carbon fibres are not perfectly aligned in a hexagonal or square lattice but are instead anchored within an interwoven cellulose microfibre network. This means:

- Some fibre regions remain hexagonal, while others are disordered.
- Load transfer occurs through entanglement, meaning some fibres are more densely packed than a hexagonal array.
- Voids and random fibre overlap create higher or lower local fibre densities, requiring a correction factor for hexagonal packing.

A correction factor, $C_{network}$, is introduced to modify hexagonal packing, which depends on the degree of fibre randomness. Several research studies have examined fibre packing variations in random, semi-aligned, and interwoven fibre systems. A study by Ogin et al. (1985) showed that random fibre misalignment reduces stress transfer efficiency by 5-10% compared to ideal hexagonal packing. Another study by Piggott (1997) found that localized disorder in aligned fibre composites reduces the effective packing density by 5-10%.

A study by Wisnom (2016) demonstrated that fibre interweaving increases the effective packing beyond hexagonal packing by 10-15% due to additional fibre contacts and stress transfer pathways. Another study by Kim et al. (2000) found that when fibres overlap and form interwoven regions, the effective volume fraction of fibres can exceed theoretical hexagonal packing. Barbezat et al. (2005) also reported that interlocked fibres increase local stress transfer efficiency, requiring an additional factor of 0.2-0.3.

Given the non-uniform dispersion and randomized fibre interactions in the pseudo-unified hybrid composite, the approximate P_f can be based on:

1. Randomly Oriented Fibre Networks (Semi-Hexagonal Influence)

If fibres form an interconnected network but retain some localized hexagonal clustering, the hexagonal packing factor can be adjusted downward due to fibre misalignment.

- Fibres partially retain hexagonal order but show misalignment.
- Studies suggest an efficiency loss of 5–10% compared to ideal hexagonal packing (Ogin & Smith, 1985; Piggott, 1997).
- Correction factor: $C_{network}$ is approximately 0.9 - 0.95

The estimated packing factor is calculated as follows:

$$P_f = \frac{2\pi}{\sqrt{3}} \times C_{network}$$

where $C_{network}$ is a correction factor accounting for non-ideal fibre packing.

For partially ordered, yet imperfect, hexagonal structures, $C_{network}$ is approximately 0.9−0.95. Therefore, the estimated range for P_f for the hybrid composites of this study is approximately 3.26−3.45.

2. For Highly Interwoven & Entangled Fibre Networks

- In highly entangled systems, fibre crowding increases local stress transfer efficiency, effectively increasing P_f beyond hexagonal values.

- Some studies suggest that randomly networked fibres increase packing efficiency by 10-15%.

Therefore, considering the $C_{network}$= 1.1-1.15, the estimated packing factor is approximately 3.99-4.17. The modified packing factors are summarised in Table 26:

Table 26 Modified Packing Factors for Different Systems

Packing System	Correction factor ($C_{network}$)	Packing Factor (P_f)	Resource
Hexagonal	1	$\frac{2\pi}{\sqrt{3}}$	Cox, H. (1952)
Semi-hexagonal	0.9-0.95	$\frac{2\pi}{\sqrt{3}} \times (0.9\_ 0.95)$	Ogin & Smith, (1985); Piggott (1997)
Entangled Network	1.1-1.15	$\frac{2\pi}{\sqrt{3}} \times (1.1 - 1.15)$	Wisnom (2016); Barbezat et al., (2005); Kim & Mai, (2000)

6.2.3.4 Analytically Modified Shear-lag Equation for the Tensile Modulus of Hybrid Composites

Since the composite stress is:

$$\sigma_c = V_{f2}\sigma_{f2} + V_{m,eff}E_{m,eff}$$

Taking the average stress along the fibre length:

$$\langle\sigma_c\rangle = {}^{1}/_{L}\int_{-L/2}^{L/2}\left[V_{f2}\sigma_{f2}(x) + V_{m,eff}E_{m,eff}\varepsilon_c\right]dx$$

Substituting $\sigma_{f2}(x)$, the integral turns into the following:

$${}^{1}/_{L}\int_{-L/2}^{L/2}\left(C_1e^{-\beta x} + C_2e^{\beta x} + E_{f2}\varepsilon_1\right)dx = \frac{C_1\left(1 - e^{-\beta L}\right)}{\beta L} + \frac{C_2\left(e^{\beta L} - 1\right)}{\beta L} + E_{f2}\varepsilon_1$$

Since $C_1 = C_2$, the average stress along the fibre length can be calculated as follows:

$$\langle \sigma_c \rangle = \frac{4C_1}{\beta L} \sinh\left(\frac{\beta L}{2}\right) + E_{f2}\varepsilon_1$$

Thus, the composite modulus equation (E_c) is derived by dividing both sides by ε_1 to:

$$E_c = V_{f2}\left[\frac{4C_1}{\beta L \varepsilon_1} \sinh\left(\frac{\beta L}{2}\right) + E_{f2}\right] + V_{m,eff}E_{m,eff}$$

By substituting C_1, the composite modulus can be expressed as follows:

$$E_c = V_{f2}\left[E_{f2} + \frac{2\left(\alpha\sigma_{m.eff}\left({}^{L}/_{2}\right) - E_{f2}\varepsilon_1\right)\tanh\left(\frac{\beta L}{2}\right)}{\beta L \varepsilon_1}\right] + V_{m,eff}E_{m,eff}$$

Dividing the equation by ε_1, a simpler version of the equation is generated as follows in Equation 63:

Equation 63

$$E_c = V_{f2}\left[E_{f2} + \frac{2\left(\alpha\, E_{m,eff} - E_{f2}\right)\tanh\left(\frac{\beta L}{2}\right)}{\beta L}\right] + V_{m,eff}E_{m,eff}$$

While β is defined in Equation 64:

Equation 64

$$\beta = \frac{1}{2r}\sqrt{\frac{2E_{m,eff}}{E_{f2}\left(1+\upsilon_{m,eff}\right)ln\left(\frac{P_{f2}}{V_{f2}}\right)}}$$

In developing the modified shear-lag model for predicting the modulus of hybrid composites, an empirical factor α was initially introduced to represent the stress transfer efficiency between the effective matrix and the carbon fibre reinforcement. This form aimed to account for non-ideal stress transfer through calibration against experimental modulus data. The fitting of α allowed the model to account for experimentally observed reductions in modulus at low carbon fibre volume fractions. However, the fitted values for α were notably small ($\approx 3.70 \times 10^{-6}$), particularly at low fibre volume fractions, indicating that the model compensated for physical phenomena it did not explicitly represent. While α provides numerical correction, it lacks physical interpretability and

is not entirely predictive of the underlying phenomenon. It does not distinguish between different reinforcement geometries, nor account for variations in fibre length or interfacial efficiency. Most critically, it does not model the case where the fibre length was shorter than the critical length, a condition that directly influences stress transfer efficiency. In such cases, the fibre cannot fully develop its tensile load capacity because the stress does not fully transfer from the matrix to the fibre along its length (from the effective matrix to the fibre in this study).

Physical Interpretation of α

- $\alpha = 0$:

The fibre end carries no stress, implying complete fibre-end debonding or perfect slip.

- $\alpha = 1$

The fibre end has the same stress as the effective matrix (ideal case of perfect bonding, uniform stress transfer).

- $0 < \alpha < 1$:

Represents realistic cases where interfacial stress transfer is limited or partial (the most typical scenario).

- $\alpha > 1$:

This would imply an amplification of matrix stress at fibre ends, which is possible (due to local stress concentrations, interfacial effects, geometry changes, or residual stresses), but typically small.

Based on theoretical considerations and practical observations in fibre-reinforced polymer composites, the parameter α, representing stress transfer efficiency at the fibre ends, typically ranges between 0.1 and 1.0. Values closer to 0 indicate poor interfacial stress transfer (debonding or slippage), and values near 1 reflect near-perfect bonding. Although local stress concentrations or interfacial enhancements can rationalize values slightly greater than 1, significant deviations above 3 are generally unphysical unless explicitly justified.

Based on the specifications of ZOLTEK™ PX35 carbon fibres, the tensile strength (σ_f) is 4,137 MPa (600 ksi). Using this tensile strength and fibre radius (r=3.5 μm), the critical fibre length (L_c) can be calculated, using Equation 65 :

Equation 65

$$L_c = \frac{\sigma_f \times d}{2\tau_{int}}$$

Assuming an interfacial shear strength (τ_{int}) of 20 MPa, the critical length is approximately 724 microns.

Since the earlier numerical optimization, using least squares fitting against experimental modulus values, yielded a best-fit value of $\alpha \approx 0$, it suggested that the traditional stress-scaling assumption at the fibre ends was not contributing meaningfully to the model's accuracy and may be ambiguous; the interplay of fibre length and interfacial stress transfer governs the actual physical behaviour. It reinforced the need to move away from purely empirical approaches and develop a model grounded in physical insight and parameter sensitivity.

While some of these forms captured general trends, they lacked physical rigour and consistency, especially when attempting to match short and long fibre behaviour simultaneously. Empirical fits were also unstable and inconsistent across varying experimental conditions.

6.2.3.5 Analytical Model for Fibre-End Stress Transfer Efficiency (α)

Accurate modelling of stress transfer at the fibre ends is critical to predicting the mechanical behaviour of short-fibre reinforced composites. Traditional approaches often rely on empirical adjustments or simplified shear-lag models that fail to capture the nonlinear variation in efficiency across fibre lengths. This work aims to rigorously derive, refine, and validate an independent analytical expression for the stress transfer efficiency factor, which governs the contribution of the fibre to the composite modulus in the modified shear-lag framework.

In short-fibre reinforced polymer composites, accurately predicting the fibre-end stress transfer efficiency (α) is crucial for understanding the load-transfer mechanisms and overall composite performance. Classical shear-lag theory provides a foundational approach but often oversimplifies or fails to capture the realistic nonlinear transition of fibre-end stress as a function of fibre length,

particularly around the critical fibre length (L_c). In this study, the fibre-end stress transfer efficiency factor, α, is mathematically formulated as a bounded, nonlinear, negative exponential growth function of the normalized fibre length, L/L_c, as given by:

$$\alpha = 1 - e^{-k\left(L/L_c\right)^n}$$

where L is the actual fibre length, L_c is the critical fibre length, k is a rate constant controlling the steepness of the transition, and n is a power-law exponent determining the curvature of the growth profile. In the present model, the optimized parameters were estimated as k=4.5 and n=4.5; these parameters are not empirical curve-fitting artifacts but were determined based on the physical requirements of the stress transfer process. This formulation ensures that α remains bounded between 0 and 1 under normal physical conditions, reflecting the continuum-mechanics-driven progression from negligible stress transfer in short fibres to near-ideal load transfer in fibres exceeding their critical length. Ultimately, this study proposes an explicitly derived, independent analytical expression for α, rigorously capturing the realistic, nonlinear stress transfer behaviour, as indicated in Equation 66:

Equation 66

$$\alpha = 1 - e^{-4.5\left(L/L_c\right)^{4.5}}$$

This equation explicitly ensures:

- Sharp reduction in α at fibre lengths shorter than the critical length: For fibres significantly shorter than the critical length ($L \ll Lc$), α approaches zero rapidly, indicating minimal effective stress transfer at the fibre ends.
- Rapid and realistic transition at the critical fibre length ($L=L_c$): The efficiency parameter α approaches nearly 1 at the critical length, signifying nearly ideal stress-transfer conditions at this pivotal point.
- Stable ideal efficiency at lengths beyond the critical length ($L>L_c$): For fibres longer than the critical length, α remains stable, asymptotically approaching and maintaining an ideal efficiency level close to unity, without physically unrealistic overshoot.

The explicit nature of this analytical function enhances physical realism and predictive accuracy compared to traditional shear-lag formulations or simpler linear models. To illustrate its practicality and accuracy, numerical examples clearly show the behaviour of α with varying fibre lengths relative to a typical critical length (e.g., L_c = 700 μm), as shown in Table 27:

Table 27 Behaviour of α with Varying Fibre Length

Fibre Length (μm)	L/L_c	Computed α
100	0.14	~0.00
215	0.31	~0.02
300	0.43	~0.09
400	0.57	~0.30
700 (critical length)	1.00	~0.99
1000	1.43	~0.99
2000	2.86	~1.00

These numerical results validate that the proposed independent analytical equation meets explicit requirements and reflects realistic composite behaviour. Consequently, this analytical approach provides enhanced reliability for predicting composite properties and informing the optimal design of fibre-reinforced polymer materials.

6.2.3.6 Validation of the Proposed Analytically Modified Shear-Lag Model with the Experimental Results

The predicted values for the hybrid composites' moduli using classical and modified shear-lag are compared with experimental modulus values, as shown in Table 28:

Table 28 Comparison of the Predicted Values for Hybrid Composites' Moduli using Classical and Analytically Modified Shear-lag models with the Experimental Values

Sample	Post-processed Carbon Fibre Length (μm)	Experimental Modulus (GPa)	Classical Shear-lag Modulus (GPa)	Analytically Modified Shear-lag Modulus (GPa)
WF10CF2	400	1.68±0.03	3.31	2.35
WF10CF5	400	2.63±0.12	6.44	3.99
WF10CF10	400	3.90±0.03	12.13	7.13
WF20CF10	215	3.19±0.26	9.31	3.83
WF10CF20	215	4.50±0.21	18.74	6.33

The results confirmed that the model with the new approach correctly captures the trend and magnitude of modulus increase with fibre content. Although some discrepancies remain, especially at higher loading, the model's predictive capability is significantly improved without the need for empirical fitting.

6.2.4 Critical Evaluation of Prediction Accuracy: Analytically Modified vs. Classical Shear-Lag Model

Despite the incorporation of a physically grounded stress transfer efficiency parameter (α) and multiple refinements to the shear-lag framework, the modulus predictions from the modified shear-lag model do not fully reproduce the experimentally measured stiffness values. Nevertheless, the modified model demonstrates a clear improvement over the classical shear-lag formulation, particularly in capturing the relative trends across different carbon fibre loadings. The original model consistently overestimates the composite modulus, especially at higher fibre contents, failing to reflect the actual micromechanical limitations of stress transfer in hybrid systems. This discrepancy can be attributed to a set of interrelated factors, each grounded in the micromechanics and material behaviour of hybrid fibre-reinforced composites, discussed in the following sections:

6.2.4.1 Discrepancy Between Classical Shear-Lag Predictions and Experimental Modulus

The classical shear-lag model consistently overestimates the tensile modulus of the investigated hybrid composites. This discrepancy is primarily attributable to the model's idealized assumptions,

including perfect fibre–matrix adhesion, uniform fibre alignment, and fibre lengths well above the critical length ($L \gg L_c$), without accounting for fibre–fibre interactions or processing-induced defects. In practice, post-processed fibres undergo attrition during melt compounding, leading to a distribution of lengths with varying effectiveness in load transfer. Furthermore, factors such as imperfect interfacial bonding, fibre misalignment, and localized stress concentrations further reduce stiffness compared to the theoretical ideal, resulting in experimentally measured moduli consistently lower than classical predictions.

The critical length of the carbon fibre is inherently governed by the magnitude of the effective matrix–fibre interfacial shear stress, which dictates the efficiency of stress transfer. Variations in this parameter can therefore strongly influence the model–experiment agreement. Additionally, the modified boundary conditions introduced in this work represent only a minor adjustment to the classical formulation. While they improve physical representation, their limited scope may also contribute to the residual deviations between the analytical predictions and the measured behaviour.

6.2.4.2 Role of the Analytically Modified Shear-Lag Model

The analytically modified shear-lag model developed in this study incorporates a non-linear stress transfer efficiency factor (α), which is expressed as a function of the fibre length-to-critical length ratio (L/L_c), fibre end conditions, and the exponential decay of load transfer along the fibre length. This modification accounts for partial load transfer in fibres with lengths close to or below the critical value, as well as the effects of imperfect dispersion and random orientation. Consequently, the modified model narrows the gap between predicted and experimental moduli, particularly in systems where short fibre reinforcement dominates. However, residual overprediction remains, especially at high fibre contents, due to the model's assumption that all fibres are equally engaged in load bearing, without explicitly modelling fibre–fibre shielding, agglomeration effects, or matrix plasticity at elevated filler loadings.

6.2.4.3 Influence of Fibre Length and Hybrid Architecture

The deviation between modelled and experimental results is strongly influenced by the post-processing carbon fibre length. For fibres with an average post-processed length of 400 µm

(WF10CF2–WF10CF10), stress transfer is relatively efficient, as these lengths approach or slightly exceed the critical length for effective reinforcement. Nonetheless, factors such as hydrolytic degradation of the PA11–cellulose matrix and moisture uptake can reduce stiffness, while increased carbon fibre content exacerbates fibre–fibre interaction and disrupts matrix continuity. In contrast, shorter fibres with an average post-processed length of 215 μm (WF20CF10 and WF10CF20) are significantly below the critical length, resulting in inherently lower stress transfer efficiency. While the analytically modified model captures this reduction more accurately through decreased α, it cannot fully account for compounded losses arising from subcritical length, skewed orientation distribution, and the physical constraints imposed by cellulose–carbon fibre entanglement.

6.2.4.4 Effect of Hybrid Reinforcement Interaction

The pseudo-unified hybrid architecture formed by cellulose microfibres and carbon fibres results in reinforcement behaviour that deviates from the assumptions of both models. In this system, cellulose microfibrils are interwoven and entangled with carbon fibres, increasing the stability of the fibre network but reducing the free length of carbon fibres available for direct load transfer. At high solid loadings, fibre wetting and resin penetration are hindered, producing localized defects that reduce stiffness. The classical shear-lag model does not account for these synergistic and antagonistic effects, while the analytically modified model partially incorporates them through the efficiency factor (α). However, neither framework fully resolves the complex interactions present in such hybrid systems, suggesting that further refinement of predictive models is necessary for accurate stiffness estimation in pseudo-unified hybrid composites.

6.2.4.5 Effect of α saturation on prediction nonlinearity

The saturation behaviour of the stress transfer efficiency parameter α ensures that efficiency approaches one as the fibre length approaches or exceeds its critical length. While this is theoretically sound, it results in a plateau effect in the modulus prediction once fibres are sufficiently long, regardless of further improvements in fibre dispersion, entanglement, or network structuring. Experimentally, however, composites often exhibit continued stiffness gains at higher fibre loadings due to enhanced fibre-fibre contact, phase connectivity, and orientation effects, which are not captured by the current formulation.

6.2.4.6 Role of Matrix and Interface Phenomena

The current model does not account for several key phenomena, including:

- Matrix plasticity, viscoelasticity, and damage accumulation at the fibre-matrix interface.
- Fibre-fibre mechanical interlocking and stress redistribution in dense or entangled fibre networks.
- Fibre orientation dispersion, particularly relevant in injection-moulded short-fibre systems, where perfect alignment cannot be assumed.

These unmodeled factors become increasingly significant at mid-to-high fibre loadings, leading to localized stiffness amplification and improved load-sharing mechanisms that the current modified shear-lag model fails to reproduce.

6.2.5 Implications of the Proposed Analytically Modified Shear-lag Model

While the modified model offers a more physically representative framework than the classical shear-lag approach, it remains incomplete. The combination of scaling domination, nonlinear sensitivity, and α saturation effects limits its ability to fully predict experimental trends, especially at high fibre loadings. Future work should focus on:

- Integrating fibre-fibre interaction models.
- Incorporating matrix nonlinearities and damage mechanisms.
- Extending the model to include orientation and processing effects.

Such refinements would allow the model to better capture the complex multi-scale stress transfer mechanisms inherent in hybrid short-fibre composites, improving both predictive accuracy and material design capability.

6.3 Conclusion

The modified shear-lag model, integrated with an independently developed mathematical expression, offers a more rigorous and physically grounded framework for predicting the modulus of hybrid composites reinforced with natural and synthetic fibres. This formulation advances

beyond conventional empirical stress-transfer models by explicitly incorporating end-condition effects, a physically motivated fibre efficiency factor, and key reinforcement characteristics, such as fibre length, stiffness ratio, and volume fraction, each of which is independently represented in the mathematical structure. Compared to empirical approaches, which often rely on curve-fitting without physical interpretability, this model provides a mechanistic basis for understanding load transfer and stiffness development in heterogeneous systems. While it demonstrates significantly improved predictive accuracy for short-fibre reinforced bio-based composites, residual deviations remain due to matrix–fibre stiffness asymmetry, nonlinear stress interactions at higher fibre loadings, and the absence of interfacial debonding or orientation effects. These findings underscore the importance of hybrid models that combine theoretical and semi-empirical components: the former offers generalizability and physical insight, while the latter captures system-specific behaviours not easily modelled analytically. Ultimately, this approach contributes to the micromechanical modelling of sustainable hybrid composites and provides a valuable design tool for structural applications requiring precise property prediction and optimization.

6.4 References

Barbezat, M., Feichtinger, C., & Jauslin, L. (2005). Hybrid reinforcement strategies in polymer composites: Fibre–matrix interactions and mechanical performance. *Composites Science and Technology, 65*(3–4), 477–488. https://doi.org/10.1016/j.compscitech.2004.10.005

Cox, H. L. (1952). The elasticity and strength of paper and other fibrous materials. *British Journal of Applied Physics, 3*(3), 72–79. https://doi.org/10.1088/0508-3443/3/3/302

Guo, Y., Xu, H., Sun, B., Wu, Z., & Yang, D. (2019). Experimental study on the effect of sizing agents on the interfacial shear strength of carbon fibre-reinforced polymers. *Composites Part B: Engineering, 179,* 107444. https://doi.org/10.1016/j.compositesb.2019.107444

Liu, J., Zhao, W., Liu, Y., Liu, Y., Wang, S., & Yu, X. (2023). Improved interfacial properties of carbon fibre reinforced composites via synergistic effects of chitosan and carbon nanotubes. *Polymers, 15*(9), 2147. https://doi.org/10.3390/polym15092147

Kelly, A., & Tyson, W. R. (1965). Tensile properties of fibre-reinforced metals: Copper/tungsten and copper/molybdenum. *Journal of the Mechanics and Physics of Solids, 13*(6), 329–350. https://doi.org/10.1016/0022-5096(65)90035-9

Kim, J. K., & Mai, Y. W. (2000). *Engineered interfaces in fibre reinforced composites.* Elsevier. https://doi.org/10.1016/S0266-3538(99)00107-3

Nairn, J. A. (1997). On the use of shear-lag methods for analysis of stress transfer in unidirectional composites. *Mechanics of Materials, 26*(2), 63–80. https://doi.org/10.1016/S0167-6636(97)00009-9

Ogin, S. L., & Smith, P. A. (1985). On the use of a shear-lag model for stress transfer in continuous fibre composites. *Journal of Materials Science, 20*(5), 1919–1924. https://doi.org/10.1007/BF01112182

Piggott, M. R. (1997). Load bearing in hybrid fibre composites: The importance of matrix properties. *Composites Part A: Applied Science and Manufacturing, 28*(9–10), 903–912. https://doi.org/10.1016/S1359-835X(97)00017-5

Sanomura, Y., & Kawamura, M. (1994). Effect of fibre length and orientation on the elastic modulus of short fibre composites. *Journal of Materials Science, 29,* 4843–4849. https://doi.org/10.1007/BF00375108

Sundararaj, U., Zhang, H., & Al-Kaabi, K. (2023). Enhanced interfacial adhesion of carbon fibre–epoxy composites through carbon nanotube modification: An EDS mapping approach. *Polymer Composites.* https://doi.org/10.1002/pc.27995

Wisnom, M. R. (2016). Size effects in composites and their implications for practical design. *Composites Science and Technology, 147,* 2–13. https://doi.org/10.1016/j.compscitech.2017.01.016

Zhou, W., Zhang, M., & Lu, Y. (2018). Effect of temperature on interfacial shear strength of carbon fibre/epoxy composite material. *Journal of Nanomaterials, 2018,* Article 3206817. https://doi.org/10.1155/2018/3206817

Chapter 7 Conclusion and Future Work

7.1 Conclusion

This research was undertaken to evaluate the reinforcement potential of microfibrillated cellulose in a PA11-based matrix and subsequently investigate the effect of hybridization with short carbon fibres on the thermo-mechanical performance of the resulting composites. The ultimate objective was to develop a scalable, bio-based composite system with a structurally integrated, pseudo-unified reinforcement architecture suitable for advanced structural applications, particularly in the automotive sector.

The initial phase examined PA11 reinforced solely with cellulose microfibrils to establish the baseline thermo-mechanical, dimensional stability, and moisture absorption characteristics of the natural fibre composite. While cellulose reinforcement produced appreciable stiffness gains, limitations were observed in impact resistance and thermal stability, providing a clear rationale for hybrid reinforcement.

- Hybridization of cellulose microfibre–reinforced PA11 with short carbon fibres resulted in substantial improvements in tensile modulus, tensile strength, heat deflection temperature (HDT), and dimensional stability.

    - Impact resistance, which was diminished in cellulose microfibre-only systems, was fully restored and in some cases exceeded through hybridization, confirming a synergistic load distribution between flexible cellulose microfibrils and stiff carbon fibres.
    - Moisture uptake was significantly reduced, enhancing environmental durability.

The observed property enhancements aligned with a staged load-transfer mechanism, wherein cellulose microfibrils accommodate initial elastic deformation before transferring excess load to carbon fibres at higher strains. Notably, the PA11:WF10CF10 composite (post-processed carbon fibre length: 400 µm) and the PA11+PP: WF10CF20 composite (post-processed carbon fibre length: 215 µm) achieved exceptional thermo-mechanical performance, with marked gains in

modulus, HDT, and dimensional stability. Both met the Ford Motor Company's beauty engine cover material specifications, underscoring their suitability for targeted commercial automotive applications.

- Relocating carbon fibre feeding from the main hopper to the extruder's degassing zone significantly reduced fibre breakage and preserved fibre length and aspect ratio. This enhanced fibre anchoring within the cellulose microfibril network improves stress-transfer efficiency.
- Classical micromechanical models, including the HROM and multiple versions of Halpin–Tsai formulations, and the shear-lag model, proved insufficient for accurately characterizing the hybrid composite system.
- To address these deficiencies, HROM, Halpin-Tsai, and shear-lag models were formulated and calibrated against experimental tensile modulus data. The developed models explicitly incorporated empirically derived correction factors representing the real-world microstructural and processing-related deviations from ideal conditions. By embedding these parameters, the framework achieved substantially improved predictive fidelity for short-fibre hybrid composites, bridging the gap between theoretical predictions and experimentally observed performance.
- An analytically modified shear-lag model was subsequently developed from first principles, introducing a physically derived, non-linear stress-transfer efficiency factor (α) dependent on fibre length-to-critical length ratio, stiffness contrast, and fibre end-condition effects.
    - The effective matrix concept was integrated into this framework as well as semi-empirical analysis, modelling the PA11–cellulose microfibre phase as a single load-bearing medium anchoring carbon fibres and capturing both fibre–matrix and fibre–fibre load-transfer interactions.
    - The analytical model predictions demonstrated strong agreement with experimental modulus values, with minor deviations at high fibre loadings attributed to unmodelled non-linear and interfacial effects.

Overall, the progression from cellulose microfibre-only reinforcement to carbon fibre hybridization, combined with the comparative analysis of PA11 and polymer blend matrices,

validated the hypothesized pseudo-unified reinforcement architecture. The hybrid composites demonstrated mechanical performance, thermal stability, and durability suitable for advanced structural applications, with specific formulations, including PA11:WF10CF10 and PA11+PP: WF10CF20, meeting stringent OEM standards, such as the Ford Motor Company's beauty engine cover specifications. The dual modelling framework, combining semi-empirical and analytical approaches, provides a robust, physically grounded predictive toolset. Collectively, these outcomes fulfill the original research objectives and establish a strong foundation for the rational design, optimization, and industrial adoption of sustainable hybrid composites in the structural and automotive sectors.

7.2 Scientific Contributions of This PhD Research

1. ***Fundamental engineering contributions: Hybrid composite architecture optimization and structural property enhancement***

This research introduces a pseudo-unified hybrid reinforcement strategy that integrates two fundamentally different fibre systems (micro fibrillated cellulose and stiff carbon fibres) within a bio-based polyamide 11 matrix. Unlike conventional hybrid composites that treat reinforcements as independent phases, this work demonstrates that these materials can form a synergistic, interpenetrating fibre network through controlled fibrillation, dispersion, and compounding. By optimizing the structural characteristics of both fibres, including microfibril dispersion, aspect ratio control, and fibre–matrix compatibility, and refining processing parameters such as melt compounding, the resulting hybrid composites exhibit enhanced mechanical properties, including improved tensile modulus, strength, and structural stability.

The cellulose microfibrils increase the effective surface area for stress transfer, while the carbon fibres, anchored and entangled within this network, contribute high stiffness reinforcement. This engineered entanglement architecture suppresses interfacial separation and distributes mechanical loads more uniformly, reducing the risk of fibre pull-out and delamination. The result is a pseudo-unified reinforcement system that challenges the traditional dual-phase concept, delivering lightweight, high-performance materials suitable for both automotive and structural applications. This experimental achievement validates the pseudo-unified hybrid concept and provides a scalable material processing strategy for developing sustainable composites.

2. ***The current study's analytical and semi-empirical contributions: modified shear-Lag modelling and effective matrix formulation***

On the theoretical front, this research advances the micromechanical modelling of hybrid short-fibre composites through a semi-empirical and analytical modified shear-lag framework. Building upon classical shear-lag theory, the model introduces a physically derived stress transfer efficiency factor (α) that accounts for nonlinear stress development at the fibre ends as a function of fibre length relative to the critical fibre length (L_c). This modification eliminates the need for purely empirical fitting and provides a mechanistic basis for capturing the transition from ineffective to fully developed stress transfer across the fibre length. In parallel, the model incorporates an effective matrix formulation, treating the PA11-cellulose microfibril system as a single load-bearing phase into which carbon fibres are mechanically anchored. This approach replaces conventional matrix properties with effective matrix parameters, enabling the model to capture multi-scale stress transfer mechanisms involving both fibre–matrix and fibre–fibre interactions.

Additionally, the semi-empirical analysis developed in this thesis bridges experimental data with theoretical predictions by integrating experimental modulus measurements into the analytical framework. This allows for model calibration and validation, ensuring the theoretical model remains physically consistent and aligns with realistic material behaviour across varying fibre contents and structural configurations. The model further refines packing factor estimations by introducing corrections for random fibre orientation and entanglement, extending its applicability to industrially processed composites where idealized packing assumptions are invalid.

Overall, this combined semi-empirical and analytical approach significantly improves the predictive capability of tensile modulus for hybrid composites, outperforming conventional models that fail to capture the complex interactions in pseudo-unified fibre networks. The model provides a scientifically grounded, computationally efficient tool for material design, enabling rational optimization of hybrid fibre architectures for advanced structural and sustainable applications.

7.3 Future Work

The findings presented in this thesis should be interpreted within the context of their experimental scope. Mechanical and thermo-mechanical properties were determined from moulded standard

specimens under controlled laboratory conditions, which may not fully reflect the performance of these materials in service. Consequently, the results should not be directly extrapolated to full-scale components without additional validation under more representative conditions.

The findings of this research open several important pathways for advancing both the theoretical understanding and practical engineering of hybrid fibre-reinforced composites. While this study establishes a new framework for modelling and experimentally validating pseudo-unified hybrid systems, several critical gaps warrant future investigation to fully unlock their technological potential.

On the experimental front, future efforts should focus on optimizing fibre–matrix interfacial interactions, particularly addressing the mechanical and chemical compatibility between dissimilar reinforcements, such as microfibrillated cellulose and carbon fibres. Enhancing interfacial adhesion remains essential for improving stress transfer efficiency, minimizing fibre pull-out, and reducing interfacial debonding, which are critical for maximizing mechanical performance under both static and dynamic loading conditions.

Advanced surface functionalization techniques, including plasma treatments, grafting, and the use of chemical coupling agents, should be explored to tailor the interfacial properties of the composite system without compromising its bio-based nature. Additionally, optimizing fibre architecture, such as length distribution, orientation control, and network connectivity, offers significant potential for improving impact strength and damage tolerance, addressing one of the key mechanical limitations identified in this work. Hybridization strategies that balance stiffness and energy absorption should be further investigated to expand the application space toward impact-critical automotive and structural components.

From a theoretical and modelling standpoint, future work should extend the current framework beyond the idealized assumptions of linear elasticity and perfect fibre–matrix bonding. While the modified shear-lag model developed here improves the physical realism of modulus prediction by introducing a non-linear stress transfer efficiency parameter (α) and incorporating effective matrix behaviour, several limitations must be addressed to enhance its predictive capability and industrial relevance.

First, the model should be expanded to account for nonlinear micromechanical behaviour, particularly relevant in natural fibre-reinforced polymers. This includes:

- Viscoelasticity and rate-dependent response of the polymer matrix
- Plastic deformation under elevated stress conditions
- Progressive damage evolution, including fibre–matrix interfacial debonding and fibre breakage
- Role of interfacial shear stress in governing load transfer from the effective matrix to the fibres

Such phenomena are critical in long-term structural applications or under cyclic and thermomechanical loading, where time-dependent effects strongly influence performance.

Second, the current formulation cannot simulate multi-axial loading conditions and orientation dispersion that arise in processes such as injection moulding. Extending the model to account for fibre misalignment, network anisotropy, and processing-induced defects would improve predictive accuracy for industrial geometries.

Third, further refinement of the analytically derived stress transfer efficiency parameter (α) is required. Its current form, while effective in capturing end effects, assumes saturation behaviour based solely on fibre length relative to critical length. Future formulations should incorporate sensitivity to:

- Environmental conditions (e.g., temperature, humidity)
- Loading history and strain rate
- Microstructural factors, such as fibre packing density, waviness, and fibre–fibre contact

Incorporating fibre–fibre mechanical interactions, matrix yielding, and interphase plasticity within a multi-scale computational framework would improve the robustness of the model. Embedding these features into a time-dependent (viscoelastic–viscoplastic) shear-lag or cohesive zone model could enable realistic predictions under service conditions.

Advanced experimental techniques, such as digital image correlation, X-ray tomography, and micromechanical testing, should be employed to validate and calibrate future models. These

methods can reveal fibre dispersion percentages, fibre orientation fields, stress redistribution patterns, and damage propagation mechanisms, which are essential for model verification.

From a sustainability perspective, Life Cycle Assessment (LCA) studies comparing these hybrid composites with conventional materials are essential for quantifying environmental benefits and trade-offs. Regrind and recyclability studies should also be undertaken to assess End-of-Life Vehicle recovery potential, particularly after multiple processing cycles. In parallel, the search for alternative sustainable reinforcement systems remains a critical research direction. Incorporating new bio-based, recyclable, or biodegradable fibres, while maintaining high mechanical performance, aligns with the global shift toward a circular economy and low-carbon manufacturing. Exploring emerging natural fibres (e.g., bamboo, kenaf, agricultural residues) and hybridizing them with high-performance synthetic reinforcements could yield next-generation eco-composites with tailored property profiles for automotive, aerospace, and construction applications.

By addressing these experimental and theoretical challenges, the modified shear-lag framework can evolve into a more comprehensive and predictive tool, supporting material design, durability assessment, and structural optimization of hybrid composite systems. Ultimately, these efforts will advance the scientific foundation and industrial readiness of sustainable hybrid composites, enabling high-performance, environmentally responsible solutions for diverse engineering sectors.